CONTROLLING THE ELECTRONIC PROPERTIES AND MORPHOLOGY OF SEMICONDUCTING POLYMERS THROUGH THE INCORPORATION OF 1,6-METHANO[10]ANNULENE

By

Benjamin C. Streifel

A dissertation submitted to the Johns Hopkins University in conformity with the requirements

for the degree of Doctor of Philosophy

Baltimore, Maryland

May, 2014

Abstract

Conducting polymers have been known since polyacetylene was discovered in the 1970s. Since then, myriad new small molecules and polymeric structures have been synthesized to optimize the properties of conducting organic materials. These materials are characterized by their highly delocalized π-orbitals and semiconductor-like band structure in their neutral state. The vast majority of these conjugated small molecules and structures are based around benzenoid Hückel 4n+2 structures where n=1. Common examples include poly-paraphenylene, polythiophene, polyaniline, and many others. These subunits perform well in certain applications and have been studied extensively, but much less attention has been focused on aromatics with larger π-electron systems. 1,6-methano[10]annulene (M10A) is one such aromatic with a 10π electron system, a non-planar structure, and a bridging methylene carbon. The non-planarity of the ring leads to low resonance energy, offering significant polyolefin character and lower energy barriers to oxidation, electrophilic addition, and other processes that require breaking of aromaticity. This polyolefin character also extends the effective conjugation length of polymers, leading to reduced bandgap and more effective delocalization of charge. These electronic features of M10A allow it to stabilize reactive species under oxidative electrochemical polymerization conditions, as well as render furan containing polymers resistant to environmental degradation.

The curved geometry of the annulene has the ability to prevent torsional strain arising from steric clashes between alkyl chains and aromatic subunits along the polymer backbone. This too leads to extended effective conjugation length and good materials properties. The bridging methylene prevents ordered aggregation, resulting in M10A-containing polymers being amorphous with a variety of comonomers. These highly disordered conducting materials are useful as transistor and thermoelectric materials,

exhibiting reasonable hole mobilities (ca. 10^{-4} cm^2/Vs) and high Seebeck coefficients (ca. 10^3 μV/K).

Thesis Advisor: John D. Tovar

Thesis Readers: Gary H. Posner and Marc M. Greenberg

Acknowledgements

Many people are to blame for the successful completion of my graduate career at Johns Hopkins University. I have had the wonderful and unique experience of working with every member (save a few summer undergraduate students) to come through JD's lab, and therefore I would like to begin by thanking my labmates Patricia Peart, Christopher Harvey, Anthony Caruso, Stephen Diegelmann, Alicia Fraind, Brian Wall, Geeta Vadehra, Giselle Elbaz, David Levine, Allix Sanders, Ashley Zacca, Herdeline "Digs" Ardoña, Justin Defrancisco, and Reid Messersmith. These individuals have offered significant scientific and social support throughout the years, and it's been a real treat to know them. I would like to thank my advisor JD Tovar for being a fantastic boss and assisting me in my research. In addition to JD, the professors I have interacted with at Johns Hopkins have been excellent educators and role models and have contributed significantly to my development as a chemist. I would also like to thank my undergraduate professors at the University of San Diego, especially Dr. Peter Iovine and Dr. Steven Morrison. They offered me substantial support during my time at USD, and are probably the people most responsible for convincing me to go to graduate school. I would also like to thank the support staff at Johns Hopkins University: Jean Goodwin, Chuck Long, Phil Mortimer, Cathy Moore, and Boris Steinberg were all fantastic people to work with.

I would also like to thank my parents, Robert and Janet Streifel, and my sister Dr. Amber Streifel. They have all been incredibly supportive of my chemical research career, from the time my parents purchased my first chemistry set, to the time I got caught brewing beer in the kitchen, to the time Amber and I spent in Baltimore attending pharmacy and graduate school. Their support has allowed me to pursue research and other adventurous chemical pursuits that have enabled me to obtain a doctoral degree.

Dedicated to my parents Robert and Janet, and my sister Amber.

Table of Contents

List of Tables

List of Figures

List of Schemes

Chapter 1 - Introduction to π-Conjugated Polymers

Foreword

The discovery of polysulfur nitride[1] and polyacetylene[2] ushered in a new era of conducting and semiconducting organic polymeric materials. These materials have been developed extensively and can compete with inorganic analogs in optoelectronic devices due to their inherent light weight nature, flexibility, and ease of processing, despite somewhat lower performance characteristics. Modern optoelectronic organic polymeric materials are often constructed from a diverse array of Hückel aromatics and have been optimized for use in devices such as photovoltaics (OPVs), field-effect transistors (OFETs), light-emitting diodes (OLEDs), and thermoelectric power generators (OTGs).

π-Conjugated Polymer Structure and Charge Transport

Polyacetylene (PA, Figure 1.1) was one of the earliest π-electron conjugated polymers to be synthesized and studied. Heeger, MacDiarmid, and Shirakawa first discovered that *trans*-polyacetylene had conductivities of up to 10^5 S/cm at room temperature when doped with I_2.[3] This high conductivity surprisingly approaches the values of common metallic conductors like copper (10^8 S/cm). The extensive delocalization of the cations formed upon chemical oxidation by iodine allows electrical current to flow relatively unhindered, resulting in the low resistance values. Polyacetylene is not an ideal organic polymeric conductor, however, as it is rather insoluble, is quite brittle, and is degraded by ambient atmospheric conditions.[4]
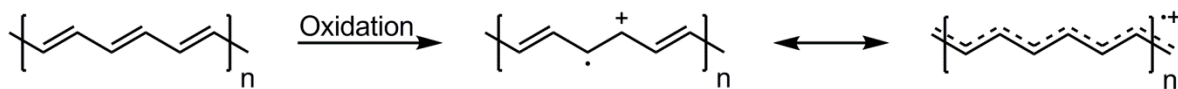
Figure 1.1. The oxidation of polyacetylene (left) showing formation of radical cation (center) and delocalized resonance structure (right).

The electronic structure of PA illustrates the effects of significant delocalization of π-electron orbital density (Figure 1.2). For alkenes such as ethylene, butadiene, and octatetraene, discrete molecular orbital levels exist with decreasing energetic spacing between orbitals and a decreasing HOMO-LUMO gap. At significant length scales, the energetic difference between orbitals is negligible and the set of filled orbitals is referred to as the valence band, while the closely-spaced unfilled orbitals are referred to as the conduction band. The bandgap becomes smaller with increasing chain length, but eventually reaches a minimum due to Peierls distortion. This distortion arises from the fact that a one-dimensional equally spaced chain with one electron per ion is unstable.[5] In the case of PA, the alternation of double and single bonds prevents from forming a truly metallic band structure. The valence and conduction bands are equally spaced about the Fermi level (E_f), which represents a hypothetical energy level at which an electron would have a 50% probability of occupying at thermodynamic equilibrium.
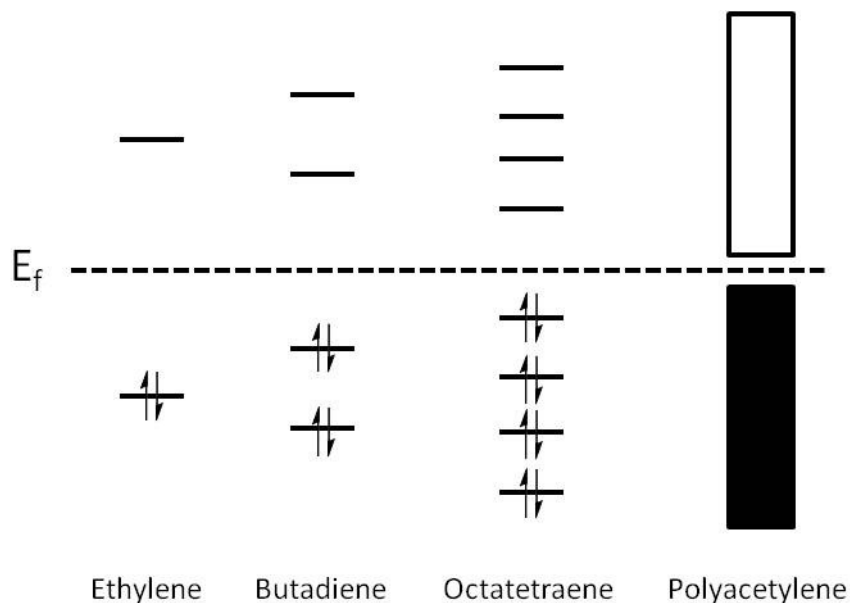
Figure 1.2. π-Electron molecular orbital diagram for oligoenes and polyacetylene showing band structure developing at long chain lengths.

Other π-conjugated subunits were subsequently developed to improve upon the materials properties of polyacetylene (Figure 1.3). Most often, these take the form of various aromatics: thiophene, fluorene, rylene diimides, acenes, diketopyrrolopyrrole, etc. Unlike polyacetylene, which pays no energetic cost for breaking aromaticity upon doping, aromatic subunits require a larger energy input to disrupt the conjugated π-electron system within each aromatic ring. The aromatic subunits, however, are more tolerant to substitution with solubilizing groups (commonly found as alkyl chains, alkoxy chains, etc) without loss of materials properties, and they are much more stable to ambient conditions than polyacetylene. These aromatic subunits can be designed to facilitate interchain π-stacking, which greatly increases rates of charge transfer through a bulk material, as charged species may propagate along a single polymer chain and 'hop' to an intimately-arranged neighboring chain to continue moving along an electric field.
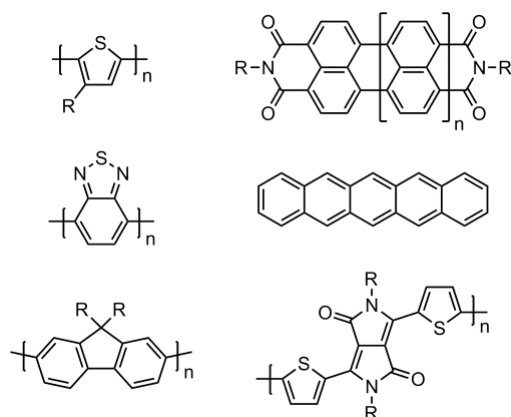
Figure 1.3. A selection of common polymeric and oligomeric π-conjugated materials used in organic semiconductors: poly(3-alkylthiophene) (top left), rylene diimides (top right), poly(2,1,3-benzothiadiazole) (middle left), pentacene (middle right), poly(9,9-dialkylfluorene) (bottom left), and poly(dithienyl-diketopyrrolopyrrole) (bottom right). R = *n*-alkyl, branched alkyl, alkoxy, etc.

π-Conjugated polymers are generally known to be extrinsic semiconductors, meaning they are weakly conducting in the undoped state, but become much more conductive upon chemical or electrochemical oxidation or reduction. By analogy to inorganic semiconductors, this oxidation or reduction process is called p- and n-doping, to describe the nature of the charge carriers created in the material. As described in Figure 1.4, oxidation of a semiconducting polymer introduces a new discrete orbital into the bandgap that contains an unpaired electron, as well as an associated unfilled orbital. This is referred to as a polaron, of which there can be several in a polymer chain. It is energetically favorable for the unpaired electrons in the polaronic states to combine to form a bipolaron, leaving two unfilled orbitals between the valence and conductions bands. Accumulation of bipolarons results in the formation of bipolaronic conduction bands that are much closer in energy to the valence band than in the original neutral polymer.
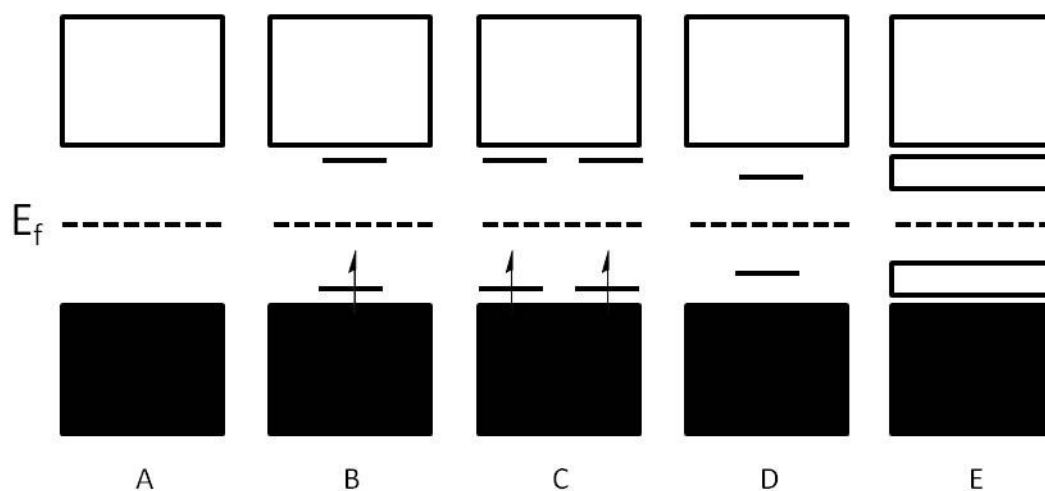
Figure 1.4. The band diagram of a semiconducting polymer (A) is oxidized to form a polaron (B) where the SOMO and LUMO move into the gap. Further oxidation results in two polarons forming (C) and combining to form a bipolaron (D) with midgap states. Significant oxidation subsequently forms a number of bipolaronic states resulting in bipolaronic bands, rendering the material conductive. Adapted from Reference 6.

Charge carriers (polarons, bipolarons) within the backbone of a polyaromatic semiconductor take the form of quinoidal structures (Figure 1.5) referred to as polarons for monocationic species and bipolarons for dications.[6] These extended quinoidal structures are thought to span a range of 8-10 aromatic rings.[7] These charge carriers move along the polymer chain and between adjacent chains in response to various stimuli (i.e. electric fields or thermal gradients). In general, intrachain transport is thought to be much more rapid that interchain transport. Charge carrier mobility is determined partially by the orientation of the conjugated subunits relative to one another. In the case of polyaromatics, a rotation out of coplanarity of 30°-40° is sufficient to effectively interrupt conjugation.[8] Thus, it is vitally important for high-performance materials to have carefully arranged pendant groups, such as solubilizing alkyl chains, as these have the ability to negatively affect coplanarity.
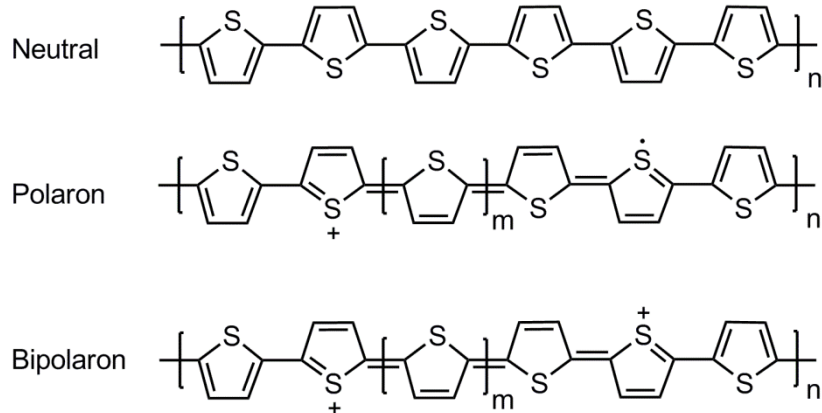
Figure 1.5. Shown are the neutral, polaronic, and bipolaronic forms of polythiophene.

Maintaining control over the spatial orientation of each ring in a polyaromatic semiconductor has important implications for the bulk film morphology. Polyaromatics with a high degree of coplanarity between adjacent rings generally form microcrystalline films due to favorable interchain quadrupolar π-π interactions. These films are often characterized by the presence of microcrystalline domains interspersed throughout more disordered regions of polymer. Increasing the degree of crystallinity in a polymer increases charge carrier mobilities and may improve other performance metrics, but high degrees of crystallinity may negatively impact charge carrier mobilities due to interfacial effects at crystal grain boundaries. It is also difficult to control the level of crystallinity on large-scale electronic devices due to the precision required in solvent evaporation rate, annealing time and temperature, purity of polymer, surface texture, substrate interfacial effects, *et cetera*.[9,10,11,12] Charge mobility in crystalline organic materials is also highly anisotropic, so attempts must be made to control the directionality of crystal growth for optimum device performance. Highly crystalline polyaromatics require high molecular weights to 'bridge' the crystalline domains and maintain efficient charge transport. If the polymer chains are too short, they

6

can form small aggregates or crystals (Figure 1.6) that are somewhat electronically insulated from the bulk film.[13]
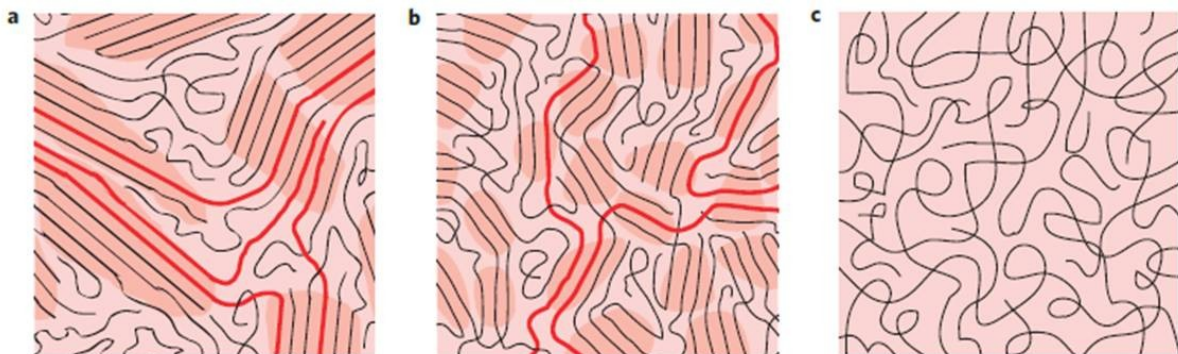
Figure 1.6. Illustration of a highly crystalline film (a), a semicrystalline film (b), and an amorphous film (c). Adapted from reference 13.

Amorphous polymers exhibit characteristics in the solid state that suggest they may be suitable replacements to more highly ordered materials. These characteristics include isotropic conductivity, nondispersive charge transport[14], tolerance of a range of solution processing conditions as well as dopant ions[15], and insensitivity to substrate type. Unlike crystalline aggregates of polymeric semiconductors, there is little charge transport anisotropy in amorphous polymers.[16] Crystallites located within polymer thin films may be randomly oriented with respect to one another and to the main direction of charge flow, hindering transport at grain boundaries and through the bulk film. In poly(3-hexylthiophene) (P3HT), for example, it is known that solvent evaporation rate (as a function of spin coating speed, for example) significantly affects both the degree of crystallinity in the film and the orientation of the crystallites relative to the substrate and one another.[17] There is generally less of a need to attempt to control aggregate orientation in amorphous films for optimum conditions.

Amorphous and otherwise highly disordered polymers films are also much more tolerant of varying processing conditions, including solvent, temperature, and concentration. Crystalline polymers may aggregate in solution and precipitate before being applied to a substrate during device fabrication. This results in inconsistent device performance as these solution aggregates and precipitates can be of a range of different sizes and have different charge transport properties. Amorphous polymers are still subject to π-stacking driven aggregation, but are less likely to form large crystalline precipitates due to the inefficiency with which the polymer chains assemble, allowing increased solvent-polymer interaction. These factors result in a high degree of spatial homogeneity in films, improving device consistency.[18] The disordered way in which the polymer chains arrange themselves negatively affects charge transport properties, with the best performing amorphous polymeric semiconductors achieving ca. 10^{-3} cm^2/Vs hole mobilities, whereas crystalline P3HT films attain hole mobilities of ca. 10^{-1} cm^2/Vs[19] and conductivities of 1000 S/cm.[20] Common subunits in amorphous conjugated polymers consist of a variety of planar aromatics, such as carbazole and isoindigo[21], decorated with branched alkyl chains to frustrate π-stacking interactions. Subunits with inherent 3-dimensional geometries like triarylamines[22], and 9,9-dialkyl fluorene,[23] frustrate π-stacking that leads to crystalline aggregates in thin films.

One factor that affects the morphology of a semiconducting film is the polymer molecular weight. The ordering of poly(3-hexylthiophene) (P3HT), for example, shows a strong dependence on polymer length (and therefore weight). Low weight (<50 kg/mol) polymers generally exist as crystalline domains of cofacially π-stacked molecules, whereas higher molecular weight (>50 kg.mol) polymers exhibit crystallites bridged by semiconducting amorphous regions as described previously.[24] The electronic results of this chain-length dependence are that high molecular weight materials show a balance of intra-

and intermolecular excitonic coupling, and therefore exhibit high exciton coherence lengths along and between polymer chains. In contrast, low molecular weight polymers show predominantly interchain excitonic coupling due to reduced spatial coherence along the polymer chain. The structural implications of these effects are that high molecular weight polymers show increased planarity compared to shorter chains. This is means that there is increased torsional strain in such highly ordered polymers with shorter chain lengths, and so the molecular weight of any material of semicrystalline nature must be carefully controlled to obtain optimum values.
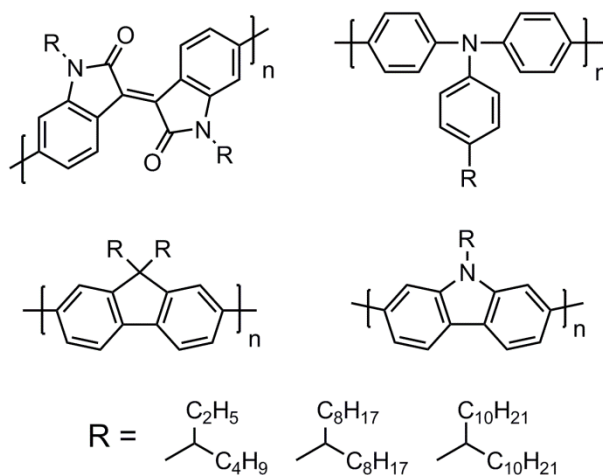
Figure 1.7. Common subunits in amorphous conjugated polymers: isoindigo (top left), triarylamines (top right), 9,9-dialkyl fluorenes (bottom right), and N-alkyl carbazoles (bottom right). Branched side chains prevent efficient π-stacking, leading to highly disordered thin films.

Side chain arrangement in a semiconducting polymer also has a significant impact on the morphology and therefore the electronic properties of the bulk material. In addition to the frustration of π-stacking caused by branched side chains, the spacing and orientation of chains along the polymer backbone is particularly important in intermolecular effects. One

such example of this is poly(5,5'-bis(3-dodecyl-2-thienyl)-2,2'-bithiophene (PQT), where the dodecyl chains are spaced and oriented in such a manner that they readily interdigitate and form highly ordered lamellar structures (Figure 1.8, left). The combination of alkyl chain interdigitation/crystallization and quadrupolar π-π interactions along the polymer backbone results in a highly ordered material with relatively high charge carrier mobilities (ca. 10^{-1} cm^2/Vs).[25] However, highly ordered alkyl segments are not necessary for good intermolecular π-π interactions. The McCullough group investigated this phenomenon by synthesizing a polymer based on thiazolothiazole with irregular spacing of alkyl chains to frustrate the alkyl-alkyl interactions, but used planar aromatics to allow for significant intermolecular interactions.[26] Poly(2,5-bis(3-dodecyl-5-(3-dodecylthiophen-2-yl)thiophen-2-yl)thiazolo[5,4-d]thiazole)s (PTzQT-12) was analyzed by X-ray diffraction and differential scanning calorimetry and it was found that there was a low degree of order in the alkyl region, but the polymer backbones exhibited significant π-π interactions. The overall morphology of this system is best described as small lamellar domains in an overall amorphous bulk film. These favorable backbone-backbone interactions result in high mobilities (ca. 10^{-1} cm^2/Vs) despite the amorphous alkyl chain portions.
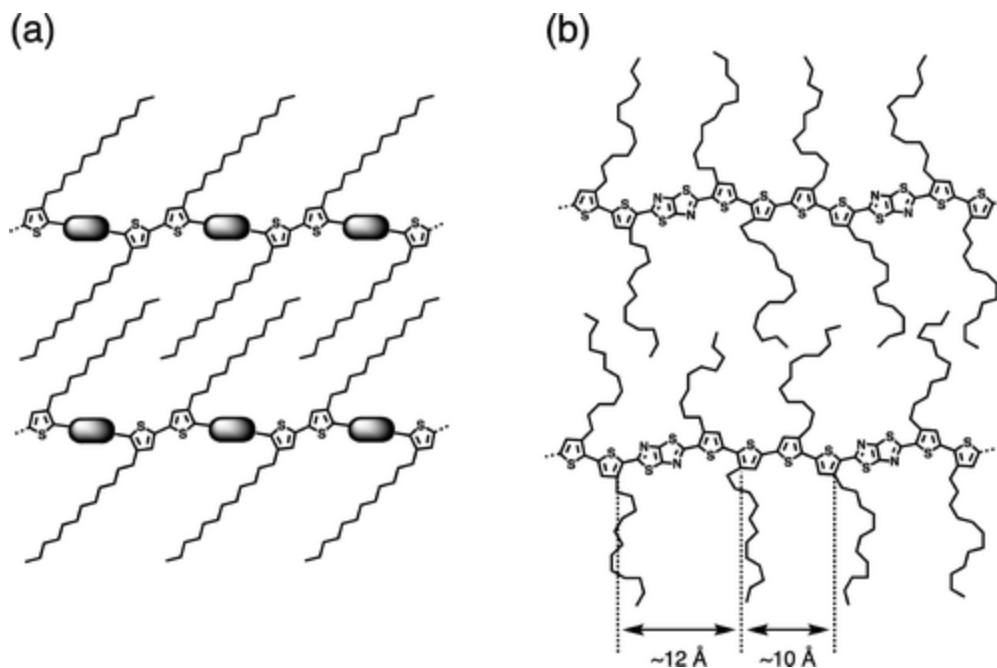
Figure 1.8. Schematic illustrations for the packing structure of PQT (a) and PTzQT-12 (b) in the solid state.

Another excellent example of the benefit of careful control over alkyl chain regioregularity and bulk film crystallinity is poly(3-hexylthiophene). P3HT is the prototypical semiconducting organic polymer and has been studied extensively.[27] P3HT has become the standard in organic electronic devices due to its ease of synthesis and good semiconductor properties. One of the main determining factors in P3HT device performance is the regioregularity of the hexyl side chains (Figure 1.9). 3-Hexylthiophene has two non-degenerate reaction sites for polymerization (the 2 and 5 positions) and the relationship of these positions to adjacent monomers determines the regioregularity. Generally, the 2 position is called the "head" (H) and the 5 position the tail (T). Successive head-to-tail (HT) couplings are preferred in the polymer as they result in the furthest spacing for the hexyl chains, reducing conjugation-breaking rotations around the bonds connecting the aromatic

subunits. HH and TT configurations result in steric interactions between hexyl chains that break the conjugation of the polymer chain. An increase in regioregularity increases the amount of planar polymer available to form stable π-stacks, which in turn increases the overall charge carrier mobility of the bulk material. Preparation of the polymer also plays a role in device performance, and annealing and solution processing conditions can affect the semiconductor properties. P3HT thin films can be annealed to form semicrystalline materials, where crystalline domains are embedded within larger areas of more disordered material. Achieving strict control over film morphology can be difficult, as dopants, solvent molecules, and assorted impurities can affect crystallization and interchain charge transport. Charge carrier mobilities also suffer when a large degree of crystallization occurs in the film, as the grain boundaries negatively affect charge transport. These effects often result in significant variation of performance metrics between similar devices.[28] For these reasons, more research is needed in the field of solution processable polymers with consistent device performance, where morphological control is carefully engineered into the material at the molecular level.
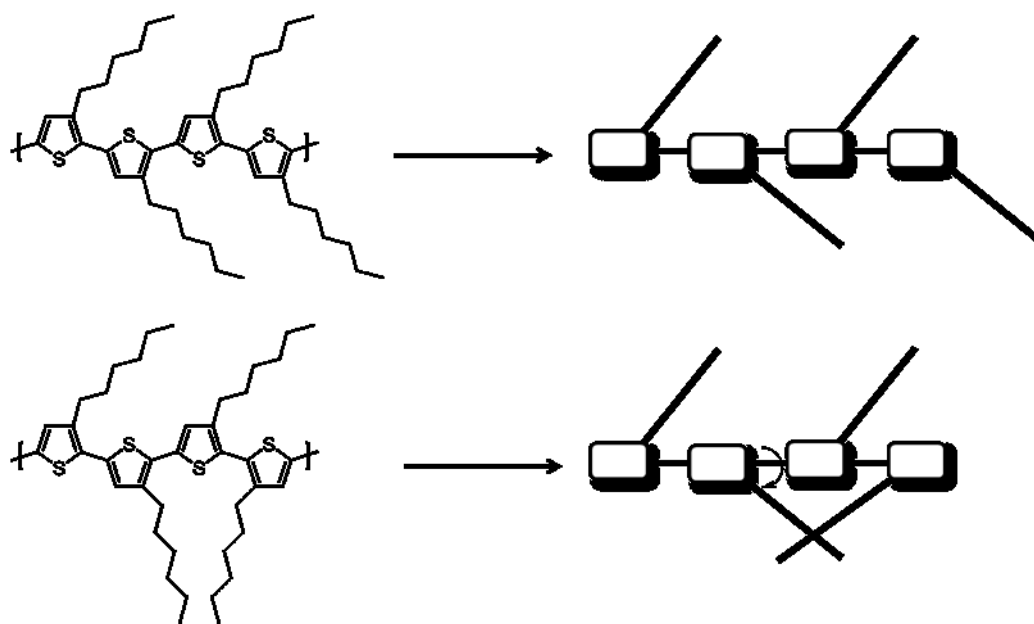
Figure 1.9. Regioregular (top) and regioirregular (bottom) repeat units of P3HT illustrating an HH defect causing torsional strain and a subsequent break in conjugation. Adapted from reference 27.

Significant work has gone into the design of efficient organic semiconducting polyaromatics using typical Hückel 4n+2 aromatics (where n=1). Larger rylene and acene type monomers (Figure 1.10) have been incorporated into polymers with hopes of making more efficient devices, but these can suffer from the same crystallinity problems as P3HT, as well as other problems arising from their unique chemical structures. The acenes can have 4n+2 electrons where n=2 or 3, but they can only have one truly aromatic sextet for any given resonance structure. A more idealized Hückel aromatic would have n=2 or 3 π-electrons but would not limit itself to one sextet. [10]Annulene should be the next largest homologue of benzene[29], but conformational preferences prevent true aromaticity and electronic delocalization. 1,6-Methano[10]annulene (M10A) has the desired stability and aromatic properties that make it a promising candidate for organic electronic device applications.
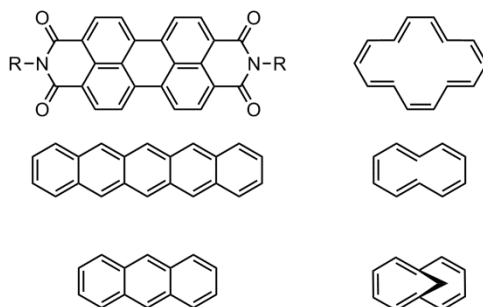
Figure 1.10. Structures of perylene diimide, pentacene, anthracene (left column), [14]-annulene, [10]-annulene, and 1,6-methano[10]annulene.

Organic Electronic Devices

Organic semiconductors will generally have lower performance metrics (i.e. charge carrier mobility, power conversion efficiency, thermoelectric figure of merit) than inorganic analogues (such as Si, Ge, Bi_xTe_y, etc.) in electronic devices. For example, the low charge carrier mobilities of organic semiconductors prohibit their use in devices that require high switching speeds. However, organic semiconducting materials are still good candidates for replacing inorganic materials due to their light weight nature, low cost, solubility in common solvents, and processability. Organic polymers and small molecules can be processed via solution-based techniques, such as inkjet and roll-to-roll (rotogravure) printing, directly onto flexible substrates. This rapid processing of large area devices is difficult to perform for inorganics, which are difficult to incorporate into structurally flexible devices. LED displays[30], photovoltaics[31], "electronic paper"[32], all-organic integrated circuits for RFID tags[33], and other devices are excellent applications for organics, as there is significant commercial interest in such devices. The three types of organic electronic devices covered in the following chapters are field effect transistors, photovoltaics, and thermoelectric generators. A basic understanding of the design, function, and performance characteristics of these particular devices is important to understanding the research presented in future chapters.

Organic Field Effect Transistors

Organic field effect transistors (OFETs) are devices that use an electric field to induce charge carriers into a semiconductor, allowing the charge carriers to flow between two electrodes.[34] OFETs come in a variety of architectures, such as a bottom-gate, top-contact arrangement (Figure 1.11). When there is no voltage bias applied to the gate electrode, no current may flow between the source and drain electrode due to the low density of charge carriers in the non-conductive film. As a bias is applied (ca. 10-100 V for organic semiconductors) to the gate, an electric field is produced across the dielectric and semiconductor, resulting in increased charge carrier density. For example, if a negative voltage is applied to the gate, holes form at the semiconductor-dielectric interface and electrons move in the opposite direction. In p-type materials, the holes form a conductive channel in the bulk semiconductor that allows current to flow when a voltage is placed across the source and drain electrodes. Charge carrier mobility is perhaps the most important performance metric of an OFET material, and is described by the equation $\sigma = \rho e \mu_h$, where σ is the electrical conductivity, ρ is the charge carrier density, e is the elementary charge, and μ_h is the hole mobility. Typical materials for the construction of an OFET include a doped silicon gate with native oxide dielectric. The SiO_2 dielectric can be coated with a variety of self-assembled monolayers, polymers, or other organic small molecules to improve semiconductor film morphology and consequently performance. The semiconductor can be evaporated on in a high vacuum chamber, or more commonly in the case of polymers, spin cast from the solution state. Electrode materials are typically gold, aluminum, or occasionally organic metals such as tetrathiafulvalene:tetracyanoquinone.[35]
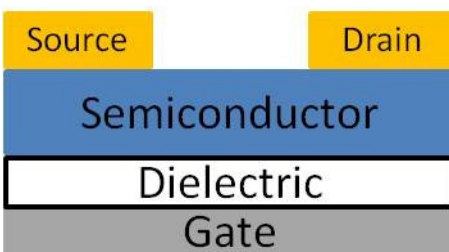
Figure 1.11. Diagram of a bottom-gate, top-contact organic field effect transistor (OFET).

The first organic polymer field-effect transistor was fabricated by Koezuka and colleagues from polythiophene (obtaining hole mobilities of ca. 10^{-5} cm^2/Vs)[36], and myriad other polymers and small molecules have been utilized in the production of OFETs since. The highest performing devices are currently made from single crystals of rubrene and can reach mobilities of 20-40 cm^2/Vs[37], but are not necessarily a good option for large area devices[38], such as display panels, due to the difficult processing requirements of growing high-quality single crystals. Semiconducting polymers generally exhibit lower mobilities, but are readily solution processable when carefully functionalized with solubilizing alkyl chains. Semicrystalline polymers such as P3HT have achieved hole mobilities of up to 0.1 cm^2/Vs.[39] Amorphous polymers are generally limited to lower mobilities or 10^{-3}-10^{-4} cm^2/Vs.[40]

Organic Photovoltaics

Organic photovoltaics (OPVs) are a popular area of research in the fields of physics, chemistry, and materials engineering. From the year 2000 to 2007, OPV publications accounted for nearly 10% of all photovoltaic publications.[41] Researchers have continued to fabricate OPV devices with power conversion efficiencies (PCE) approaching 10%, whereas inorganic silicon-based devices are currently achieving ca. 25% efficiency.[42] OPVs convert sunlight into electrical power by absorbing a photon and simultaneously promoting an electron from the valence band to the conduction band of the material. The electron in the

conduction band separates from the hole in the valence band and diffuses to an electrode. A very common architecture for OPVs is the bulk heterojunction (BHJ), which makes use of a blend of an electron-donating semiconductor and an electron-accepting semiconductor. The donor and acceptor materials in a BHJ-OPV device typically are not miscible in the solid state and are annealed after solution processing to allow some degree of phase separation. This annealing step is crucial as it allows the donor and acceptor materials to phase segregate into channels that can conduct holes or electrons. The ideal channel or domain size in the annealed heterojunction roughly matches the exciton diffusion length of the polymer, on the order of 10 nm for common organic semiconducting polymers.

The prototypical BHJ OPV (Figure 1.13) consists of a transparent electrode/substrate such as indium tin oxide (ITO) on glass or a flexible transparent polymer support. The semiconducting materials often consist of regioregular P3HT and a buckminsterfullerene derivative, phenyl-C_{61}-butyric acid methyl ester (PCBM). These materials are dissolved in a solvent, blended in the appropriate ratios (i.e. 1:1 P3HT:PCBM w/w), spin cast or printed onto the transparent electrode and annealed. A metallic electrode is then evaporated on, common materials being Ca or $CsCO_3$ followed by Al or Au.

BHJ-OPV devices based on P3HT:PCBM can attain PCEs of up to ~6% when polymer molecular weight, dispersity, purity, processing conditions, substrate cleanliness, and other factors are very carefully accounted for.[43] These factors can be difficult to control and may lead to inconsistent device performance.[44] In fact, over a decade of research has yielded very diverse published results for the same P3HT:PCBM system (Figure 1.12), with low-performance devices still being published in the literature.
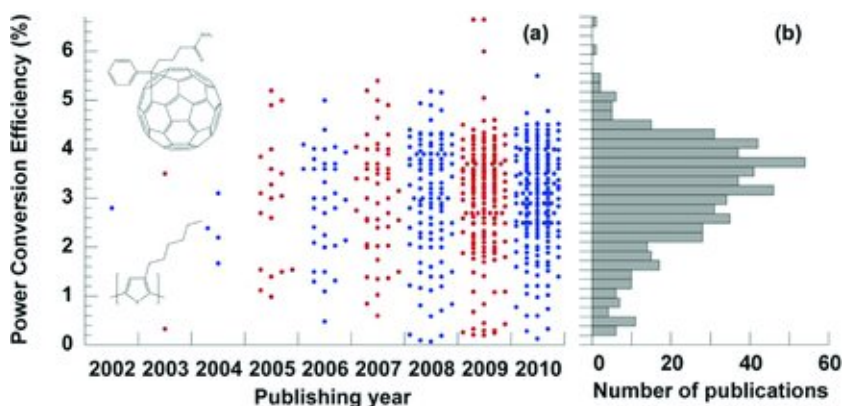
Figure 1.12. a) Power conversion efficiencies of P3HT:PCBM BHJ-OPVs published in the years between 2002-2010. b) Histogram of PCE and number of publications. Adapted from Reference 44.
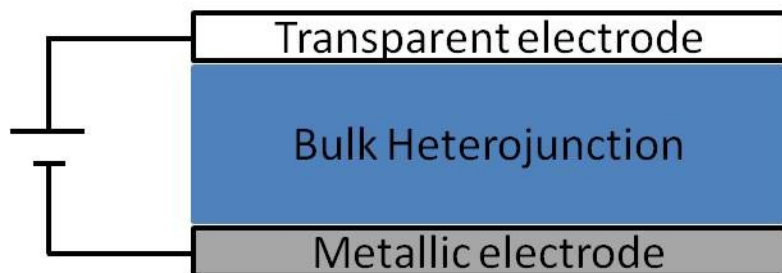
Figure 1.13. Diagram of an organic photovoltaic device (OPV).

Organic Thermoelectric Generators

Conjugated polymers are promising materials for thermoelectric applications.[45] Desirable qualities such as light weight, flexibility, solution processability, and low cost make them interesting replacements for more expensive low-natural-abundance materials such as Bi_2Te_3.[46] One particularly interesting application of polymeric thermoelectric devices is waste heat recovery. According to the U.S. Department of Energy, approximately 1.8×10^{12} BTU of waste heat is available for recapture and use. The average household in the US consumes 10^7 BTU annually, with all homes consuming roughly 10^{13} BTU.[47] This includes waste heat

18

in the form of gasses and liquids from a variety of large-scale industrial processes: power generation, refining processes, petroleum and chemical product manufacture, et cetera.[48] Polymeric thermoelectric materials are good candidates for this role due to their light weight, solution processability, and ease of large scale production.

The efficiency of thermoelectric materials is given by Equation 1.1, where η is the maximum efficiency of the material, T_H and T_C are the temperatures of the hot and cold side of the device, respectively, and ZT is the dimensionless figure of merit. ZT is given by Equation 1.2, where S is the Seebeck coefficient (dV/dT), σ is the electrical conductivity, κ is the thermal conductivity, and T is the average temperature of the device. An additional quantity, power factor (PF), is reported as a simple metric for the quality of a thermoelectric material and is described by the numerator of Z ($S^2\sigma$), in units of W m^{-1} K^{-2}. Organic polymers often have higher Seebeck coefficients and lower thermal conductivities than inorganic materials, but at the expense of much lower electrical conductivity.[49,50] The high Seebeck coefficient of organic materials may be explained by an increase in phonon drag relative to inorganic semiconductors and metals.[51] Because thermal conductivity is dominated in polymers by phonon conductivity due to the low-σ regime in which they operate[52], the strong phonon-electron coupling associated with conjugated polymer charge transport may offer a suitable explanation for this phenomenon.[53,54] Phonon drag is an important contributor to thermoelectric charge transport at relatively low temperature[55], so organic materials may be ideal candidates for this type of power generation.

Equation 1.1. The maximum efficiency of a thermoelectric device depends on a Carnot term as well as a term dependent on ZT, the dimensionless figure of merit.

$$\eta = \frac{T_H - T_C}{T_H} \frac{\sqrt{1 + ZT} - 1}{\sqrt{1 + ZT} + \frac{T_C}{T_H}}$$

Equation 1.2. The dimensionless figure of merit ZT is dependent on the Seebeck coefficient, electrical conductivity, thermal conductivity, and average temperature of the material.

$$ZT = \frac{S^2 \sigma}{\kappa} T$$

Another way to describe the high Seebeck coefficient is through a density of states model.[56] If the material, either pristine or a blend, is energetically structured such that the density of states in the conduction band is much greater than that of the valence band, the possibility for high Seebeck and moderate electrical conductivity is maintained, leading to high PF values and ultimately ZT. This is generally accomplished by introducing a minor additive with low carrier energy to a bulk material with high carrier energy, although other methods are possible. Thermal excitation of carriers in the minor additive should migrate into the bulk and diffuse against the temperature gradient, yielding a high Seebeck coefficient. An inverse relationship generally exists between the Seebeck coefficient and the electrical conductivity. With increasing dopant addition the Seebeck coefficient of a material typically declines, but the PF may continue to increase due to orders-of-magnitude increases in electrical conductivity. After passing a certain concentration of dopant, however, the PF begins to decline[57] due to the change in the Fermi level, resulting in a more symmetric density of states and therefore a lower Seebeck. Practical testing of a thermoelectric material will seek to optimize both S and σ by optimizing the dopant concentration.
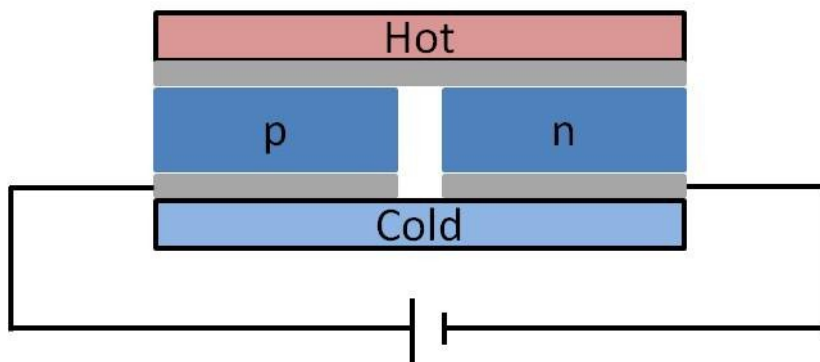
Figure 1.14. Diagram of an organic thermoelectric generator (OTEG).

A complete thermoelectric device will generally consist of two semiconducting materials, one n-type and one p-type, located between a heat source and a heat sink (Figure 1.14). Charge carriers (holes in the p-type material and electrons in the n-type) will flow against the temperature gradient, resulting in an electromotive force that may be used to power a variety of electronic devices. Individual devices are frequently wired together in series and parallel in order to achieve voltages and currents appropriate for the required power generation.

Conclusions

Amorphous polymeric semiconductors hold significant promise in terms of the development of organic electronic devices. In the following chapters, I will detail the use of the unusual Hückel aromatic 1,6-methano[10]annulene as a component of these polymers to control both the morphology and electronic properties in thin film devices. This aromatic subunit has been developed as a component of semiconducting polymers in the Tovar group, and this work continues in that vein of research.

References

[1] M.M. Labes; P. Love; L.F. Nichols *Chem. Rev.* **1979**, *79*, 1-15

[2] S. Etemad; A.J. Heeger *Ann. Rev. Phys. Chem* **1982**, *33*, 443-469

[3] H. Shirakawa; E.J. Louis; A.G. MacDiarmid; C. Chiang; A.J. Heeger *J. Chem. Soc., Chem. Commun.* **1977**, 577-580.

[4] E.V. Anslyn; D.A. Daugherty Ch. 17: Electronic Organic Materials *Modern Physical Organic Materials* University Science Books, Sausalito CA, **2006**, 1001-1045

[5] W.A. Little *Phys. Rev.* **1964**, *134*, A1416

[6] J.L. Brédas; G.B. Street *Acc. Chem. Res.* **1985**, *18*, 309

[7] P. Audebert; F. Miomandre Chapter 18 In *Handbook of Conducting Polymers: Theory, Synthesis; Properties; and Characterization*, 3rd Ed; T.A. Skotheim; J.R. Reynolds, Eds., CRC Press, Boca Raton FL, **2007**, 18-1 – 18-39

[8] J.L. Brédas *J. Chem. Phys.* **1985**, *82*, 3808-3811

[9] W. Zhang; J. Smith; S.E. Watkins; R. Gysel; M. McGehee; A. Salleo; J. Kirkpatrick; S. Ashraf; T. Anthopoulos; M. Heeney; I. McCulloch *J. Am. Chem. Soc.* **2010**, *132*, 11437-11439

[10] H. Sirringhaus; P.J. Brown; R.H. Friend; M.M. Nielsen; K. Bechgaard; B.M.W. Langeveld-Voss; A.J.H Spiering; R.A.J. Janssen; E.W Meijer; P. Herwig; D.M. de Leeuw *Nature* **1999**, *401*, 685-688

[11] D.P. McMahon; D.L. Cheung; L. Goris; J. Dacuna; A. Salleo; A. Troisi *J. Phys. Chem. C.* **2011**, *115*, 19386-19393

[12] J. Rivnay; M.F. Toney; Y. Zheng; I.V. Kauvar; Z. Chen; V. Wagner; A. Facchetti; A. Salleo *Adv. Mater.* **2010**, *22*, 4359-4363

[13] R. Noriega; J. Rivnay; K. Vandewal; F.P.V. Koch; N. Stingelin; P. Smith; M.F. Toney; A. Salleo *Nature Materials* **2013**, *12*, 1038-1044

[14] P.M. Borsenberger; L.T. Pautmeier; H. Bässler *Phys. Rev. B* **1992**, *46*, 12145-12153

[15] P.M. Borsenberger; P. Richert; H. Bässler *Phys. Rev. B* **1993**, *47*, 4289-4295

[16] D.W. Breiby; E.J. Samuelson; *J. Polym. Sci., Part B: Polym. Phys.* **2003**, *41*, 2375

[17] D.M. DeLongchamp; B.M. Vogel; Y. Jung; M.C. Gurau; C.A. Richter; O.A. Kirillov; J. Obrzut; D.A. Fischer; S. Sambasivan; L.J. Richter; E.K. Lin *Chem. Mater.* **2005**, *17*, 5610-5612

[18] T. Yasuda; T. Suzuki; M. Takahashi; L. Han *Solar Energy Mater. and Solar Cells* **2011**, *95*, 3509-3515

[19] J.F. Chang; B. Sun; D.W. Breiby; M.M. Nielsen; T.I. Sölling; M. Giles; I. McCulloch; H. Sirringhaus *Chem. Mater.* **2004**, *16*, 4772-4776

[20] R.D. McCullough; S. Tristram-Nagle; S.P. Williams; R.D. Lowe; M. Jayaraman *J. Am. Chem. Soc.* **1993**, *115*, 4910

[21] Y. Deng; J. Liu; J. Wang; L. Liu; W. Li; H. Tian; X. Zhang; Z. Xie; Y. Geng; F. Wang *Adv. Mater.* **2013**, *26*, 471-476

[22] T. Yasuda; T. Suzuki; M. Takahashi; L. Han *Solar Energy Mater. and Solar Cells* **2011**, *95*, 3509-3515

[23] S. Kilina; E.R. Batista; P. Yang; S. Tretiak; A. Saxena; R.L. Martin; D.L. Smith *ACS Nano*, **2008**, *2*, 1381-1388

[24] F. Paquin; H. Yamagata; N.J. Hestand; M. Sakowicz; N. Berube; M. Cote; L.X. Reynolds; S.A. Haque; N. Stingelin; F.C. Spano; C. Silva *Phys. Rev. B.* **2013**, *88*, 155202

[25] B.S. Ong; Y. Wu; P. Liu; S. Gardner *J. Am. Chem. Soc.* **2004**, *126*, 3378-3379

[26] I. Osaka; R. Zhang; G. Sauve; D.M. Smilgies; T. Kowalewski; R.D. McCullough *J. Am. Chem. Soc.* **2009**, *131*, 2521-2529

[27] R.D. McCullough *Adv. Mater.* **1999**, *10*, 93-116

[28] J. Rivnay; L.H. Jimison; J.E. Northrup; M.F. Toney; R. Noriega; S. Lu; T.J. Marks; A. Facchetti; A. Salleo *Nature Materials* **2009**, *8*, 952-958

[29] Van Tamelen, E.E., Burkoth, T.L., *J. Am. Chem. Soc.*, **1967**, *89*, 151-152

[30] B. Comiskey; J.D. Albert; H. Yoshizawa; J. Jacobson *Nature* **1998**, *394*, 253

[31] C.J. Brabec; S. Gowrisanker; J.J.M. Halls; D. Laird; S. Jia; S.P. Williams *Adv. Mater.* **2010**, *22*, 3839-3856

[32] R. Wisnieff *Nature* **1998**, *394*, 225

[33] C. J. Drury; C. M. J. Mutsaers; C. M. Hart; M. Matters; D. M. de Leeuw *Appl. Phys. Lett.* **1998**, *73*, 108.

[34] H. Sirringhaus *Adv. Mater.* **2005**, *17*, 2411-2425

[35] A.N. Bloch; D.O. Cowan; T.O. Poehler *Energy and Charge Transfer in Organic Semiconductors* **1974**, 167-174

[36] H. Koezuka; A. Tsumura; T. Ando *Synth. Met.* **1987**, *18*, 699-704

[37] T. Hasegawa; J. Takea *Sci. Technol. Adv. Mater.* **2009**, *10*, 024314

[38] C.D. Dimitrakopoulos; P.R.L. Malenfant *Adv. Mater.* **2002**, *14*, 99-117

[39] C. Tanase; E.J. Meijer; P.W.M. Blom; D.M. de Leeuw *Phys. Rev. Lett.* **2003**, *91*, 216601

[40] J. Veres; S.D. Ogier; S.W. Leeming; D.C. Cupertino; S.M. Khaffaf *Adv. Funct. Mater.* **2003**, *13*, 199

[41] T. Ameri; G. Dennler; C. Lungernschmied; C.J. Brabec *Energy Environ. Sci.* **2009**, *2*, 347

[42] L. Dou; J. You; J. Yang; C.-C. Chen; Y. He; S. Murase; T. Moriarty; K. Emery; G. Li; Y. Yang *Nature Photonics* **2011**, *6*, 180-185

[43] C.J. Brabec; S. Gowrisanker; J.J.M. Halls; D. Laird; S. Jia; S.P. Williams *Adv. Mater.* **2010**, *22*, 3839-3856

[44] M.T. Dang; L. Hirsch; G. Wantz *Adv. Mater.* **2011**, *23*, 3597-3602

[45] M. He; F. Qiu; Z. Lin *Energy Environ. Sci.* **2013**, *6*, 1352-1361

[46] X. Lu; D.T. Morelli *Phys. Chem. Chem. Phys.* **2013**, *15*, 5762

[47] US Energy Information Adminstration *Residential Energy Consumption Survey* Washington. US Department of Energy **2009**

[48] US Department of Energy. *Technology Roadmap: Energy Loss Reduction and Recovery in Industrial Energy Systems*. Washington. Office of Energy Efficiency and Renewable Energy. **2004**

[49] N. Dubey; M. Leclerc *J. Polym Sci., Part B: Polym Phys.* **2011**, *49*, 467-475

[50] Y. Xuan; X. Liu; S. Desbief; P. Leclere; M. Fahlman; R. Lazzaroni; M. Berggren; J. Cornil; D. Emin; X. Crispin *Phys. Rev. B: Condens. Matter Mater. Phys.* **2010**, *82*, 115454

[51] C. Herring *Phys. Rev.* **1954**, *96*, 1163-1187

[52] T.O. Poehler; H.E. Katz *Energy Environ. Sci.*, **2012**, *5*, 8110-8115

[53] A. S. Karabunarliev; E.R. Bittner *J. Chem. Phys.* **2003**, *118*, 4291-4296

  B. J.-F. Chang; M. Giles; M. Heeney; I. McCulloch; H. Sirringhaus *Phys. Rev. B.* **2007**, *76*, 205204

[54] A.B. Kaiser *Rep. Prog. Phys.* **2001**, *64*, 1

[55] T.H. Geballe; G.W. Hull *Phys. Rev.* **1954**, *94*, 1134-1140

[56] J. Sun; M.L. Yeh; B.J. Jung; B. Zhang; J. Feser; A. Majumdar; H.E. Katz *Macromolecules* **2010**, *43*, 289-2903

[57] O. Bubnova; U. Khan; A. Malti; S. Braun; M. Fahlman; M. Berggren; X. Crispin *Nat. Mater.* **2011**, *10*, 429

Chapter 2 - 1,6-Methano[10]annulene as a Component of π-Conjugated Optoelectronic Polymers

Introduction

First synthesized by Vogel in the 1960s, 1,6-methano[10]annulene (M10A) has been studied as a novel aromatic with interesting properties, as the bridging methylene group constrains the geometry to a Hückel aromatic conformation.[1] The parent [10]annulenes of varying double bond configurations lack significant electron delocalization due to steric interactions within the ring.[23] The addition of a methylene group allows a close approximation of a Hückel aromatic, but also forces a slightly curved geometry, resulting in quite a bit of olefinic character that affects the reactivity and materials properties of M10A.[4,5] The aromatic character of larger 10π e$^-$ systems is attenuated by the polyene nature of the molecules, lowering the lattice distortion energy required to undergo the change from a benzenoid to a quinoidal structure[6]. Experimentally, M10A-thiophene polymers show trends in the UV-visible spectrum characteristic of longer conjugation length and increased planarity, as compared to similar naphthalene based systems (Figure 2.1). Annulene based polymers also show a lower oxidation potential than furan and thiophene based derivatives, while helping to maintain stability of the notoriously moisture-sensitive polyfuran.[7]

methano[10]annulene polymers:
extensive intrapolymer delocalization ...

... vs. naphthalene polymers:
localized structure imposed by energetic barriers
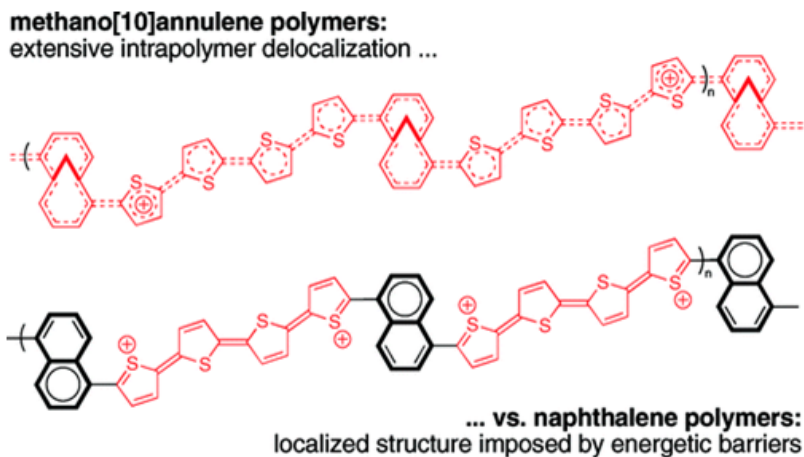
Figure 2.1. Exaggerated quinoidal bipolaronic resonance structures associated with doped M10A (top) and naphthalene polymers (bottom). [6]

The electronic characteristics and experimental results build the case for incorporating M10A into semiconducting polymers in an attempt to create more efficient devices and probe the fundamental science of polymeric organic semiconductors. Simplifying the process of chemically synthesizing polymerizable annulene-based monomers, M10A is easily functionalized according to known procedures, and its aromatic nature allows for a wide variety of transition metal-catalyzed cross coupling reactions to be performed. Simple techniques allow for a variety of monomers to be created in good yields using mild conditions. As shown in Figure 2.2, synthesis of the M10A core begins with two Birch reductions of naphthalene to isotetralin, followed by selective cyclopropanation of the central alkene using dichlorocarbene. A dissolving metal reduction of the *gem*-dihaloalkane results in a tricyclic-undecadiene derivative. Oxidative aromatization with DDQ completes the synthesis of M10A.
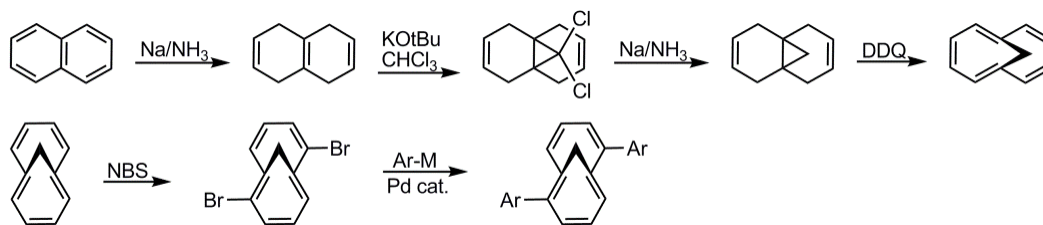
Figure 2.2. Vogel synthesis of M10A (top) and bromination-cross coupling scheme used for making aryl-flanked annulene derivatives (bottom). Ar-M represents any organometallic typically used in Pd cross couplings (organomagnesium, organolithium, organotin, organoboron, etc).

One particularly interesting feature of M10A is the curved shape of the annulene, forced into such a conformation by the bridging methylene group. The implications of this curved, bridged structure are huge; not only does the bridging carbon maintain the semi-planarity (and thus the aromaticity) of the ring, but it also presents a steric blocking group that interferes with normal π-stacking interactions that lead to potentially problematic aggregates. By far the most important driving force for the aggregation of conjugated polymers is $\pi-\pi$ quadrupolar interactions. While these are typically weak interactions, over the length of a polymer chain they can add up to significant binding forces between large molecules. The π-stack-interrupting methylene bridge of M10A results in the need for fewer, or even complete removal of, alkyl solubilizing chains from thiophene-based polymers. The lack of side chains would increase the proportion of π-conjugated material versus 'greasy' side chain per unit weight of bulk material. It should also be noted that when M10A is 2,7-disubstituted via typical succinimide halogenations, a racemic product is formed. Polymerizing a racemic mixture of aromatics will even further reduce the likelihood of self-assembly and aggregation into crystalline domains. The effects of the bridging methylene and racemic nature of a 2,7-disubstituted M10A are enough to create amorphous polymers.

While not necessarily good for interchain charge transport, amorphous conducting materials can be processed reliably and reproducibly. The amorphous nature of annulene polymers may prevent the aforementioned problems with crystalline regions from forming in the bulk.

The curved structure of M10A also holds promise in organic photovoltaics. A common problem in bulk heterojunction OPVs is poor interfacing between the donor polymer and the electron accepting portion of the cell. Polymers and small molecules that preferentially phase separate from each other typically have poor interfaces between them, limiting charge separation and transport. Frechét and coworkers got around this by reducing the overall order of the donor (P3HT) so as to limit exclusion of the acceptor (PCBM) and to maintain ideal domain sizes.[8] This of course has a negative impact on the absorption properties within the P3HT channels that form, but charge carrier mobilities were not negatively affected by the reduction in crystallinity of the P3HT domains.[9] Instead of reducing order slightly and introducing conjugation-breaking defects into the polymer, M10A could be used to ameliorate some of the phase separation. Although no studies have been performed on M10A in this particular regard, close analysis of the structure of M10A reveals excellent shape complementarity to C_{60} derivatives (Figure 2.3). If this complementarity can be translated into $\pi-\pi$ interactions, perhaps a better donor-acceptor interface can develop upon annealing. By having multiple weak interactions between the polymer chain and the fullerene acceptor, there will be a reduced tendency to fully phase separate upon annealing, as is known to happen with P3HT and PCBM. If the correct proportions of donor and acceptor are used, annealing should allow creation of hole and electron transporting channels required for efficient charge extraction while M10A "solubilizes" the fullerenes and maintains a close interaction. This idea is inspired by the work of Nuckols and colleagues, who utilized bowl-shaped hexabenzocoronenes[10] to form molecular "ball and socket joints" with fullerenes.[11]
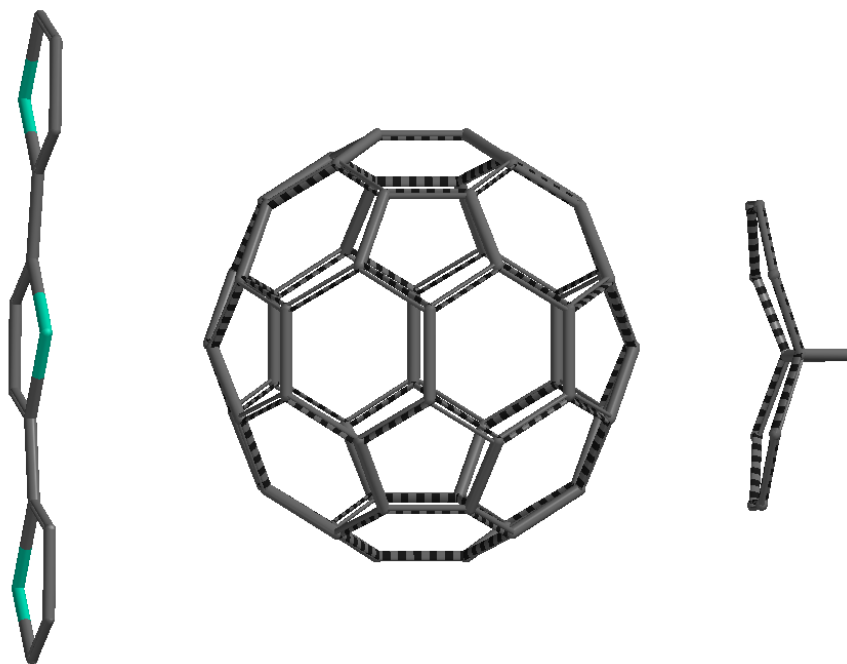
Figure 2.3. Depiction of the geometries of M10A, C_{60}, and terthiophene using energy minimized structures set approximately at van der Waals contact distance.

Another benefit of the curved structure of M10A is the potential for the reduction of conjugation-breaking side chain steric interactions. As previously described, defects in the regiochemistry of solubilizing side chains can have deleterious effects on mobilities and conductivity. The curved nature of the annulene could potentially allow for less steric clash when H-H or T-T defects are encountered in carefully synthesized hexylthiophene-annulene polymers, by simply presenting the side chains with less steric hindrance than another hexyl chain would give. Given that conjugation is directly related to planarity in polymer systems, and both are correlated to the optical bandgap of the polymer, UV-visible spectroscopy is an excellent way to qualitatively measure the degree of conjugation and planarity between different hexyl chain orientations. For the aforementioned reasons, M10A is an excellent

candidate for further research with the aim of developing new π-conjugated semiconducting polymers and small molecules for use in organic electronic devices.

Semiconducting polymers based on 1,6-methano[10]annulene

Organic semiconductors have proven to be commercially viable alternatives to traditional inorganic electronic materials for light emitting, charge transporting, and energy harvesting applications that require large area, light weight, and flexible active materials. High performance polymers suitable for these applications are often designed to foster extensive π-stacking in the solid state, but this can make the material prone to aggregation, crystallization, and undesired degrees of phase segregation after device fabrication.[12] There currently exists an unmet need for disordered or otherwise amorphous materials for these types of applications that show useful thermal stability[13], processability[14], and carrier mobility.[15] Amorphous materials are desirable for such applications as light-emitting diodes and thermoelectrics. Steric interactions within or between conjugated polymers directly influence overall intrapolymer planarity and subsequent interpolymer ordering of the resulting thin-film materials.[16] However, it is not completely understood how to control by design the effects of such interactions, particularly when attempting to control interpolymer stacking and crystallization.[17] Because solution processable polymers generally require some sort of solubilizing groups (often long alkyl chains pendant to the main conjugated chain), steric interactions arising from torsional strain between repeat units that contain them play an important role in disturbing the effective conjugation length of these polymers.

Several structure-property relationships have revealed the effects of solubilizing chain regiochemistry on different polymeric materials (Figure 2.4).[18,19,20,21] UV-visible and fluorescence spectroscopy revealed that altering only the position of pendant alkyl chains

relative to various aromatic polymer backbone subunits was enough to influence planarity within the conjugated polymer backbone.

The effect of poly(3-hexylthiophene) (P3HT) regioregularity on electronic properties is a particularly well-studied example.[22,23,24,25,26,27] When positioned in a regiorandom fashion, these alkyl chains caused the conjugated aromatic molecules to experience torsional strain and rotate out of co-planarity, thus breaking the conjugation along the polymer backbone.[28] Torsional strain was exacerbated when large, sterically demanding electron-accepting units such as benzothiadiazole and diketopyrrolopyrrole were incorporated into thiophene-based donor-acceptor polymers. Despite unfavorable torsional interactions, donor-acceptor polymers made up of components bearing relatively large molecular footprints nevertheless exhibit low optical bandgaps and increased charge transfer and/or separation than all-donor or all-acceptor homopolymers.[29, 30] These studies compared the torsional interactions among planar aromatic molecules and found that, in general, when the alkyl chains were directed away from the most sterically demanding group, the polymers showed a bathochromic shift in absorption and emission spectra to lower energy due to enhanced electronic delocalization.
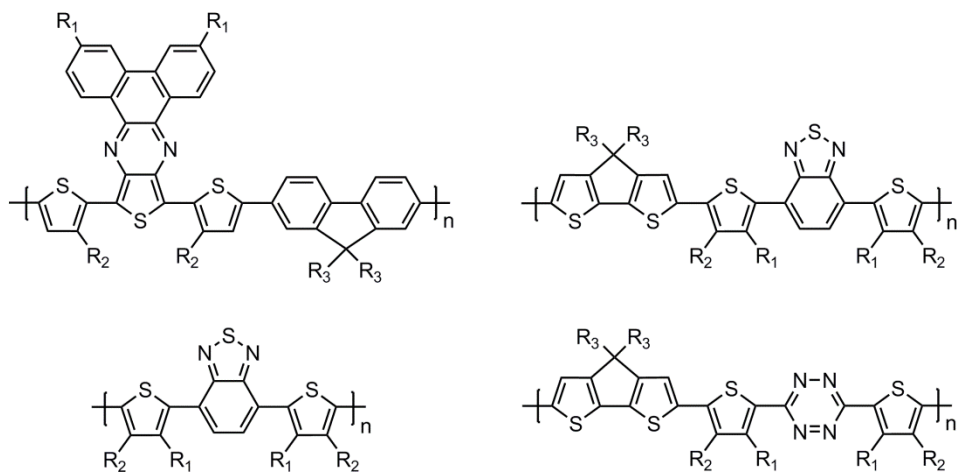
Figure 2.4. Examples of polymer structures exploring solubilizing alkyl chain regiochemistry. R groups consist of *n*-hexyl, *n*-octyl, *n*-dodecyl, and 2-ethylhexyl groups or protons.

Previous work in our lab explored 1,6-methano[10]annulene (M10A) as a candidate building block for semiconducting polymeric materials based on this molecule's unusual non-benzenoid aromaticity.[31,32,33,34] This landmark aromatic system was first synthesized by Vogel and Roth in 1964[35] and can be viewed as a valence isomer of a bisnorcaradiene motif present on substituted fullerenes such as PC$_{61}$BM.[36] M10A offers lower oxidation potentials, increased effective conjugation lengths, and decreased bandgaps in polymers that contain it relative to benzenoid building blocks. The bridged, curved structure of M10A should frustrate inter-chain π-stacking, possibly leading to amorphous solid-state materials. Although seemingly counterintuitive, amorphous materials exhibit good device characteristics in thin films and result in enhanced processability due to reduced tendency to experience π-stacking-driven aggregation in solution, and reduced phase segregation in thin films.[37,38,39] For high-throughput applications, such as inkjet printing, where undesired aggregation and precipitation are major factors, these properties are highly desired. In addition to these characteristics, the curved molecular geometry of M10A has the potential to reduce the steric clashes resulting from alkyl chains on neighboring aromatic rings. For

these reasons, M10A may be useful in extending conjugation length in alkylated conjugated polymers due to reduced annulene-alkyl torsional strain relative to other larger planar aromatic subunits.

In this section the synthesis of M10A-based conjugated polymers and small molecule models with different alkyl chain orientations relative to the annulene core in order to probe the amount of steric relief granted by aromatics exhibiting a curved molecular geometry is detailed. This study incorporates M10A and a variety of commonly used aromatics such as thiophene, benzothiadiazole, and diketopyrrolopyrrole. Each series consists of a "Tail In" and a "Tail Out" version with hexyl chains attached to the 3- or 4-positions, respectively, of the 2-thienyl units directly attached to the 2,7-positions of 1,6-methano[10]annulene (e.g. Tail In in Figure 2.5 is 2,7-bis(3-hexyl-2-thienyl)-1,6-methano[10]annulene), as well as a "No Tail" version with no hexyl groups. Regioregular co-polymers prepared from these carefully designed subunits showed differences in torsional interactions as determined by the relative positions of the hexyl chains. The electronic properties of polymers and small molecules were characterized by UV-visible and photoluminescence spectroscopy, and the polymers were characterized by ^{1}H NMR and gel permeation chromatography. Cyclic voltammetry was used to investigate their solution electrochemistry. A clear correlation between electronic properties and hexyl chain regiochemistry was found. The implications of these correlations are that curved aromatics can be used to influence and interrogate torsional interactions along the backbone of conjugated polymers while promoting solubility and disordered π-stacking in the solid state.
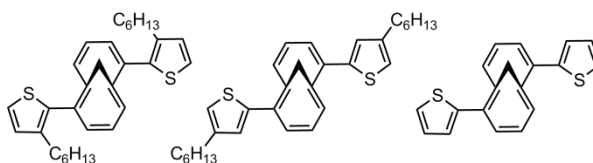
Figure 2.5. The Tail In (left), Tail Out (center), and No Tail (right) configurations of the TMT monomers refer to the relative relationship of the hexyl chain on the thiophenes relative to the annulene.

Synthesis of 1,6-Methano[10]annulene Polymers

Several polymers and molecular models were synthesized, built upon the aforementioned Tail In, Tail Out, and No Tail thiophene-M10A-thiophene (TMT) subunits. The orientation of the hexyl chains in the polymers should change little as far as electron donation into the aromatic backbone of the polymer, but is expected to dramatically alter the torsional influences involved in maintaining an extended effective conjugation length (ECL). For example, the curved nature of M10A should alleviate the steric clashing with solubilizing groups relative to larger or more planar aromatic subunits (Figure 2.6).
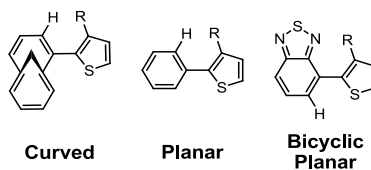
Figure 2.6. The structures of curved M10A, planar aromatics, and bicyclic planar aromatics offer differing degrees of torsional strain, affecting conjugation length in polymers.

These TMT monomers were synthesized by palladium-catalyzed cross couplings between 2,7-dibromo-1,6-methano[10]annulene and various 2-(tributylstannyl)thiophenes to afford the Tail In, Tail Out, and No Tail TMT products (Scheme 2.1). Neidlein established the utility of Pd-catalyzed cross coupling on M10A cores for optical materials,[40] and we

34

subsequently employed this for electropolymerizable molecules.[31] Tail In and Tail Out TMT were purified via column chromatography, and the No Tail variant was purified by recrystallization according to our previously reported procedure.[32] The TMT molecules are readily stannylated at the thienyl 5-positions by lithiation and quenching with tributylstannyl chloride (Scheme 2.2). These reactions proceed in high yields, but the excess tin electrophile required to drive the reactions to completion makes final purification difficult. The bis(tributylstannyl)-TMT compounds were carried on to the next reaction as isolated, with NMR integrations being used to estimate purity for accurate stoichiometry in subsequent reactions. Nevertheless, the lack of analytical purity for the stannylated comonomers led to unavoidable stoichiometry imbalances that could have potentially impacted the observed molecular weights. The TMT molecules are also easily brominated at the same 5-thienyl positions with NBS in dichloromethane. The dibromo-TMT compounds are purifiable by column chromatography and are isolated in acceptable yields. The distannane and the dibromide precursors are set up to perform a variety of transition-metal catalyzed cross-couplings to access either polymers (Scheme 2.3) or small molecules (Scheme 2.4).
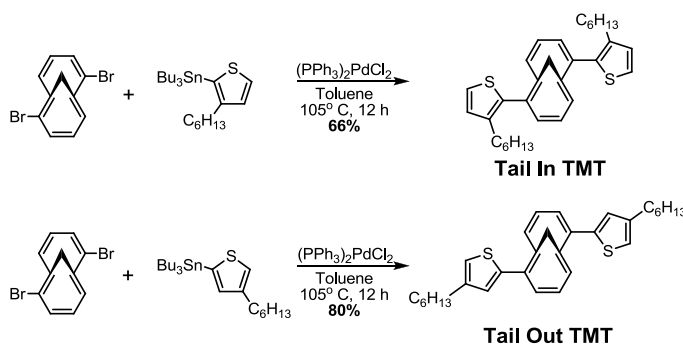
Scheme 2.1. Synthesis of thiophene-M10A-thiophene (TMT) monomers.
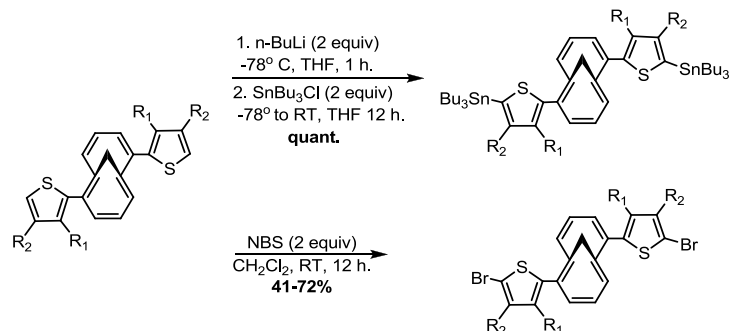
Scheme 2.2. Stannylation and bromination of the TMT monomers. Tail In: R_1= hexyl, R_2= H; Tail Out: R_1= H, R_2= hexyl; No Tail: R_1=R_2= H.

Homopolymers of the TMT subunits (PTMT, Scheme 2.3) were synthesized by Yamamoto reductive couplings of the dibromo-TMT units using a bipyridyl-nickel complex formed *in situ* from $Ni(COD)_2$ and 2,2'-bipyridine. The polymerization of the dibromo-TMT monomers proceeded by heating to 60°C for 2-4 days in dry DMF. The PTMT-T series was synthesized from the copolymerization of the dibromo-TMT monomers with 2,5-bis(tributylstannyl)thiophene via Stille couplings.   The standard Stille coupling procedure was modified by addition of copper (I) iodide to activate the thienyl bromide towards oxidative addition, as well as cesium fluoride to activate the (tributylstannyl)thiophene towards transmetalation.[41] PTMTs and PTMT-Ts were precipitated from methanol and filtered. The Tail In and Tail Out PTMTs and PTMT-Ts were soluble in common organic solvents, but the No Tail polymers were rather insoluble.
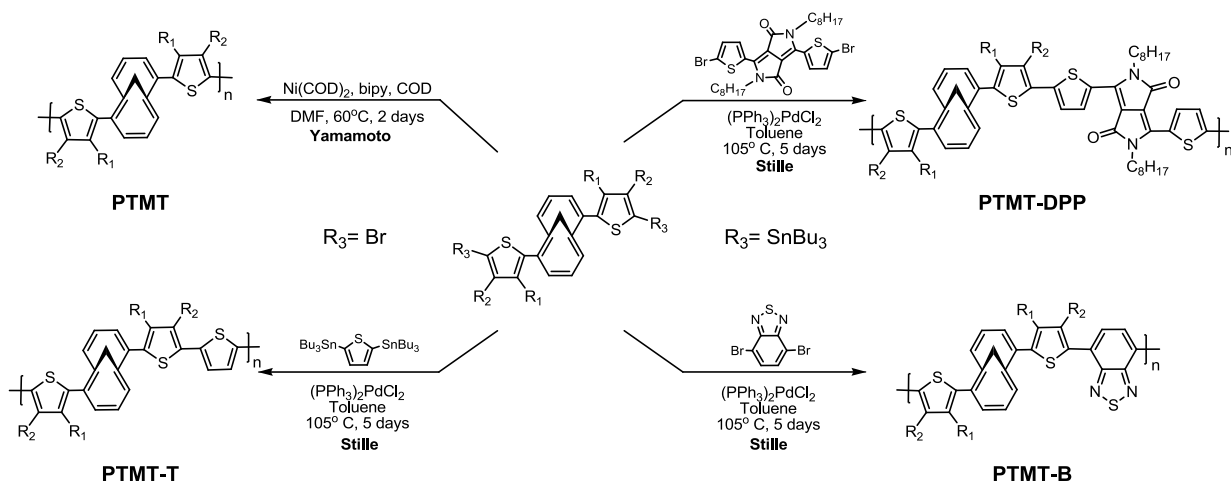
Scheme 2.3. Polymer syntheses from TMT monomers. Tail In: R_1= hexyl, R_2= H; Tail Out: R_1= H, R_2= hexyl; No Tail: R_1=R_2=H.

The PTMT-B and PTMT-DPP polymer series were synthesized from the bis(tributylstannyl)-TMT monomers by Stille coupling with the electron-poor dibromides of 2,1,3-benzothiadiazole[42] and bis(thienyl)-diketopyrrolopyrrole[43]. The PTMT-B and PTMT-DPP syntheses utilize enhanced Stille coupling procedures similar to those used in the PTMT-T synthesis but without the catalytic CuI to activate the aryl bromide, because electron deficient aromatics typically undergo rapid oxidative addition. The PTMT-B and PTMT-DPP series were precipitated directly into methanol and filtered to obtain final product. All variants were soluble in chlorinated organic solvents, although the No Tail polymers seemed to be less soluble in the same solvents than the tailed counterparts.

All polymers were analyzed by gel permeation chromatography to determine their approximate molecular weights relative to polystyrene standards. The values were not corrected and are assumed to be overestimates due to the rod-like structure of the polymers and the possibility of aggregation leading to exaggerated molecular weight measurements.[44] Although in some cases the molecular weights were low, we suspect that the number of individual pi-conjugated components in the polymer repeat units is sufficient to yield

37

polymers capable of maintaining the inherent effective conjugation length (that usually comprise ca. 10 aromatic rings).[45] The solvent used for this particular chromatography setup was THF at ambient temperature, which did not allow analysis of the No Tail polymers within any of the polymer series due to severe insolubility even after extended sonication and heating. However, the No Tail polymers were sparingly soluble in *o*-dichlorobenzene-*d*₄, allowing for ^{1}H NMR characterization. Peak broadening in the NMR spectrum indicates degrees of polymerization comparable to those of the Tail In and Tail Out within the same series.

Table 2.1. Polymer molecular weight data obtained by gel permeation chromatography.

Series / Orientation		M_n (g/mol)	M_w (g/mol)	PDI=[a]	DP$_n$=[b]
	Tail In	3800	6200	1.61	8
PTMT	Tail Out	2400	4900	2.05	5
	No Tail	Insoluble in THF			
	Tail In	3600	11100	3.11	6
PTMT-T	Tail Out	5700	15000	2.63	10
	No Tail	Insoluble in THF			
	Tail In	3800	7800	2.05	6
PTMT-B	Tail Out	3000	7700	2.57	9
	No Tail	Insoluble in THF			
	Tail In	3200	5500	1.72	3
PTMT-DPP	Tail Out	3000	4700	1.58	6
	No Tail	Insoluble in THF			

[a] Polydispersity index (PDI) is calculated as M_w/M_n.

[b] Degree of polymerization (DP$_n$) is calculated as M_n/repeat unit formula weight.

Oligomeric model systems were synthesized to mimic the polymeric series in structure and hexyl chain orientation. These small molecule models were designed to help elucidate torsional interactions without any dependence on molecular weight differences. The TTMTT and BTMTB systems are synthesized by Stille coupling (Scheme 2.4), by

endcapping the TMT monomer with thiophene or benzothiadiazole groups, respectively. The molecular models were purified by column chromatography and characterized by ^{1}H and ^{13}C NMR, as well as HR-MS.
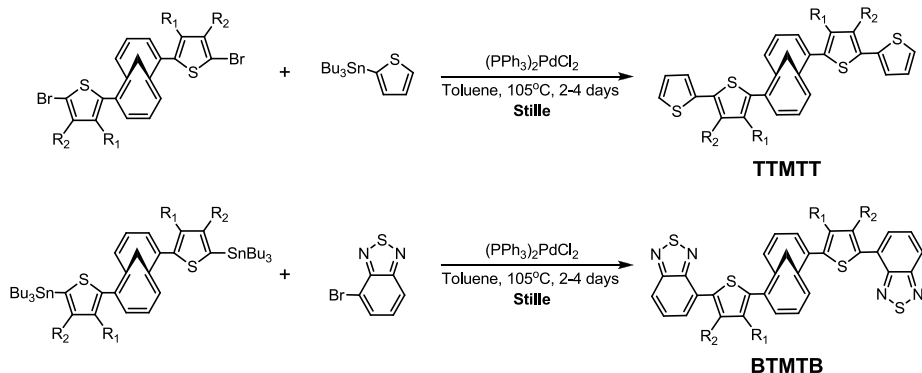
Scheme 2.4. Syntheses of TTMTT (top) and BTMTB (bottom) small molecule model systems. Tail In: R_1= hexyl, R_2= H; Tail Out: R_1= H, R_2= hexyl; No Tail: R_1=R_2=H.

Another set of small molecule model systems were made; the TNT series serves as a model of the TMT series but uses a planar bicyclic naphthalene subunit (Scheme 2.5). The synthesis proceeds via the same Stille methodology as the TMT, TTMTT, and BTMTB series described previously, starting with 1,5-diiodonaphthalene and various 2-tributylstannylthiophenes. Due to low yields of the diiodonaphthalene synthesis[46], only small amounts of TNT were able to be synthesized, and analytical purity was not achieved through column chromatography. Nonetheless, the product was sufficiently pure to allow spectroscopic analysis as in the case of the other model systems.
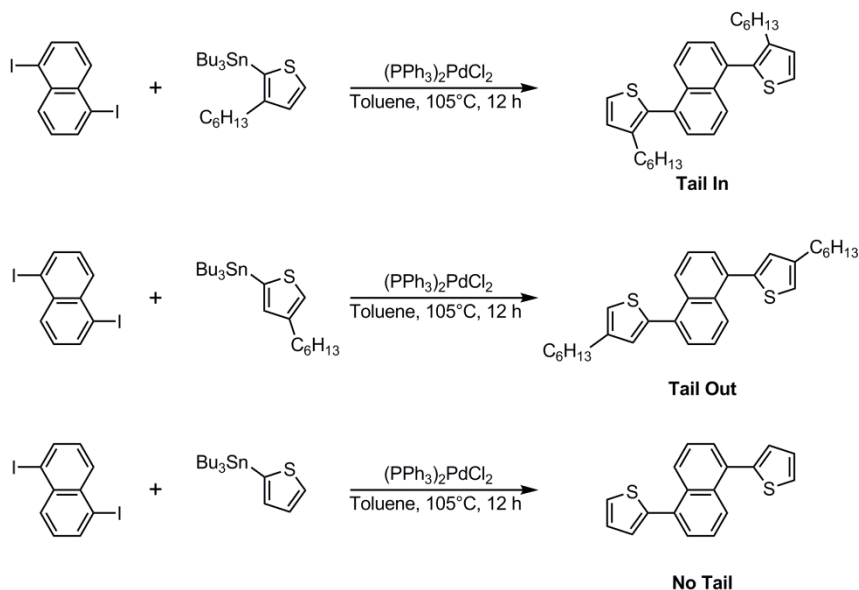
Scheme 2.5. Synthesis of the TNT series of small molecule model systems.

Study of Torsional Strain Within 1,6-Methano[10]annulene-Containing Polymers

UV-visible spectrophotometry was used to determine the relative degree of electronic delocalization along each polymer chain and within the small molecule models. For a polymer with a specific π-conjugated repeating unit, a longer effective conjugation length leads to lower energy absorption, so any forces that may cause the aromatic rings to deviate dramatically from planarity should be apparent in the electronic absorption spectrum by way of hypsochromic shifts in the onsets and/or maxima of absorption to higher energy. A torsional deviation of around 30-40° from co-planarity has been shown computationally to effectively interrupt conjugation.[47]

Tail In PTMT has a slightly red-shifted absorption maximum and onset compared to Tail Out PTMT (12 nm and 7 nm, respectively, Figure 2.7). The thiophene linkages within this series can be viewed as models of head-to-head (HH) and tail-to-tail (TT) couplings, as defined generally by McCullough for P3ATs.[48]   The bithiophene units in the Tail Out configuration correspond to a HH coupling, a torsional defect known to result in conjugation-

breaking rotation out of co-planarity. The Tail In structure corresponds to a TT defect but we hypothesize that the extent to which this affects the conjugation is mitigated by the presence of the curved M10A ring. No Tail PTMT appears to show an even further red-shifted absorption maximum and onset, and can be interpreted as a baseline of dihedral orientations inherent to the polymer backbone without alkyl chain influence. However, No Tail PTMT aggregates strongly in solution, leading to excessive scattering and a nonzero baseline in the absorption spectrum, so the observed values could also reflect planarized and/or aggregate structures. The photoluminescence spectra of the PTMT series show similar emission maxima, but different Stokes' shifts (106 nm Tail In, 133 nm Tail Out). The larger Stokes' shift for Tail Out polymer suggests it must undergo more reorganization in the excited state to reach a more planar lower energy structure necessary to better stabilize the excited state. This follows from the more sterically demanding HH linkage present in Tail Out PTMT.
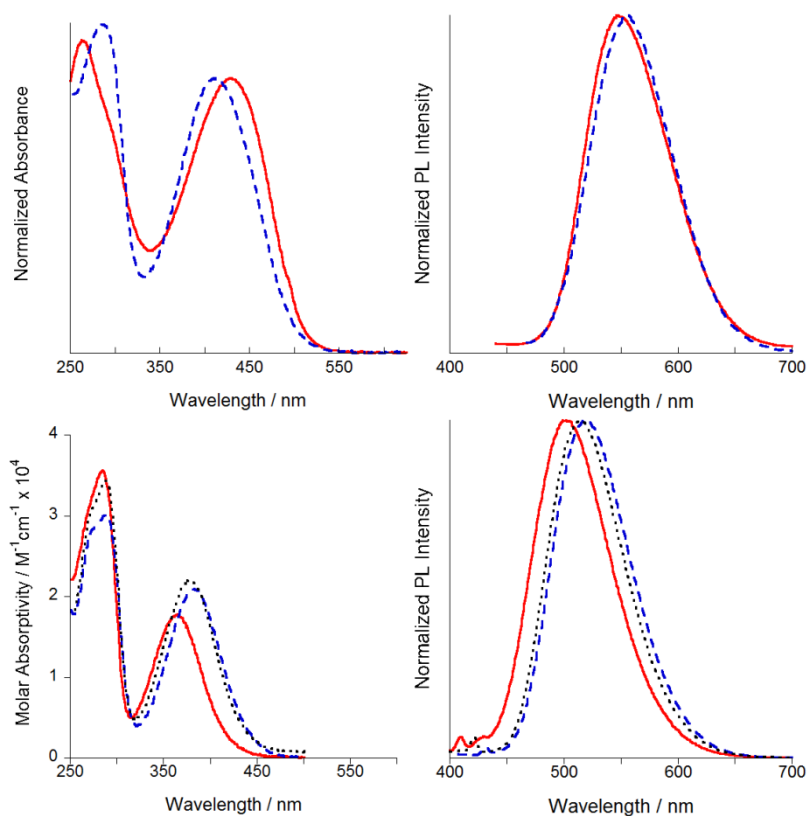
Figure 2.7. UV-Vis (left) and photoluminescence (right) for the PTMT (top) and TMT (bottom) series. Polymer absorption profiles are normalized relative to the lowest energy maxima. Excitation for each polymer occurred at the λ_{max} of the individual polymers. Tail In (red,—), Tail Out (blue, ---), No Tail (black, ···).

The TMT monomers show the opposite trend of the PTMT series in the absorption spectrum (Figure 2.7, bottom). Tail Out TMT shows a lower energy onset and absorption maximum compared to the Tail In (by 18 nm and 22 nm, respectively). This trend is expected due to the lack of significant steric interference acting on the hexyl chain of the Tail Out TMT compared to the presence of the annulene adjacent to the hexyl group for Tail In TMT. The photoluminescence spectrum also reflects these differences, with an 18 nm shift in the emission maxima from Tail In to Tail Out. Given the lack of sterically demanding groups adjacent to the portion of the thiophene ring furthest from the annulene, it is

42

unsurprising that No Tail TMT shows similar spectral behavior to Tail Out TMT, with both showing basically identical absorption and emission profiles.

The PTMT-T series shows the opposite trend of PTMT (Figure 2.8); the absorption maximum and onset of the Tail Out configuration are lower in energy than the Tail In (13 nm and 35 nm, respectively). The PTMT-T series assesses the difference between adjacent hexyl-annulene (large, curved) and hexyl-thiophene (small, planar) torsional interactions. In this particular case, the geometry of the annulene is not enough to make up for the size difference between the thiophene and [10]annulene. When the hexyl chains are directed towards the annulene there is some degree of freedom for the solubilizing chain that can lead to a reduction in torsional angle, as evidenced by the PTMT series, but not as much as is available when the hexyl chain is directed towards a relatively non-sterically demanding thiophene ring. The photoluminescence of the PTMT-T series shows the same trend as the TMT model series; the Tail In shows a higher energy emission, but smaller Stokes' shift than the Tail Out. The more conjugated Tail Out polymer has a lower energy emission maximum than does the Tail In. The Stokes' shifts indicate that less energy is needed to relax the excited state of the Tail In polymer due to it pre-existing in a relatively restricted conformation compared to the Tail Out analog and therefore cannot achieve a comparable extent of co-planarity in the excited state. The No Tail polymer shows the furthest red shift in the absorption and the lowest Stokes' shift, giving a baseline of co-planarity and extended conjugation for this polymer series due to the inherent hexyl-thienyl interactions.

Figure 2.8. UV-Vis (left) and photoluminescence (right) spectra for the PTMT-T (top) and TTMTT (bottom) series. Polymer absorption profiles are normalized relative to the lowest energy maxima. Excitation for each polymer occurred at the λ_{max} of the individual polymers. Tail In (red,−), Tail Out (blue, ---), No Tail (black, ⋯).

The TTMTT molecular models show the same trends as their PTMT-T counterparts, with Tail Out TTMTT exhibiting lower energy absorption features than Tail In TTMTT (25 nm maximum and 21 nm onset redshifted differences). The rationale invoked for the TMT and PTMT-T series is also valid here: the terminal thiophenes of these models present, in essence, the same steric environment as the thiophene comonomer subunit of the PTMT-T series, giving the Tail Out configuration the opportunity to achieve a more co-planar conformation. The photoluminescence of the TTMTT models also follows the aforementioned trends of the PTMT-T series, exhibiting a redshifted Tail Out emission

44

maximum. The Stokes' shift of the TTMTT series shows a greater shift for the Tail In relative to the Tail Out model (141 nm and 135 nm, respectively). This supports the proposal that the terminal thiophenes of the TTMTT series present a similar steric environment to the thiophene comonomer subunits in PTMT-T, without the formation of an HH defect commonly seen in regioirregular polythiophenes. The greater Stokes' shift for Tail In TTMTT suggests that the Tail In system pre-exists in a relatively restricted conformation, much like the parent polymer. No Tail TTMTT follows the same trend as No Tail PTMT-T: red-shifted absorption and the smallest Stokes' shift of the series, and the reasoning remains the same as for the polymer series.

With an assessment of how solubilizing hexyl groups influence torsional properties of thiophene-based conjugated polymers containing the non-planar M10A segment, we sought to study other polymers with broader absorption across the visible spectrum. The PTMT-B series interrogates the difference between hexyl-annulene and hexyl-benzothiadiazole interactions. This differs in several ways from the PTMT-T series; the benzothiadiazole core is bicyclic and presents a larger surface to interfere with the adjacent hexyl chains, and the electron-poor nature of benzothiadiazole creates a donor-acceptor system in the polymer chain that significantly lowers the optical band gap. As seen in Figure 2.9, the Tail In polymer has a lower energy absorption maximum and onset than the Tail Out (by 34 nm and 15 nm, respectively). The lone pairs on the heteroatoms forming the bicyclic ring system as well as the greater bond angles in the 6-membered ring versus a 5-membered thiophene may have an effect on the ECL by inducing significant torsional strain on the polymer backbone. These effects add up to allow the Tail In polymer, on average, to reach a more planar and conjugated state than Tail Out PTMT-B.

The photoluminescence data follows the trends previously seen in the PTMT and PTMT-T series. The emission maxima for all three polymers are within 3 nm and the emission profiles overlap nearly perfectly, but the Stokes' shifts follow similar trends (124 nm

Tail In, 137 nm Tail Out). Considering the alternating donor-acceptor structure of the polymers and the tendency for such systems to undergo intramolecular charge transfer, it is possible that the excited states of the polymers are able to overcome steric interactions in order to better adopt comparably planar structures that can emit photons of similar energy. Because electronic transitions between states happen prior to nuclear reorganization, all three polymers could emit from a comparably planarized fluorophore, and then relax back to their ground state conformations. An alternative explanation for the similarity in PL wavelengths in the polymers with stronger acceptors could originate from twisted intramolecular charge transfer (TICT) states. [49] Although these TICT states are a possibility, the polymer dispersities and the lack of strong vibronic features in the PL spectra preclude the unambiguous assessment of any spectral attenuation as a function of molecular solvent parameters or other definitive spectroscopic characterizations of these states that would be necessary to suggest TICT over other electronic processes. As such, the previous rationale for the similarity of the PL spectra is the preferred explanation in this case. No Tail PTMT-B follows a trend similar to the previous series: redshifted absorption maximum and onset and lower Stokes' shift compared to the Tail Out polymer, but relatively similar values compared to Tail In PTMT-B.
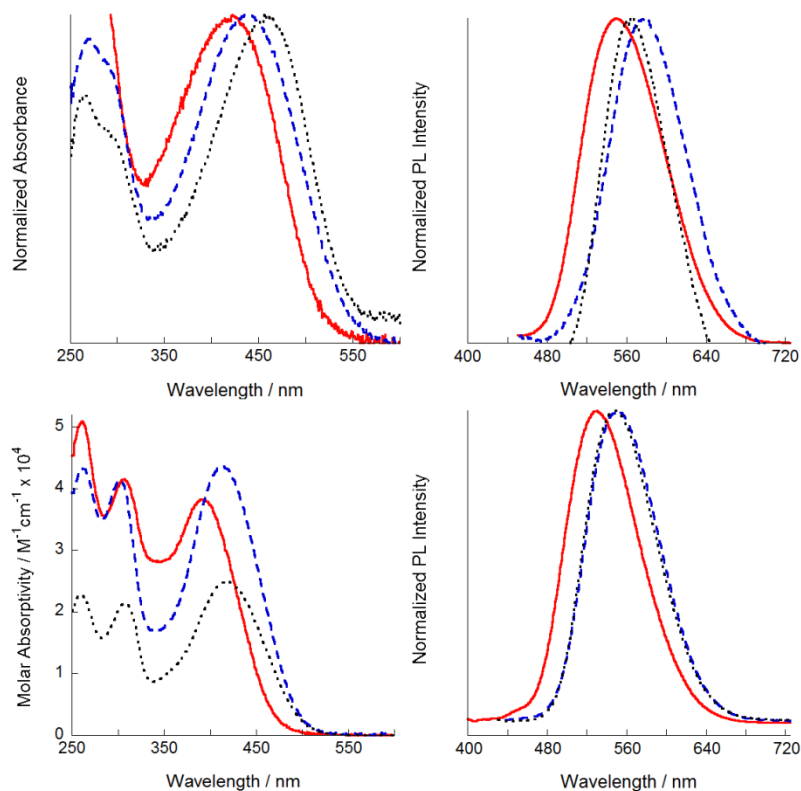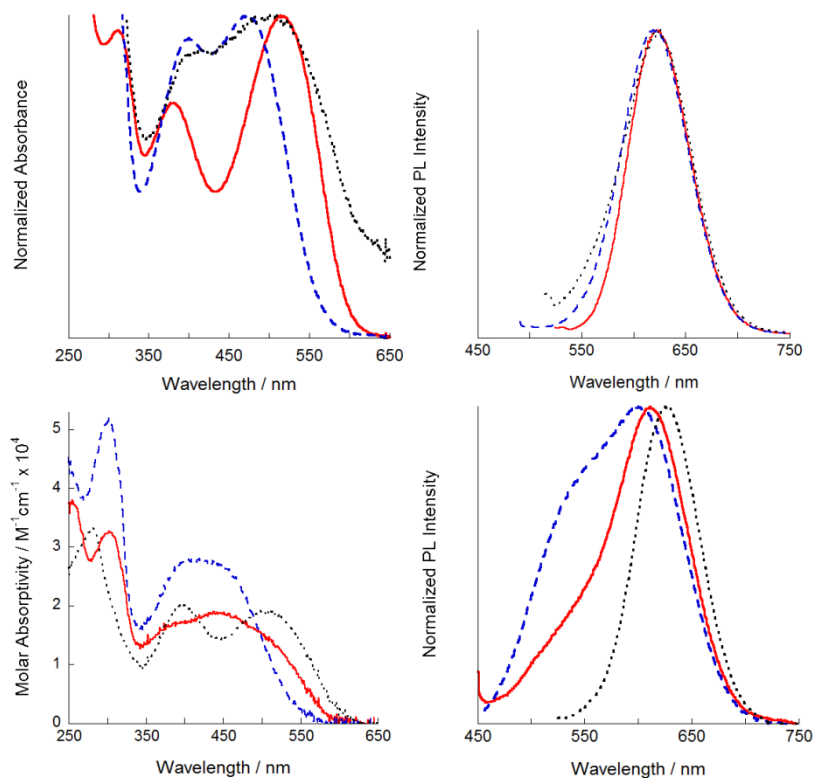
Figure 2.9. UV-Vis (left) and photoluminescence (right) data for the PTMT-B (top) and BTMTB (bottom) series. Polymer absorption profiles are normalized relative to the lowest energy maxima. Excitation for each polymer occurred at the λ_{max} of the individual polymers. Tail In (red,−), Tail Out (blue, ---), No Tail (black, ···).

The BTMTB models show similar absorption trends to the respective PTMT-B polymers. Although the multiple features in the absorption profile makes it difficult to pick definitive absorption maxima, the onset difference in this model series clearly shows the Tail In configuration is red-shifted 16 nm from the onset of the Tail Out. This differs from the TTMTT series where the terminal aromatic rings could adopt a conformation that contributed to the delocalized electronic system without inducing steric strain. The size and bond angles of benzothiadiazole restrict the degree to which the terminal rings can adopt coplanar structures, resulting in the Tail In model having a lower energy onset of absorption. Thus,

the hexyl-annulene interactions may be more amenable to coplanar conformations than hexyl-benzothiadiazole interactions.

In an effort to study even more broadly absorbing, low-bandgap polymers, the PTMT-DPP series was designed and synthesized. The PTMT-DPP series shows an interesting absorption trend not yet demonstrated in the other polymer and oligomeric model systems reported here (Figure 2.10). The lowest energy absorption maxima and onsets of all three polymers in the series are essentially identical. This is likely due to the domination of the low energy portion of the spectrum by a charge transfer band resulting from the stronger donor-acceptor nature of the DPP-containing polymers. Although the molecular weights are very small for the DPP-containing polymers, they should be of sufficient length to accommodate the inherent ECL. Prior work with carbazole-DPP alternating copolymers has shown that there is very little optical variation (λ_{max} ranging from 630 to 642 nm in dilute $CHCl_3$ solutions) arising from molecular weight differences (between 4,000 and 30,000 g/mol) even with the inclusion of the stronger carbazole electron donor unit.[50] There are interesting features at higher energies that reveal a trend similar to that of the PTMT-T series. The local maxima occur at 403 nm, 416 nm, and 434 nm for the Tail In, Tail Out, and No Tail polymers respectively. The PTMT-T and PTMT-DPP series have a similar portion of repeat unit that could influence the high energy section of the spectrum. The reasoning for this trend is similar to the reasoning for the PTMT-T series as well: because there is a 2,5-disubstituted thiophene adjacent to the hexyl-substituted thiophenes of the TMT core, the Tail Out configuration has the freedom to adopt a planar conformation without the restricting influence of a directly adjacent larger aromatic group. The PTMT-DPP series is not photoluminescent.
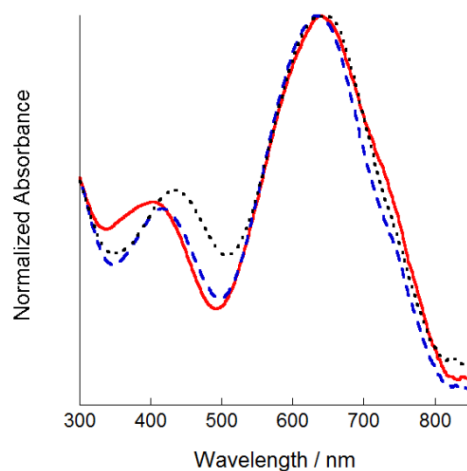
Figure 2.10. Absorption spectra of PTMT-DPP series. Polymer absorption profiles are normalized relative to the lowest energy maxima. Tail In (red,—), Tail Out (blue, ---), No Tail (black, ⋯).

In order to compare the current work to previous M10A-naphthalene studies, we synthesized a series of naphthalene-based small molecules (1,5-bis(thiophen-2-yl)-naphthalene and 3- or 4-hexylthiophen-2-yl derivatives) to determine if the spectroscopic trends were consistent with the TMT series (Figure 2.11). There is a smaller spread in λ_{max} values between the TMT Tail In and No Tail compounds (10 nm) relative to the related naphthalene molecules shown below (16 nm). Furthermore, there is a larger difference in Stokes' shift in the same molecules relative to the TMT (ca. 30 nm vs. 3 nm!). This indicates that the sterics of the hexyl vs. protio are more pronounced with the planar aromatic relative to the curved annulene.
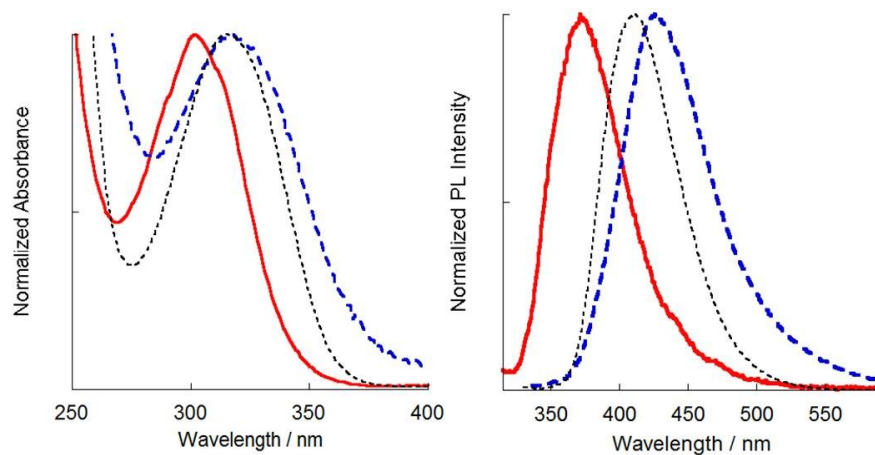
Figure 2.11. Absorption and PL spectra of TNT series. Absorption and PL profiles are normalized relative to the lowest energy maxima. Tail In (red,−), Tail Out (blue, ---), No Tail (black, ⋯).

Table 2.2. UV-Vis and photoluminescence data for polymers and molecular models.

Series / Orientation		λ_{max} (nm)	Onset (nm)	PL_{max} (nm)	Stokes' Shift (nm)
PTMT	Tail In	430	520	546	116
	Tail Out	418	513	551	133
	No Tail	468	540	601	133
PTMT-T	Tail In	422	540	546	124
	Tail Out	435	575	572	137
	No Tail	455	550	560	105
PTMT-B	Tail In	512	595	622	110
	Tail Out	478	580	619	141
	No Tail	520	610	621	101
PTMT-DPP	Tail In	637	810	---	---
	Tail Out	636	810	---	---
	No Tail	644	803	---	---
TMT	Tail In	365	438	499	134
	Tail Out	383	460	571	188
	No Tail	375	467	512	137
TTMTT	Tail In	389	490	530	141
	Tail Out	414	511	549	135
	No Tail	417	510	550	133
BTMTB	Tail In	446	576	611	165
	Tail Out	425	560	599	174
	No Tail	509	598	627	118

All spectra recorded in chloroform at ambient temperature. Onset was determined to be the wavelength at which the absorption reached 5% above the baseline.

Each of the polymer and small molecule systems was studied by cyclic voltammetry (CV) to determine the HOMO energy. After measurement of the onset of oxidation and calculation of the HOMO level (using Fc/Fc$^+$ as an external reference), the previously measured optical bandgap could be applied to obtain the LUMO energy. The general trend extracted from the data that across all polymers and molecular models, the Tail Out systems have an earlier onset of oxidation than do the Tail In of similar composition. The difference between them is relatively small, however and may be an artifact of the complex interplay of surface effects, electrolyte interactions, solution capacitance, etc. that can influence solution cyclic voltammetry. What seems to be a bigger difference than the subtle changes in the HOMO level is the change in the LUMO for each polymer and small molecule series (except the PTMT-T series). Attempts to perform cathodic CV did not yield useful results, despite the electron-accepting nature of the DPP subunit.
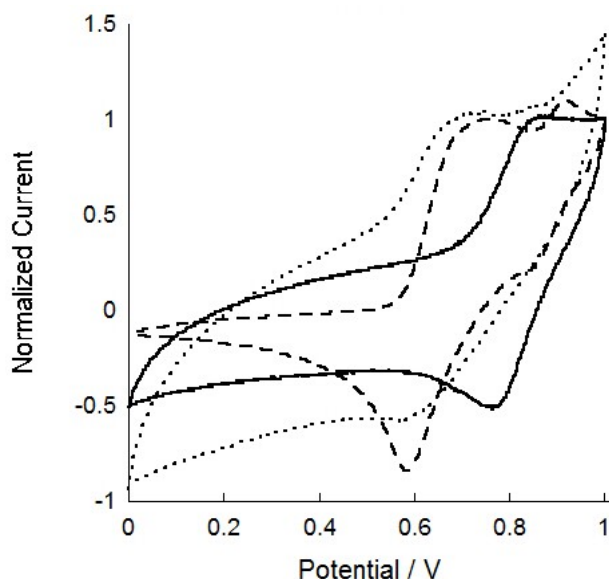
Figure 2.12. Cyclic voltammetry of the PTMT series (potential vs Ag/Ag$^+$). Tail In (—), Tail Out (---), No Tail (•••).
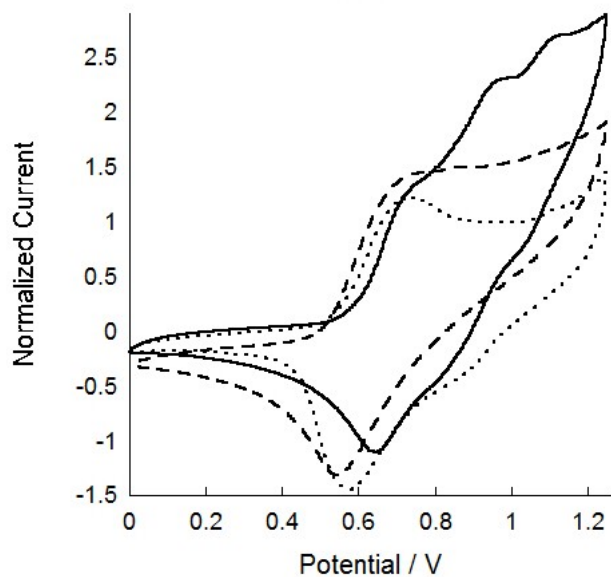
Figure 2.13. Cyclic voltammetry of the PTMT-T series (potential vs Ag/Ag$^+$). Tail In (—), Tail Out (---), No Tail (•••).
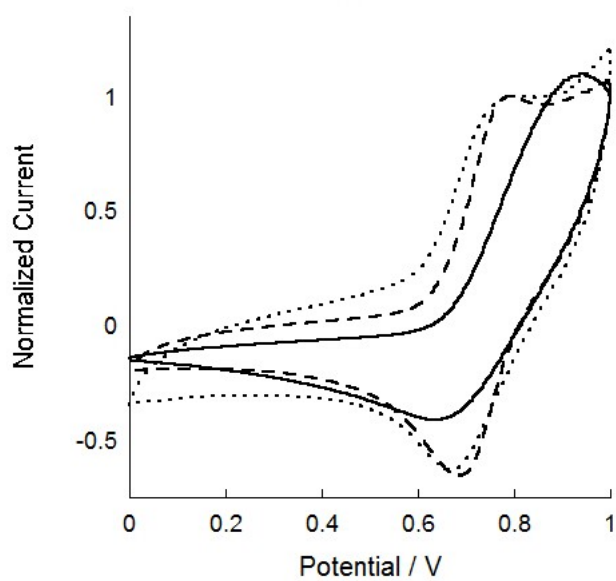
Figure 2.14. Cyclic voltammetry of the PTMT-B series (potential vs Ag/Ag$^+$). Tail In (—), Tail Out (---), No Tail (•••).
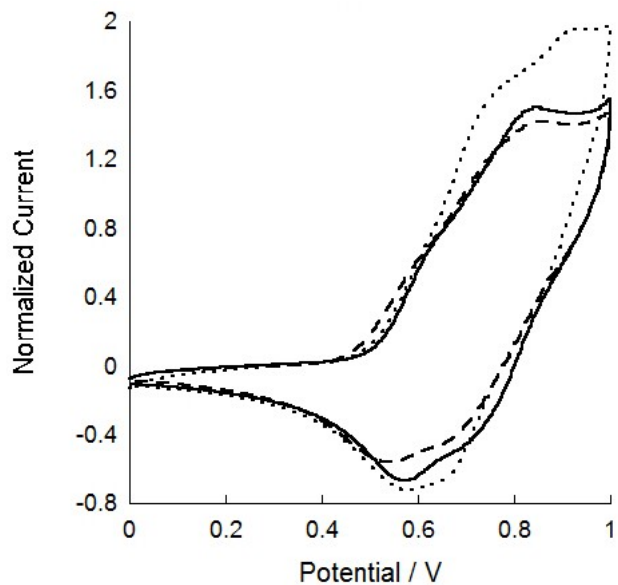
Figure 2.15. Cyclic voltammetry of the PTMT-DPP series (potential vs Ag/Ag$^+$). Tail In (—), Tail Out (---), No Tail (•••).
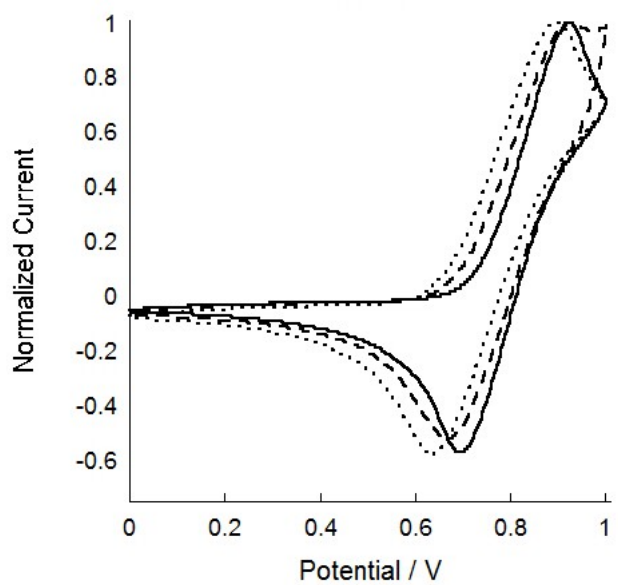
Figure 2.16. Cyclic voltammetry of the TTMTT series (potential vs Ag/Ag$^+$). Tail In (—), Tail Out (---), No Tail (•••).
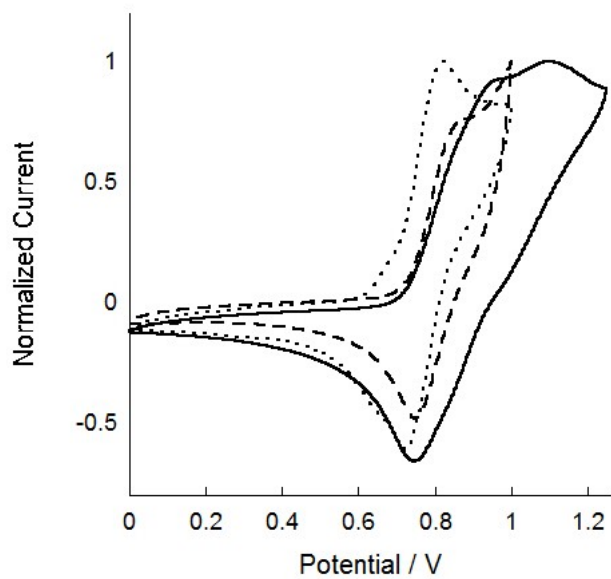
Figure 2.17. Cyclic voltammetry of the BTMTB series (potential vs Ag/Ag$^+$). Tail In (—), Tail Out (---), No Tail (•••).

Table 2.3. Electrochemical data for all polymer and small molecule systems was measured by cyclic voltammetry, and the HOMO level is reported from vacuum using Fc/Fc$^+$ as an external standard.[51] The HOMO energy and the optical bandgap (E_g) were used to calculate the LUMO level.

Series / Orientation		$E_{1/2}$ (mV)	Onset (mV)	HOMO (eV)	LUMO (eV)	E_g (eV)
PTMT	Tail In	812	670	-5.22	-2.83	2.39
	Tail Out	667	540	-5.09	-2.67	2.42
	No Tail	635	540	-5.09	-2.79	2.30
PTMT-T	Tail In	687	551	-5.09	-2.80	2.29
	Tail Out	632	474	-5.01	-2.86	2.15
	No Tail	617	495	-5.03	-2.77	2.26
PTMT-B	Tail In	786	650	-5.20	-3.11	2.09
	Tail Out	739	620	-5.17	-3.03	2.14
	No Tail	742	620	-5.17	-3.14	2.03
PTMT-DPP	Tail In	705	490	-4.98	-3.45	1.53
	Tail Out	696	460	-4.95	-3.42	1.53
	No Tail	663	490	-4.98	-3.44	1.54
TTMTT	Tail In	808	678	-5.18	-2.65	2.53
	Tail Out	811	649	-5.15	-2.73	2.42
	No Tail	796	664	-5.16	-2.73	2.43
BTMTB	Tail In	925	771	-5.27	-3.12	2.15
	Tail Out	875	718	-5.22	-3.01	2.21
	No Tail	773	661	-5.60	-3.53	2.07

X-ray diffraction analysis was used to determine if conjugated polymers containing 1,6-methano[10]annulene would form disordered aggregates when subjected to standard solution processing conditions. These conditions included dropcast films of polymers and blends of electron-donor polymers and electron-accepting fullerenes to simulate common bulk heterojunction organic photovoltaic device compositions (BHJ-OPV).[52] Films of P3HT,

each previously described polymer, and a PTMTB:PCBM blend (1:1 by weight) as a prototypical BHJ-OPV composition were dropcast from 5 mg/mL (10 mg/mL for the polymer:fullerene blend) $CHCl_3$ solutions onto glass substrates that had been treated with a thin layer of PEDOT:PSS to allow proper solvent wetting and film formation. P3HT (a well established crystalline organic semiconducting polymer[53]) showed a diffraction peak at around $2\theta = 5°$, while the other polymers and the blend showed no diffraction. The lack of ordered aggregates in the polymer:fullerene blend may make these interesting targets for further OPV research. Excessive phase segregation is a known issue in bulk heterojunction photovoltaics and M10A-containing polymers may help to prevent or slow the kinetics of polymer phase segregation while being able to interact with domains of crystalline curved PCBM molecular surfaces.
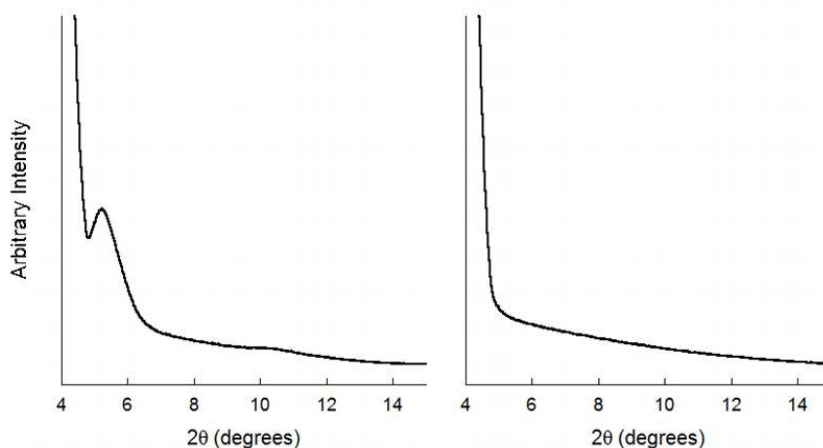
Figure 2.18. X-ray diffractograms of annealed films of P3HT (left), Tail In PTMT-B (right).

Thin films were prepared in the same manner for UV-Vis analysis, but were spin-coated onto glass-PEDOT:PSS substrates to yield films suitable for absorption analysis. The polymer films showed very slightly broadened UV-visible absorption traces relative to their solution spectra, indicating similar amounts of intermolecular interactions in the solid state and in solution. There was a notable amount of scattering in many of the thin film spectra, so

it is possible that unordered aggregates are present in the annealed solid state. We speculate that the curved and racemic nature of the annulene unit in these polymers effectively suppresses π-π interactions or other specific types of polymer aggregation.

Tail Out and No Tail PTMT-DPP were tested as p-type semiconducting materials using bottom-gate top-contact field-effect transistors (OFET).[54] The devices were prepared and tested under ambient atmospheric conditions using heavily n-doped Si wafers with 100nm thermally grown native oxide. As shown in Figure 2.19, the No Tail and Tail Out PTMT-DPP both performed as p-type semiconductors, but did not show n-type behavior despite the presence of the commonly ambipolar diketopyrrolopyrrole-co-thiophene motif. No Tail PTMT-DPP had a hole mobility of 1.44×10^{-4} ($\pm 0.17 \times 10^{-4}$) cm^2/Vs and a threshold voltage of -24 V. Tail Out PTMT-DPP had a hole mobility of 1.21×10^{-4} ($\pm 0.09 \times 10^{-4}$) cm^2/Vs and a threshold voltage of -29 V. These mobility values are lower than seen for semicrystalline DPP-containing polymers, but are comparable to disordered polymeric systems reported in the literature (ca. 10^{-3}-10^{-4} cm^2/Vs). [55,56,57]
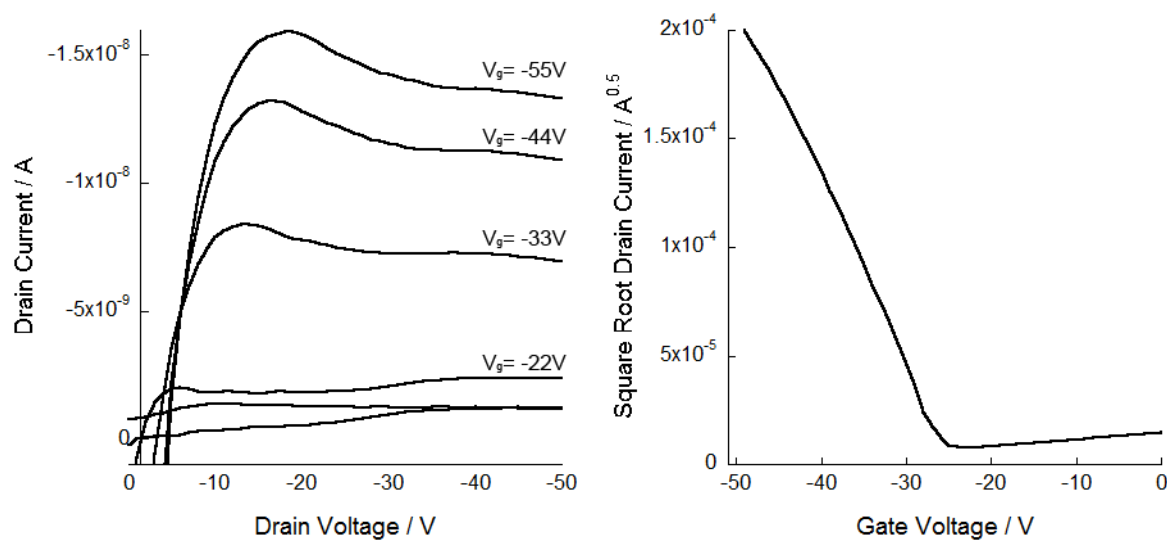
Figure 2.19. The transistor characteristics of Tail Out PTMT-DPP are shown in plots of I_d vs. I_v (left) and $I_d^{0.5}$ vs. V_g (right).

In conclusion, four polymeric and two small molecule systems based on 1,6-methano[10]annulene were synthesized, with each system consisting of three different solubilizing side-chain arrangements: Tail In, Tail Out, and No Tail regioisomers. The polymer and oligomer families were designed to probe the reduction of torsional strain granted to nearby solubilizing alkyl chains by the curved geometry of the annulene, the extent of which was characterized by UV-visible and photoluminescence spectroscopy, as well as electrochemistry. It was determined that 1,6-methano[10]annulene –when incorporated into certain polymeric or oligomeric materials-does grant a degree of steric relief that results in a longer effective conjugation length. The degree to which the conjugation is extended depends on the particular aromatic rings in the polymer, and the placement of any solubilizing alkyl chains. For the PTMT, PTMT-B, and BTMTB series, 1,6-methano[10]annulene was found to grant a certain amount of steric relief when the hexyl chain was directed towards the annulene instead of towards another aromatic group. For the PTMT-T, PTMT-DPP, and TTMTT systems, the opposite effect was found due to the relatively small steric demands of the 2,5-thienyl group (2-thienyl in TTMTT series). The low

energy regions of the PTMT-DPP absorption spectra were dominated by the strongly absorbing DPP chromophores and their associated charge transfer bands. Cyclic voltammetry revealed that the polymers and small molecules maintain relatively similar HOMO energy levels. In addition to these electronic subtleties arising from torsional considerations, the polymers as thin films, including a PTMTB:PCBM blend, were all found to be disordered and possibly amorphous by XRD after drop casting and annealing. P-type field-effect transistors were prepared with No Tail and Tail Out PTMT-DPP and showed comparable mobilities and threshold values to other disordered polymeric systems operating under ambient conditions. The spectroscopic and device data reveal that conjugated polymers containing 1,6-methano[10]annulene may be useful in applications requiring highly disordered conjugated polymers. Further research is warranted to determine the long term stability of polymer blends and the applicability of such curved aromatics for contemporary electronic devices.

Thermoelectric Devices Based on Amorphous 1,6-Methano[10]annulene π-Conjugated Polymers

The literature precedent for conducting polymer thermoelectrics is growing at a rapid pace, but there are few examples of amorphous conjugated polymers for such applications. Conjugated amorphous polymers are promising candidates for thermoelectrics because their highly disordered structure leads to low thermal conductivity relative to more crystalline materials (polymeric or otherwise).[58] In this section the utility of M10A based polymers for thermoelectric devices is demonstrated. M10A has been shown previously to increase effective conjugation length, lower oxidation potentials, reduce solution aggregation, and many polymers that incorporate it are highly disordered or amorphous.[59] A particular M10A-based polymer, Tail Out PTMT-DPP (Figure 2.20) yields hole mobilities of ca. 10^{-4} cm^2/Vs under ambient conditions, and is readily soluble (>10 mg/mL) in chlorinated solvents and

tetrahydrofuran. These factors make Tail Out PTMT-DPP a promising candidate for thermoelectric power generation applications.
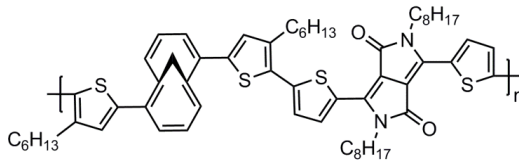
Figure 2.20. Structure of Tail Out PTMT-DPP where C_8H_{17} = 2-ethylhexyl

X-ray diffraction has been performed on annealed films of the polymer and no diffraction peaks were present, indicating a highly disordered system, yet the material still functioned as a thin film transistor semiconductor. Differential scanning calorimetry was performed on the polymer, confirming the amorphous nature of this material (Figure 2.21).
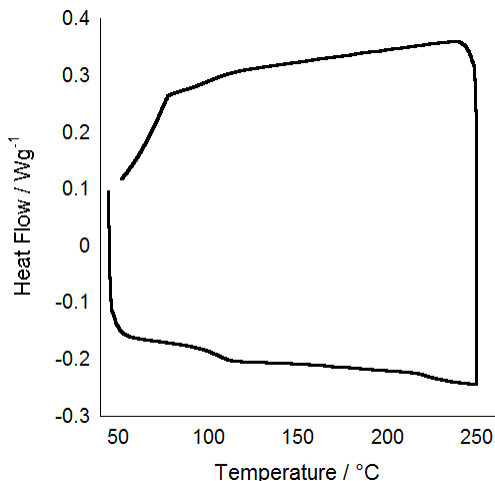
Figure 2.21. Differential scanning calorimetry shows the amorphous nature of Tail Out PTMT-DPP. This is the second scan from 45-250 °C.

Tail Out PTMT-DPP was blended with the oxidant 2,3,5,6-tetrafluoro-7,7,8,8-tetracyanoquinodimethane (F_4TCNQ) in varying weight percents of dopant and dropcast

61

onto prepared glass slides with bottom-contact gold electrodes. These devices were measured for their Seebeck coefficient and electrical conductivity in order to calculate PF. It was found that Tail Out PTMT-DPP:F_4TCNQ blends have high Seebeck coefficients but at the expense of relatively low conductivity (Figure 2.22). Doping levels ranged from 10% to 16% w/w. Below 10% the films were not suitably conductive and above 16% the films were generally of poor quality, possibly due to precipitation of polymer-dopant aggregates.
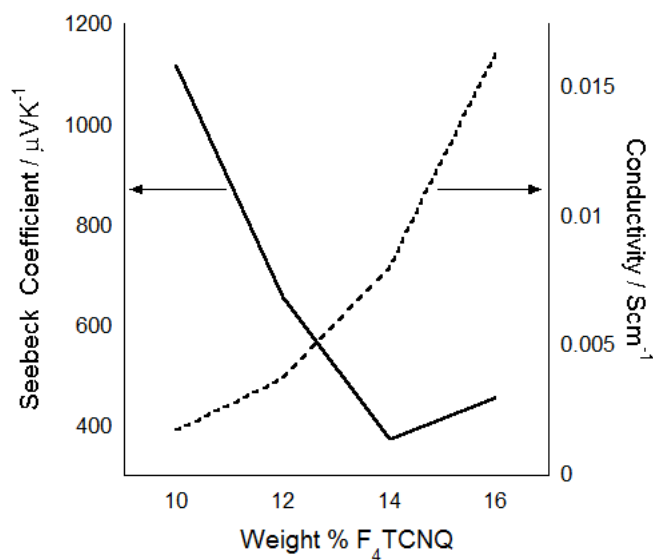
Figure 2.22. Shown is a plot of Seebeck coefficient versus doping percent for various blends of PTMTDPP and F_4TCNQ.

The power factor of Tail Out PTMT-DPP is limited by the low conductivity of the sample in this system (Figure 2.23). It is known for P3HT that the identity of the dopant can alter the thermoelectric properties of the material by several orders of magnitude.[5,11,60,61,62] PF values range from 0.006 to 26 μW/mK^2, electrical conductivites from 3.8x10^{-4} to 21 S/cm and Seebeck coefficients from 25 to 5400 μV/K by changing the dopant and optimizing for that particular set of conditions. Thus it is not entirely clear what effects each dopant may have on polymer morphology and electrical and thermal transport, so screening dopants and

concentrations is necessary to maximize the usefulness of a particular polymer for thermoelectric applications.
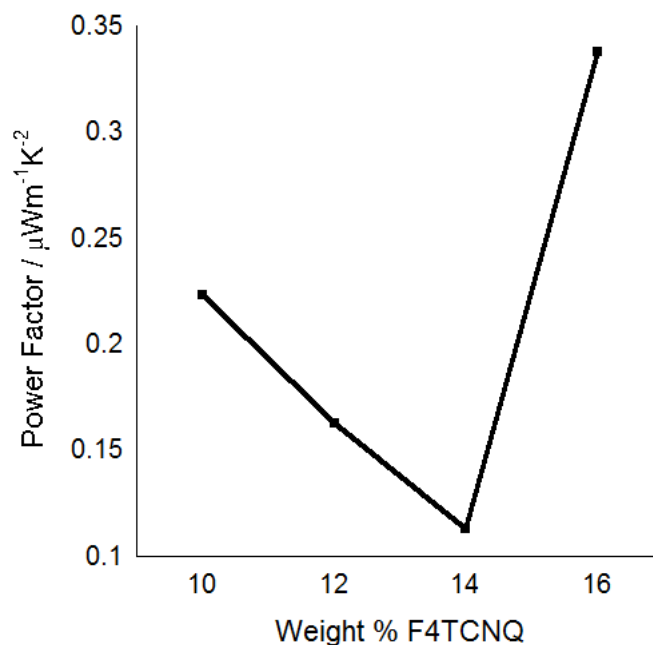
Figure 2.23. The power factor ($S^2\sigma$) of PTMTDPP-F$_4$TCNQ blends range from 0.11 to 0.34 μW/mK^2.

M10A-based polymer Tail Out PTMT-DPP was found to be a suitable candidate for thermoelectric devices due to its high Seebeck coefficient (1100 μV/K). However, the electrical conductivity of the polymer when doped with F$_4$TCNQ is relatively low (1.6x10^{-2} S/cm), resulting in power factor values of 0.34 μW/mK^2. Possible options for increasing the electrical conductivity and maintaining the high Seebeck values are changing the dopant or making a blend of polymer and a conducting nanostructure. As previously discussed, the reduction potential of the dopant (among other qualities) can drastically alter the conductivity of the material without detrimental effects on the Seebeck coefficient. Polymer nanocomposites have been recently reviewed and show great promise for maximizing thermoelectric figures of merit.[63] Despite low σ and PF values, the results obtained in this

study of Tail Out PTMT-DPP-F$_4$TCNQ blends may indicate the utility of amorphous conjugated polymers as an interesting candidate for thermoelectric devices.

Organic Photovoltaic Devices Based on 1,6-Methano[10]annulene-Benzothiadiazole Copolymers

No Tail and Tail In PTMT-B polymers were used in BHJ-OPV devices with PCBM (1:3 PTMT-B:PCBM w/w). The devices were fabricated by spin coating the polymer:fullerene blends onto ITO glass, annealing, and evaporating 7 mm^2 Al electrodes onto the bulk heterojunction material. The devices were rather inefficient, achieving PCEs of 0.013% and 0.020% for No Tail and Tail In PTMT-B, respectively under AM 1.5G simulated solar illumination conditions. Tail In PTMT-B is noticeably more soluble than the No Tail polymer, so solubility-based morphological differences may explain the lower PCE for No Tail relative to Tail In. The fill factors of the polymers were 0.25 and 0.26 for No Tail and Tail In, respectively, which are also quite poor when compared to contemporary polymer:fullerene BHJ-OPVs. One explanation for this is the low open circuit voltages of 0.44 V and 0.28 V and low short circuit currents of 8.2x10^{-6} A and 1.9x10^{-5} A for No Tail and Tail In, respectively. These low values are likely due to a host of factors: contact resistance between polymer and metal electrode, poor surface morphology at polymer:electrode interfaces, poor polymer morphology in the bulk film, among other issues. Ultimately, these particular polymers make for poor solar cells under these relatively standard conditions. This may be due to the amorphous nature of the polymers resulting in poor morphology, or the annulene-fullerene interactions may play a role in lowering performance by allowing facile geminate charge recombination. Further characterization of the polymer:fullerene film morphology by AFM, X-ray diffraction, or other techniques is needed to determine the limiting factors in these materials.
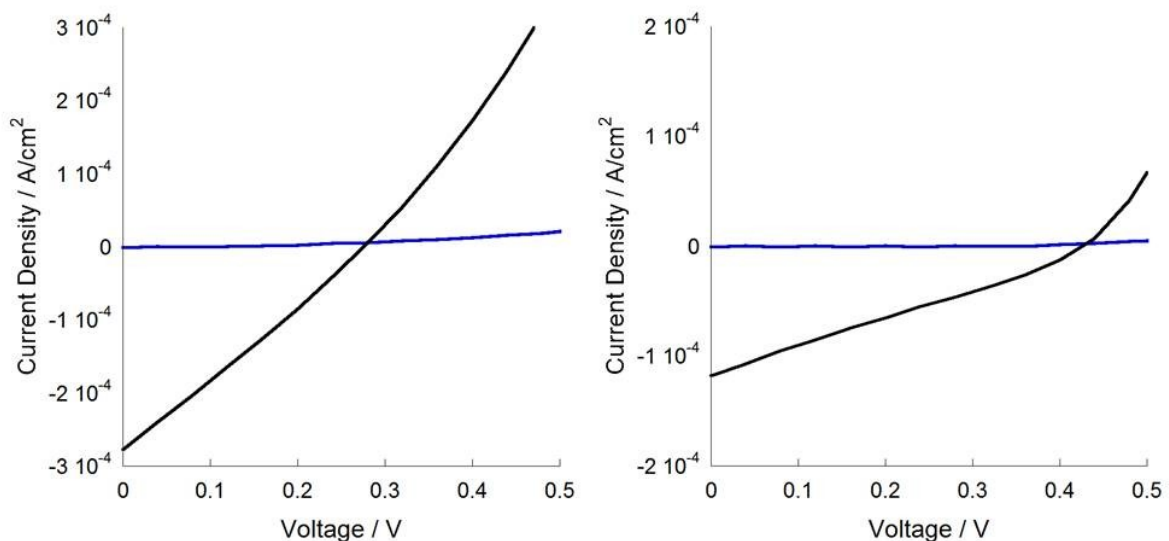
Figure 2.24. Current density versus voltage plots for Tail In (left) and No Tail (right) PTMT-B, under AM 1.5G illumination (black) and in the dark (blue).

Experimental

General Synthetic Methods:

All column chromatography solvents were distilled technical grade. All palladium and nickel catalysts were obtained from Strem Chemicals and used as received. 2,2'-bipyridyl, 2-bromothiophene, 2-tributylstannylthiophene, *n*-butyllithium, toluene, and DMF were obtained from Sigma Aldrich and used as received, except for toluene and DMF, which were dried over 4Å molecular sieves and sparged for 0.5-1 h with dry N_2. *N*-bromosuccinimide (NBS) was obtained from Sigma Aldrich and was recrystallized from water before use. 1,5-cyclooctadiene (COD) was obtained from JT Baker Chemicals and distilled prior to use. 1,6-methano[10]annulene,[64] 2,7-dibromo-1,6-methano[10]annulene,[65] No Tail TMT,[66] 4,7-dibromo-2,1,3-benzothiadiazole,[67] and 3,6-bis(2-bromo-5-thienyl)-2,5-di(2-ethylhexyl)pyrrolo[3,4-*c*]-pyrrole-1,4-dione[68] were prepared according to literature procedures.

NMR Spectroscopy:

All ^{1}H and ^{13}C NMR spectra were recorded in CDCl$_3$ or o-dichlorobenzene (o-DCB) (Cambride Isotope Laboratories) on a Bruker Avance 400 MHz instrument, and data were collected with either Bruker Topspin V.1.3 or 2.1, unless otherwise noted. Data was processed with either Topspin V.2.1 or SpinWorks V.3.1.7.0 (2010, University of Manitoba). All ^{1}H spectra were calibrated against either residual protio-chloroform (7.26 ppm) or TMS (0.00 ppm) in the deuterated solvent. ^{13}C spectra were calibrated against the CDCl$_3$ triplet (77 ppm).

Gel Permeation Chromatography:

Polymer molecular weight analysis was carried out by gel permeation chromatography (GPC) on a Waters 1515 Isocratic HPLC equipped with two 5 mm Waters Styragel HR4 and HR3 columns (300 mm x 7.8 mm), connected in series with increasing pore size, and a Waters 2489 UV-Visible Detector. Polymers are dissolved in HPLC grade tetrahydrofuran (0.5-1 mg/mL), and filtered through a 0.2 mm PVDF filter. GPC was performed with submicron filtered HPLC grade THF (Fisher) eluent at 1 ml/min. The apparent molecular weight and polydispersity (PDI) was determined from a calibration curve based on linear polystyrene standards.

UV-Vis and Photoluminescence:

UV-Vis spectra were taken on a Varian Cary 50 Bio UV-Vis spectrometer in CHCl$_3$ (spectroscopic grade, Sigma Aldrich) at ambient temperature using quartz cuvettes, unless otherwise noted. Solutions were spectroscopically dilute (ca. 10^{-6} M) and had optical densities under 0.2. The data were collected and analyzed using Cary WinUV V.3.00(182) software.

All fluorescence spectra were taken on a Photon Technology International fluorimeter fitted with a PTI 814 PMT for detection and PTI excitation and emission monochrometers. Spectra were recorded in $CHCl_3$ (spectroscopic grade, Sigma Aldrich) at ambient temperature, using quartz cuvettes, unless otherwise noted. Excitation occurred at the lowest energy absorption maximum. PTI FeliX32 V.1.2(Build 56) was used for data processing.

Thin films were prepared by cleaning glass slides (Fisher) by sonication for 5 min each in Alconox solution, acetone, and isopropanol. Residual solvent was removed by blowing dry with nitrogen. The cleaned slides were treated with PEDOT:PSS (Sigma Aldrich, high conductivity grade) and spun at 2000 RPM for 90 s, then annealed at 90°C for one hour and allowed to cool to ambient temperature. Polymer solutions (1mg/mL in o-dichlorobenzene) were spun onto the treated slides at 1200 RPM for 90 s and then annealed again at 90°C for 15 min. A slide with only PEDOT:PSS was used as a 100% transmittance background sample. The samples were then placed in the beam path and their absorption spectra recorded.

Electrochemistry:

All electrochemistry was performed on an Autolab potentiostat with a 2 mm Pt button working electrode, Pt wire counter electrode, and Ag/AgCl reference electrode, in either MeCN or DCM (spectroscopic grade, Sigma Aldrich) with 0.1 M tetrabutylammonium hexafluorophosphate (TBAP) as the electrolyte. A ferrocene/ferrocenium external standard was used for all measurements. TBAP and ferrocene were obtained from Sigma Aldrich, and the TBAP was recrystallized from anhydrous ethanol prior to use. Electrolyte solutions were stored over 4Å molecular sieves. Data was collected and processed using GPES software.

X-Ray Diffraction:

5 mg/mL solutions in $CHCl_3$ of each polymer (5 mg/mL each of Tail In PTMTB and $PC_{61}BM$ for the bulk heterojunction film) were prepared by heating and sonicating the mixture extensively. Glass slides (Fisher premium) were sonicated for 5 min each in DI H_2O, isopropanol, and acetone (all spectroscopic grade), before drying with dry nitrogen. A thin layer of PEDOT:PSS (Sigma Aldrich, high conductivity grade) was spin-coated onto the clean substrates at 2500 RPM for 90 s and annealed for 1 h at 90°C before being allowed to cool. The films were dropcast on and annealed at 90°C for 3 min. A Cu Kα source and PIXcel-3D detector were used to effect a 2θ scan with a set omega at 0.3°, a scan range of 1.996°-25.000°, step size of 0.0131303°, and a scan speed of 0.016726 degrees/second.

Transistor Fabrication:

Bottom gate-top contact transistors were fabricated on highly-doped n-type Si wafers (SI-Tech, Process Solutions) with a thermally-grown 100 nm oxide layer. All wafers were sonicated in warm acetone and IPA, and dried in a stream of dry nitrogen. Active layers of 1,6-methano[10]annulene-containing polymers were spin coated (Laurell Technologies Corporation) at 1500 rpm for 90 s, and annealed at 90° C for 5 min. Wafers were loaded overnight for thermal evaporation of 125 nm Au electrodes (Edwards Auto 306) through a shadow mask with W/L ratio of 32, where W = 8 mm and L = 250 µm. Si gates were scratched with a diamond scribe and contacted with Ga-In eutectic (Sigma-Aldrich). All electrical characterization was performed on an Agilent 4155C Semiconductor Parameter Analyzer using a medium integration time (16.7 ms), under ambient fluorescent lighting conditions, in air. Devices were probed with low-resistance probes from Micromanipulator, onto which small (~100 µm) drops of Ga-In eutectic were placed for contacting source and drain electrodes.

Thermoelectric Device Fabrication and Testing:

Three 50nm Au electrodes were evaporated on the glass substrates, leaving ~0.5 cm bare glass between each electrode, which ran the length of the slide. Novec fluoropolymer was applied to create individual sections measuring ~0.5cm x ~0.75cm, such that a dropcast film would cover the bare channel and contact the Au electrodes on either side. 14-16 devices were prepared on each slide. Polymer-dopant blends were made by dissolving each in a suitable solvent ($CHCl_3$ or THF) at concentrations of 10 mg/mL and 1 mg/mL, respectively. Varying ratios of polymer:dopant were then pipetted into a vial and swirled by hand for 30 s to mix. The blends were then dropcast under ambient conditions onto prepared substrates and allowed to dry. Once dry, the substrates were placed in a vacuum desiccator overnight (>12h) to remove any residual solvent. The Novec and underlying electrode between devices were removed to isolate the individual devices, which were then measured. Devices were tested according to published procedures.[69]

General procedure for TMT and TNT synthesis:

Dihaloarene (1.0 equiv), tributylstannyl thiophene (2.2 equiv), and $(PPh_3)_2PdCl_2$ (0.05 equiv) were added to a flame dried Schlenk flask charged with a magnetic stir bar and evacuated/refilled with dry N_2 three times. 20 mL dry, degassed toluene was added via syringe and the solution was stirred and heated to 105°C for 15 h. At this point, the solution was allowed to cool while stirring and then poured into a rapidly stirring mixture of diethyl ether and 1M KF (aq) (50 mL of each). This suspension was stirred for 5-10 min and vacuum filtered. 50 mL of the KF solution was added and stirred for 5 more min before vacuum filtration. The organic layer was separated and dried with $MgSO_4$, the solvent was removed by rotary evaporation, and the crude solid dried under high vacuum. The crude material was purified by column chromatography on SiO_2 with hexanes as the eluent.

[Tail Out TMT]: 2,7-Bis(4-hexyl-2-thienyl)-1,6-methano[10]annulene

Prepared according to general TMT synthesis procedure using 2,7-dibromo-1,6-methano[10]annulene (0.5003 g, 1.6667 mmol), 5-tributylstannyl-3-hexylthiophene (1.9121 g, 4.1809 mmol), and Pd(PPh$_3$)$_2$Cl$_2$ (49.6 mg, 0.0706 mmol). The product was isolated as a fluorescent yellow oil (0.6318 g, 1.331 mmol, 80%). ^{1}H NMR (400 MHz, CDCl$_3$) δ: 7.86 (d, J = 9 Hz, 2H), 7.40 (d, J = 9 Hz, 2H), 7.32 (s, 2H), 7.08 (t, J = 9 Hz, 2H), 6.94, (s, 2H), 2.65 (t, 4H, J = 6.0 Hz), 1.68 (m, 4H), 1.34 (m, 12H), 0.90 (t, 6H, J = 6.0 Hz), -0.08 (s, 2H); ^{13}C NMR (100 MHz, CDCl$_3$) δ: 144.2, 142.8, 135.4, 130.0, 129.0, 128.0, 121.4, 117.9, 36.0, 31.8, 30.7, 30.6, 29.1, 22.7, 14.2. UV-Vis (CHCl$_3$): λ_{max} 289 nm (ε = 30100 M^{-1}cm^{-1}), 383 nm (ε = 20900 M^{-1}cm^{-1}). HRMS (EI) Calcd for C$_{31}$H$_{38}$S$_2$: 474.2417 [M$^{+\bullet}$], Found m/z= 474.2415.

[Tail In TMT]: 2,7-Bis(3-hexyl-2-thienyl)-1,6-methano[10]annulene

Prepared according to general TMT synthesis procedure using 2,7-dibromo-1,6-methano[10]annulene (0.5007 g, 1.6667 mmol), 2-tributylstannyl-3-hexylthiophene (1.6851 g, 3.6846 mmol), and Pd(PPh$_3$)$_2$Cl$_2$ (49.8 mg, 0.0708 mmol). The product was isolated as a fluorescent yellow oil (0.5212 g, 1.0978 mmol, 66%). ^{1}H NMR (400 MHz, CDCl$_3$) δ: 7.29 (d, J = 10 Hz, 2H), 7.17 (d, J = 5 Hz, 2H), 7.13 (d, J = 10 Hz, 2H), 6.96 (m, J = 5, 10 Hz, 4H), 2.90 (m, 2H) 2.74 (m, 2H), 1.40 (m, 4H), 1.07 (m, 12H), 0.71 (t, J = 6 Hz, 6H), -0.15 (s, 2H); ^{13}C NMR (100 MHz, CDCl$_3$): δ 140.6, 136.2, 133.8, 129.4, 128.8, 126.5, 124.7, 117.0, 34.9, 31.2, 30.2, 28.7, 22.2, 13.8. UV-Vis (CHCl$_3$): λ_{max} 285 nm (ε = 35800 M^{-1}cm^{-1}), 365 nm (ε = 18000 M^{-1}cm^{-1}). HRMS (EI) Calcd for C$_{31}$H$_{38}$S$_2$: 474.2415 [M$^{+\bullet}$] Found m/z= 474.2402

Tail Out TNT: 1,5-Bis(4-hexyl-2-thienyl)-naphthalene

Prepared according to general TMT/TNT synthesis procedure using 1,5-diiodonaphthalene (100.0 mg, 0.2632 mmol), 2-tributylstannyl-4-hexylthiophene (264.8 mg, 0.5791 mmol), and

Pd(PPh$_3$)$_4$ (12.2 mg, 0.0105 mmol). The product was isolated as a fluorescent yellow oil (77.6 mg, 0.168 mmol, 64%).^{1}H NMR (400 MHz, CDCl$_3$) δ: 7.98 (m, 2H), 7.67 (m, 2H), 7.51 (m, 2H), 7.17 (m, 2H), 7.00 (m, 2H), 2.40 (m, 4H), 1.50 (m, 4H), 1.05 (m, 12H), 0.72 (m, 6H).

Tail In TNT: 1,5-Bis(3-hexyl-2-thienyl)-naphthalene

Prepared according to general TMT/TNT synthesis procedure using 1,5-diiodonaphthalene (100.0 mg, 0.2632 mmol), 2-tributylstannyl-3-hexylthiophene (264.8 mg, 0.5791 mmol), and Pd(PPh$_3$)$_4$ (12.2 mg, 0.0105 mmol). The product was isolated as a fluorescent yellow oil (63.0 mg, 0.14 mmol, 52%). ^{1}H NMR (400 MHz, CDCl$_3$) δ: 8.10 (m, 2H), 7.74 (m, 2H), 7.59 (m, 2H), 7.12 (m, 2H), 7.05 (m, 2H), 2.32 (m, 4H), 1.43 (m, 4H), 1.13 (m, 12H), 0.77 (m, 6H).

No Tail TNT: 1,5-Di(2-thienyl)-naphthalene

Prepared according to general TMT/TNT synthesis procedure using 1,5-diiodonaphthalene (100.0 mg, 0.2632 mmol), 2-tributylstannylthiophene (216.1 mg, 0.5791 mmol), and Pd(PPh$_3$)$_4$ (12.2 mg, 0.0105 mmol). The product was isolated as a fluorescent yellow solid (56.9 mg, 0.195 mmol, 74%).^{1}H NMR (400 MHz, CDCl$_3$) δ: 8.22 (m, 2H), 7.59 (m, 2H), 7.48 (m, 2H), 7.44 (m, 2H), 7.25 (m, 2H), 7.19 (m, 2H).

 General procedure for bromination of TMTs:

TMT (0.80 mmol, 1.0 equiv) and NBS (1.69 mmol, 2.1 equiv) were added to a roundbottom flask charged with a stir bar. The flask was completely wrapped in aluminum foil to exclude light. Dichloromethane (5 mL) was added and flask vented by insertion of a needle through a septum in the neck of the flask. The reaction was stirred at ambient temperature for 2-3 d. The mixture was diluted with 20 mL hexanes and the organic layer washed with water (2x15

mL) and brine (1x15 mL) before the organic layer was dried with MgSO$_4$. The solvent was removed by rotary evaporation and the crude product placed under high vacuum. The crude material was purified by column chromatography on SiO$_2$, with hexanes as the eluent. Note: the dibromo- No Tail TMT was purified by recrystallization from boiling ethanol.

[Dibromo-Tail Out TMT]: 5', 5"-Dibromo-2,7-bis(4-hexyl-2-thienyl)-1,6-methano[10]annulene

Prepared according to the general TMT bromination procedure using 2,7-bis(4-hexyl-2-thienyl)-1,6-methano[10]annulene (0.2506 g, 0.2633 mmol), N-bromosuccinimide (0.0961 g, 0.5397 mmol), dichloromethane (7 mL). Column chromatography (silica/hexane) gave pure compound (0.2399 g, 0.3793 mmol, 72%). ^{1}H NMR (400 MHz, CDCl$_3$) δ: 7.82 (d, *J* = 8.8 Hz, 2H), 7.31 (d, *J* = 9.0 Hz, 2H), 7.14 (s, 2H), 7.07 (t, *J* = 9.0 Hz, 2H), 2.60 (t, *J* = 6.0 Hz, 4H), 1.64 (m, 4H), 1.34 (m, 12H), 0.90 (m, 6H), -0.013 (s, 2H). ^{13}C NMR (100 MHz, CDCl$_3$) δ: 142.9, 142.2, 134.3, 129.9, 128.2, 127.9, 126.9, 117.6, 109.8, 35.6, 31.5, 29.6, 29.5, 28.8, 22.4, 13.9. HR-MS (EI) Calcd for C$_{31}$H$_{36}$S$_2$Br$_2$: 634.0605 [M$^{+\bullet}$] Found *m/z*= 634.0605

[Dibromo-Tail In TMT]: 5', 5"-Dibromo-2,7-bis(3-hexyl-2-thienyl)-1,6-methano[10]annulene

Prepared according to the general TMT bromination procedure using 2,7-bis(3-hexyl-2-thienyl)-1,6-methano[10]annulene (0.4747 g, 0.9999 mmol), N-bromosuccinimide (0.3663 g, 2.0581 mmol), dichloromethane (10 mL). Column chromatography (silica/hexane) gave pure compound (0.4553 g, 0.7198 mmol, 72%). ^{1}H NMR (400 MHz, CDCl$_3$) δ: 7.39 (d, *J* = 8.7 Hz, 2H), 7.16 (d, *J* = 9.5 Hz, 2H), 7.03 (t, *J* = 9.1 Hz,2H), 6.99 (s, 2H), 2.85-2.65 (m, 4H), 1.51 (m, 4H), 1.14 (m, 12H), 0.79 (t, *J* = 6.0 Hz, 6H), -0.013 (s, 2H). ^{13}C NMR (100 MHz, CDCl$_3$) δ: 141.6, 138.2, 133.0, 132.0, 130.0, 129.3, 127.0, 117.5, 111.8, 34.9, 31.6, 30.4,

29.3, 28.9, 22.7, 14.0. HR-MS (EI) Calcd for $C_{31}H_{36}S_2Br_2$ [M$^+$]: 632.06015 Found m/z= 632.06047.

[Dibromo-No Tail TMT]: 5', 5"-Dibromo-2,7-bis(2-thienyl)-1,6-methano[10]annulene

Prepared according to the general TMT bromination procedure using 2,7-bis(2-thienyl)-1,6-methano[10]annulene (0.2504 g, 0.8160 mmol), N-bromosuccinimide (0.3061 g, 1.7199 mmol), dichloromethane (4 mL). Recrystallization from MeOH gave a pure solid product (0.1546 g, 0.3331 mmol, 41%). ^{1}H NMR (400 MHz, CDCl$_3$) δ: 7.81 (d, J = 8.6 Hz, 2H), 7.31 (d, J = 9.6 Hz, 2H), 7.18 (d, J = 3.9 Hz, 2H), 7.10-7.07 (m, 4H), -0.05 (s, 2H). ^{13}C NMR (100 MHz, CDCl$_3$) δ: 144.4, 133.9, 130.6, 130.0, 128.1, 127.5, 127.1, 117.5, 113.0, 35.5.

General procedure for bis(tributylstannyl)-TMT synthesis:

TMT (0.33 mmol, 1.0 equiv) was added to a flame dried Schlenk flask charged with a stir bar and evacuated/refilled with dry N$_2$ three times. Distilled THF (10 mL) was added and the solution stirred while cooling to -78°C in a dry ice/acetone bath for 20 min. N-Butyllithium solution (1.6 M, 0.50 mL, 2.2 equiv) was added dropwise, and the solution stirred for an hour while maintaining the temperature at -78°C. Tributyltin chloride (0.2 mL, 2.2 equiv) was added via syringe and the solution stirred at -78°C for one hour before removing the cooling bath and allowing the mixture to warm to room temperature overnight. The reaction was quenched with DI H$_2$O (10 mL) and extracted with dichloromethane (25mL). The organic layer was washed with water (3x15 mL) and brine (1x15 mL) before drying with MgSO$_4$. The solvent was removed by rotary evaporation, and the crude material placed under high vacuum. The crude product was carried on as is, using NMR integrations as estimates of purity for accurate additions in later reactions.

[Bis-stannyl Tail Out TMT]:

5', 5"-Bis(tributylstannyl)-2,7-bis(4-hexyl-2-thienyl)-1,6-methano[10]annulene

2,7-Bis(4-hexyl-2-thienyl)-1,6-methano[10]annulene   (.2492 g, 0.5249 mmol), n-butyllithium (0.85 mL, 1.62 M), tributyltin chloride (0.33 mL, 1.1058 mmol), THF (15 mL). The product was isolated as a crude yellow oil. The crude product showed a very clean aromatic ^{1}H NMR region, but contained excess tributyltin chloride which proved very difficult to remove. ^{1}H NMR (400 MHz, CDCl$_3$) δ: 7.87 (d, J = 8.8 Hz, 2H), 7.48 (s, 2H), 7.42 (d, J = 9.7 Hz,2H), 7.08 (t, J = 9.3 Hz, 2H), 2.61 (m, 4H), 1.75-1.50 (m, 16H), 1.35 (m, 24H), 1.14 (m, 8H), 0.91 (t, J = 6.0 Hz, 24H), -0.07 (s, 2H).

[Bis-stannyl Tail In TMT]:

5', 5"-Bis(tributylstannyl)-2,7-bis(3-hexyl-2-thienyl)-1,6-methano[10]annulene

 2,7-Bis(3-hexyl-2-thienyl)-1,6-methano[10]annulene (.2642 g, 0.5266 mmol), n-butyllithium (0.85 mL, 1.62 M), tributyltin chloride (0.33 mL, 1.1058 mmol), THF (15 mL). The product was isolated as a crude yellow oil. The crude product showed a very clean aromatic ^{1}H NMR region, but contained excess tributyltin chloride which proved very difficult to remove. ^{1}H NMR (400 MHz, CDCl$_3$) δ: 7.87 (d, J = 8.8 Hz, 2H), 7.50 (s, 2H), 7.42 (d, J = 9.7 Hz,2H), 7.08 (t, J = 9.3 Hz, 2H), 2.61 (m, 4H), 1.75-1.50 (m, 16H), 1.35 (m, 24H), 1.14 (m, 8H), 0.91 (t, J = 6.0 Hz, 24H), -0.07 (s, 2H).

[Bis-stannyl No Tail TMT]: 5', 5"-Bis(tributylstannyl)-2,7-bis(2-thienyl)-1,6-methano[10]annulene

2,7-Bis(2-thienyl)-1,6-methano[10]annulene   (.1002 g, 0.3263 mmol), n-butyllithium (0.52 mL, 1.62 M), tributyltin chloride (0.19 mL, 0.6820 mmol), THF (15 mL). The product was isolated as a crude yellow oil. The crude product showed a very clean aromatic ^{1}H NMR

region, but contained excess tributyltin chloride which proved very difficult to remove. ^{1}H NMR (400 MHz, CDCl$_3$) δ: 7.86 (d, J = 8.8 Hz, 2H), 7.50 (d, J = 8.0 Hz, 2H), 7.43 (d, J = 9.7 Hz,2H), 7.08 (t, J = 9.3 Hz, 2H), 1.62 (m, 12H), 1.36 (m, 12H), 1.14 (m, 12H), 0.91 (t, J = 6.0 Hz, 18H), -0.05 (s, 2H).

General procedure for Stille cross-coupling polymerization:

Aryl dibromide (0.5 mmol, 1.0 equiv.), aryl distannane (0.5 mmol, 1.0 equiv.), Pd(PPh$_3$)$_2$Cl$_2$ (0.025 mmol, 0.05 equiv), CsF (2.2 mmol, 4.4 equiv), and CuI (0.1 mmol, 0.2 equiv) are added to a flame dried Schlenk flask and evacuated/refilled with N$_2$ three times. Toluene that has been degassed with dry N$_2$ over 4Å sieves for 30 min is added to dibromide and distannane and magnetically stirred to dissolve. The solution is heated to 105°C and stirred for 1-5 d until the reaction mixture is allowed to cool and concentrated by rotary evaporation. The resulting crude solid is dissolved in CHCl$_3$ and precipitated into rapidly stirring room temperature MeOH. The precipitate is then washed with excess MeOH to remove monomer and catalyst.

 [Tail Out PTMT-B]: Prepared according to general Stille polymerization procedure.

5', 5"-Bis(tributylstannyl)-2,7-bis(4-hexyl-2-thienyl)-1,6-methano[10]annulene (0.3502, 0.3324 mmol), 4,7-dibromo-2,1,3-benzothiadiazole (0.0769g, 0.2618 mmol), Pd(PPh$_3$)$_4$ (0.0074g, 0.0105 mmol). ^{1}H NMR (400 MHz, CDCl$_3$) δ: 8.02 (m, br), 7.75 (s, br), 7.55 (m, br), 7.18 (m, br), 2.78 (m, br), 1.74 (m, br), 1.57 (s, br), 1.30 (m, br), 0.84 (m, br), 0.07 (s). GPC: M_w = 7743 g/mol, M_n = 3019 g/mol, PDI = 2.57, DP_w: 12.8. UV-Vis (CHCl$_3$): λ_{max} 480 nm, onset 600 nm.

[Tail In PTMT-B]: Prepared according to general Stille polymerization procedure.

5', 5"-Bis(tributylstannyl)-2,7-bis(3-hexyl-2-thienyl)-1,6-methano[10]annulene (0.3508g, 0.3325 mmol), 4,7-dibromo-2,1,3-benzothiadiazole (0.0772g, 0.2621 mmol), Pd(PPh$_3$)$_4$ (0.0073g, 0.0105 mmol). ^{1}H NMR (400 MHz, CDCl$_3$) δ: 8.12 (s, br), 7.89 (s, br), 7.54 (d, J = 8.4 Hz), 7.36 (d, J = 10.5 Hz), 7.14 (t, J = 9.1 Hz), 7.06 (m, br), 3.07 (m, br), 2.90 (m , br), 1.79-1.51 (m, br), 1.38-1.16 (m, br), 0.82 (m, br), 0.03 (s). GPC: M_w = 7822 g/mol, M_n = 3820 g/mol, PDI = 2.05, DP$_w$: 12.9 UV-Vis (CHCl$_3$): λ_{max} 523 nm, onset 630 nm.

[No Tail PTMT-B]: Prepared according to general Stille polymerization procedure.

5', 5"-Bis(tributylstannyl)-2,7-bis(2-thienyl)-1,6-methano[10]annulene (0.1101g, 0.1242 mmol), 4,7-dibromo-2,1,3-benzothiadiazole (0.0320g, 0.1089 mmol), Pd(PPh$_3$)$_4$ (0.0030g, 0.0049 mmol). ^{1}H NMR (400 MHz, o-DCB) δ: 8.21 (m, br), 7.96 (m, br), 7.60 (m, br), 7.23 (m, br), 3.15 (s, br), 2.37 (s, br), 1.30 (m, br), 0.92 (s, br), 0.08 (s, br) . GPC: Poor solubility prevents analysis using THF. UV-Vis (CHCl$_3$): λ_{max} 520 nm, onset 610 nm.

[Tail Out PTMT-T]: Prepared according to general Stille polymerization procedure.

5', 5"-Bibromo-2,7-bis(4-hexyl-2-thienyl)-1,6-methano[10]annulene (100.0 mg, 0.1581 mmol), 2,5-bis-tributylstannylthiophene (104.7 mg, .1581 mmol), PdCl$_2$(PPh$_3$)$_2$ (5.6 mg, 0.0079 mmol), 5 mL Toluene. Yielded 21.8 mg (59%) of an orange powder. ^{1}H NMR (400 MHz, CDCl$_3$) δ: 7.93-7.87 (m, br), 7.44-7.33 (m, br), 7.15-7.10 (m, br), 6.97 (s, Ar), 2.87 (m, br), 2.66 (m, br), 1.80-1.57 (m, br), 1.35 (s, br), 0.91 (m, br), -0.04 (s, CH$_2$). GPC: M_w = 14987 g/mol, M_n = 5691 g/mol, PDI = 2.63, DP$_w$: 27.0. UV-Vis (CHCl$_3$): λ_{max} 435 nm, onset 575 nm.

[Tail In PTMT-T]: Prepared according to general Stille polymerization procedure.

5', 5"-Dibromo-2,7-bis(3-hexyl-2-thienyl)-1,6-methano[10]annulene (100.0 mg, 0.1581 mmol), 2,5-bis-tributylstannylthiophene (104.7 mg, .1581 mmol), PdCl$_2$(PPh$_3$)$_2$ (5.6 mg, 0.0079 mmol), 5 mL Toluene. Yielded 20.4 mg (58%) of an orange powder. ^{1}H NMR (400 MHz, CDCl$_3$) δ: 7.47 (m, br), 7.35 (m, br), 7.15 (s), 7.07 (m), 2.91 (m, br), 2.75 (m, br), 2.00-1.71 (m), 1.65 (m, br), 1.42 (m), 1.18 (m, br), 0.95 (t, J = 7.2 Hz), -0.05 (s). GPC: M$_w$ = 11141 g/mol, M$_n$ = 3587 g/mol, PDI = 3.11, DP$_w$: 20.0. UV-Vis (CHCl$_3$): λ$_{max}$ 422 nm, onset 540 nm.

[No Tail PTMT-T]: Prepared according to general Stille polymerization procedure.

5', 5"-Dibromo-2,7-bis(2-thienyl)-1,6-methano[10]annulene (100.0 mg, 0.1581 mmol), 2,5-bis-tributylstannylthiophene (104.7 mg, .1581 mmol), PdCl$_2$(PPh$_3$)$_2$ (5.6 mg, 0.0079 mmol), 5 mL Toluene. Yielded 14.0 mg of an orange powder. ^{1}H NMR (400 MHz, *o*-DCB) δ: 7.90 (m, br), 7.85 (d, J = 8.8 Hz), 7.48 (m, br), 7.44-7.42 (m, br), 7.36 (d, J = 5.2 Hz), 7.15-7.10 (m, br), -0.02 (s). GPC: Poor solubility prevents analysis using THF. UV-Vis (CHCl$_3$): λ$_{max}$ 455 nm, onset 560 nm.

[Tail Out PTMT-DPP]: Prepared according to general Stille polymerization procedure.

5', 5"-Bis(tributylstannyl)-2,7-bis(4-hexyl-2-thienyl)-1,6-methano[10]annulene (0.1542g, 0.1465 mmol), 3,6-bis(2-bromo-5-thienyl)-2,5-di(2-ethylhexyl)pyrrole[3,4-*c*]-pyrrole-1,4-(2*H*,5*H*)-dione (50.0 mg, 0.0733 mmol), CsF (49.0 mg, 0.3223 mmol), CuI (2.8 mg, 0.014 mmol), (PPh$_3$)$_4$Pd (42.3 mg, 0.037 mmol), and toluene (7 mL). Yielded 85.3 mg of dark blue-green powder (39%). ^{1}H NMR (400 MHz, CDCl$_3$) δ: 9.07 (m), 7.95-7.88 (m, br), 7.48-7.32 (m, br), 7.14 (q, J = 9.7 Hz), 6.97 (s), 4.06 (m, br), 2.90 (m, br), 2.65 (m, br), 1.95 (s,

br), 1.77 (m ,br), 1.68 (m, br), 1.53 (s), 1.44-1.24 (m, br), 0.90 (m, br), 0.06 (s). GPC: M_w: 4742 g/mol M_n: 3003 g/mol PDI: 1.58 DP_w: 4.8. UV-Vis (CHCl$_3$): λ_{max} 636 nm, onset 810 nm.

[Tail In PTMT-DPP]: Prepared according to general Stille polymerization procedure.

5', 5"-Bis(tributylstannyl)-2,7-bis(3-hexyl-2-thienyl)-1,6-methano[10]annulene (0.1546 g, 0.1466 mmol), 3,6-bis(2-bromo-5-thienyl)-2,5-di(2-ethylhexyl)pyrrole[3,4-*c*]-pyrrole-1,4-(2*H*,5*H*)-dione (50.4 mg, 0.0733 mmol), CsF (48.7 mg, 0.3223 mmol), CuI (3.0 mg, 0.013 mmol), (PPh$_3$)$_4$Pd (4.2 mg, 0.0037 mmol), and toluene (5 mL). Yielded 79.2 mg of dark blue-green powder (36%). ^{1}H NMR (400 MHz, CDCl$_3$) δ: 8.97 (m, br), 7.44 (m, br), 7.30 (m, br), 7.09 (m, br), 4.06 (m, br), 1.94 (s, br), 1.54 (s, br), 1.54-1.42 (m, br), 0.94-0.78 (m, br), 0.06 (s). GPC: M_w: 5517 g/mol M_n: 3203 g/mol PDI: 1.72 DP_w: 5.5. UV-Vis (CHCl$_3$): λ_{max} 637 nm, onset 810 nm.

[No Tail PTMT-DPP]: Prepared according to general Stille polymerization procedure.

5', 5"-Bis(tributylstannyl)-2,7-bis(2-thienyl)-1,6-methano[10]annulene (64.9 mg, 0.0733 mmol), 3,6-bis(2-bromo-5-thienyl)-2,5-di(2-ethylhexyl)pyrrole[3,4-*c*]-pyrrole-1,4-(2*H*,5*H*)-dione (50.0 mg, 0.0733 mmol), (PPh$_3$)$_2$PdCl$_2$ (2.6 mg, 0.0037 mmol), and toluene (5 mL). Yielded 65.0 mg of dark blue-green powder (30%). ^{1}H NMR (400 MHz, *o*-DCB) δ: 8.97 (m, br), 7.92 (br), 7.49-7.43 (m, br), 7.38 (m, br), 7.16 (m, br), 4.05 (s, br), 1.94 (s, br), 1.46-1.19 (m, br), 0.89 (m, br), 0.07 (s). GPC: Poor solubility prevents analysis using THF. UV-Vis (CHCl$_3$): λ_{max} 644 nm, onset 803 nm.

General procedure for Yamamoto polymerization: Prepared according to literature procedures.[70] Ni(COD)$_2$ (0.1000 mmol, 1.2 equiv), 2,2'-bipyridine (0.1000 mmol, 1.2 equiv), and COD (0.8333 mmol, 1.0 equiv) are added to a flame dried Schlenk flask charged with a

stir bar. The flask is evacuated and refilled 3 times with N_2, after which a portion of dry, degassed DMF (1-3 mL) is added. The mixture is stirred for 30 min at room temperature, during which the mixture goes from yellow to deep purple. While stirring, aryl dibromide (0.08 mmol, 1.0 equiv) is added to a separate Schlenk flask, evacuated/ refilled three times and dissolved in dry, degassed DMF (1-2 mL). This solution is added via syringe to the Ni(bipy)COD complex in the first flask, and heated to 60°C for 48-96 h. Upon completion the reaction mixture is precipitated from rapidly stirring MeOH and the polymer collected via vacuum filtration.

[Tail Out PTMT]: Prepared according to general Yamamoto polymerization procedure. 5', 5"-Dibromo-2,7-bis(4-hexyl-2-thienyl)-1,6-methano[10]annulene (108.4 mg, 0.1714 mmol), Ni(COD)$_2$ (56.6 mg, 0.2056 mmol), COD (18.0 mg, 0.1714), 2,2'-bipyridyl (32.1 mg, 0.2056 mmol), 5 mL DMF. Yielded 51.0 mg (63.0%) of an orange powder. ^{1}H NMR (400 MHz, CDCl$_3$) δ: 7.96 (br), 7.84 (br), 7.47 (m, br), 7.40 (s, br), 7.15 (m, br), 2.66 (s, br), 1.67 (s, br), 1.30 (s, br), 0.88 (s, br), -0.05 (br). GPC: M_w = 4920 g/mol, M_n = 2402 g/mol, PDI = 2.05, DP_w: 10.4. UV-Vis (CHCl$_3$): λ_{max} 418 nm, onset 513 nm.

[Tail In PTMT]: Prepared according to general Yamamoto polymerization procedure. 5', 5"-Dibromo-2,7-bis(3-hexyl-2-thienyl)-1,6-methano[10]annulene (50.0 mg, 0.0790 mmol), Ni(COD)$_2$ (26.1 mg, 0.0949 mmol), COD (8.5 mg, 0.0790), 2,2'-bipyridyl (14.8 mg, 0.0949 mmol), 2 mL DMF. Yielded 21.8 mg (58.4%) of an orange powder. ^{1}H NMR (400 MHz, CDCl$_3$) δ: 7.49 (m, br), 7.15 (m, br), 2.95-2.75 (m, br), 1.64 (m, br), 1.21 (m, br), 0.82 (m, br), -0.01 (s, br). GPC: M_w = 6169 g/mol, M_n = 3828 g/mol, PDI = 1.61, DP_w: 13.0 UV-Vis (CHCl$_3$): λ_{max} 430 nm, onset 520 nm.

[No Tail PTMT]: Prepared according to general Yamamoto polymerization procedure. 5', 5"-Dibromo-2,7-bis(2-thienyl)-1,6-methano[10]annulene (100.0 mg, 0.2154 mmol), Ni(COD)$_2$ (71.1 mg, 0.2583 mmol), COD (23.3 mg, 0.2154), 2,2'-bipyridyl (40.4 mg, 0.2583 mmol), 5 mL DMF. Yielded 9.5 mg (14.4%) of a red powder. ^{1}H NMR (400 MHz, o-DCB) δ: 7.92 (m, br), 7.85 (d, J = 8.5 Hz), 7.49-7.35 (m, br), 7.16-7.07 (m, br), 0.05, (s). GPC: Poor solubility prevented analysis using THF. UV-Vis (CHCl$_3$): λ$_{max}$ 468 nm, onset 540 nm.

General procedure for Stille cross-coupling of small molecule systems:

Aryl dibromide (0.1000 mmol, 1.0 equiv), bisstannylarene (0.2250 mmol, 2.25 equiv), and PdCl$_2$(PPh$_3$)$_2$ (0.0050 mmol, 0.05 equiv)or Pd(PPh$_3$)$_4$ (0.0050 mmol, 0.05 equiv), were added to a flame dried, N$_2$ filled Schlenk flask with a stir bar. The flask was evacuated/refilled 3x, at which point dry, degassed toluene (DMF) is added. The solution is heated to 105°C (80°C) while stirring for 48-96 h, while monitoring progress with TLC. Upon completion the reaction mixture is diluted with ethyl ether and stirred with ~50 mL 1M KF for 10 min. The resulting precipitate is vacuum filtered and the organic layer is separated and stirred with another 50 mL KF solution. Again the solution is filtered, the organic layer separated, washed with saturated aq. NH$_4$Cl, and dried over MgSO$_4$. The solvent is removed via rotary evaporation, and the crude material purified by column chromatography (SiO$_2$).

[Tail Out TTMTT]: 5', 5"-Bis(2-thienyl)-2,7-bis(4-hexyl-2-thienyl)-1,6-methano[10]annulene Prepared according to general Stille TTMTT procedure. 5', 5"-dibromo-2,7-bis(4-hexyl-2-thienyl)-1,6-methano[10]annulene (50.0 mg, 0.0790 mmol), 2-tributylstannylthiophene (66.5 mg, 0.1778 mmol), PdCl$_2$(PPh$_3$)$_2$ (5.4 mg, 0.0079 mmol), 3 mL toluene. After 72 hours reaction was quenched, and chromatographed using 95:5 hexane : ethyl acetate mixture as

eluent. Yielded 23.3 mg (46.1%) orange powder. ^{1}H NMR (400 MHz, CDCl$_3$) δ: 7.91 (d, J = 8.7 Hz, 2H), 7.42 (d, J = 9.6 Hz, 2H), 7.31 (m, 2H), 7.17 (s, 2H), 7.11 (m, 4H), 2.81 (m, 4H), 1.71 (m, 4H), 1.43 (m, 4H), 1.33 (m, 8H), 0.90 (m, 6H), -0.04 (s, 2H). ^{13}C NMR (100 MHz, CDCl$_3$): δ 140.9, 140.5, 136.3, 132.1, 130.2, 128.1, 127.5, 127.2, 118.1, 36.0, 31.8, 30.7, 29.6, 29.4, 22.7, 14.2. HRMS (EI) Calcd for C$_{39}$H$_{42}$S$_4$: 638.21694 [M$^+$] Found m/z= 638.21691. UV-Vis (CHCl$_3$): λ_{max} 414 nm (ε = 43500 M^{-1}cm^{-1}).

[Tail In TTMTT]: 5', 5"-Bis(2-thienyl)-2,7-bis(3-hexyl-2-thienyl)-1,6-methano[10]annulene

Prepared according to general Stille TTMTT procedure. 5', 5"-bis(tributylstannyl)-2,7-bis(3-hexyl-2-thienyl)-1,6-methano[10]annulene (50.5 mg, 0.0475 mmol), 2-bromothiophene (17.1 mg, 0.1045 mmol), Pd(PPh$_3$)$_4$ (2.7 mg, 0.0024 mmol), 3 mL DMF. After 48 hours reaction was quenched, and chromatographed using hexane as eluent. Yielded 6.4 mg (21.1%) orange powder. ^{1}H NMR (400 MHz, CDCl$_3$) δ: 7.46 (d, J = 8.8 Hz, 2H), 7.20 (d, J = 5.4 Hz, 2H), 7.17 (d, J = 3.0 Hz, 2H), 7.14 (s, 2H), 7.08 (t, J = 9.4 Hz, 4H), 7.02 (m, 2H) 2.92 (m, 4H), 2.76 (m, 4H), 1.56 (m, 4H), 1.19 (m, 8H), 0.81 (m, 6H), -0.05 (s, 2H). ^{13}C NMR (100 MHz, CDCl$_3$) δ: 141.7, 140.9, 140.4, 137.6, 136.7, 135.5, 133.7, 130.2, 129.1, 127.8, 126.9, 125.8, 124.2, 123.3, 117.5, 35.5, 31.7, 30.4, 29.4, 28.9, 22.5, 14.0. HRMS (EI) Calcd for C$_{39}$H$_{42}$S$_4$: 638.21694 [M$^+$] Found m/z= 638.21518. UV-Vis (CHCl$_3$): λ_{max} 389 nm (ε = 38000 M^{-1}cm^{-1}).

[No Tail TTMTT]: 5', 5"-Bis(2-thienyl)-2,7-bis(2-thienyl)-1,6-methano[10]annulene

Prepared according to general Stille Small Molecule Procedure. 5', 5"-bis(tributylstannyl)-2,7-bis(2-thienyl)-1,6-methano[10]annulene (50.5 mg, 0.1077 mmol), 2-tributylstannylthiophene (90.4 mg, 0..2423 mmol), PdCl$_2$(PPh$_3$)$_2$ (3.8 mg, 0.0054 mmol), 3 mL Toluene. After 96 hours reaction was quenched, and chromatographed using hexane as

eluent. Yielded 7.8 mg (15.4%) orange powder. ^{1}H NMR (400 MHz, CDCl$_3$) δ: 7.82 (d, J = 8.6 Hz, 2H), 7.35 (d, J = 9.5 Hz, 2H), 7.17 (m, 2H), 7.17 (s, 2H), 7.14 (m, 4H), 7.04 (t, J = 9.2 Hz, 4H), 6.96 (m, 2H) -0.08 (s, 2H). ^{13}C NMR (100 MHz, CDCl$_3$) δ: 142.9, 141.9, 138.3, 137.3, 134.5, 130.0, 127.9, 126.9, 124.4, 123.5, 117.8, 35.7. HRMS (EI) Calcd for C$_{27}$H$_{18}$S$_4$: 470.02914 [M$^+$] Found m/z= 470.02866. UV-Vis (CHCl$_3$): λ_{max} 417 nm (ε = 25000 M^{-1}cm^{-1}).

[Tail Out BTMTB]:

5', 5"-Bis(4-2,1,3-benzothiadiazole)-2,7-bis(4-hexyl-2-thienyl)-1,6-methano[10]annulene

Prepared according to General Stille Small Molecule Procedure. 5', 5"-bis(tributylstannyl)-2,7-bis(4-hexyl-2-thienyl)-1,6-methano[10]annulene (100.0 mg, 0.956 mmol), 4-bromo-2,1,3-benzothiadiazole (42.9 mg, 0.1995 mmol), (PPh$_3$)$_4$PdCl$_2$ (3.3 mg, 0.0047 mmol), and toluene (5 mL). Yielded 7.5 mg of a red powder (11%). ^{1}H NMR (400 MHz, CDCl$_3$) δ: 8.01 (t, J = 10.0 Hz, 2H), 7.68 (m, 2H), 7.52 (d, J = 8.4 Hz, 2H), 7.15 (t, J = 9.0 Hz, 1H), 2.70 (m, 4H), 1.69 (m, 4H), 1.25 (m, 12H), 0.83 (m, 6H), 0.05 (s, 2H). ^{13}C NMR (100 MHz, CDCl$_3$) δ: 131.7, 130.7, 129.7, 128.6, 127.9, 127.0, 125.55, 120.7, 119.8, 31.5, 30.4, 29.5, 29.0, 28.8, 13.9 HRMS (EI) Calcd for C$_{43}$H$_{42}$N$_4$S$_4$: 742.22923 [M$^+$] Found m/z= 742.22805. UV-Vis (CHCl$_3$): λ_{max} 425 nm (ε = 28000 M^{-1}cm^{-1}).

[Tail In BTMTB]:

5', 5"-Bis(4-2,1,3-benzothiadiazole)-2,7-bis(3-hexyl-2-thienyl)-1,6-methano[10]annulene

Prepared according to General Stille Small Molecule Procedure. 5', 5"-bis(tributylstannyl)-2,7-bis(3-hexyl-2-thienyl)-1,6-methano[10]annulene (100.0 mg, 0.0950 mmol), 4-bromo-2,1,3-benzothiadiazole (42.9 mg, 0.1995 mmol), (PPh$_3$)$_4$PdCl$_2$ (3.3 mg, 0.0047 mmol), and toluene (5 mL). Yielded 10.9 mg of a red powder (15%). ^{1}H NMR (400 MHz, CDCl$_3$) δ: 8.11 (d, J = 7.5 Hz, 2H), 8.02 (m, 1H), 7.88 (m, 2H), 7.61 (m, 2H), 7.53 (dd, J = 2.5, 9.0 Hz, 2H),

7.36 (dd, J = 3.1, 9.4 Hz, 2H), 7.14 (t, J = 9.4 Hz, 2H), 3.06 (m, 2H), 2.89 (m, 2H), 1.70 (m, 4H), 1.22 (m, 12H), 0.82 (m, 6H), 0.03 (s, 2H). HRMS (EI) Calcd for $C_{43}H_{42}N_4S_4$ [M+]: 742.22923 Found m/z= 742.23034. UV-Vis (CHCl$_3$): λ_{max} 446 nm (ε = 19000 M^{-1}cm^{-1}).

[No Tail BTMTB]:

5', 5"-Bis(4-2,1,3-benzothiadiazole)-2,7-bis(2-thienyl)-1,6-methano[10]annulene

Prepared according to General Stille Small Molecule Procedure. 5', 5"-bis(tributylstannyl)-2,7-bis(2-thienyl)-1,6-methano[10]annulene (150.0 mg, 0.1692 mmol), 4-bromo-2,1,3-benzothiadiazole (7.5 mg, 0.36 mmol), (PPh$_3$)$_4$PdCl$_2$ (5.9 mg, 0.0090 mmol), and toluene (3 mL). Yielded 4.6 mg of a red powder (5%). ^{1}H NMR (400 MHz, CDCl$_3$) δ: 8.21 (d, J = 3.9 Hz, 2H), 7.98 (d, J = 8.8 Hz), 7.95 (s, 2H), 7.89 (d, J = 8.8 Hz, 2H), 7.63 (d, J = 3.9 Hz, 2H), 7.55 (d, J = 9.9 Hz, 2H), 7.51 (dd, J = 3.5 Hz, 1 Hz, 2H), 7.46 (d, J = 9.8 Hz, 2H), 7.39 (dd, J = 5.0 Hz, 1 Hz, 2H), 7.19-7.13 (m, 6H), 0.07 (s, 2H). UV-Vis (CHCl$_3$): λ_{max} 509 nm (ε = 19000 M^{-1}cm^{-1}).

Portions of this chapter were adapted from:

Torsional Influences within Disordered Organic Electronic Materials Based upon Non-Benzenoid 1,6-Methano[10]annulene Rings

B.C. Streifel; P.A. Peart; J.F. Martinez Hardigree; H.E. Katz; J.D. Tovar

Macromolecules **2012**, *45* (18), 7339-7349

References

[1] Vogel, E., Roth, H.D., *Angew. Chem.*, **1964**, *76*, 145

[2] Vogel, E *Pure & Appl. Chem.* **1982**, *54*, 1015-1039

[3] Masamune, S. *Acc. Chem. Res.* **1972**, *5*, 272

[4] Vogel, E., *Chem. Soc. Spec. Publ.*, Ollis, W.D. ed. **1967**, *27*, 113

[5] Sabljic, A., Trinajstic, N., *J. Org. Chem.*, **1981**, *46*, 357-3461

[6] Peart, P.A., Tovar, J.D., *Org. Lett.*, **2007**, *9*(16), 3041-3044

[7] Peart, P.A., Tovar, J.D., *Macromolecules*, **2009**, *42*(13), 4449-4455

[8] K. Sivula; C.K. Luscombe; B.C. Thompson; J.M.J. Fréchet *J. Am. Chem. Soc.* **2006**, *128*, 13988-13989

[9] C.H. Woo; B.C. Thompson; B.J. Kim; M.F. Toney; J.M.J. Fréchet *J. Am. Chem. Soc.* **2008**, *130*, 16324-16329

[10] A.C. Whalley; K.N. Plunkett; A.A. Gorodetsky; C.L. Schenk; C.-Y. Chiu; M.L. Steigerwald; C. Nuckolls *Chem. Sci.* **2010**, *2*, 132-135

[11] N. J. Tremblay, A. A. Gorodetsky, M. Cox, T. Schiros, B. Kim, R. Steiner, Z. Bullard, A. Sattler, W-Y. So, Y. Itoh, M. F. Toney, H. Ogasawara, A. P. Ramirez, I. Kymissis, M. L. Steigerwald, and C. Nuckolls *Chem. Phys. Chem.* **2010**, *11*, 799-803

[12.] Zhokhavets, U.; Erb, T.; Hoppe, H.; Gobsch, G.; Sariciftci, N.S. *Thin Solid Films* **2006**, *496*, 679

[13.] Sivula, K.; Luscombe, C.K.; Thompson, B.C.; Frechét, J.M.J. *J. Am. Chem. Soc.* **2006**, *128*, 13988

[14.] (a) Brabec, C.J. *Solar Energy Materials & Solar Cells* **2004**, *83*, 273
 (b) Yip, H.-L.; Jen, Alex K.-Y. *Energy Environ. Sci.* **2012**, *5*, 5994

[15.] (a) Chen, T-A.; Rieke, R.D. *Synth. Met.* **1993**, *60*, 175.

 (b) Chen, T-A.; Wu, X.; Rieke, R.D. *J. Am. Chem. Soc.* **1995**, *117*, 233

[16.] (a) McCullough, R.D.; Tristram-Nagle, S.; Williams, S.P.; Lowe, R.D.; Jayaraman, M. *J. Am. Chem. Soc.* **1993**, *115*, 4910

 (b) McCullough, R.D.; Lowe, R.D. *J. Chem. Soc., Chem. Commun.* **1992**, *70*

 (c) McCullough, R.D.; Williams, S.P.; Tristram-Nagle, S.; Jayaraman, M.; Eqbank, P.C.; Miller, L. *Synth. Met.* **1995**, *69*, 279.

 (d) McCullough, R.D.; Lowe, R.D.; Jayaraman, M.; Anderson, D.L. *J. Org. Chem.* **1993**, *58*, 904-912

[17.] Woo, C.H.; Thompson, B.C.; Bumjoon, J.K.; Toney, M.F.; Frechet, J.M.J. *J. Am. Chem. Soc.* **2008**, *130*, 16324

[18.] Jayakannan, M.; Van Hal, P.A.; Janssen, R.A.J. *J. Polym Sci. Part A: Polym. Chem.* **2002**, *40*, 251

19. Mondal, R.; Ko, S., Verploegen, E.; Becerril, H.A.; Toney, M.F.; Bao, Z. *J. Mater. Chem.* **2011**, *21*, 1537

20. Ding, J.; Li, Z.; Cui, Z.; Robertson, G.P.; Song, N.; Du, X.; Scoles, L. *J. Polym Sci. Part A: Polym. Chem.* **2011**, *49*, 3374

21. Lee, S.K.; Cho, S.; Tong, M.; Seo, J.H.; Heeger, A.J., *J. Polym. Sci. Part A: Polym. Chem.* **2011**, *49*, 1821

22. Elsenbaumer, R.L.; K-Y. Jen; G. G. Miller; H. Eckhardt; L. W. Shacklette; R. Jow In *Electronic Properties of Conjugated Polymers* H.Kuzmany, M. Mehring, S. Roth, Eds., Springer Series in Solid State Sciences, Springer, Berlin 1987, Vol. 76, *p* 400.

23. Souto-Maior, R.M.; Hinkelmann, K.; Wudl, F., *Macromolecules* **1990**, *23*, 1268

24. Zagorska, M.; Kulszewicz-Bajer, I.; Pron, A.; Firlcj, L.; Berier, P.; Galtier, G. *Synth. Met.* **1991**, *45*, 385

25. Zagorska, M.; Krishe, B. *Polymer* **1990**, *31*, 1379

26. Krishe, B.; Hellberg, J.; Lilja, C. *J. Soc. Chem. Commun.* **1987**, *19*, 1476

27. An excellent review of poly(3-alkylthiophene) regioregularity is found in the following: McCullough, R.D. *Adv. Mater.* **1998**, *10*, 93

28. Hong, S.Y.; Kim, C.Y.; Kim, D.Y.; Hoffman, R. *Macromolecules* **2001**, *34*, 6475

29. Havinga, E.E.; ten Hoeve, W.; Wynberg, H. *Polym. Bull.* **1992**, *29*, 119

30. Havinga, E.E.; ten Hoeve, W.; Wynberg, H. *Synth. Met.* **1993**, *55-57*, 299

31. Peart, P. A.; Tovar, J. D. *Org. Lett.* **2007**, 9, 3041

32. Peart, P. A.; Repka, L. M.; Tovar, J. D. *Eur. J. Org. Chem.* **2008**, 2193

33. Peart, P. A.; Tovar, J. D. *Macromolecules* **2009**, *42*, 4449

34. Peart, P. A.; Elbaz, G.; Tovar, J. D. *Pure Appl. Chem.* **2010**, *82*, 1045

35. E. Vogel; H. D. Roth *Angew. Chem.* **1964**, *76*, 145

36. Hummelen, J.C.; Knight, B.W.; LePeq, F.; Wudl, F.; Wilkins, C. *J. Org. Chem.* **1995**, *60*, 532-538

37. Sirringhaus, H. *Adv. Mater.* **2005**, *17*, 2411

38. Baek, N.S.; Hau, S.K.; Yip, H-L.; Acton, O.; Chen, K-S.; Jen, A. K.-Y. *Chem. Mater.* **2008**, *20*, 5734

39. Osaka, I.; Zhang, R.; Sauvé, G.; Smilgies, D-M.; Kowalewski, T.; McCullough, R.D. *J. Am. Chem. Soc.* **2009**, *131*, 2521

[40.] (a) Bryant-Friedrich, A.C.; Neidlein, R. *Helv. Chim. Acta.* **1997**, *80*, 128

   (b) Bryant-Friedrich, A.C.; Neidlein, R. *Helv. Chim. Acta.*, **1997**, *80*, 1639

[41.] Mee, S.P.H.; Lee, V.; Baldwin, J.E. *Angew. Chem. Int. Ed.* **2004**, *43*, 1132

[42.] Karikomi, M.; Kitamura, C.; Tanaka, S.; Yamashita, Y. *J. Am. Chem. Soc.* **1995**, *117*, 6791-6792

[43.] (a) Bijleveld, J.C.; Zoombelt, A.P.; Mathijssen, S.G.J.; Wienk, M.M.; Turbiex, M.; de Leeuw, D.M.; Janssen, R.A.J. *J.   Am. Chem. Soc.* **2009**, *131*, 16616

   (b) Woo, C. H.; Beaujuge, P.M.; Holcombe, T.W.; Lee, O.P.; Fréchet, J.M.J. *J. Am. Chem. Soc.*, **2010**, *132*, 15547

[44.] Holdcroft, S., *J. Polym. Sci., Part B: Polym. Phys.* **1991**, *29*, 1585-1588

[45.] Wohlgenannt, M.; Jiamng, X.M.; Vardeny, Z.V. *Phys. Rev. B* **2004**, *69*, 241204(R)

[46] J.G. Rodriguez; J.L. Tejedor *J. Org. Chem.* **2002**, *67*, 7631-7640

[47.] Brédas, J.L. *J. Chem. Phys.*, **1985**, *82*, 3809

[48.] McCullough, R.D. *Adv. Mater.*, **1998**, *10*, 93

[49.] Grabowski, A.R.; Rotkiewicz, K. *Chem. Rev.* **2003**, *103*, 3899-4032

[50.] Zou, Y.; Gendron, D.; Neagu-Plesu, R.; Leclerc, M. *Macromolecules* **2009**, *42*, 6361

[51.] Pommerehne, J.; Vestweber, H.; Guss, W.; Mahrt, R.F.; Baessler, H.; Porsch, M.; Daub, J. *Adv. Mater.* **1995**, *7*, 551

[52.] Brabec, C.J.; Dyakonov, V.; Scherf, U.; Eds., *Organic Photovoltaics*, Wiley-VCH: New York, 2008

[53.] McCullough, R.D.; Tristram-Nagle, S.; Williams, S.P.; Lowe, R.D.; Jayaraman, M. *J. Am. Chem. Soc.* **1993**, *115*, 4910

[54.] No measurable transistor performance was observed from Tail In PTMT-DPP.

[55.] Sonar, P.; Singh, S.P.; Li, Y.; Soh, M.S.; Dodabalapur, A. *Adv. Mater.* **2010**, *22*, 5409

[56.] Li, Y.; Sonar, P.; Singh, S.P.; Zeng, W.; Soh, M.S. *J. Mater. Chem.* **2011**, *21*, 10829

[57.] Chua, L.-L.; Zaumseil, J.; Chang, J.-F.; Ou, E.C.-W.; Ho, P.K.-H.; Sirringhaus, H.; Friend, R.H. *Nature* **2005**, *434*, 194

[58] Knappe, W *Adv. Polym. Sci.* Warmeleitung in Polymeren, **1971**, *7*, 477-535

[59] A. P.A. Peart; J.D. Tovar *Org. Lett.* **2007**, *9*, 3041-3044

B. P.A. Peart; L.M. Repka; J.D. Tovar *Eur. J. Org. Chem.* **2008**, 2193-2206

C. P.A. Peart; J.D. Tovar *Macromolecules* **2009**, *42*, 4449-4455

D. B.C. Streifel; P.A. Peart; J.F. Martínez-Hardigree; H.E. Katz; J.D. Tovar *Macromolecules*, **2012**, *45*, 7339-7349

[60] Q. Zhang; Y. Sun; W. Xu; D. Zhu *Energy Environ. Sci.* **2012**, *5*, 9639-9644

[61] Y. Shinohara; K. Ohara; H. Nakanishi; Y. Imai; Y. Isoda *Mater. Sci. Forum* **2005**, *141*, 492-493

[62] M. He; J. Ge; Z. Lin; X. Feng; X. Wang; H. Lu; Y. Yang; F. Qiu *Energy Environ. Sci.* **2012**, *5*, 8351

[63] Y. Du; S.Z. Shen; K. Cai; P.S. Casey *Prog. Polym. Sci.* **2012**, *37*, 820-841

[64] Vogel, E.; Roth, H.D.; *Angew. Chem.* **1964**, *76*, 145

[65] Vogel, E., Klug, W., Breuer, A., *Org. Synth*. **1974**, *54*, 11

[66] Peart, P.A., Repka, L.M., Tovar, J.D., *Eur. J. Org. Chem.*, **2008**, *22*, 3875

[67] Pilgram, K.J., *J. Het. Chem.*, **1970**, *7*, 629

[68] Woo, C. H., Beaujuge, P.M., Holcombe, T.W., Lee, O.P., Fréchet, J.M.J., *J. Am. Chem. Soc.*, **2010**, *132*, 15547

[69] J. Sihna; R.M. Ireland; S.J. Lee; H.E. Katz *MRS Communications* **2013**, *3*, 9-100

[70] Yamamoto, T., et al., *Macromolecules*, **1992**, *25*(4), 1214

Chapter 3 - Furan-1,6-Methano[10]Annulene Copolymers

Introduction to Furan-M10A π-Conjugated Copolymers

Over the past few years, furan has become an increasingly important component of π-conjugated optoelectronic polymers.[1] Poly- and oligofuran are more soluble[2], more planar[3], and have more extensive π-stacking[4] than their thiophene-containing counterparts, and they typically show lower oxidation potentials and higher photoluminescence quantum yields than related poly- and oligothiophenes. Being bioavailable and biodegradable, furan also has a "green" element. These qualities are offset by the presence of a more sensitive heterocyclic core prone to side reactions such as ring-opening and hydrolysis,[5,6] particularly under oxidative conditions required to polymerize furan and oligofurans through chemical or electrochemical means.[7,8] Oligofurans have been shown to be more tolerant to regioregularity defects relative to thiophene analogues due to their enhanced planarity and rigidity.[9] Tolerance of substitution defects and the broader ability to maintain planarity in the presence of torsional strain are desirable when designing π-conjugated polymeric semiconductors due to the enhanced propensity to foster interchain π-electron interactions among planarized polymers over nonplanar polymers. For example, semiconductive π-conjugated furan copolymers have shown efficient ambipolar charge transport,[10,11] and photovoltaic devices employing furan-based copolymers have shown power conversion efficiencies similar to or higher than other chalcogen analogues.[12,13]

Bendikov and coworkers showed that field effect mobilities and conductivities of oligofurans are actually comparable to thiophene analogs, which refutes earlier claims[14] that unfavorable electronic effects of the oxygen atom would decrease conductivity in polymeric semiconductors.[15] This work also challenges the long held assertion that the polarizability of sulfur is vital to the improved charge transport characteristics of conjugated materials.[16, 17] Sexithiophene (6T) substituted with hexyl chains at the terminal thienyl α-positions displayed

field effect hole mobilities in the 10^{-2}-10^{-1} cm^2/Vs range[18] while sexifuran (6F) showed similar

values of up to 0.05 cm^2/Vs. Unsubstituted 8F and 8T displayed similar hole mobilities as

well. Two mutually opposing factors were proposed for the similarity in performance of these

representative devices: the polarizability of sulfur (important in the electronic delocalization

of the π-conjugated system), the small van der Waals radius of oxygen (resulting in tighter

crystal packing) and the lower reorganizational energy when changing from aromatic to

quinoidal structures. With such small differences between the two chalcogen atoms, it

stands to reason that substitution patterns and film morphology have a much larger impact

on overall device performance characteristics than do the identity of the heteroatoms.

Recent device work with furan-containing polymers has generally focused on

complex π-conjugated systems, often incorporating electron-donating and electron-

accepting groups to decrease optical bandgaps and increase charge transfer and

separation. Wang and coworkers studied the effects of using different π "bridges" between

donor and acceptor moieties (benzodithiophene and benzothiadiazole derivatives,

respectively).[19] The change in the spacer group from thiophene to furan changed the

photophysical properties of the polymer both in photovoltaic devices and *in silico* estimations

of co-planarity. These photovoltaic devices are often characterized by several figures of

merit, two of which are open circuit voltage (V_{oc}) and power conversion efficiency (PCE).

Compared to the thiophene derivative (Figure 3.1, bottom), the furan based polymer showed

a higher V_{oc} (0.94 V versus 0.82 V for thiophene) but a lower PCE (2.81% versus 4.93% for

thiophene). The optical bandgap for the furan based polymer was slightly larger than the

thiophene system, 1.96 eV for furan and 1.82 eV for thiophene. Computations of the

optimized torsional angles of the aromatic subunits flanking the π-bridge suggest that furan

(A=4.88°, B=-1.02°) is slightly more planar than with thiophene as the bridge (A=8.51°,

B=8.67°) although neither deviates dramatically out of planarity.
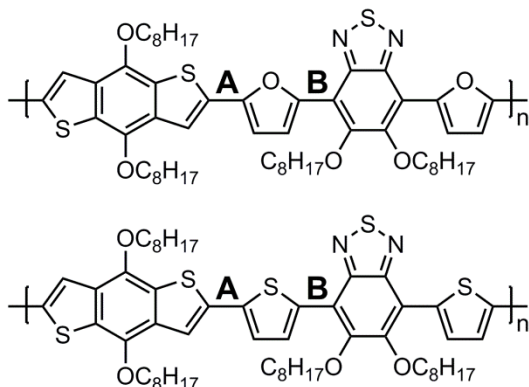
Figure 3.1. Donor-π-acceptor polymer shown with variable heterocyclic spacer groups. The optimized torsional angles of bonds A and B were computed to determine relative co-planarity of the conjugated backbone.

The groups of Frechét[20] and Janssen[21] synthesized a variety of furan and thiophene-containing polymers built around the diketopyrrolopyrrole subunit a now-popular electron deficient building block (Figure 3.2). By varying the heteroatom on each of the three 5-membered aromatics in the polymer repeat unit, the optical and electronic properties could be tuned. Of particular interest in Frechét's work on this system was the ability of furan to increase the solubility of the polymer such that branched alkyl chains were not needed to maintain the same solution processability. By using furans to solubility, less alkyl steric bulk was needed to prevent solution aggregation and precipitation, which decreased the π-stacking distance between polymer backbones for furan based systems relative to the thiophene derivatives. The highest PCE observed using these polymers was 6.5% (X=O, Y=S, R=n-C_{14},), which is an improvement over the ca. 5% efficiencies found for all-thiophene systems that required branched alkyl chains in order to be solution processable.

FFF   **FPF**
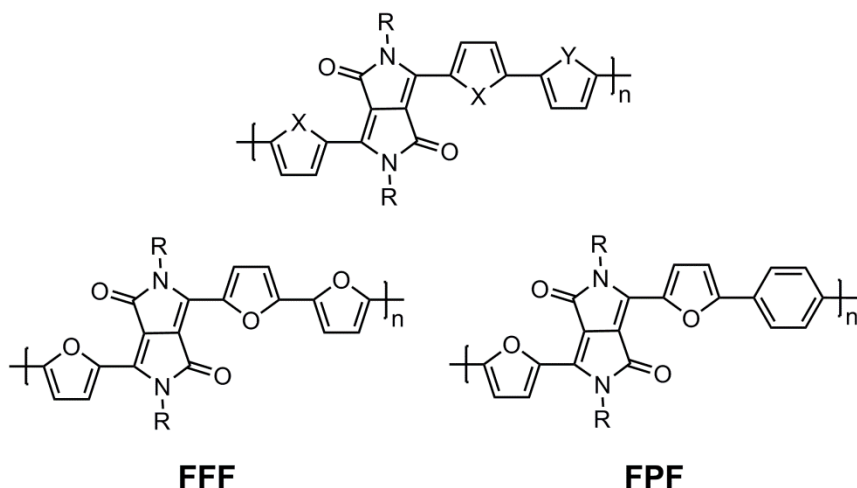
Figure 3.2. Generic diketopyrrolopyrrole-based conjugated polymer (top). X = O or S, Y = O, S, or -CH=CH-. R= branched or linear C_8 through C_{16} alkyl chains. FPF and FFF polymer structures are also shown.

Janssen and coworkers examined the effect of different π bridges within the polymers on ambipolar field-effect mobility in thin film transistors (OFET). For a series of bridges such as FFF and FPF it was found that, in general, replacing a thiophene ring with furan resulted in slightly lower hole and electron mobilities, except in the case of the terfuran bridge which showed drastically diminished electron mobility. Regardless, the measured values (except FFF) were all in the 10^{-2}-10^{-3} cm^2/Vs range typical of donor-acceptor ambipolar polymers. In the case of OFET performance, there is such a small difference that the increased solubility of furan-based systems may make them more commercially interesting from a processing standpoint, but not necessarily from a high-performance perspective.

Skene and Dufresne used azomethine-substituted aromatic rings to probe the differences between pyrrole, N-methylpyrrole, thiophene, and furan as π bridges in conjugated oligomers and polymers (Figure 3.3).[22] UV-Vis and electrochemistry revealed the extent of conjugation and how other optoelectronic properties depended on the identity of

the heterocyclic aromatic. A bathochromic shift in the absorption was observed for the monomers and polymers with the general trend being furan<thiophene<pyrrole $\approx$ N-methylpyrrole, meaning these systems are consistent with theory and other experimentally derived trends in organic semiconductor bandgaps. It was also found by X-ray crystallography that the symmetric homo-aryl systems generally showed less co-planarity than the asymmetric hetero-aryl dyads. Of particular interest were the donor-acceptor interactions between furan and pyrrole moieties of a hetero-aryl dyad (Figure 3.3, X=O, Y=NMe, n=1). This led to regioregular crystal packing and greatly increased co-planarity of the molecule compared to other systems. These types of ordered supramolecular interactions are often accompanied by increases in device performance characteristics, although these studies were not explicitly addressed.
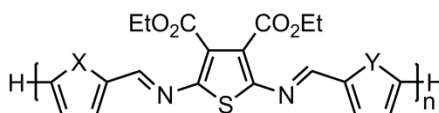
Figure 3.3. Structure of a representative azomethine compound where X=Y=S, NH, NMe, or O for homo-aryl dyads and X≠Y=S, NH, NMe, or O for hetero-aryl dyads. For monomers n=1.

New extended pi-electron units that incorporate fused furan moieties can also harness the advantageous electronic properties of furan for organic semiconductor applications. One such emerging class is made up of the benzodifurans (BDFs, Figure 3.4). BDFs are known to have pharmacological activity[23], and recent research into their materials properties has shown significant promise. Modern synthetic methods have enabled facile syntheses of both small molecule materials as well as polymers, providing access to highly functionalized BDF cores where conjugation can be through the long or short axis of the

BDF molecule.[24] Donor-acceptor copolymers have recently be synthesized by Liu and Jeffries-EL for use in OPV applications thus achieving PCEs up to 5%,[37a,37e] comparable to 5.6% for thiophene analogs[25], and hole mobilities were measured in transistor devices to be ca. 10^{-4}-10^{-2} cm^2/Vs[37b]. Complex BDF structures also maintain the high fluorescence intensity common in oligofurans species.[37d] BDFs are one example of the current trend in organic electronic materials to incorporate well-studied subunits into larger and more complex polymer structures in an attempt to modify semiconductor properties for specific applications.
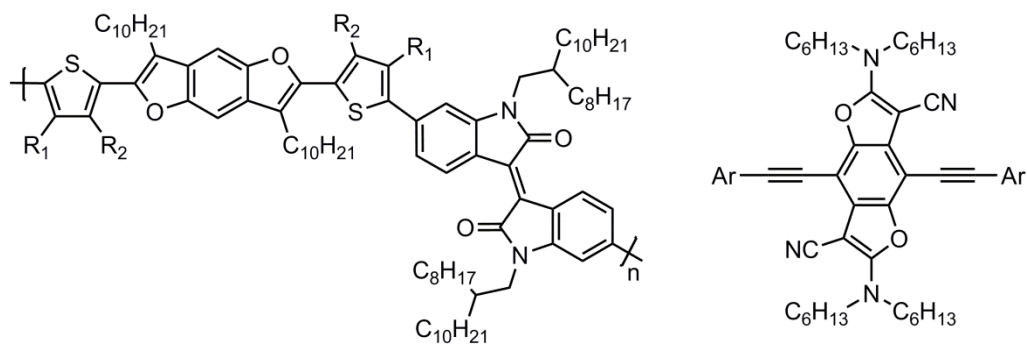
Figure 3.4. Structures of two *trans*-benzodifuran-containing conjugated systems: BDF-*co*-isoindigo donor-acceptor polymer with variable side chain positions where R=n-decyl or H (left) and a highly functionalized BDF small molecule (right).

Former student Patricia Peart previously demonstrated that M10A can attenuate the reactivity of attached furan rings yet still allows for anodic electropolymerization into an annulene-furan π-conjugated copolymer.[26] M10A is a non-planar non-benzenoid π-electron system that has been shown to extend the effective conjugation lengths and lower the oxidation potentials of oligomers and polymers that incorporate it.[27] Furthermore, the methylene bridge on the M10A ring frustrates extensive intermolecular π-electron interactions among the polymers. Although perhaps counterintuitive, M10A copolymers yield

amorphous, yet functional p-type semiconducting materials. Polymer thin films will invariably possess large areas of disordered aggregates regardless of the extent of their molecularly engineered crystallinity, and thus tuning the ability of a polymer to tolerate this disorder while maintaining effective charge transport is the key to high-performance devices.[28] Toney, Salleo, and colleagues have shown that disordered semiconducting materials can have high charge carrier mobilities if they can foster efficient charge transfer/transport at the intra- and interdomain levels. The synthesis and characterization of novel amorphous semiconducting polymers allows the study of tolerance for disorder as well as the deconvolution of various charge transport mechanisms through crystalline and disordered regions in thin films.[29,30,31]

M10A-furan copolymers were previously subjected to electroanalytical investigations[14], but these types of polymers have not yet been prepared chemically for study in solution or the preparation of solid state devices. In this work, we study a series of M10A and diketopyrrolopyrrole (DPP) copolymers with varied furan and thiophene substitution. The polymers consist of two monomer units, a thiophene- or furan-flanked M10A subunit, and a thiophene- or furan-flanked DPP subunit. The polymers are denoted PXY, where X and Y are either furan (F) or thiophene (T) located on the M10A or DPP subunits, respectively (Figure 3.5). By changing the heteroatom substitution on either the electron-donating M10A segment or the electron-accepting DPP segment, subtle electronic effects are evident from spectral, electrochemical, and thermal analysis. The polymers were characterized in the solution and solid states to determine their electronic properties. Carrier mobility measurements and morphology studies also yield insight into the electronic effects of heteroatom substitution. A correlation between the identity and location of the heteroatom substituent in the polymer backbone was made to the bulk semiconductor properties of the material, showing an increase in hole mobility with an increase in furan substitution.
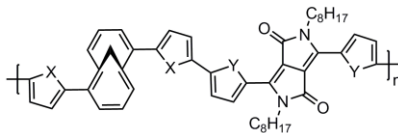
Figure 3.5. Generic PXY polymer structure, where X and Y = S or O, and C_8H_{17} = 2-ethylhexyl.

Synthesis and Properties of Furan-1,6-Methano[10]annulene Copolymers

The four PXY polymers synthesized in this work (Scheme 3.1) were prepared via Pd(0)-mediated Stille polymerization in dry, degassed toluene at 105 °C from the corresponding dibromo and distannyl monomers. Polymers were formed after 48 hours, and the cooled reaction mixtures were precipitated directly into methanol. The precipitates were filtered off and washed with copious amounts of methanol and hexanes to remove residual monomers and oligomers. GPC was used to determine the approximate molecular weight and dispersity of each polymer, relative to polystyrene standards. The values presented in Table 1 are uncorrected and can be assumed to be overestimates,[32] but still show trends in molecular weight depending on furan content and location in the polymer. PTT precipitated early during the polymerization and is too insoluble in THF to obtain meaningful GPC analysis. In contrast, no precipitate was observed during the polymerization of PFF, which is quite soluble in THF (ca. 10 mg/mL). PTF and PFT show similar degrees of solubility in THF (5-7 mg/mL), albeit between the PTT and PFF extremes. Solubility and its effects on processing conditions are important considerations for the ink-based printing of large-area optoelectronic devices. The PXY polymers have roughly half the alkyl chain content compared to common polyaromatics such as P3HT (33% and 60% alkyl carbon content for PXY and P3HT, respectively).
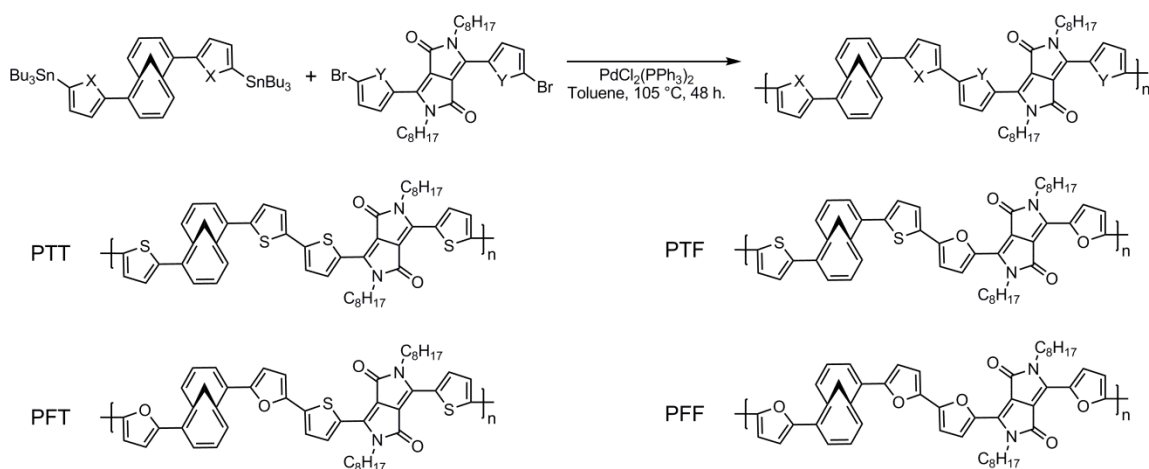
Scheme 3.1. Stille polymerizations leading to PXY polymers, where C_8H_{17} = 2-ethylhexyl.

Table 3.1. UV-Vis, electrochemical, and molecular weight data for PXY polymers.

	λ_1 (nm)	λ_2 (nm)	Onset[a] (nm)	E_g (eV)	HOMO[b] (eV)	LUMO[b] (eV)	M_w[c] (g/mol)	M_n[c] (g/mol)	Đ	DP_n
PTT	432	662	950	1.31	-4.98	-3.67	---Insoluble in THF---			
PTF	421	660	760	1.63	-5.04	-3.41	7900	5100	1.54	6.4
PFT	440	672	850	1.46	-4.99	-3.53	2800	1900	1.47	2.4
PFF	438	668	830	1.49	-4.94	-3.45	8700	4400	1.96	5.8

a.   UV-Vis spectra were collected in $CHCl_3$ at ambient temperature. The onset was determined by the wavelength at which the absorption reached 5% above baseline.
b.   HOMO levels were calculated from the onset of anodic current from the cyclic voltammogram. LUMO levels were calculated using the optical bandgap.
c.   Polymer molecular weights are relative to polystyrene standards and are uncorrected.

The optical bandgap and electronic features in the solution UV-vis absorption spectrum for each polymer are dependent upon the identity and location of the heterocyclic rings in the polymer (Figure 3.6, left). The heterocycle adjacent to the electron-withdrawing DPP subunits appears to determine the optical bandgap: polymers bearing the thienyl-DPP subunit (PTT and PFT) have lower energy onsets of absorption (950 nm and 850 nm, respectively) than those bearing furyl-DPP subunits (PTF and PFF, 760 nm and 830 nm, respectively). This trend is expected based upon the absorption spectra of the dibromo-DPP monomers, as the dibromo-dithienyl-DPP monomer has an absorption onset of 600 nm and

the difuryl analogue has an onset of 586 nm. Low energy shoulders are prominent in the PTT and PFF polymers. The substitution of the electron donating M10A subunit seems to control the λ_{max} values of both the high and low energy peaks, with furyl-M10A polymers (PFT, PFF) having lower energy absorption maxima (672 nm and 668 nm, respectively) than the thienyl-M10A analogues (PTF, PTT, 660 nm and 662 nm, respectively). The high energy peaks of PFT and PFF (440 nm and 438 nm, respectively) are lower in energy than those of PTF and PTT (421 nm and 432, respectively). This is expected in the higher energy portion of the spectrum which is attributed to the M10A segments of the polymer, based on the absorption spectra of the M10A based small molecules FMF[9] (λ_{max} = 386 nm, onset = 450 nm) and TMT[20] (λ_{max} = 375 nm, onset = 467 nm). Thin film UV-vis showed a different trend than the solution state (Figure 3.6, right). Thin films of PTT showed an onset of absorption similar to the solution spectrum, whereas PTF, PFT, and PFF films all showed lower energy onsets than in the solution state. This indicates some degree of planarization in the solid state. PTF and PFF show nearly identical absorption onsets, indicating a similar degree of π-π interactions and planarity in the solid state. The high energy absorption peaks (400-500 nm region) in the solid state show a similar trend to the solution, where PFT and PFF have lower energy maxima (465 nm and 446 nm, respectively) than PTT and PTF (443 nm and 439 nm, respectively) in this region. The PXY polymers were tolerant of a range of processing conditions as the peak shape and maxima remained the same in as-spun films and films annealed for 1 hour at 100°C.

97
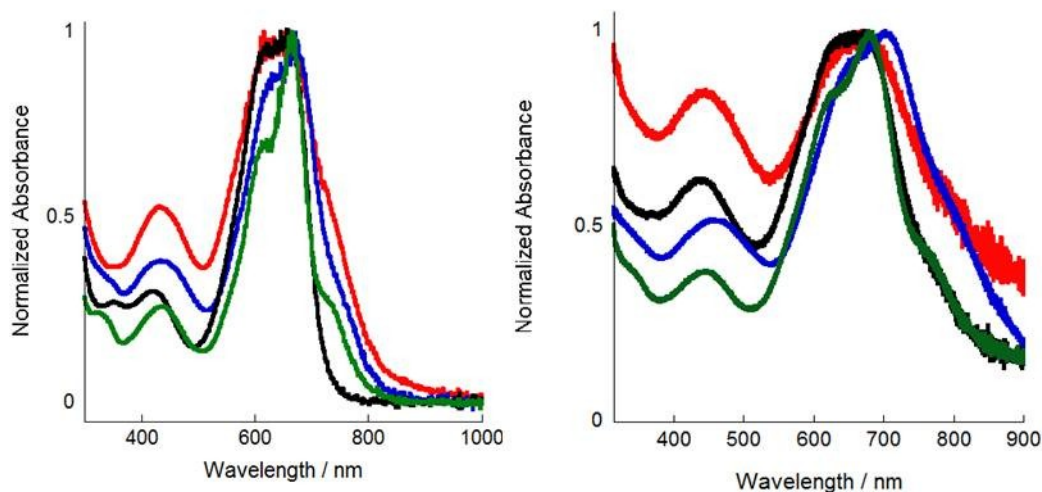
Figure 3.6. Solution (CHCl₃, left) and thin film (right) UV-vis absorption spectra of the PXY polymers. Red = PTT, Black = PTF, Blue = PFT, and Green = PFF.

The electrochemically-derived HOMO levels of the polymers are within 0.1 eV as determined by onset of oxidation in the solution CV, a consequence of the extended electron-rich segments common to all polymers regardless of heteroatom substitution. The LUMO energies are closely linked to the acceptor unit due to the fact that they are calculated from the optical bandgap data, which is controlled primarily by the electron accepting DPP subunit (Table 3.1). Thin film UPS measurements showed larger HOMO level differences than the solution CV (Figure 3.7). When plotted relative to the Fermi band edge of P3HT[33], the binding energy of the polymers scales inversely with the degree of furan substitution: PFF has a binding energy 0.6 eV lower than that of PTT, which had the same binding energy as P3HT. PTF and PFT band edges had binding energies of 0.4 eV and 0.3 eV lower than P3HT, respectively. This trend of decreasing HOMO energy with increasing furan substitution may result from the morphological differences in the films arising from solubility differences.
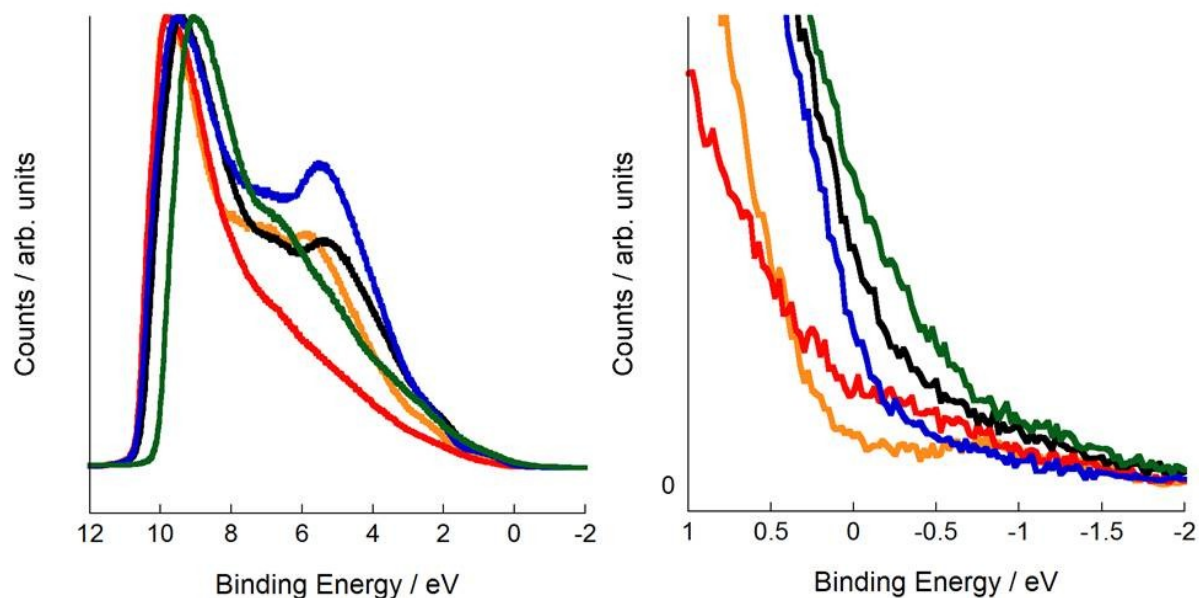
Figure 3.7. Normalized ultraviolet photoelectron spectroscopy of P3HT and PXY polymers plotted relative to the band edge of P3HT (full spectrum left, Fermi edge right). Red = PTT, Black = PTF, Blue = PFT, Green = PFF, and Orange = P3HT.

The polymers presented in this report show no crystallinity in the solid state (Figure 3.8). This is likely due to the presence of M10A, whose racemic three-dimensional structure is expected to frustrate intermolecular packing relative to the more traditional crystalline nature of high-performance π-conjugated semiconductive polymers. Differential scanning calorimetry showed only minor melting of the DPP side chains in all cases, with no clear glass transitions or crystal melting points. PTT showed a feature in the endotherm around 225 °C, but this is not maintained in the exotherm and is thus not likely a crystal melting point.
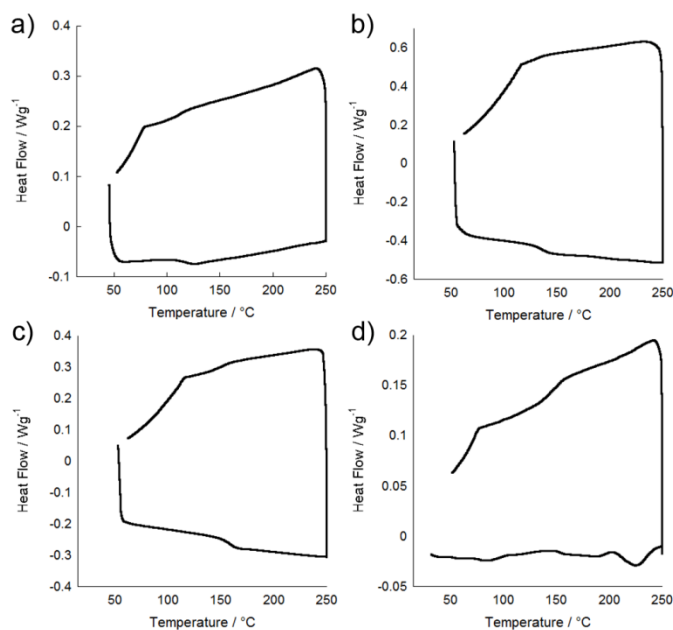
Figure 3.8. Shown are the differential scanning calorimetry second scans, plotted with the exotherm up. a) PFF b) PFT c) PTF d) PTT.

OFETs prepared with PXY polymer active layers showed a trend of increasing charge carrier mobility with increasing furan substitution (Figure 3.9). The polymers functioned as p-type materials with mobilities on the order of 10^{-4} cm^2/Vs. The μ_h values (cm^2/Vs) were 1.64 x 10^{-4} ($\pm$ 6.7 x 10^{-6}) for PTT, 1.98 x 10^{-4} ($\pm$ 1.3 x 10^{-5}) for PTF, 3.34 x 10^{-4} ($\pm$ 1.5 x 10^{-5}) for PFT, and 7.05 x 10^{-4} ($\pm$ 8.2 x 10^{-5})for PFF. These unoptimized mobility values, although low compared to crystalline organic semiconductors, are on the same order of magnitude for other amorphous polymers[34], and they were comparable to those obtained in similar devices fabricated in our labs with regioregular P3HT (μ_h = 2.76 x 10^{-4} cm^2/Vs). Calculation of mobility ratio μ_h^* (μ_h^*=μ_{PXY}/μ_{P3HT}) gives an estimate of the relative mobility values with respect to P3HT, which range from 0.59 for PTT to 2.5 for PFF. With proper optimization of device fabrication conditions for each polymer, it is reasonable to expect greater mobilities for any new organic semiconductor. Indeed, regioregular P3HT has demonstrated hole mobilities of ca. 10^{-1} cm^2/Vs.[35]

PXY	$\mu_h{}^*$
PTT	0.59
PTF	0.72
PFT	1.2
PFF	2.5
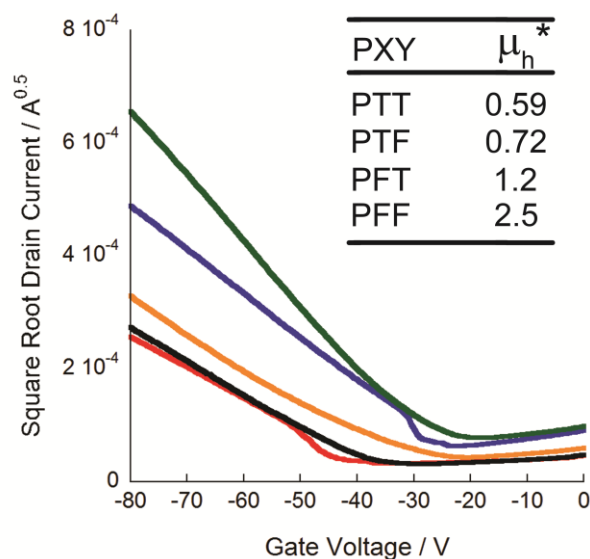
Figure 3.9. I_d-V_g curves for OFET devices for the PXY series and P3HT and table of $\mu_h{}^*$ values where $\mu_h{}^* = \mu_{PXY}/\mu_{P3HT}$. Red = PTT, Black = PTF, Blue = PFT, Green = PFF, Orange = P3HT

AFM phase images were taken of the area between contacts in the OFET devices (Figure 3.10). RMS roughness values were similar for all films (PFF = 1.62 nm, PFT = 2.66 nm, PTF = 2.69 nm, PTT = 1.02 nm), measured across a 2 μm x 2 μm area. The images reveal that increasing thiophene substitution results in increased phase contrast within the film, suggesting the growth of large aggregates or precipitates in the film.[36] It is likely that the lower solubility of the thiophene-containing polymers (PFT, PTF, PTT) causes larger aggregates to form under solution processing conditions. The presence of larger disordered aggregates in the thiophene-containing polymers may be a factor in the trend seen in hole mobility measurements.[37]
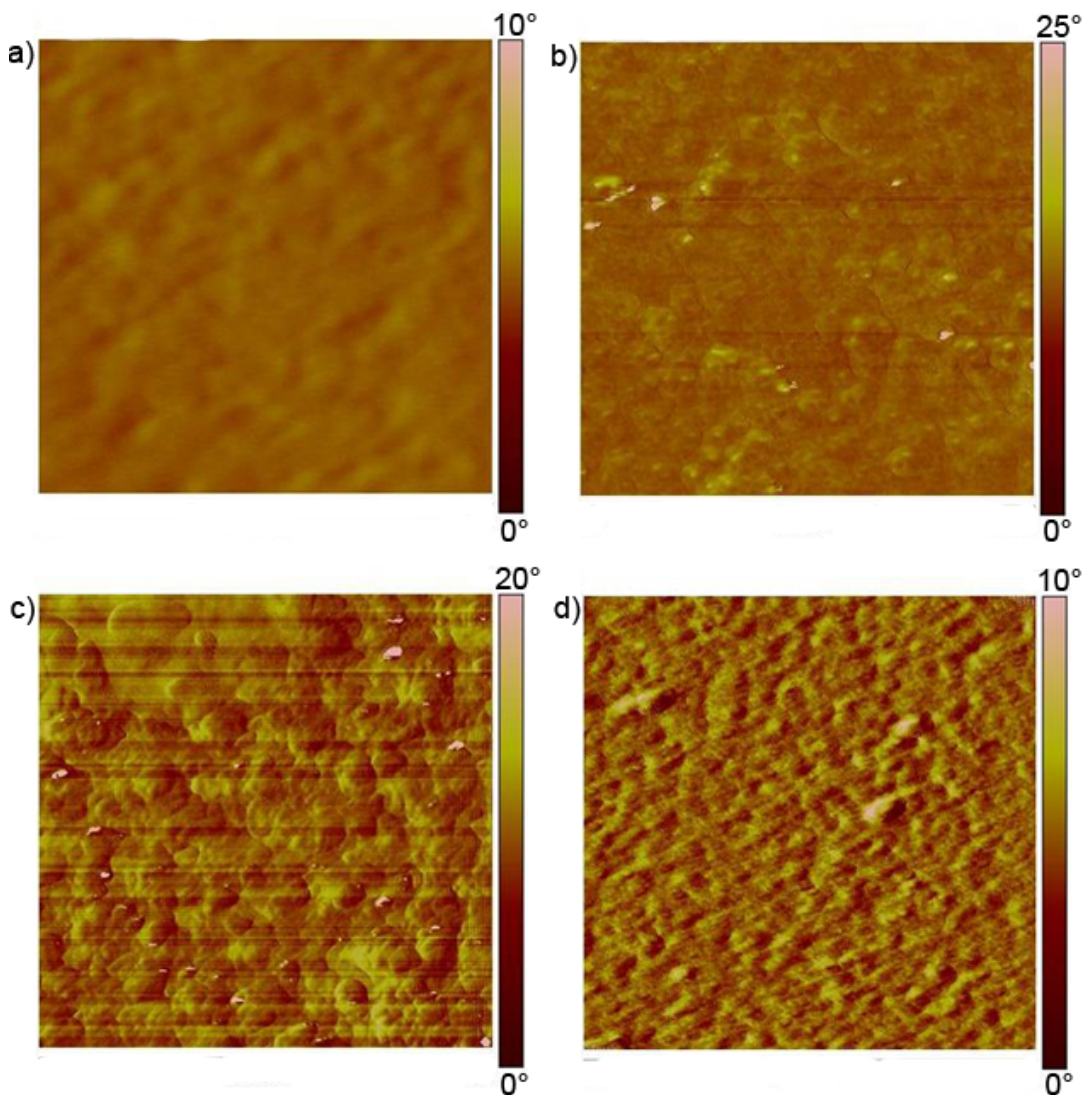
Figure 3.10. AFM phase images of PXY polymers spin cast onto OTS/SiO$_2$ substrates (2μm x 2μm image area). a) PFF b) PFT c) PTF d) PTT.

Conclusions

Four furan- and thiophene-containing M10A-based polymers were synthesized to determine the electronic effects of furan and thiophene substitution in amorphous M10A-based polymers. These new polymers are soluble, amorphous, electronically tunable, and easily synthesized. Their solubilities and amorphous nature arise from the geometric properties of M10A rather than side-chain engineering. The heteroaromatic attached to the

electron-withdrawing DPP subunit controlled the optical bandgap, whereas those associated with the electron-donating M10A subunit controlled the absorption maxima. The thienyl-DPP subunits showed lower bandgaps than the furyl-DPP analogues, and the furyl-M10A subunits showed lower energy absorption maxima than the thienyl-M10A analogues. Polymer thin film absorption spectra remained relatively unchanged in as-spun and annealed films. The polymers are amorphous as determined by DSC, and OFET devices prepared from these polymers yielded hole mobilities of ca 10^{-4} cm^2/Vs, which are comparable to other known amorphous organic semiconductors in the literature. AFM images of polymer thin films suggest that the presence of larger aggregates in the thiophene-containing polymers (PFT, PTF, PTT) may contribute to lower hole mobilities than the furan containing polymers. These results suggest that the PXY series may be useful in applications where amorphous semiconductors are desired, such as light-emitting diodes, thermoelectric devices, or as blends with high-performance semiconducting polymers.

Experimental

General: Dichloromethane (DCM) and hexanes were purchased from Sigma Aldrich and distilled prior to use. Toluene and tetrahydrofuran (THF) were obtained from a solvent purification system (Innovative Technologies), stored over 4Å molecular sieves, and sparged with dry N$_2$ for 15 minutes before use. Palladium catalysts (Strem Chemicals Inc.) were used as received. 2,7-Di(2-furyl)-1,6-methano[10]annulene (FMF)[27], 5', 5"-di(tributylstannyl)-2,7-di(2-thienyl)-1,6-methano[10]annulene (di-stannyl TMT)[38], 3,6-di(2-bromo-5-furyl)-2,5-di(2-ethylhexyl)-pyrrolo[3,4-*c*]-pyrrole-1,4-dione (dibromo-F$_2$DPP), 3,6-di(2-bromo-5-thienyl)-2,5-di(2-ethylhexyl)-pyrrolo[3,4-*c*]-pyrrole-1,4-dione (dibromo-T$_2$DPP)[39], and PTT[38] were prepared according to procedures reported in the literature.

NMR: All NMR spectra were recorded in $CDCl_3$ (Cambridge Isotope Laboratories) on a Bruker Avance 400 MHz instrument and data were collected with Bruker Topspin V. 2.1 unless otherwise noted. Data were processed with either Topspin V.2.1 or SpinWorks V.3.1.7.0 (2010, University of Manitoba). All ^1H spectra were calibrated against either residual $CHCl_3$ (7.26 ppm) or TMS (0.00 ppm) in the deuterated solvent.

UV–Vis: Spectra were recorded on a Varian Cary 50 Bio UV–vis spectrometer in $CHCl_3$ (spectroscopic grade, Sigma-Aldrich) at ambient temperature using quartz cuvettes, unless otherwise noted. Solutions had optical densities of ca. 0.8. Thin film UV-Vis samples were prepared by spin coating (WS-650MZ-23NPP, Laurell Technologies Co) PEDOT:PSS (3.0% in H_2O high conductivity grade, Sigma Aldrich) onto glass slides (Fisher, cleaned with acetone and dried in a 120 °C oven) at 3000 rpm for 60 seconds and annealed for 1 h at 100 °C to promote polymer adhesion. Polymers were then spun from 5 mg/mL $CHCl_3$ (Sigma Aldrich) solutions and annealed at 100 °C for 1 h. The data were collected and analyzed using Cary WinUV V.3.00(182) software.

Electrochemistry: Cyclic voltammetry was performed on an Autolab potentiostat with a 2 mm^2 Pt button working electrode, Pt wire counter electrode, and Ag/Ag^+ reference electrode, in either THF or DCM (spectroscopic grade, Sigma-Aldrich) with 0.1 M tetrabutylammonium hexafluorophosphate (TBAP) as the electrolyte. A Fc/Fc^+ external standard was used to calibrate measurements ($E_{1/2}$ = 0.281 V vs. Ag/Ag^+). TBAP and ferrocene were obtained from Sigma-Aldrich, and the TBAP was recrystallized from anhydrous ethanol prior to use. Electrolyte solutions were stored over 4 Å molecular sieves and sparged with dry N_2. Data were collected and processed using GPES software.

Gel permeation chromatography (GPC): Polymer molecular weights were measured by GPC (Agilent 1260 with photodiode array detector) using unstabilized THF as the eluent (1 mL/min, 40 °C) through a Resipore guard column (50x7.5 mm, Agilent) and two Resipore columns (300x7.5mm, Agilent). Polystyrene standards (Easivial PS-L, Agilent) were used to build a calibration curve. Processing was done using Cirrus GPC Software (Version 3.4, Agilent). Polymers were dissolved in THF (0.25-0.5 mg/mL), filtered (Millex FG 0.20 μm PTFE filters, Millipore), and manually injected (10 μL).

Differential scanning calorimetry (DSC): Calorimetry was performed on a DSC Q20 (TA Instruments) using DSC Q20 software (V24.9 build 121,TA Instruments). Polymer powders (2-10 mg) were weighed and placed into aluminum pans, pressed to seal, and placed into the sample compartment. The samples were heated from 25-250°C in two cycles, and the second cycle reported. Tungsten was used as a reference and N_2 as a purge gas (50 mL/min).

Ultraviolet photoelectron spectroscopy (UPS): Photoelectron spectroscopy was performed on a Phi 5600 X-ray photoelectron spectrometer (Physical Electronics) with UV40A UPS source (Prevac) tuned to operate at the He Iα line (21.2 eV). Samples were prepared identically to thin film UV-vis samples (Glass : PEDOT:PSS : Polymer) and mounted on a sample holder with steel screws so as to provide electrical contact between the polymer film and the instrument. A -6V bias was applied to the sample before data collection.

Carrier mobility measurements: Bottom gate-top contact organic field effect transistors (OFETs) were fabricated on highly doped n-type Si wafers (SI-Tech, Process Solutions) with

a thermally grown 300 nm oxide layer. All wafers were sonicated in warm acetone and isopropanol and dried in a stream of dry N_2. The oxide layer was treated with octadecyltrichlorosilane vapor (OTS, Sigma Aldrich) under high vacuum. Polymers were dissolved in $CHCl_3$ (5 mg/mL) and filtered (0.20 μm PTFE filter, Millipore FG) prior to use. Active layers of PXY polymers were spin-coated (Laurell Technologies Corporation) at 1500 rpm for 90 s and annealed at 100 °C for 1 h. Wafers were loaded overnight for thermal evaporation of 125 nm Au electrodes (Edwards Auto 306) through a shadow mask with *W*/*L* ratio of 32, where *W* = 8 mm and *L* = 250 µm. Si gates were scratched with a diamond scribe and contacted with Ga–In eutectic (Sigma-Aldrich). All electrical characterization was performed on an Agilent 4155C Semiconductor Parameter Analyzer using a medium integration time (16.7 ms), under vacuum. Devices were probed with low-resistance probes from Micromanipulator, onto which small (∼100 µm) drops of Ga–In eutectic were placed for contacting source and drain electrodes. Mobility measurements are reported as the average of 12 devices.

Atomic Force Microscopy (AFM): AFM images were taken on a Digital Instruments (USA) Multi Mode SPM in tapping mode and a scan rate of 2 Hz. Height and phase images were taken of the area between the source and drain electrodes of the OFET devices described previously.

5', 5''-di(tributylstannyl)-2,7-di(2-furyl)-1,6-methano[10]annulene: Prepared according to published procedures for the related TMT molecules.[38] 2,7-Di(2-furyl)-1,6-methano[10]annulene (50.0 mg, 0.182 mmol) was added to a flame dried Schlenk flask charged with a stir bar and evacuated/refilled with dry N_2 three times. Dry, degassed THF (5 mL) was added and the solution stirred while cooling to -78 °C in a dry ice/acetone bath for 20 min. N-butyllithium solution (0.240 mL, 1.6 M in hexanes, 0.383 mmol) was added

dropwise and stirred for 1 h at -78 °C. SnBu$_3$Cl (0.103 mL, 0.382 mmol) was added to the reaction mixture and stirred at -78 °C for 1 h before removing the cooling bath and allowing the reaction mixture to warm to room temperature and stir for 12 h. The reaction was quenched with deionized water (10 mL) and extracted with DCM (3 x 10 mL). The organic layers were washed with deionized water (3 x 15 mL) and brine (1 x 15 mL) before drying over MgSO$_4$. The solvent was removed by rotary evaporation and the crude material placed under high vacuum to yield 175 mg of a dark yellow oil (117% by weight due to excess tin electrophile) that was used without purification. The product was not stable to ambient light and air and was stored under nitrogen in the dark. ^{1}H NMR (400 MHz, CDCl$_3$) δ: 7.88 (d, J = 9.4 Hz, 2H), 7.50 (d, J = 9.4 Hz, 2H), 7.12 (t, J = 9.4 Hz,2H), 6.70 (m, 2H), 6.65 (m, 2H), 1.62 (m, 12H), 1.37 (m, 12H), 1.14 (m, 12H), 0.91 (m, 18H), -0.06 (s, 2H).

General procedure for Stille polycondensation (Adapted from Reference 38 for PTT): Aryl dibromide (0.50 mmol, 1.0 equiv.), aryl distannane (0.60 mmol, 1.2 equiv.), and Pd(PPh$_3$)$_2$Cl$_2$ (0.025 mmol, 0.050 equiv.) were added to a flame dried 25 mL Schlenk flask charged with a magnetic stir bar and evacuated and refilled with dry N$_2$ three times. Dry, degassed toluene was added and heated to 105 °C and stirred. After 48 h, the reaction mixture was allowed to cool to ambient temperature and then poured directly into rapidly stirring methanol (100 mL). The precipitate was collected via vacuum filtration and washed with methanol (~200 mL) and hexanes (50 mL).

PFT: The general procedure for Stille polycondensation was followed using 3,6-bis(2-bromo-5-thienyl)-2,5-di(2-ethylhexyl)pyrrole[3,4-*c*]-pyrrole-1,4-dione (84.4 mg, 0.124 mmol), 5', 5"-di(tributylstannyl)-2,7-di(2-furyl)-1,6-methano[10]annulene (132 mg, 0.161 mmol), Pd(PPh$_3$)$_2$Cl$_2$ (8.9 mg, 0.0062 mmol), and toluene (10 mL) to yield 78.7 mg of dark blue-green powder (80%). ^{1}H NMR (400 MHz, CDCl$_3$) δ: 7.99 (m, br), 7.62-7.47 (m, br), 7.18 (m,

br), 6.84 (m, br), 4.06 (m, br), 1.97 (m, br), 1.47-1.20 (m, br), 1.00-0.79 (m, br), 0.06 (s, 2H). GPC: M_w: 2800 g/mol M_n: 1900 g/mol Đ: 1.47 DP_n: 2.4. UV-Vis (CHCl$_3$): λ_{max} 672 nm, onset 850 nm.

PTF: The general procedure for Stille polycondensation was followed using 3,6-di(2-bromo-5-furyl)-2,5-di(2-ethylhexyl)pyrrole[3,4-*c*]-pyrrole-1,4-dione (176.5 mg, 0.1143 mmol), 5', 5"-di(tributylstannyl)-2,7-di(2-thienyl)-1,6-methano[10]annulene (113 mg, 0.137 mmol), Pd(PPh$_3$)$_2$Cl$_2$ (6.8 mg, 0.0097 mmol), and toluene (15 mL) to yield 77.5 mg of dark blue-green powder (74%). ^{1}H NMR (400 MHz, CDCl$_3$) δ: 8.54 (m, br), 7.90 (m, br), 7.48-7.36 (m, br), 7.14 (m, br), 6.76 (m, br), 4.18 (m, br), 2.85 (m, br), 1.51-1.12 (m, br), 0.96-0.77 (m, br), 0.00 (s, 2H). GPC: M_w: 7900 g/mol M_n: 5100 g/mol Đ: 1.54 DP_n: 6.4. UV-Vis (CHCl$_3$): λ_{max} 660 nm, onset 760 nm.

PFF: The general procedure for Stille polycondensation was followed using 3,6-di(2-bromo-5-furyl)-2,5-di(2-ethylhexyl)pyrrole[3,4-*c*]-pyrrole-1,4-dione (74.3 mg, 0. mmol), 5', 5"-di(tributylstannyl)-2,7-di(2-furyl)-1,6-methano[10]annulene (286 mg, 0.271 mmol), Pd(PPh$_3$)$_2$Cl$_2$ (16.0 mg, 0.0135 mmol), and toluene (25 mL) to yield 157.4 mg of dark blue-green powder (73%). ^{1}H NMR (400 MHz, CDCl$_3$) δ: 8.51 (m, br), 7.95 (m, br), 7.57 (m, br), 7.23 (m, br), 7.18 (m, br), 6.99 (m, br), 6.87 (m, br), 4.16 (m, br), 1.92 (m, br), 1.51-1.14 (m, br), 0.96-0.74 (m, br), 0.06 (s, 2H). GPC: M_w: 8700 g/mol M_n: 4400 g/mol Đ: 1.96 DP_n: 5.8. UV-Vis (CHCl$_3$): λ_{max} 668 nm, onset 830 nm.

References

[1] a) B.C. Streifel; J.D. Tovar "Pi-conjugated furan-based polymers" Encyclopedia of Polymer Science and Technology, **2012**, Wiley and Sons

b) Gonzales-Tejera, M.J., Sanchez de la Blanca, E., Carrillo, I., *Synth. Met.*, **2008**, *158*(5), 165-189

c) S.S. Zade; N. Zamoshchik; M. Bendikov *Acc. Chem. Res.* **2011**, *44*, 14-24

d) O. Gidron; M. Bendikov *Angew. Chem. Int. Ed.* **2014**, *53*, 2546-2555

[2] Y. Miyata; M. Terayama; T. Minari; T. Nishinaga; T. Nemoto; S. Isoda; K. Komatsu *Chem.-Asian J.* **2007**, *2*, 1492-1504

[3] O. Gidron; Y. Diskin-Posner; M. Bendikov *J. Am. Chem. Soc.* **2010**, *132*, 2148-2150

[4] J.K. Politis; J.C. Nemes; M.D. Curtis *J. Am. Chem. Soc.* **2001**, *123*, 2537-2547

[5] S. Glenis; M. Benz; J.L. Schindler; C.R. Kannewurk; M.G. Kanatzidis *J. Am. Chem. Soc.* **1993**, *115*, 12519-12525

[6] K. Gollnick; A. Griesbeck *Tetrahedron* **1985**, *41*, 2057

[7] M.J. Gonzales-Tejera; E. Sanchez de la Blanca; I. Carrillo *Synth. Met.* **2008**, *158*, 165-189

[8] T. Ohsawa; K. Kaneto; K. Yoshino *Jpn. J. Apply. Phys.* **1984**, *23*, L663

[9] X.-H. Jin; D. Sheberla; L.J.W. Shimon; M. Bendikov *J. Am. Chem. Soc.* **2014**, *136*, 2592-2601

[10] M.S. Chen; O.P. Lee; J.R. Niskala; A.T. Yiu; C.J. Tassone; K. Schmidt; P.M. Beaujuge; S.S. Onishi; M.F. Toney; A. Zettl; J.M.J Frechét *J. Am. Chem. Soc.* **2013**, *135*, 19229-19236

[11] Y. Li; P. Sonar; S.P. Singh; W. Zeng; M.S. Soh *J. Mater. Chem.* **2011**, *21*, 10829-10835

[12] Z. Zeng; Y. Li; J. Deng; Q. Huang; Q. Peng *J. Mater. Chem. A* **2014**, *2*, 653-662

[13] Y. Kim; C.E. Song; A. Cho; J. Kim; Y. Eom; J. Ahn; S.-J. Moon; E. Lim *Mater. Chem. and Phys.* **2014**, *143*, 825-829

[14] Ando, S., Nishida, J., Fujiwara, E., Tada, H., Inoue Y., Tokito, S., Yamashita, Y., *Chem. Lett.*, **2004**, 1170

[15] Politis, J.K., Nemes, J.C., Curtis, M.D., *J. Am. Chem. Soc.*, **2001**, *123*, 2537-2547

[16] K. Takimiya, Y. Kunugi, Y. Konda, N. Niihara, T. Otsubo, *J. Am. Chem. Soc.*, **2004**, *126*, 5084

[17] T. Okamoto, K. Kudoh, A. Wakamiya, S. Yamaguchi, *Org. Lett.*, **2005**, *7*, 5301

[18] (a) Horowitz, G., Fichou D., Peng, X., Xu, Z., Garnier, F., *Solid State Commun.*, **1989**, *72*, 381

(b) Garnier, F., Yassar, A., Hajlaoui, R., Horowitz, F., Deloffre, F., Servet, B., Ries, S., Alnot, P., *J. Am. Chem. Soc.*, **1993**, *115*, 8716

(c) Hajlaoui, R. El Kassmi, A., Horowitz, G., Laigre, L., Porzio, W., Armanini, M., Provasoli, F., *Chem. Mater.*, **1998**, *10*, 3334

(d) Hajlaoui, R., Fichou, D., Horowitz, G., Nessakh, N., Constant, M., Garnier, F., *Adv. Mater.*, **1997**, *9*, 557

(e) Horowitz, G, Hajlaoui, M.E., *Adv. Mater.*, **2000**, *12*, 1046

[19] (a) Wang, X., Chen, S., Sun, Y., Zhang, M., Li, Y., Li, X., Wang, H., *Polym. Chem.*, **2011**, *2*, 2872

(b) Wang, X., Sun, Y., Chen, S., Guo, X., Zhang, M., Li, X., Li, Y., Wang, H., *Macromolecules*, **2011**, *45*, 1208-1216

[20] (a) Woo, C.H., Beaujuge, P.M., Holcombe, T.W., Lee, O.P., Frechét, J.M.J., *J. Am. Chem. Soc.*, **2010**, *132*, 15547-15549

(b) Yiu, A.T., Beaujuge, P.M., Lee, O.P., Woo, C.H., Toney, M.F., Frechet, J.M.J., *J. Am. Chem. Soc.*, **2012**, *134*(4), 2180-2185

[21] Bijleveld, J.C., Karsten, B.P., Matijssen, S.G.J., Wienk, M.M., de Leeuw, D.M., Janssen, R.A.J., *J. Mater. Chem.*, **2011**, *21*, 1600-1606

[22] Dufresne, S., Skene, W.G., *J. Phys. Org. Chem.*, **2012**, *25*, 211-221

[23] (a) Chambers, J. J.; Kurrasch-Orbaugh,D.M.; Parker,M.A.; Nichols, D. E. *J. Med. Chem.* **2001**, *44*, 1003.

(b) Chambers, J. J.; Kurrasch-Orbaugh, D.M.;Nichols,D.E. *Bioorg.Med.Chem. Lett.* **2002**, *12*, 1997.

(c) Verghese, J.; Liang, A.; Sidhu, P. P. S.; Hindle, M.; Zhou, Q.; Desai, U. R. *Bioorg. Med. Chem. Lett.* **2009**, *19*, 4126.

(d) Kim, I.; Choi, *J. Org. Biomol. Chem.* **2009**, *7*,2788.

(e) Manna, K.; Agrawal,Y.K. *Bioorg. Med. Chem. Lett.* **2009**, *19*, 2688.

(f) De Luca, L; Nieddu, G.; Porcheddu, A.; Giacomelli, G. *Curr. Med. Chem*. **2009**, *16*, 1.

(g) Liang, Z.; Ma, S.; Yu, J.; Xu, R., *Tetrahedron* **2007**, *63*, 12877.

[24] (a) Kobilka, B.M., Dubrovskiy, A.V., Ewan, M.D., Tomlinson, A.L., Larock, R.C., Chaudhary, S., Jeffries-EL, M., *Chem. Commun.*, **2012**, Advance Article, DOI: 10.1039/C2CC34070D

(b) Tsuji, H., Mitsui, C., Ilies, L., Sato, Y., Nakamura, E. *J. Am. Chem. Soc.*, **2007**, *129*, 11902-11903

(c) Huo, L., Huang, Y., Fan, B., Guo, X., Jing, Y., Zhang, M., Li, Y., Hou, J., *Chem. Comm.*, **2012**, *48*, 3318-3320

(d) Keller, S., Yi, C., Li, C., Liu, S.-X., Blum, C., Frei, G., Sereda, O., Neels, A., Wandlowski, T., Decurtins, S., *Org. Biomol. Chem.*, **2011**, *9*, 6410-6416

(e) Yi, E., C., Blum, Lehmann, M., Keller, S., Liu, S.-X., Frei, G., Neels, A., Hauser, J., Schuerch, S., Decurtins, S., *J. Org. Chem.*, **2010**, *75*, 3350-3357

[25] Huo, L., Huo, J., Zhang, S., Chen, H., Yang, Y., *Angew. Chem. Int. Ed.*, **2010**, *49*, 1500

[26] P.A. Peart; J.D. Tovar *Macromolecules* **2009**, *42*, 4449-4455

[27] P.A. Peart; J.D. Tovar *Org. Lett.* **2007**, *9*, 3041-3044

[28] R. Noriega; J. Rivnay; K. Vandewal; F.P.V. Koch; N. Stingelin; P. Smith; M.F. Toney; A. Salleo *Nature Materials* **2013**, *12*, 1038-1044

[29] A. Bhuwalka; J.F. Mike; M. He; J.J. Intemann; T. Nelson; M.D. Ewan; R.A. Roggers; Z. Lin; M. Jeffries-EL *Macromolecules*, **2011**, *44*, 9611-9617

[30] B.M. Kobilka; B.J. Hale; M.D. Ewan; A.V. Dubrovskiy; T.L. Nelson; V. Duzhko; M. Jeffries-EL *Polym. Chem.* **2013**, *4*, 5329-5336

[31] P. Sonar; T.R.B. Foong; S.P. Singh; Y. Li; A. Dodabalapur *Chem. Commun.* **2012**, *48*, 8383-8385

[32] S.J. Holdcroft *J. Polym. Sci., Part B: Polym. Phys.* **1991**, *29*, 1585-1588

[33] Y. Shen; L. Scudiero; M.C. Gupta *IEEE J. Photovoltaics* **2012**, *2*, 512-518

[34] C. Celle; C. Suspene; M. Ternisien; S. Lenfant; D. Guerin; K Smaali; K. Lmimouni; J.P. Simonato; D. Vuillaume *Organic Electronics* **2014**, *15*, 729-737

[35] C. Tanase; E.J. Meijer; P.W.M. Blom; D.M. de Leeuw *Phys. Rev. Lett.* **2003**, *91*, 216601

[36] B.T. de Villers; C.J. Tassone; S.H. Tolbert; B.J. Schwartz *J. Phys. Chem. C Lett.* **2009**, *113*, 18978-18982

[37] G. Balaji; M.S. Esfahani; P. Joshi; J. Bhattacharaya; M. Jeffries-EL; V. Dalai *Eur. Polym. J.* **2013**, *49*, 3921-3928

[38] B.C. Streifel; P.A. Peart; J.F. Martínez Hardigree; H.E. Katz; J.D. Tovar *Macromolecules* **2012**, *45*, 7339-7349

[39] C.H. Woo; P.M. Beaujuge; T.W. Holcombe; O.P. Lee; J.M.J. Frechét *J. Am. Chem. Soc.* **2010**, *132*, 15547-15549

Chapter 4 - 1,6-Methano[10]annulene as a Component of Oligomeric Tetracyanoquinodimethanes

Introduction to Tetracyanoquinodimethanes for Optoelectronics

π-Conjugated molecules with distinctly quinoidal electronic structures have unique electronic and magnetic properties that make them well suited for a variety of organic electronic[1], spintronic[2], and energy storage applications[3]. A common motif for these molecules is the presence of terminal dicyanomethylene groups, similar to tetracyanoquinodimethane (TCNQ) and related molecules with extended π-electron systems. These extended conjugated molecules often exhibit strong electron-accepting behavior, with some even possessing amphoteric redox properties.[4] Oligothiophene-based tetracyanoquinodimethane derivatives (OT-TCNQ, Figure 4.1), for example, have demonstrated electron mobilities as high as 0.2 cm^2/Vs.[5] One particularly interesting feature in these extended OT-TCNQ derivatives is the ability to form open-shell singlet and triplet biradical states. Synthesis of a sexithiophene OT-TCNQ derivative by Otsubo and colleagues resulted in ambient temperature EPR activity[6] and Raman spectra[7] characteristic of a thermally-accessible triplet biradical electronic state. The biradical results when the thiophene rings are aromatized, and is in equilibrium with the quinoidal and open-shell singlet states. The barrier to biradical formation is lowered by the large stabilization granted by aromatization of the thienoquinoid rings[8]. The triplet biradical is only observed in the quinque- and sexithiophene derivatives and not in smaller systems, indicating that a certain degree of aromatic stabilization is required for stable biradical formation.
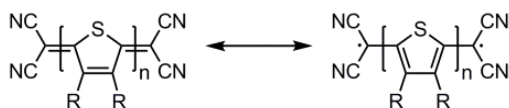
Figure 4.1. OT-TCNQ derivative illustrating quinoidal (left) and biradical (right) structures.

Over the past decade, tetracyanoquinodimethylene units have been incorporated into a variety of aromatic platforms such as variously substituted thiophenes[9], rylenes[10], and other, larger polycyclic benzenoid hydrocarbons[11,12] (Figure 4.2). These motifs have the potential to regain aromaticity and thus support the persistence of singlet or triplet biradicals near ambient temperatures.
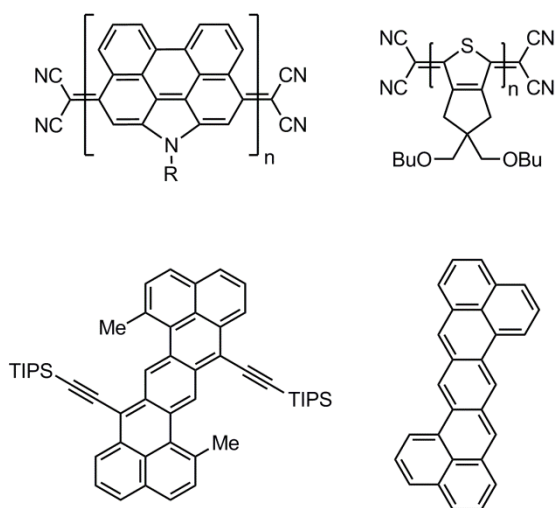
Figure 4.2. Structurally diverse extended π-conjugated quinoidal molecules: rylenes (top left), oligothiophenes (top right), and heptazethrenes (bottom left, bottom right).

In this report, we describe the use of 1,6-methano[10]annulene (M10A) as a comparable biradical-stabilizing subunit. M10A can be viewed as on the border between a classical Hückel aromatic and a "cyclic polyene" due to its non-planarity and relatively low resonance stabilization energy.[13] Although NICS calculations predict strong aromaticity,

M10A undergoes olefin-like reactions during bromination.[14] These competing factors result in an aromatic core that is capable of stabilizing radical species through extensive delocalization. This stabilization via delocalization has been demonstrated by Creary through computational investigations into relative stabilities of M10A and benzyl radical species.[15] We have also shown how M10A can be a useful component of conjugated aromatic polymers and oligomers by lowering oxidation potentials, increasing effective conjugation length over other 10 π-electron systems, and stabilizing reactive co-monomers.[16,17] The bridging methylene of M10A frustrates intermolecular π-stacking interactions and results in solution-processable polymers that form amorphous semiconducting films.[18] The radical-stabilizing, conjugation-extending, and solubilizing qualities of M10A make the annulene a good candidate for incorporation into tetracyanoquinodimethylene derivatives with the aim of creating thermally-accessible singlet or triplet biradical species. In this chapter, the synthesis and spectroscopic characterization of a tetracyanoquinodimethane derivative 2,7-bis(5'-dicyanomethylenethiophen-2'-ylidene)-1,6-methano[10]annulene (TMTQ, Figure 4.3) is presented.
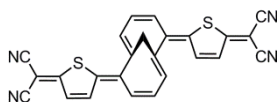
Figure 4.3. Chemical structure of the small molecule TMTQ.

Synthesis and Characterization of TMTQ

Synthesis of TMTQ was accomplished by Takahashi coupling.[19] The sodium salt of malononitrile was prepared using an excess of sodium hydride, which was then added to a solution of Pd(PPh$_3$)$_4$ and dibromo-TMT and refluxed overnight. The reaction was quenched and diluted with 2M HCl and the coupling product oxidized with Br$_2$ in water. TMTQ was

isolated from the crude mixture by column chromatography in 55% yield as a dark blue solid.
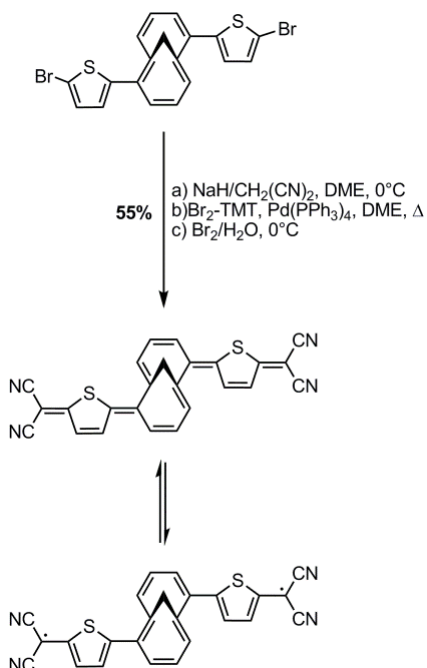
Scheme 4.1. Takahashi method of synthesizing TMTQ.

The UV-Vis spectrum of TMTQ shows an absorption peak at 683 nm (ε = 37000 M^{-1}cm^{-1}) with an onset at 850 nm. Intense low energy absorption features are common among tetracyanoquinodimethanes due to low lying LUMO levels, particularly in molecules with some donor-acceptor qualities or amphoteric behavior.[6,10,18] Cyclic voltammetry results in a reversible peak at -320 mV vs. Ag/Ag$^+$ ($E_{1/2}$), indicating the strong electron-accepting nature of TMTQ, as illustrated in Figure 4.4 (right). Using a ferrocene/ferrocenium couple as a reference at 4.8 eV below vacuum[20], this corresponds to an electrochemical LUMO of 4.18 eV. Attempts at anodic electrochemical measurements resulted in irreversible decomposition of the molecule.
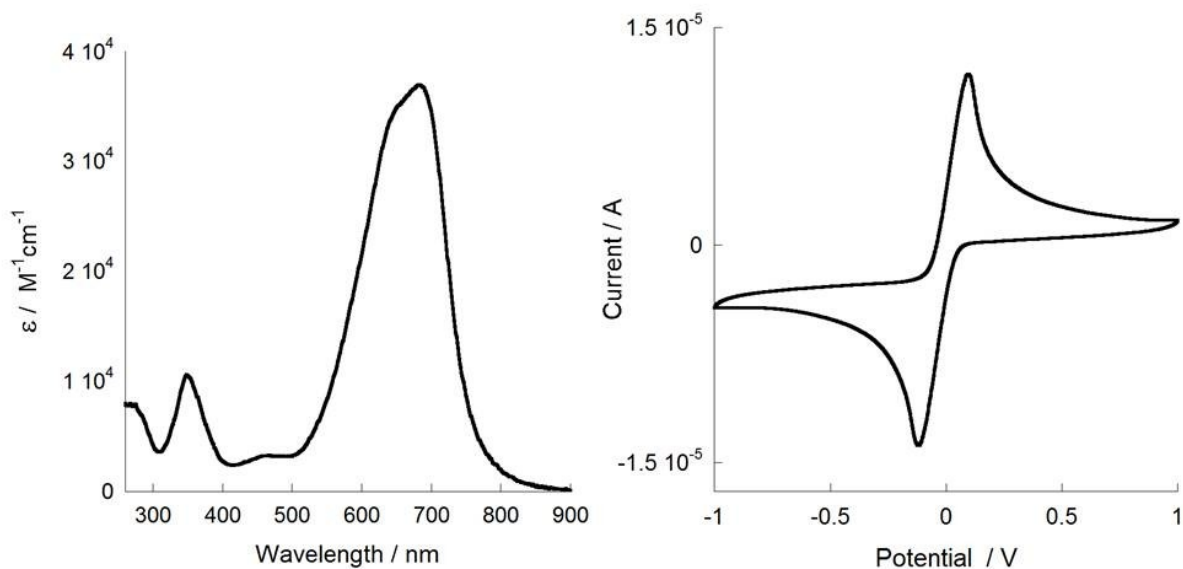
Figure 4.4. UV-vis absorption spectrum (CHCl₃, left) and cyclic voltammogram (THF/TBAPF₆, right) of TMTQ.

Variable temperature ^{1}H NMR experiments suggest interconversion between quinoidal and biradical electronic states as evidenced by broadening of the signals and the growth of additional broad peaks in the spectrum as the temperature is increased (Figure 4.5).[21,22] At 25 °C, there is evidence of some paramagnetic broadening of the peaks, indicating a possible open shell singlet or triplet biradical structure. Upon cooling to 0°C, the resolution of the peaks is enhanced, suggesting less paramagnetic character (Figure 4.6). As the temperature is raised to 100 °C, there is a loss of resolution and a growth of broad, featureless peaks around 7.26, 6.40, and 5.85 ppm. These additional peaks may be due to differing amounts of electronic shielding due to different electronic structures, but the broad nature of the peaks does not allow the assignment of any particular structure.
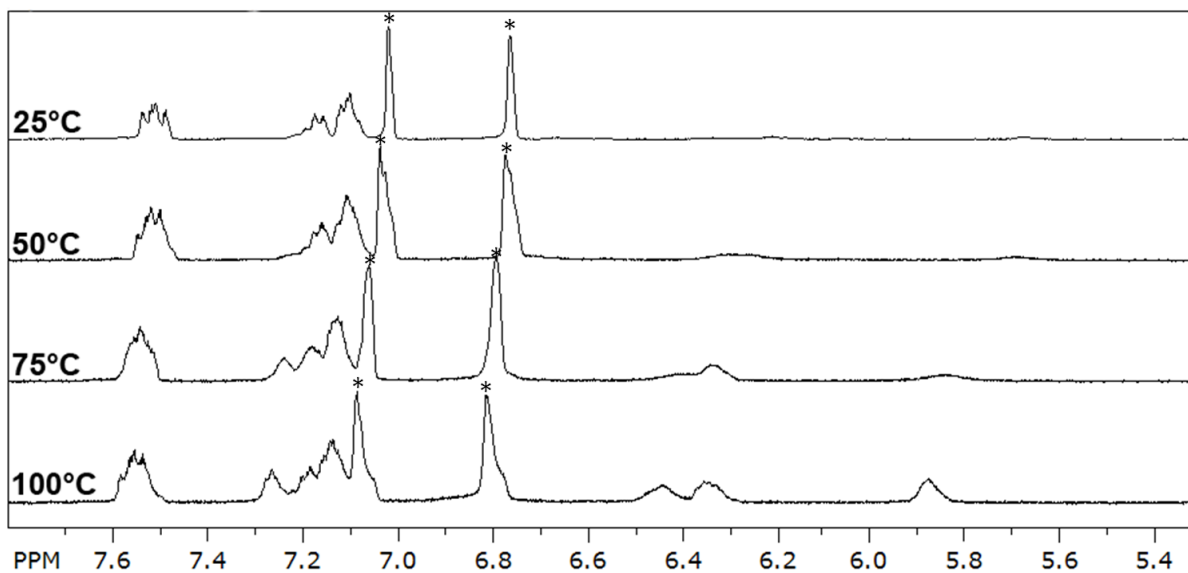
Figure 4.5. ^{1}H NMR (400 MHz) spectra of TMTQ at various temperatures in d_4-o-dichlorobenzene (* = residual protio solvent peaks).
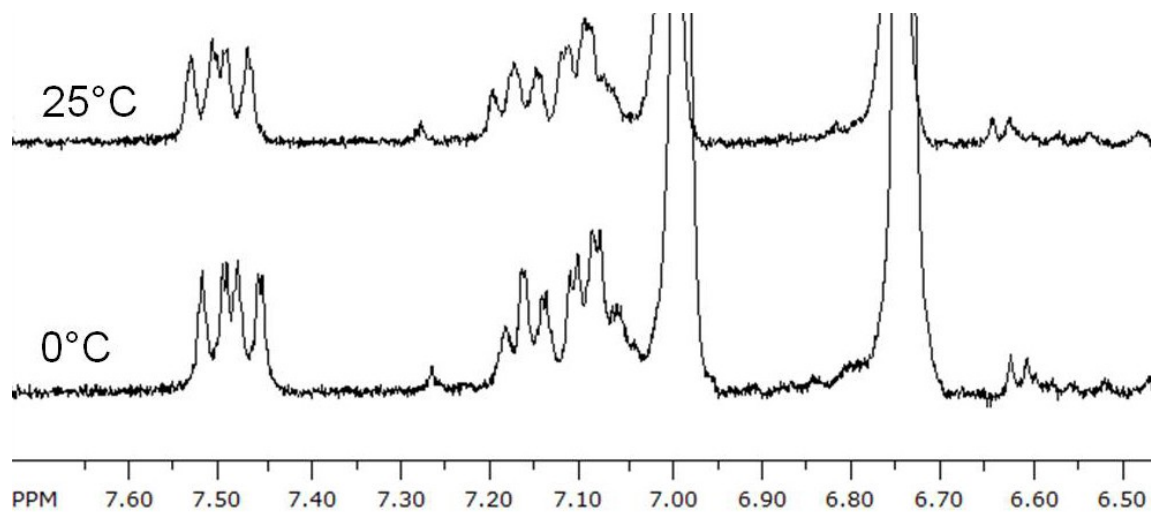
Figure 4.6. ^{1}H NMR (300 MHz) spectra of TMTQ at ambient temperature and 0°C in d_4-o-dichlorobenzene.
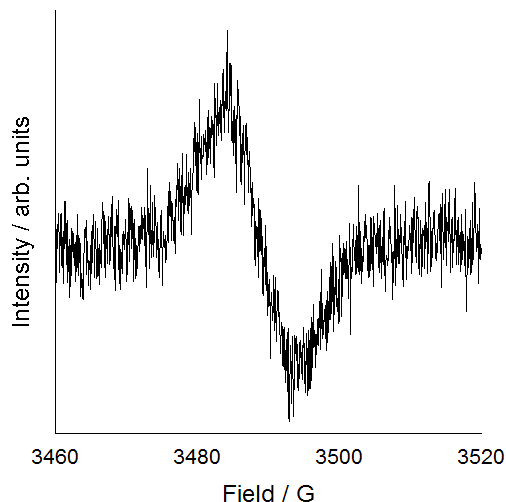
Figure 4.7. EPR spectrum of TMTQ obtained in $CHCl_3$ at 25 °C.

TMTQ shows a weak EPR signal at 25 °C, indicating the presence of a triplet biradical species in solution (Figure 4.7). At cryogenic temperatures (-100 °C) no signal was observed, nor was any signal observed at higher concentrations (10 mg/mL). In other neutral biradical species, strong π-π interactions and even covalent bonds have been noted in the solid state, so it is likely that the effects of concentration on the EPR signal are due to solution aggregation and diminishing of the concentration of the triplet species.[23,24]

DFT (B3LYP/6-31G*) calculations of the HOMO and LUMO energy levels and molecular orbitals were performed to determine if a thermally-accessible triplet state was theoretically feasible (Figure 4.8). The structure of TMTQ was geometrically optimized and the energy levels calculated. Mulliken spin density maps were generated for the triplet species to illustrate the spin distribution. The HOMO and LUMO levels of the S_0 state were computed to be -5.79 eV and -4.14 eV, respectively. The *in silico* LUMO level compares nicely with the electrochemically measured value of -4.18 eV. The HOMO-LUMO gap is 1.65 eV, which is consistent with the experimentally determined absorption spectrum. The HOMO and LUMO of the T_1 state occurred at -5.68 eV and -2.83 eV, respectively.

The difference between the calculated S_0-T_1 HOMO levels is 0.11 eV, making a small population of the T_1 state available at room temperature. In the simplest case of non-interacting spins, a Boltzmann distribution (F(singlet)/F(triplet)=$e^{\Delta E/kT}$) would predict a ratio of 98.6% S_0 and 1.4% T_1 states at 25 °C.[25] This can be used to explain the weak EPR signal near ambient temperature. A Boltzmann distribution at 100 °C predicts a ratio of 96.8% S_0 and 3.2% T_1, still a small proportion of triplet biradical, perhaps explaining the relatively small change in the ^{1}H NMR spectrum at elevated temperatures.
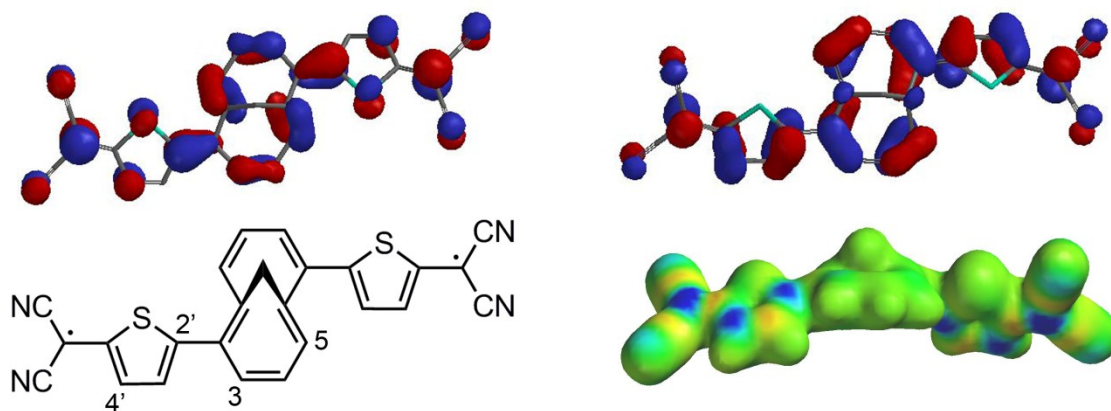
Figure 4.8. DFT (B3LYP/6-31G*) molecular orbitals of TMTQ singlet state (top left), triplet state (top right), chemical structure drawing of the biradical-aromatic state (bottom left), and Mulliken spin density diagram (bottom left; blue = high spin density, green = low spin density).

A spin density surface was also computed using DFT to determine the extent of biradical delocalization in TMTQ. Delocalization occurs well into the thiophene ring and radical character extends into the M10A ring, as evidenced by the blue areas in the spin density structure. Mulliken spin densities indicate that the central malononitrile carbons contain the highest density of spin (Mulliken density of 0.44), the 2' and 4' positions (2- and 4-thienyl) have similar spin densities (0.26 for both), and the 3- and 5-M10A carbons have

slightly lower density (0.20, and 0.18, respectively). This large amount of delocalization explains the low temperature at which TMTQ shows biradical-aromatic behavior, as the polyolefinic and radical stabilizing nature of M10A is able to greatly reduce the energy cost of biradical formation compared to planar, benzenoid aromatics.

Singlet biradical character is common in longer tetracyanoquinodimethanes, and is evidenced by low degrees of bond length alteration in the singlet state. Bond lengths were measured in the computed structures (B3LYP/6-31G*) for the C-C skeleton of the molecule (Figure 4.9). The singlet state showed bond alteration similar to that of tetracyano-terthiophenequinodimethane, and is therefore predicted to have a low degree of singlet biradical character.[26] The triplet state shows a low degree of bond length alteration within the aromatic rings (bonds 2,3,4 for thiophene and 6,7,8,9 for M10A), confirming the proposed aromatic-biradical structure.[27] Bond 5 in the triplet state is much longer than others likely due to steric interactions between the thiophene and annulene rings, and bond 10 is relatively long in both the triplet and singlet states due to ring strain imposed by the bridging methylene group. The bond length alteration (BLA) values within the thiophene ring (defined as the average length of bonds 2 and 4 minus bond 3)[28] for the singlet and triplet states are 0.071 Å and 0.009 Å, respectively. The singlet BLA value corresponds to similar singlet terthiophenequinodimethane analogues as determined by Kishi and Nakano[27], and the triplet BLA value corresponds to triplet terthiophenequinone analogues as determined by Navarrete and Ortí[28].
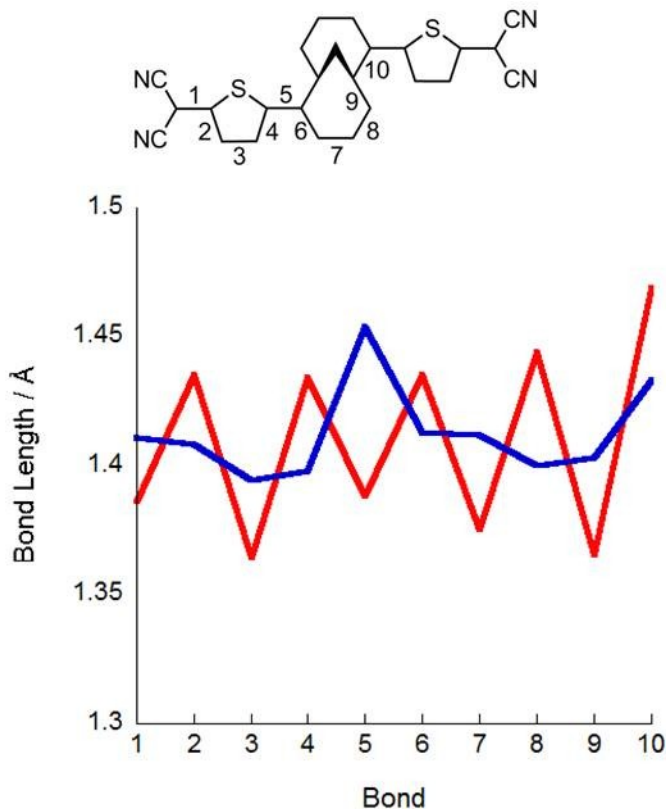
Figure 4.9. Bond number scheme (top) and bond lengths (bottom) of the singlet (red) and triplet (blue) structures of TMTQ.

Oligoquinones of similar size, such as terphenoquinone[29], tetracyanomethylene-terthiophenequinone[30], and thienyl heteroquaterphenoquinones[31], do not show triplet biradical character. To our knowledge, TMTQ is the shortest known molecule capable of formation of a stable triplet biradical state at ambient temperatures. By taking advantage the ability of the central M10A ring to stabilize the triplet state, TMTQ is able to create stable triplet biradical species at relatively low temperatures.

Infrared spectroscopy revealed no significant differences between the solution (CHCl$_3$) and solid states. The nitrile stretches occurred at 2208 cm^{-1} for both states, and the aromatic C=C stretching peaks were identical in the 1525-1400 cm^{-1} region of the spectrum. There was a small shift in the C-H stretching frequency, with the solid state at 3043 cm^{-1} and

the solution at 3010 cm^{-1}. The lower frequency of the stretch could signal an alkene-to-aromatic transition, but there could also be solvent interactions that affect the frequency of stretch. Given the identical values of the nitrile C≡N and aromatic C=C stretching frequencies, it seems that this spectrum relates primarily to the quinoidal form. The solution used for the experiment was necessarily quite concentrated (10 mg/mL) in order to obtain a spectrum, so π-π interactions could be inhibiting formation of the quinoidal biradical form.
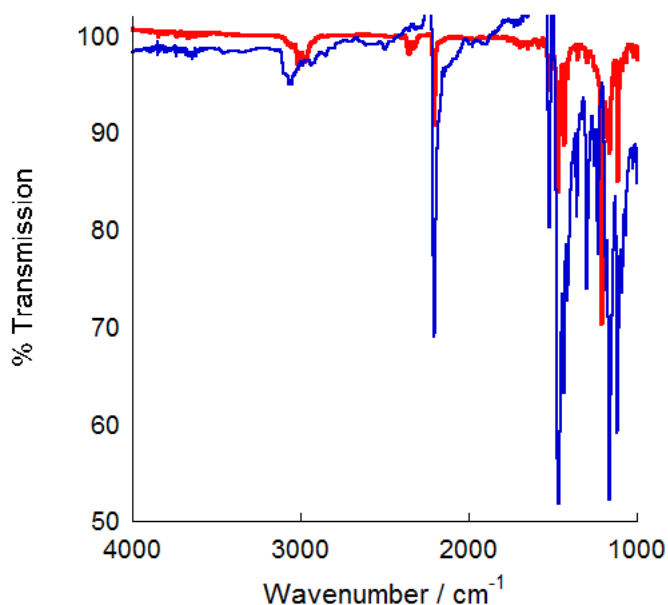
Figure 4.10. Fourier transform infrared spectrum of solid-(blue) and solution-(CHCl$_3$, red) state TMTQ.

Attempts to synthesize extended M10A and naphthalene derivatives were unsuccessful after repeated attempts using the same methodology as for TMTQ (Figure 4.11). Due to solubility concerns after initial attempts, toluene was substituted for glyme, but to no avail. It was then reasoned that the extended π-systems might have lower oxidation potentials and molecular bromine might be too harsh. Air oxidation was then attempted, but again with no product formation. For future synthetic studies, different oxidants may need to

be used to generate the quinoidal species in significant yields. Another option may be the use of solubilizing side chains to increase solubility.
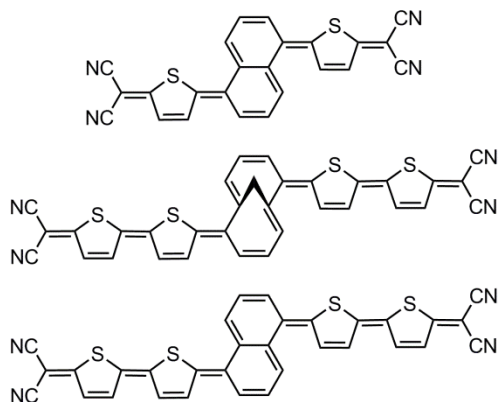
Figure 4.11. Structures of tetracyanoquinodimethane derivatives whose syntheses proved unworkable by the Takahashi coupling/bromine oxidation methodology.

Conclusions

The extended tetracyanoquinodimethane derivative TMTQ was synthesized via Takahashi coupling and investigated by UV-vis spectroscopy, NMR, cyclic voltammetry, EPR spectroscopy, and DFT computations. The experimental data strongly suggest that the molecule has a thermally accessible triplet biradical excited state as evidenced by broad NMR features at elevated temperatures and the presence of a weak EPR signal at ambient temperature. A strong low energy UV-vis absorption band reveals a small HOMO-LUMO gap commonly found among OT-TCNQ derivatives. Cathodic cyclic voltammetry reveals a reversible reduction peak around -320 mV versus Ag/Ag$^+$ (E$_{1/2}$), corresponding to a LUMO level of -4.18 eV. DFT computation (B3LYP, 6-31G*) of HOMO and LUMO energy levels, molecular orbitals, and spin density surfaces, and Mulliken spin values agreed strongly with the experimental data. By using Boltzmann distribution analysis, the weak EPR signal was postulated to be a result of a relatively small population of the triplet biradical state near

ambient temperatures. Bond length measurements from the computational data suggest that there is a small amount of singlet-biradical contribution to the singlet ground state, although it is unlikely that this contributes to the EPR signal based on studies of related oligothiophenequinodimethanes.[6] To our knowledge, TMTQ is the shortest molecule to show stable room-temperature triplet biradical behavior to date. The molecule is easily synthesized and is readily soluble in common organic solvents. This has important implications for studying spintronics, magnetic materials, and other applications where neutral paramagnetic π-conjugated molecules may prove useful.

Future studies of TMTQ in particular and other M10A-quinone derivatives in general will involve further characterization of the quinoidal-radical equilibrium states. Raman spectroscopy and EPR at elevated temperatures will allow analysis of thermodynamics of the transition from singlet to triplet state. EPR characterization of the radical anion of TMTQ and accompanying theoretical modeling may reveal more information about spin delocalization within M10A. For these purposes, TMTQ has been mailed to the group of Juan Casado in Spain at the time this document was prepared.

Experimental

General: All chemicals were obtained from Sigma Aldrich and used without further purification unless otherwise noted. Dichloromethane (DCM) was distilled prior to use. Tetrahydrofuran (THF) was obtained from an Innovative Technology solvent purification system and stored over 4Å molecular sieves under dry N_2. Anhydrous 1,2-dimethoxyethane (DME) was purified by distillation from $CaCl_2$ and stored over 4Å molecular sieves under N_2. 5', 5"-Dibromo-2,7-di(2-thienyl)-1,6-methano[10]annulene was synthesized according to published procedures. $Pd(PPh_3)_4$ was purchased from Strem Chemicals Inc. and used without further purification.

NMR: All NMR spectra were recorded in d_4-o-dichlorobenzene (o-DCB) or CDCl$_3$ (Cambridge Isotope Laboratories) on a Bruker Avance 400 MHz instrument and data were collected with Bruker Topspin V. 2.1 unless otherwise noted. Data were processed with either Topspin V.2.1 or SpinWorks V.3.1.7.0 (2010, University of Manitoba). All ^{1}H spectra were calibrated against either residual CHCl$_3$ (7.26 ppm) or TMS (0.00 ppm) in the deuterated solvent.

UV–vis: Spectra were recorded on a Varian Cary 50 Bio UV–vis spectrometer in CHCl$_3$ (spectroscopic grade, Sigma-Aldrich) at ambient temperature using quartz cuvettes, unless otherwise noted. Solutions had optical densities of ca. 0.8. The data were collected and analyzed using Cary WinUV V.3.00(182) software.

Electrochemistry: Cyclic voltammetry was performed on an Autolab potentiostat with a 2 mm Pt button working electrode, Pt wire counter electrode, and Ag/Ag$^+$ reference electrode, in dry, degassed THF with 0.1 M tetrabutylammonium hexafluorophosphate (TBAP) as the electrolyte. A Fc/Fc$^+$ external standard was used to calibrate measurements and the E$_{1/2}$ was found to be 301 mV versus Ag/Ag$^+$. TBAP and ferrocene were obtained from TCI America. TBAP was recrystallized from anhydrous ethanol and dried under vacuum prior to use. Data were collected and processed using GPES software.

Electron paramagnetic resonance (EPR): EPR spectroscopy was performed on a Bruker EMX X-band spectrometer and the data collected and analyzed by WinEPR. Samples were dissolved in CHCl$_3$ at a concentration of 3 mg/mL, and the sample chamber was purged with nitrogen prior to data collection.

Infrared Spectroscopy (FTIR): FTIR was performed on a Nicolet iS5 spectrometer with iD5 ATR diamond gate (Thermo-Fisher). TMTQ samples were in the forms of powder and 10 mg/mL $CHCl_3$ solutions, both at ambient temperature. The spectra were collected with OMNIC 9.2.98 software (Thermo-Fisher).

Computations: Computational chemistry was performed using density functional theory (DFT/B3LYP 6-31G*) in Spartan '04 (Wavefunction Inc, Build 1,0,3). Equilibrium geometries were optimized using symmetry constraints. Mulliken spin densities were calculated for the triplet species using UB3LYP/6-31G*, and orbital energies recorded for HOMO and LUMO of both the singlet and triplet states.

2,7-bis(5'-dicyanomethylenethiophen-2'-ylidene)-1,6-methano[10]annulene (TMTQ): TMTQ was prepared by adapting procedures known in the literature.[32] Sodium hydride (131.1 mg, 5.464 mmol) was added to a flame dried Schlenk tube charged with a stir bar and evacuated/refilled with dry N_2 three times. The flask was placed in an ice bath (0 °C) and dry, degassed DME (5 mL) was added and stirred. Malononitrile (108.3 mg, 1.631 mmol) was added to a separate Schlenk tube and evacuated/refilled with dry N2 three times. DME (5 mL) was added and the flask cooled to 0 °C in an ice bath. Once the malononitrile was dissolved, the solution was added to the sodium hydride/DME suspension dropwise and kept at 0 °C and stirred for 4 hours. 5', 5"-Dibromo-2,7-bis(2-thienyl)-1,6-methano[10]annulene (317.1 mg, 0.6831 mmol) and Pd(PPh3)4 (78.9 mg, 0.0683 mmol) were added to a flame dried 25 mL Schlenk flask charged with a stir bar and evacuated/refilled three times with dry N_2. DME (40 mL) was added and stirred to dissolve at ambient temperature. The sodium hydride/malononitrile reaction mixture was added dropwise to the aryldibromide/catalyst solution, heated to reflux (85 °C), and stirred overnight (14 hr), during which the mixture became a deep red color. The reaction mixture

was cooled to 0 °C with an ice bath. 2M HCl$_{aq}$ (10 mL) was cooled to 0 °C and added slowly to the reaction mixture, which formed a light yellow precipitate. After stirring for 2 hr at 0 °C, a saturated bromine/water solution (5 mL, 0 °C) was added and allowed to stir for 2 hr, during which the color changed to a blue-green color. The mixture was extracted with DCM (3 x 25 mL), the organic layers dried over MgSO$_4$, and the solvent removed by rotary evaporation. The crude solid was purified by column chromatography (SiO2, 1% MeOH in DCM as eluent) to give 161.4 mg (0.373 mmol, 55%) of blue solid. ^{1}H NMR (400 MHz, CDCl3) δ: 7.70-7.64 (m, br, 4H), 7.57-7.53 (m, br, 2H), 7.49-7.44 (m, br, 4H). ^{13}C NMR (100 MHz, CDCl3) δ: 142.1, 132.1, 132.0, 131.9, 131.8, 128.5, 128.4, 36.3. HRMS (EI) Calcd for C$_5$H$_{12}$N$_4$S$_2$ [M+•]: 432.05034 Found m/z= 432.04988. FTIR (neat) cm^{-1}: 2208, 1525, 1473, 1437. UV-Vis (CHCl$_3$): λ$_{max}$ 683 nm (ε = 37000 M^{-1}cm^{-1}).

References

[1] T.M. Pappenfus; R.J. Chesterfield; C.D. Frisbie; K.R. Mann; J. Casado; J.D. Raff; L.L. Miller *J. Am. Chem. Soc.* **2002**, *124*, 4184-4185

[2] Y.W. Son; M.L. Cohen; S.G. Louie; *Phys. Rev. Lett.* **2006**, *97*, 216803

[3] Y. Morita; S. Nishida; T. Murata; M. Noriguchi; A. Ueda; M. Satoh; K. Arifuku; K. Sato; T. Takui; *Nat. Mater.* **2011**, *10*, 947-951

[4] T.M. Pappenfus; J.D. Raff; E.J. Hukkanen; J.R. Burney; J. Casado; S.M. Drew; L.L. Miller; K.R. Mann *J. Org. Chem.* **2002**, *67*, 6015-6024

[5] R.J. Chesterfield; C.R. Newman; T.M. Pappenfus; P.C. Ewbank; M.H. Haukaas; K.R. Mann; L.L. Miller; C.D. Frisbie *Adv. Mater.* **2003**, *15*, 1278-1282

[6] T. Takahashi, K.-I. Matsuoka; K. Takimiya; T. Otsubo; Y. Aso; *J. Am. Chem. Soc.* **2005**, *127*, 8928-8929

[7] J. Casado; J.T.L. Navarrete *The Chemical Record* **2010**, *11*, 45-53

[8] I. Hoogmartens; P. Adriaensens; D. Vanderzande; J. Gelan; C. Quattrocchi; R. Lazzaroni; J.L. Brédas *Macromolecules* **1992**, *25*, 7347-7356

[9] D. Fazzi; E.V. Canesi; F. Negri; C. Bertarelli; C. Castiglioni *Chem. Phys. Chem.* **2010**, *11*, 3685-3695

10 Z. Zeng; S. Lee; J.L. Zafra; M. Ishida; X. Zhu; Z. Sun; Y. Ni; R.D. Webster; R.-W. Li; J.T.L. Navarrete; C. Chi; J. Ding; J. Casado; D. Kim; J. Wu *Angew. Chem. Int. Ed.* **2013**, *52*, 8561-8565

11 Y. Li; K.-W. Huang; Z. Sun; R.D. Webster; Z. Zeng; C. Chi; K. Furukawa; J. Wu *Chem. Sci.* **2014**, Advance Article DOI: 10.1039/c3sc53015a

12 Y. Li; W.-K. Heng; B.-S. Lee; N. Aratani; J.-L. Zafra; N. Bao; R. Lee; Y.-M. Sung; Z. Sun; K.-W. Huang; R.D. Webster; J.T.L. Navarrete; J. Casado; D.-H. Kim; J. Ding; A. Osuka; J. Wu *J. Am. Chem. Soc.* **2012**, *134*, 14913-14922

13 W.R. Roth; M. Böhm; H.-W. Lennartz; E. Vogel *Angew. Chem. Int. Ed.* **2003**, *22*, 1007-1008

14 G.F. Caramori; K.T. de Oliveira; S.E. Galembeck; P. Bultinck; M.G. Constantino *J. Org. Chem.* **2007**, *72*, 76-85

15 X. Creary; K.M. Miller *Org. Lett.* **2002**, *4*, 3493-3496

16 P.A. Peart; J.D. Tovar *Org. Lett.* **2007**, *9*, 3041-3044

17 P.A. Peart; J.D. Tovar *Macromolecules* **2009**, *42*, 4449-4455

18 B.C. Streifel; P.A. Peart; J.F. Martinez-Hardigree; H.E. Katz; J.D. Tovar *Macromolecules* **2012**, *45*, 7339-7349

19 M. Uno; K. Seto; S.J. Takahashi *J. Chem. Soc. Chem. Comm.* **1984**, 932

20 H.-M. Koepp; H. Wendt; H. Strehlow *Z. Electrochem* **1960**, *64*, 483

21 Z. Sun; K.-W. Huang; J. Wu *J. Am. Chem. Soc.* **2011**, *131*, 11896-11899

22 Y. Li; W.-H. Heng; B.S. Lee; N. Aratani; J.L. Zafra; N. Bao; R. Lee; Y.M. Sung; Z. Sun; K.-W. Huang; R.D. Webster; J.T.L. Navarette; D. Kim; A. Osuka; J. Casado; J. Ding; J. Wu *J. Am. Chem. Soc.* **2012**, *134*, 14913-14922

23 T. Kubo; A. Shimizu; M. Sakamoto; M. Uruichi; K. Yakushi; M. Nakano; D. Shiomi; K. Sato; T. Takui; Y. Morita; K. Nakasuji *Angew. Int. Ed.* **2005**, *44*, 6564-6568

24 D.E. Janzen; M.W. Burand; P.C. Ewbank; T.M. Pappenfus; H. Higuchi; D.A. da Silva Filho; V.G. Young; J.L. Brédas; K.R. Mann *J. Am. Chem. Soc.* **2004**, *126*, 15295-15308

25 S.G. Vulfson Molecular Magnetochemistry, Gordon and Breach Science Publishers, Amsterdan, **1998**

26 R.Kishi; M. Dennis; K. Fukuda; Y. Murata; K. Morita; H. Uenaka; M. Nakano *J. Phys. Chem. C* **2013**, *117*, 21498-21508

27 R.P. Ortiz; J. Casado; V. Hernandez; J.T.L. Navarrete; E. Orti; P.M. Viruela; B. Milian; S. Hotta; G. Zotti; S. Zecchin; B. Vercelli *Adv. Funct. Mater.* **2006**, *16*, 531-536

[28] R.P. Ortiz; J. Casado; S. Rodriguez Gonzales; V. Hernandez; J.T.L. Navarrete; P.M. Viruela; E. Orti; K. Takimiya; T. Otsubo *Chem.-Eur. J.* **2010**, *16*, 470-484

[29] R. West; J.A. Jorgenson; K.L. Stearly; J.C. Calabrese *J. Chem. Soc., Chem. Commun.* **1991**, 1234-1235

[30] Y. Suzuki; M. Shimawaki; E. Miyazaki; I. Osaka; K. Takimiya *Chem. Mater.* **2011**, *23*, 795-804

[31] E.V. Canesi; D. Fazzi; L. Colella; C. Bertarelli; C. Castiglioni *J. Am. Chem. Soc.* **2012**, *134*, 19070-19083

[32] Y. Qiao; Y. Guo; C. Yu; F. Zhang; W. Xu; Y. Liu; D. Zhu *J. Am. Chem. Soc.* **2012**, *134*, 4084-4087

Chapter 5 - Towards Möbius Aromatics for Optoelectronic Materials Applications

Introduction to Möbius Aromaticity

Conducting and semiconducting oligomers and polymers have become popular since Heeger, MacDiarmid, and Shirakawa discovered the unexpected metallic nature of polyacetylene. Due to environmental instability, polyaromatic materials were developed to attenuate some of the atmospheric reactivity and potentially increase electronic device performance. Although these polyaromatic materials represent a broad range of structures, connectivities, and elemental compositions, all of them fall into the category of Hückel aromatics. Except a few unusual structures, the overwhelming majority of these molecules are planar, benzenoid structures (e.g. thiophene, benzene, pyrrole, furan, etc) that follow Hückel's 4n+2 rule of aromaticity. As of the writing of this document, there have been no published instances of using Möbius aromatics (4n, with a half-twist) for optoelectronic devices. However, significant research has been directed towards understanding Möbius aromaticity in general. The work of Rainer Herges in particular has been instrumental in understanding the theoretical, synthetic, and experimental aspects of Möbius aromatics.[1] Most interesting of Herges work is his combination of 'normal' aromatics with 'belt-like' aromatics to form p-conjugated structures with a built-in half-twist.[2] Möbius aromatics are characterized by adopting a half-twist that allows previously 4n Hückel antiaromatic molecules to adopt a stabilized aromatic geometry. The Frost circle mnemonic (Figure 5.1) for 4n-annular systems shows the difference in stabilization for Hückel versus Möbius geometries.

Hückel Annulenes

secular equation

$$E_j = \alpha + 2\beta \cos \frac{2\pi j}{N}$$

N: number p-orbitals
E_j: π MO energies
j = 0,1,2,3 ⋯ (N-1)
α : Coulomb integral
β : Resonance integral

hypothetical planar cyclooctatetraene
(open shell)

Möbius Annulenes

secular equation

$$E_j = \alpha + 2\beta \cos \frac{\pi(2j+1)}{N}$$

hypothetical Möbius cyclooctatetraene
(closed shell)
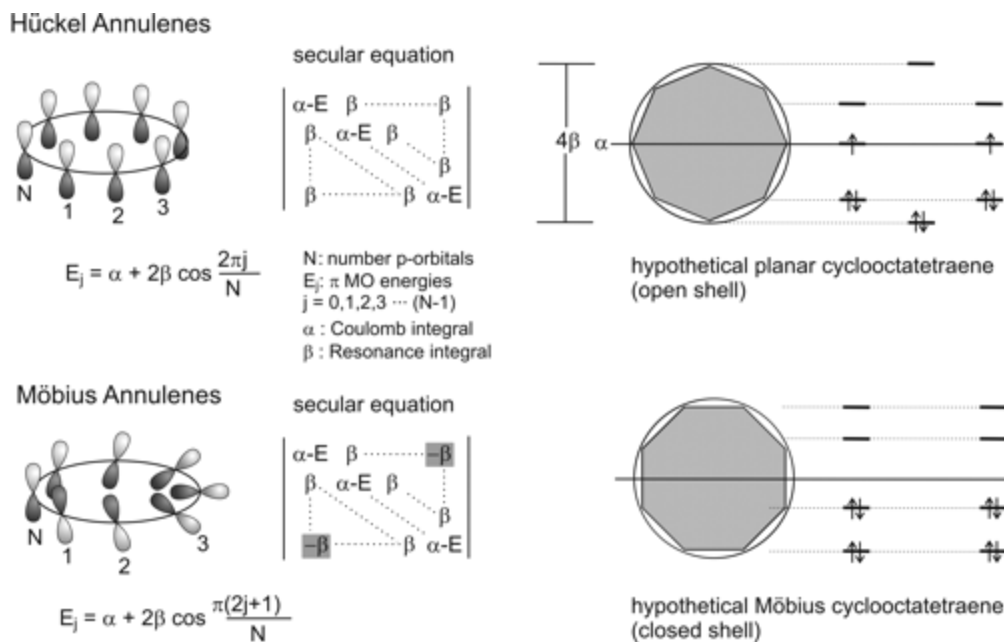
Figure 5.1. Orbital diagrams, secular matrices, and Frost circle diagrams describing the stability gained in 4n annulenes with a Möbius topology.

This typically can only occur for molecules of sufficient size such that a half-twist does not induce significant strain. Figure 5.2 illustrates this by showing relative energy differences of various [n]-annulenes in the most stable Hückel and Möbius conformations. Unsurprisingly, Möbius-benzene (M-benzene) is significantly higher in energy than Hückel benzene (H-benzene). This difference between M- and H-[n]-annulene forms decreases as the value of n increases, due to the larger rings' ability to adopt a relatively unstrained, half-twisted conformation. Shrinking energetic gaps notwithstanding, the annulenes from [6]-[20] are more stable in a planar conformation. Herges and coworkers approached this problem synthetically and were able to make the first example of a stable Möbius aromatic.[3]
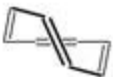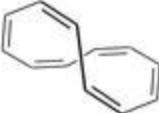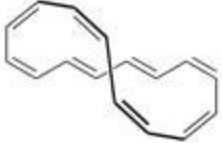
Figure 5.2. Relative energies of the most stable Hückel and Möbius isomer of [6]-, [8]-, [12]-, [16]-, and [20]-annulene calculated at B3LYP/6-31G* level of DFT.

Also worthy of note is the work done on expanded porphyrin systems by the groups of Kobayashi, Kim, Osuka, and Latos-Grazynski.[4, 5] These systems are large [28]hexaphryn systems that have been characterized as relatively "floppy" in the literature (Figure 5.3). The authors were able to use selective crystallization (via careful choice of solvents) to unambiguously assign Möbius structures to the expanded porphyrin systems. Theoretical calculations confirmed that these systems had low energy Möbius conformations, but both theory and experiment suggest that these half-twist states are short lived and in equilibrium with planar Hückel-like conformers.
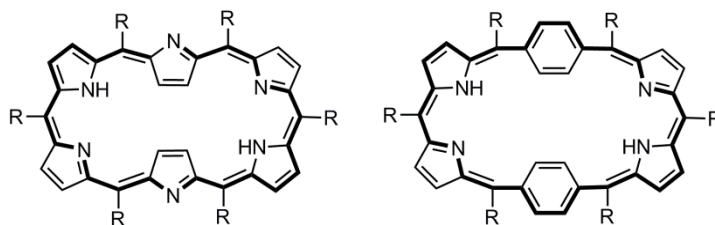
Figure 5.3. Examples of [28]hexaphryn (left) and [28]-di-*p*-benzihexaphryn (right) with Möbius π-electron pathways in bold. R = phenyl, mesityl, or perfluorophenyl.

The academically interesting nature of Möbius aromatics aside, the aforementioned molecules seem to have little to offer in terms of materials utility. Because organic electronic devices operate by transporting charge carriers, a more ideal Möbius system will be able to tolerate oxidative or reductive processes while maintaining its stabilized aromatic nature. Similar to the Hückel analogy of tropyllium cation, P. von R. Schleyer found that cyclononatetraenyl cation, adopts a surprisingly stable half-twist conformation (Figure 5.4)[6,7] upon formation and is stable for a short period of time even in aqueous conditions, before reacting further to form a [4.3]-bicyclic ring system.[8] Although this is not an isolable molecule, there is promise that this could lower oxidation potentials of bulk semiconductors and perhaps alter charge-transport characteristics. An interesting option for this system is the use of small molecule transient cationic species generated by thermolysis to introduce charge carriers in a semiconducting material across a temperature gradient.
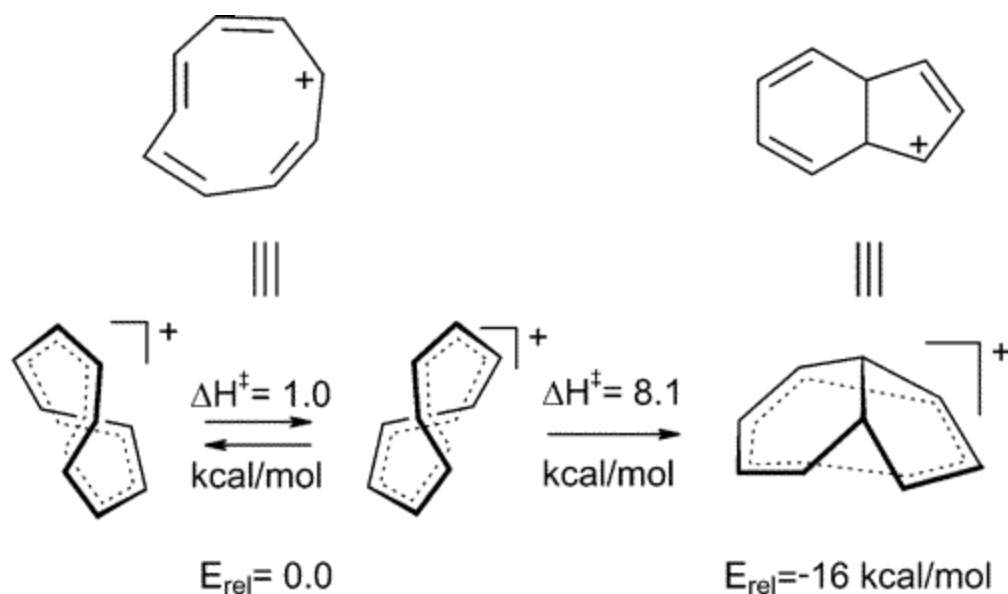
Figure 5.4. DFT calculated structures for the Schleyer $C_9H_9^+$ system showing Möbius half-twist. Adapted from Reference 7.

Few systems are capable of attaining aromaticity upon oxidation or reduction. One closely related example is poly(isothianaphthene) (PITN) where the thiophene portion loses aromaticity upon adopting a quinoidal structure, but the attached ring gains aromaticity in the process. This trait places PITN in the class of low bangap polymers that exhibit high conductivities and low oxidation potentials.[9] Perhaps a cyclononatetraenyl cationic system can exhibit a similar tendency towards low oxidation potentials and efficient charge transport.

Some potential difficulties in realizing Möbius aromatic are readily apparent. The planarity of Hückel aromatics certainly aids in both inter- and intramolecular charge transport, as conjugated systems can align with quadrupolar forces to form crystalline organic conductors. There has been no work done on the bulk behavior of Möbius aromatics, and thus will require significant study should any candidate molecules be successfully synthesized. It is unlikely that any Möbius aromatic will posses more aromatic

stabilization than a Hückel aromatic due to the required twist and overall preference for π-systems to adopt a planar structure. The inability of a molecule to adopt a half-twist conformation in the solid state also remains to be proven. This does not mean, however, that these molecules cannot be studied with specific applications in mind.

Synthetic Development of Möbius Aromatic Small Molecules

A brief retrosynthetic outline below (Figure 5.5) shows possible routes to obtaining the molecules required to form functionalized cyclononatetraenyl cationic species. These routes include several different methods of reaching 1,5-diphenylcyclooctatetraene (1,5-Ph$_2$-COT), including Heck couplings, ring-closing metathesis, and addition-elimination schemes (listed as general alkene formation). These routes seek to take advantage of the rich alkene chemistry known in the literature. The 1,5-disubstituted COT isomer was selected because it results in two distinct alkenes, which may be selectively targeted for cyclopropanation. A 1,3-disubstituted COT, for example, would have less symmetry and could prove more synthetically challenging. Multiple routes were investigated to determine an optimum route to scalable routes that yield amounts of material suitable for solution and solid-state testing of the initial materials. Initial attempts were only concerned with oligomeric species as a proof of principle for π-electron-expanded cyclononatetraenyl cationic systems, specifically containing phenyl groups. These pendant phenyl groups give a handle for further functionalization and incorporation into polymeric systems. They also serve as placeholders for more commonly used aromatics, such as thiophene, furan, etc.
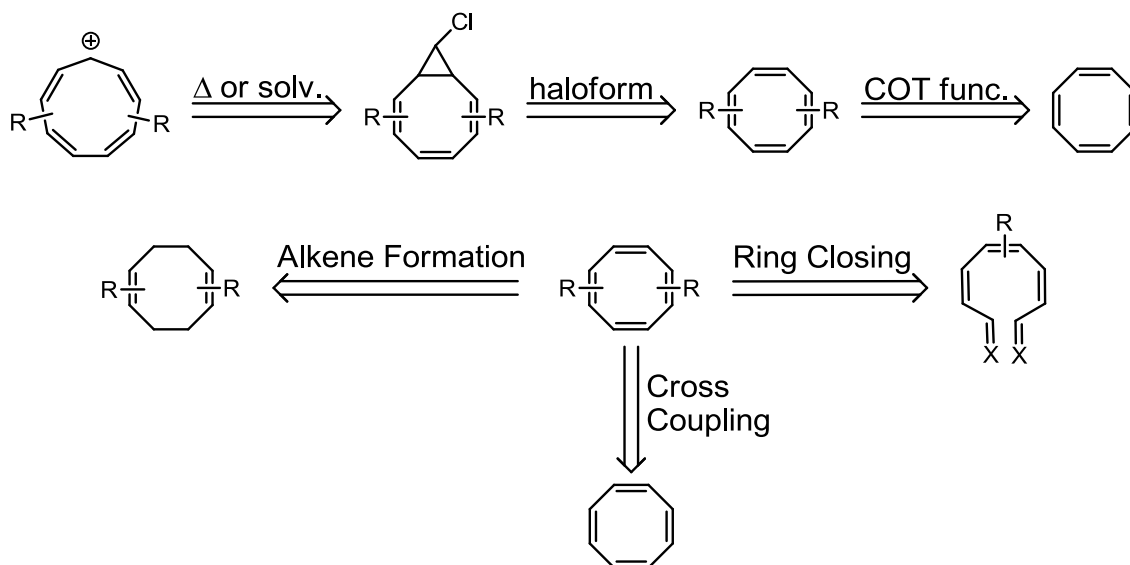
Figure 5.5. Retrosynthetic scheme detailing potential routes to difunctionalized $C_9H_9^+$ Möbius aromatic intermediates. R = phenyl.

Multiple attempts to synthesize various 1,5-diaryl-1,5-cyclooctadienes (1,5-Ar$_2$-COD) and 1,5-diaryl-1,3,5,7-cyclooctatetraenes (1,5-Ar$_2$-COT) through Heck couplings were unsuccessful. Both the di- and tetraene are known to be good bidentate ligands and therefore are undesirable substrates for palladium-catalyzed cross coupling reactions. Another route to 1,5-diaryl-COT derivatives was designed, borrowing from available literature sources and incorporating new methodology as necessary.

Starting with 1,5-cyclooctadiene (COD), the addition of two equivalents of bromine yields the desired compound 1,2,5,6-tetrabromocyclooctane (Scheme 5.1). Precipitation from dichloromethane by addition of hexanes gives pure product in 33% yield, somewhat in contrast to the literature yield of 86%.[10] The tetrabrominated product was then subjected to basic elimination conditions, resulting in primarily 1,5-dibromo-1,5-cyclooctadiene after recrystallization from methanol in 27% yield.[11] Some 1,6-dibromo-1,5-cyclooctadiene was apparent in the crude product by ^{1}H NMR, but this compound was removed during purification. It should be noted that there is no inherent preference by the author of this

report, it just so happened that the 1,5-dibromo product was more readily obtained. In the future, the 1,6-dibromo product may also be investigated for the sake of comparing the two regioisomers. A Kumada-type cross-coupling was then performed on the divinyl-dihalide to yield 1,5-diphenyl-1,5-cyclooctadiene.[12] After purification by column chromatography (SiO$_2$, hexanes), the product was isolated as a light yellow oil in a 28% yield.
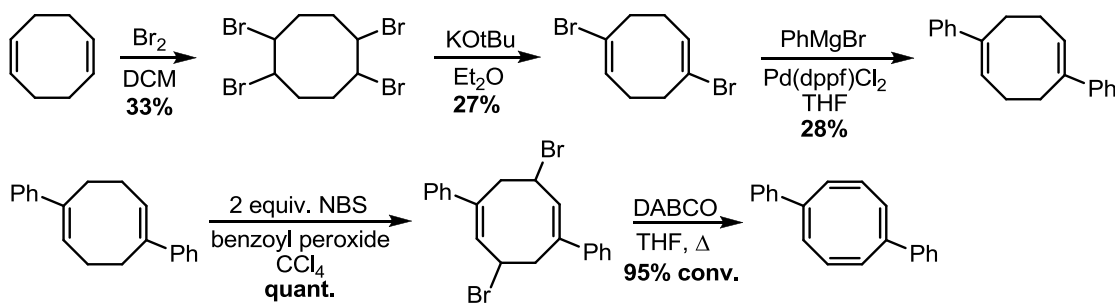
Scheme 5.1. Synthetic scheme for the synthesis of 1,5-diphenyl-COT.

At this point, significant work was done following a synthetic preparation of COT from COD in one step using a lithiation-oxidation-elimination scheme developed by the Edelmann group (Scheme 5.2).[13] This preparation successfully converted the unsubstituted diene to the tetraene in a one-pot reaction. COD was treated with two equivalents of n-butyllithium and N,N,N,N-tetramethylethylenediamine (TMEDA) at -78°C, and then quenched with di-*tert*-butyl peroxide. The cyclooctyl-dianion is assumed to attack the peroxide, creating a t-butyl ether and one equivalent of t-butoxide. This can subsequently undergo elimination to form the cyclooctatetraene product. However, no such diphenyl-tetraene product was formed in repeated trials at different temperatures, even after the addition of *tert*-butyllithium/TMEDA. After repeated attempts to modify the reaction conditions proved unsuccessful, a deuterium-quenching study was performed. Aliquots of the reaction were taken after addition of *t*-butyllithium, TMEDA, and di-*tert*-butyl peroxide, and immediately quenched with d_4-methanol. After removal of solvent, ^{1}H NMR spectra were taken and it was

noticed that all three stages of the reaction yielded the same molecule. None of the olefinic proton resonances were affected in either shift or splitting pattern, rather the phenyl portion of the spectrum showed changes in both splitting, shift, and integration values, although it was not readily apparent which aryl proton was replaced with a deuterium atom. Given this evidence, this particular method was abandoned.
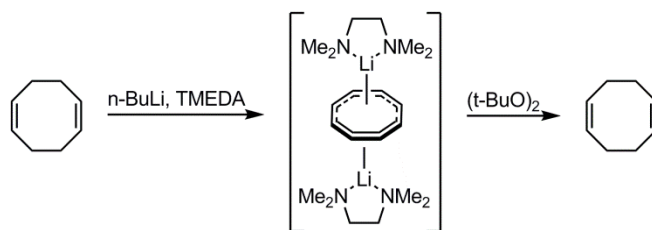
Scheme 5.2. Edelmann synthesis of COT from 1,5-COD using *n*-butyllithium, TMEDA, and di-*tert*-butoxide.

Being that 1,5-diphenyl-1,5-COD has two distinct allylic positions, and thinking along the lines of the same elimination reactions used previously in the synthesis, a radical bromination and subsequent elimination scheme was designed. Reacting the diene with exactly two equivalents of N-bromosuccinimide (NBS) and twenty mole percent benzoyl peroxide in CCl_4 at reflux yielded the indicated product in quantitative yield, although further purification proved difficult. The diallyl-dibromide compound was found to disintegrate on silica and was not stable to recrystallization from ethanol, but the reaction runs cleanly enough to yield approximately 95% pure material after an extractive workup. The specific location of bromine substitution was confirmed by ^{1}H, and ^{13}C NMR spectra. The ^{1}H NMR spectrum (Figure 5.6) reveals a symmetric substitution pattern, with a doublet (a) at 6.10 ppm and a triplet (c) at 4.13 ppm, which can only arise from 3,7-dibromo-1,5-diphenyl-cycloocta-1,5-diene of the various possible regioisomers.
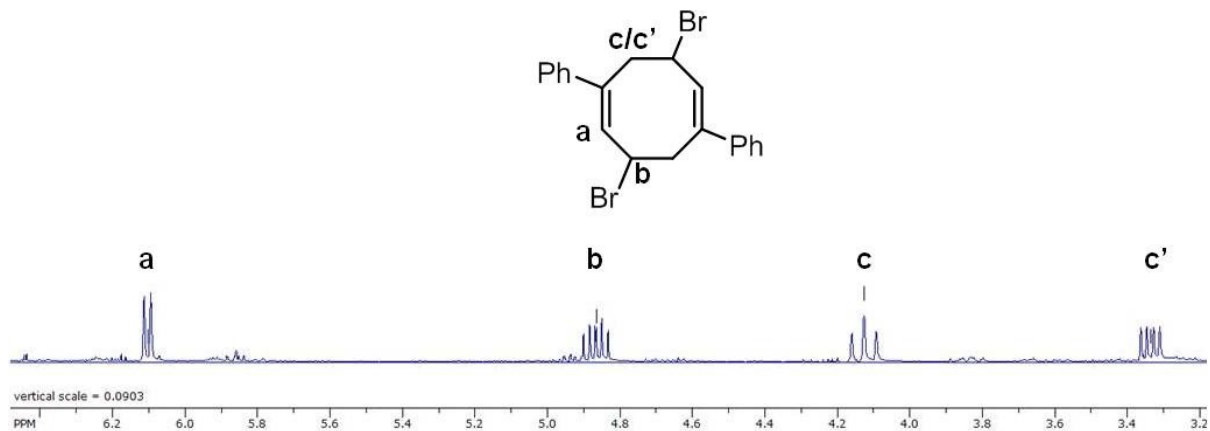
Figure 5.6. ^{1}H NMR spectrum (400 MHz, CDCl$_3$) of 3,7-dibromo-1,5-diphenyl-cycloocta-1,5-diene.

This dibromo-diphenyl-COD derivative was subjected to conditions identical to the synthesis of 1,5-dibromo-1,5-COD (KOtBu in diethyl ether) in order to effect an elimination, but no product was formed and the starting material was destroyed in the process. Several tertiary amines were then screened as bases suitable to cause elimination to occur. Eight equivalents of base (Et$_3$N, DABCO, and 2,4,6-trimethylpyridine) were added to one equivalent of 3,7-dibromo-1,5-diphenyl-1,5-COD and stirred at ambient temperature in dry THF. Neither triethylamine nor 2,4,6-trimethylpyridine showed any reaction, but DABCO showed slight formation of product and after setting up another reaction, this time at reflux overnight, nearly complete conversion of starting material to 1,5-diphenyl-1,3,5,7-COT by NMR integration. Attempts at purification on silica gel also resulted in the loss of the compound, but a small portion was submitted for nominal mass spec. ^{13}C NMR was taken of the crude material, but there were enough impurities to make the spectrum unassignable. The olefinic portion of the ^{1}H spectrum however agrees with literature data for this molecule, although slight shift and *J* value differences are reported (Figure 5.7).[14] It's worthwhile to note that the synthetic scheme in the Miller report is a 10-step process from 1,5-COD and for this reason time was spent developing a new 5-step route to disubstituted-COT

derivatives. Except for the final elimination, all steps have been performed on a multi-gram

scale, albeit with a few low-yielding reactions.
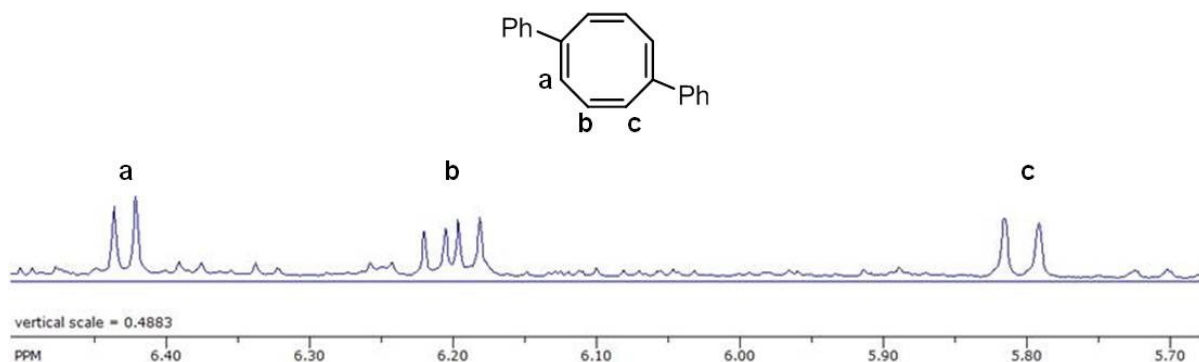
Figure 5.7. ^{1}H NMR spectrum (400 MHz, CDCl$_3$) of crude 1,5-diphenyl-cycloocta-1,3,5,7-

tetraene.

Conclusions

Progress was made towards Möbius aromatic cationic intermediates based on a

disubstituted cyclononatetraenyl cation. The synthesis made use of literature precedent set

by Miller, but devised a new iterative bromination-elimination scheme using NBS and

various bulky bases to effect the desired transformations. 1,5-Diphenyl cyclooctatetraene

was successfully synthesized and characterized by ^{1}H NMR and HR-MS, but the compound

proved difficult to purify. Further synthetic work will need to explore cyclopropanation

conditions of Ph$_2$-COT and the subsequent thermolysis/solvolysis reactions. Kinetics

experiments and *in silico* models will be necessary for confirmation of a Möbius-type

intermediate of the disubstituted cyclononatetraenyl cationic species. If a Möbius

intermediate is feasible under thermolysis conditions, the molecule may be incorporated into

the backbone of a conjugated polymer, or it may be used as an additive/dopant. One

interesting idea is the creation of a thermal doping gradient across a polymeric

thermoelectric generator to alter the bandgaps of the material and affect the phonon-charge carrier interactions in the device.

Experimental

General Methods:

All column chromatography solvents were distilled technical grade from Sigma Aldrich. All palladium catalysts were obtained from Strem Chemical and used as received. 2-tributylstannylthiophene, *n*-butyllithium, 1,5-cyclooctadiene, bromine, benzoyl peroxide, and toluene were obtained from Sigma Aldrich and used as received, except for toluene, which were dried over 4Å molecular sieves and sparged for 0.5-1 h with dry N_2. *N*-bromosuccinimide (NBS) was obtained from Acros and was recrystallized from deionized water before use. THF was obtained from an Innovative Technologies solvent purification system and stored over 4Å molecular sieves under N_2. 1,5-dibromo-1,5-cyclooctadiene[10] and 1,5-diphenyl-1,5-cyclooctadiene[11] was synthesized according to literature procedures.

NMR Spectroscopy:

All ^1H and ^{13}C NMR spectra were recorded in $CDCl_3$ or *o*-dichlorobenzene (*o*-DCB) (Cambride Isotope Laboratories) on a Bruker Avance 400 MHz instrument, and data were collected with either Bruker Topspin V.1.3 or 2.1, unless otherwise noted. Data were processed with either Topspin V.2.1 or SpinWorks V.3.1.7.0 (2010, University of Manitoba). All ^1H spectra were calibrated against either residual protiochloroform (7.26 ppm) or TMS (0.00 ppm) in the deuterated solvent. ^{13}C spectra were calibrated against the $CDCl_3$ triplet (77.23 ppm).

3,7-dibromo-1,5-diphenyl-1,5-cyclooctadiene

1,5-Diphenyl-1,5-cyclooctadiene (1.0050 g, 3.841 mmol), N-bromosuccinimide (1.3672 g, 7.681 mmol), and benzoyl peroxide (0.1861 g, 0.768 mmol) were added to a round bottom flask charged with a stir bar. CCl_4 (200 mL) was added and the mixture heated to reflux while stirring for 45 minutes, at which point the mixture is allowed to cool to ambient temperature. The mixture was diluted with hexanes (200 mL) and extracted with DI water (3 x 100 mL) and brine (1 x 100 mL). The organic layer was dried over $MgSO_4$ and the solvent removed. The resulting waxy orange solid (1.7338 g, quant.) is ~95% pure by ^{1}H NMR integration and is used without further purification. The compound appears to disintegrate on silica. ^{1}H NMR (400 MHz, CDCl$_3$) δ: 7.36-7.28 (m, br, 10H), 6.10 (d, J = 8.2 Hz, 2H), 4.87 (m, 2H), 4.12 (t, J = 13.9 Hz, 2H), 3.33 (dd, J = 13.9, 5.6 Hz, 2H). HR-MS (EI): Calcd for $C_{20}H_{17}{}^{79}Br^{81}Br$: 416.96765 [M-H$^+$] Found m/z= 416.96916.

1,5-diphenyl-1,3,5,7-cyclooctatetraene

3,7-Dibromo-1,5-diphenyl-1,5-cyclooctadiene (25 mg, 0.0598 mmol), 1,4-diazabicyclo[2.2.2]octane (53.7 mg, 0.478 mmol), and dry, air free THF (5 mL) were added to a N$_2$-purged 25 mL round bottom flask charged with a stir bar and fitted with a reflux condenser. The mixture was heated to reflux and stirred for 20 h before being allowed to cool to ambient temperature. The solvent was removed from the crude product, which appeared to reach 95% conversion and degraded on silica gel in hexanes. ^{1}H NMR (400 MHz, CDCl$_3$) δ: 7.5-7.1 (m, 10H), 6.43 (d, J = 6.1 Hz, 2H), 6.20 (dd, J = 6.1, 9.5 Hz, 2H), 5.80 (d, J = 9.5 Hz, 2H). NMR characterization data agrees with literature values.[15] HR-MS (EI): Calcd for $C_{20}H_{16}$: 256.12520 [M+H$^+$] Found m/z= 256.12444.

References

[1] Herges, R., *Chem. Rev.*, **2006**, *106*, 4820

[2] D. Ajami; O. Oekler; A. Simon; R. Herges *Nature*, **2003**, *426*, 819-821

[3] Ajami, D., Hess, K., Köhler, F., Nather, C., Oeckler, O., Simon, A., Yamamoto, C., Okamoto, Y., Herges, R., *Chem.-Eur. J.*, **2006**, *12*, 5434

[4] Kobayashi, N., Kim, D., Osuka, A., et al, *J. Am. Chem. Soc.*, **2008**, *130*, 13568

[5] Stepien, M., Latos-Grazynski, L., Sprutta, N., Chwalisz, P., Szterenberg, L., *Angew. Chem. Int. Ed.*, **2007**, *46*, 7869

[6] M. Mauksch; V. Gogonea; H. Jiao; P. v.R. Schleyer *Angew. Chem. Int. Ed.* **1998**, *37*, 2395

[7] R. Herges *Chem. Rev.* **2006**, *106*, 4820-4842

[8] Barborak, J.C., Su, T.-M., Schleyer, P. von. R., *J. Am. Chem. Soc.*, **1971**, *93*, 279

[9] Rasmussen, S.C., Pomerantz, M., Ch. 12., *Handbook of Conducting Polymers 3rd Edition* (Eds. Skotheim and Reynolds), CRC Press, New York, **2007**.

[10] B.R. Varga; M. Kallay; K. Hegyi; S. Beni *Chem. Eur. J.* **2012**, *18*, 822-828

[11] H. Detert; B. Rose; W. Mayer; H. Meier *Chemische Berichte* **1994**, *127*, 1529-1532

[12] K. Asato; K. Ueyama; T. Hayashi *Org. Lett.* **2005**, *7*, 5889-5892

[13] J. Gottfriedsen; A. Miloslavina; F.T. Edelmann *Tet. Lett.* **2004**, *45*, 3583-3584

[14] M. Lyttle; A. Streitweiser; M.J. Miller *J. Org. Chem.* **1989**, *54*, 2331-2335

[15] M.H. Lyttle; A. Streitweiser; M.J. Milller *J. Org. Chem.* **1989**, *54*, 2331-2335

Chapter 6 – Appendix: Additional Spectra
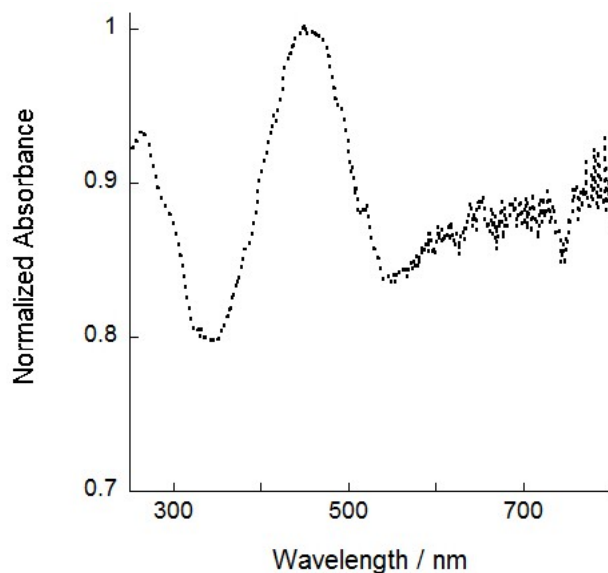
Figure A1. UV-Vis spectrum of No Tail PTMT in CHCl$_3$ at RT.
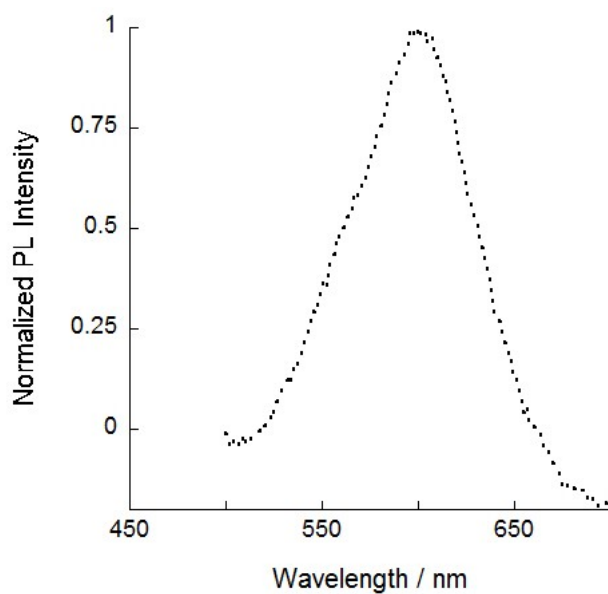
Figure A2. Photoluminescence spectrum of No Tail PTMT in CHCl$_3$ at RT.
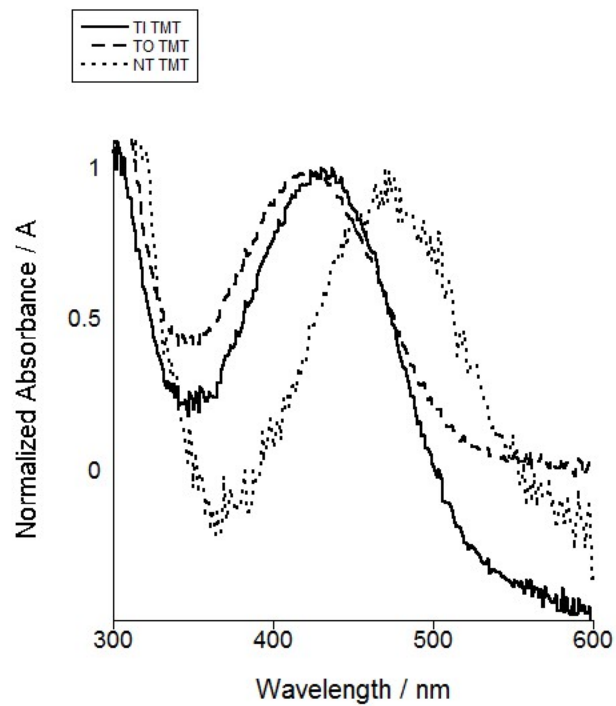
Figure A3. UV-Vis spectrum of the PTMT series on PEDOT:PSS/glass slides at RT.
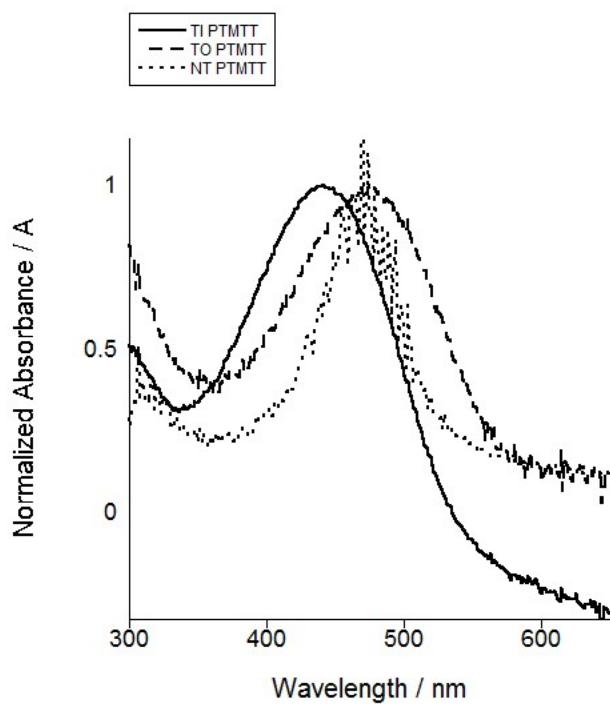
Figure A4. UV-Vis spectrum of the PTMT-T series on PEDOT:PSS/glass slides at RT.
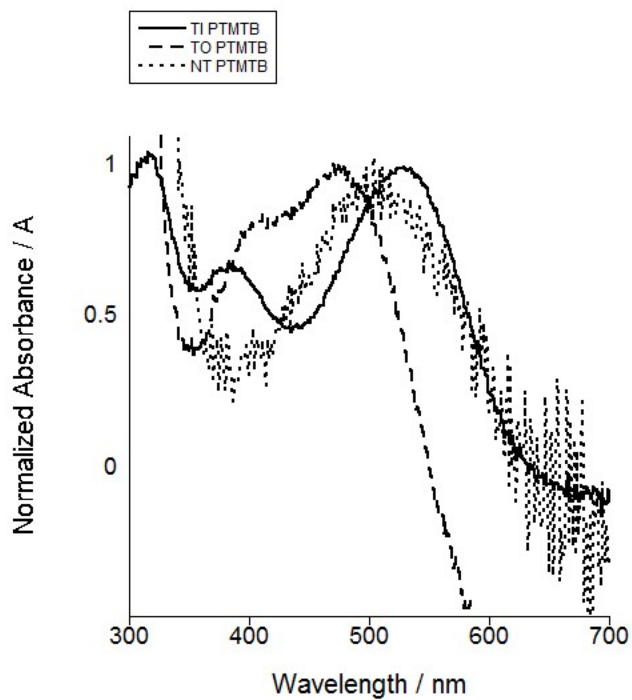
Figure A5. UV-Vis spectrum of the PTMT-B series on PEDOT:PSS/glass slides at RT.
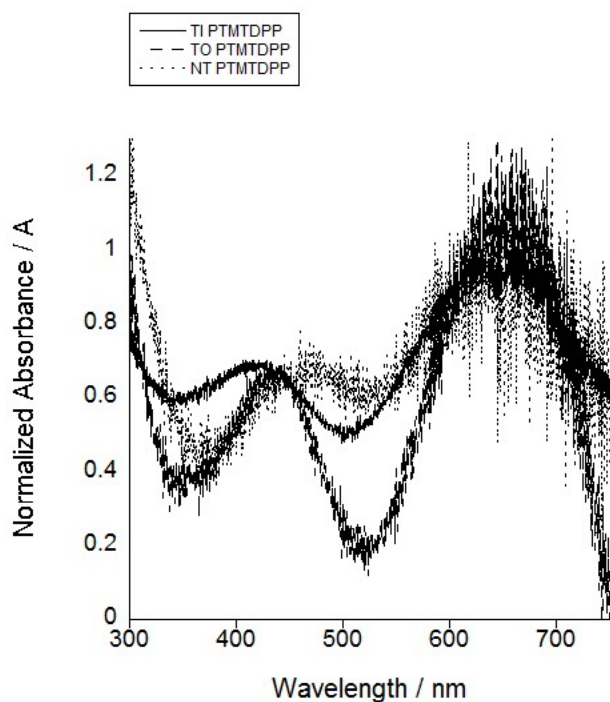
Figure A6. UV-Vis spectrum of the PTMT-DPP series on PEDOT:PSS/glass slides at RT.
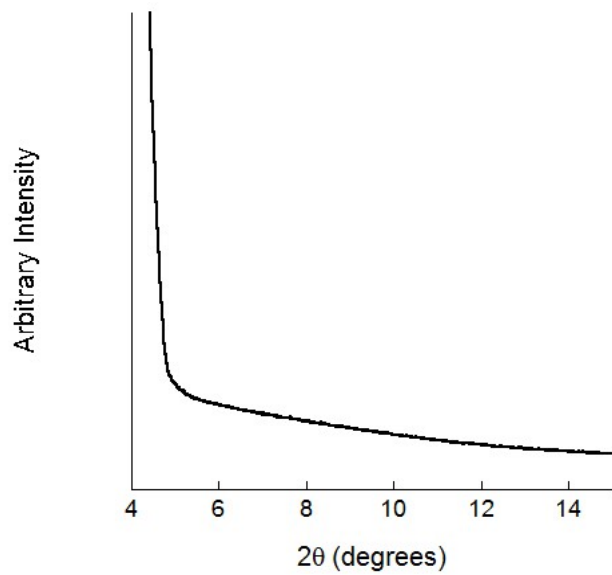
Figure A7. Thin film XRD of Tail Out PTMT.
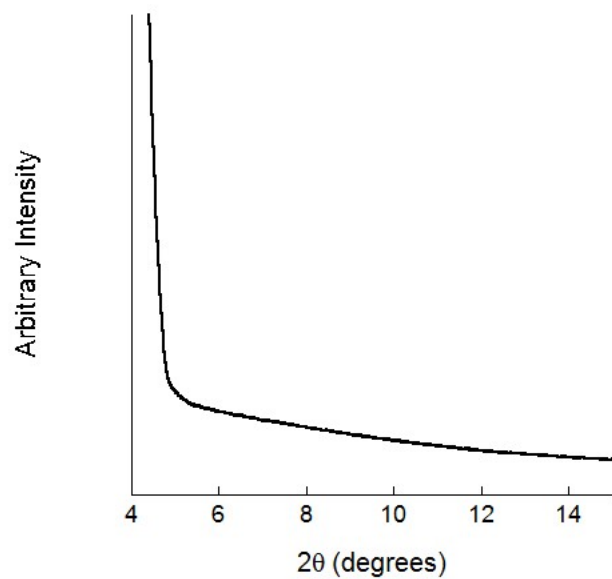
Figure A8. Thin film XRD of Tail In PTMT.
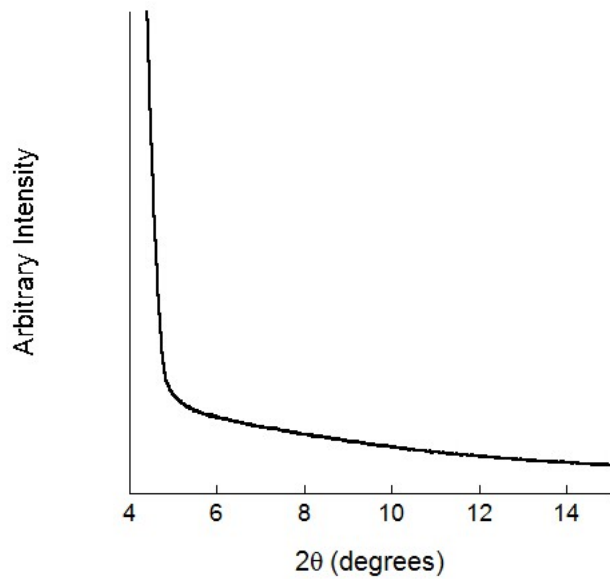
Figure A9. Thin film XRD of No Tail PTMT.
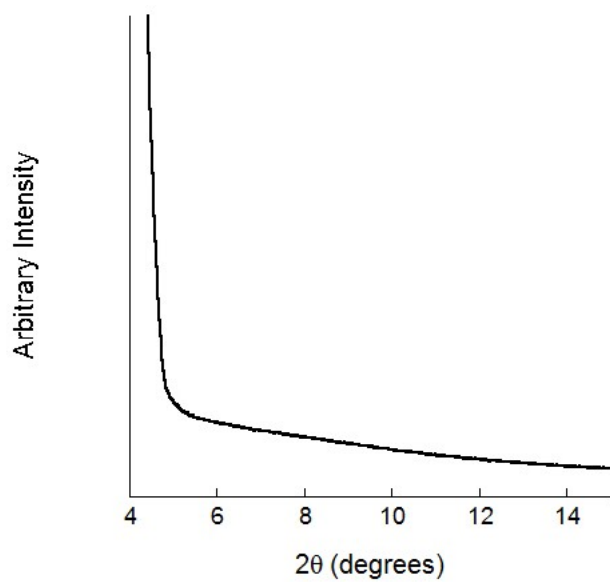
Figure A10. Thin film XRD of Tail Out PTMT-T.
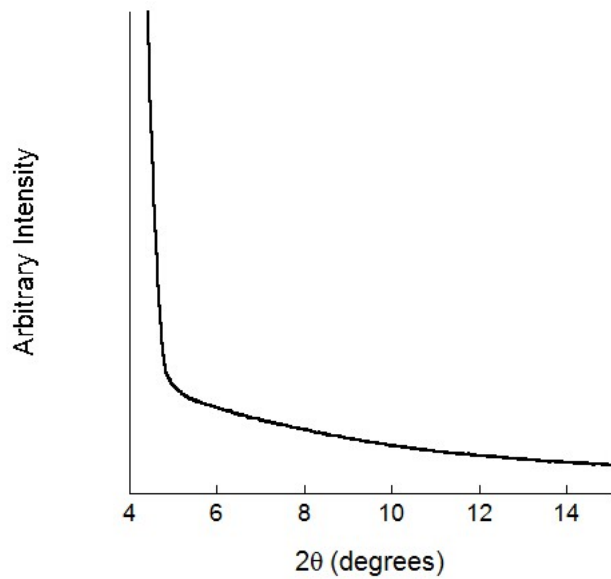
Figure A11. Thin film XRD of Tail In PTMT-T.
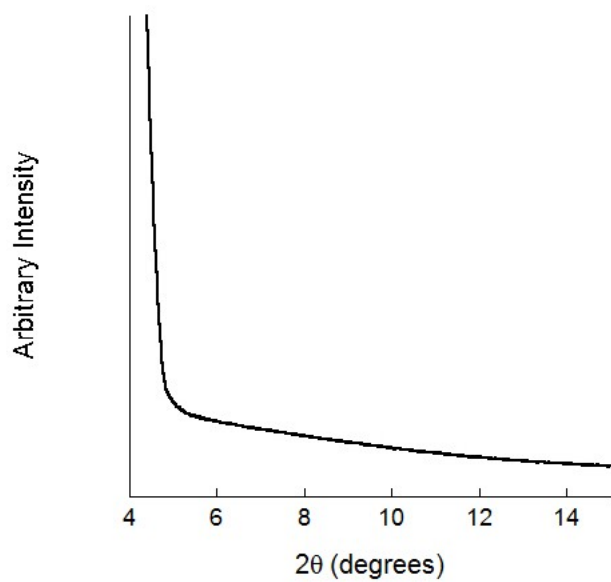
Figure A12. Thin film XRD of No Tail PTMT-T.

149
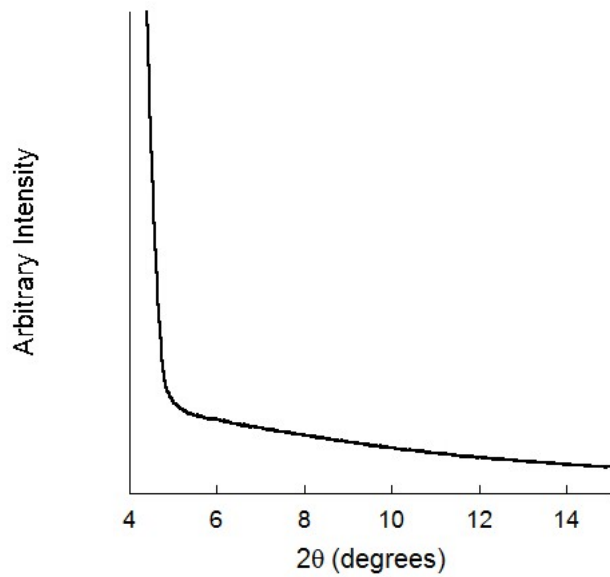
Figure A13. Thin film XRD of Tail Out PTMT-B.
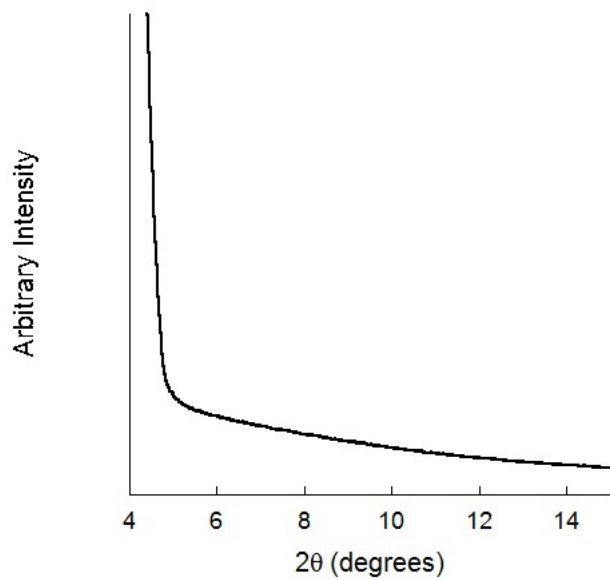
Figure A14. Thin film XRD of Tail In PTMT-B.
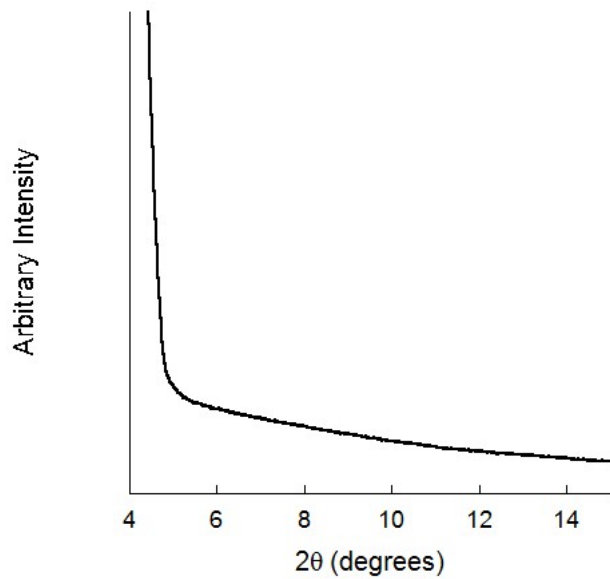
Figure A15. Thin film XRD of No Tail PTMT-B.
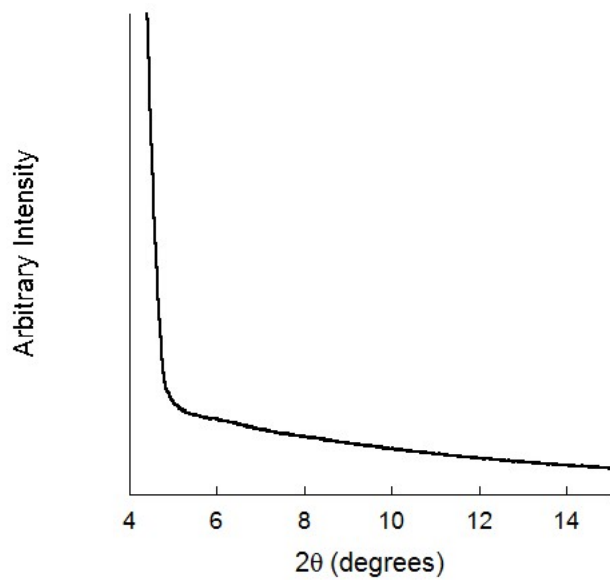
Figure A16. Thin film XRD of Tail Out PTMT-DPP.
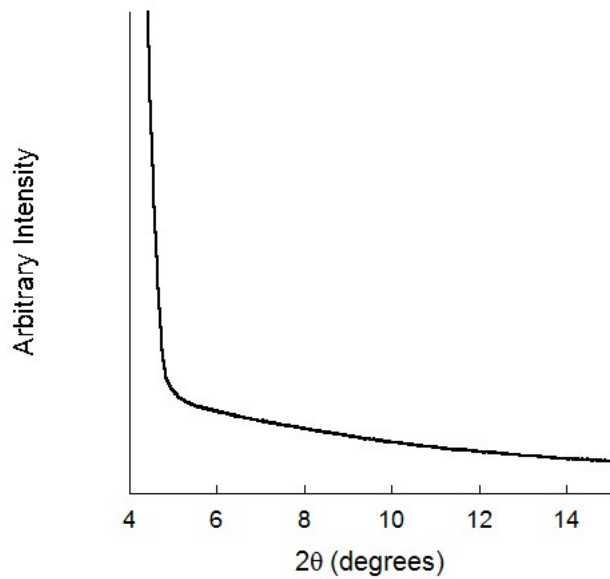
Figure A17. Thin film XRD of Tail In PTMT-DPP.
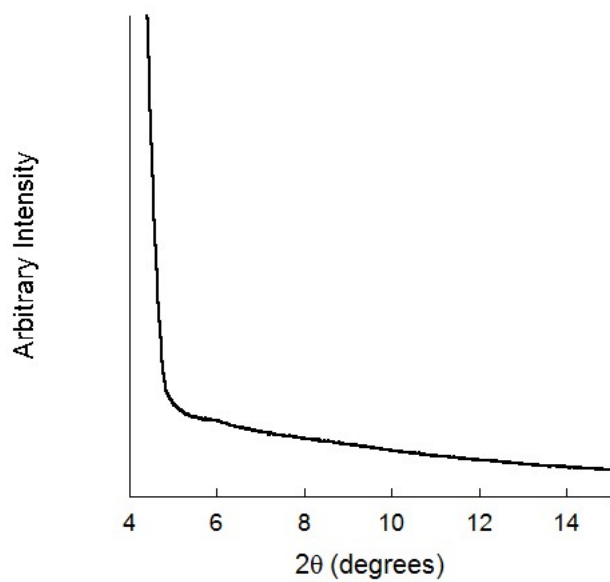
Figure A18. Thin film XRD of No Tail PTMT-DPP.
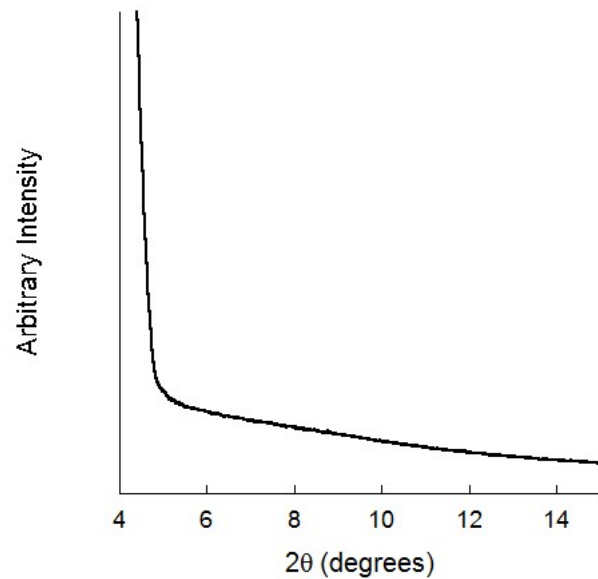
Figure A19. Thin film XRD of a 1:1 blend of Tail In PTMT-B and $PC_{61}BM$ (wt:wt).
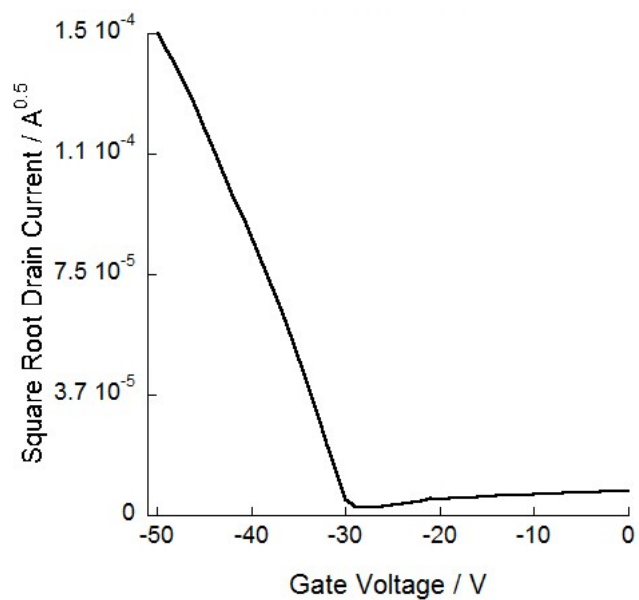
Figure A20. Sq. rt. drain current versus gate voltage for Tail Out PTMT-DPP OFET device.
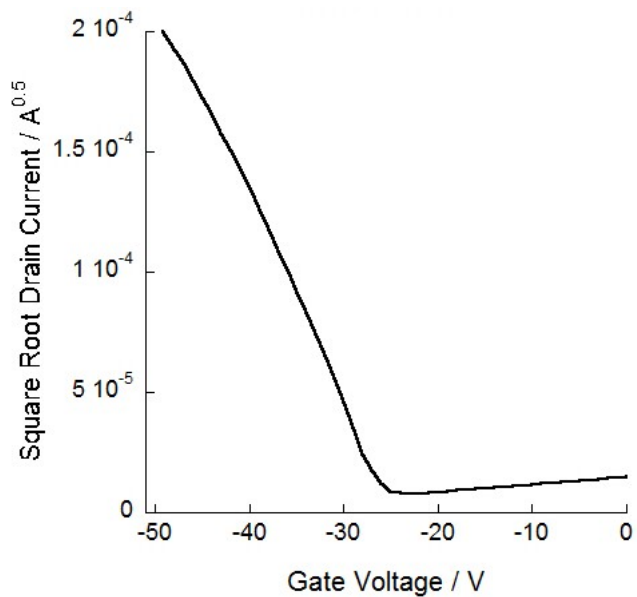
Figure A21. Sq. rt. drain current versus gate voltage for No Tail PTMT-DPP OFET device.
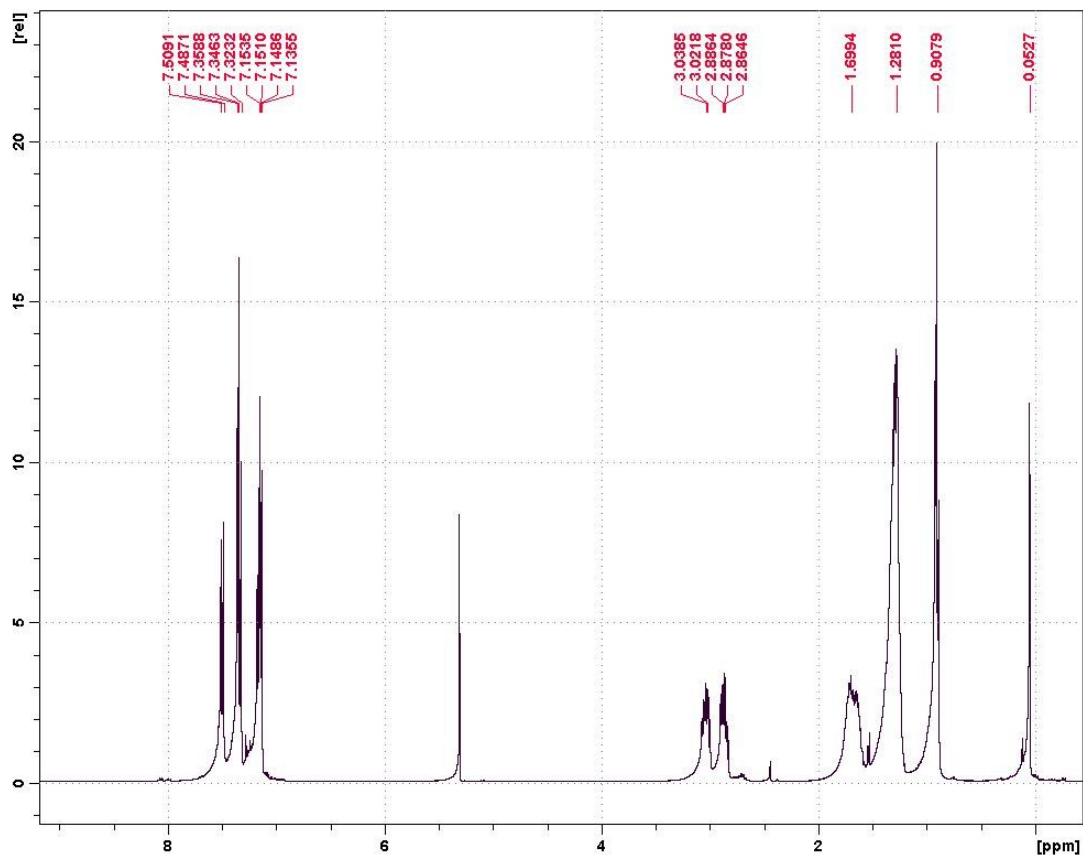
Figure A22. ^{1}H NMR of Tail Out TMT (400 MHz, CDCl$_3$).
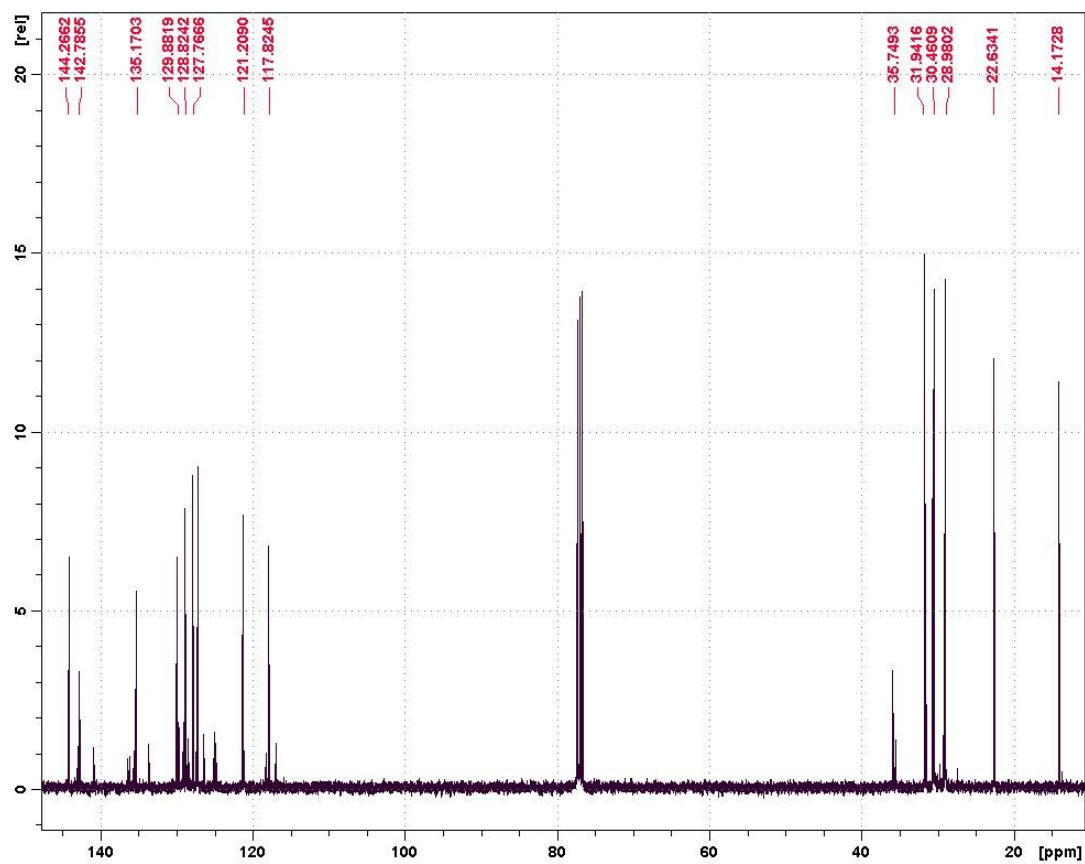
Figure A23. ^{13}C NMR of Tail Out TMT (100 MHz, CDCl$_3$).

Figure A24. ^{1}H NMR of Tail In TMT (400 MHz, CDCl$_3$).
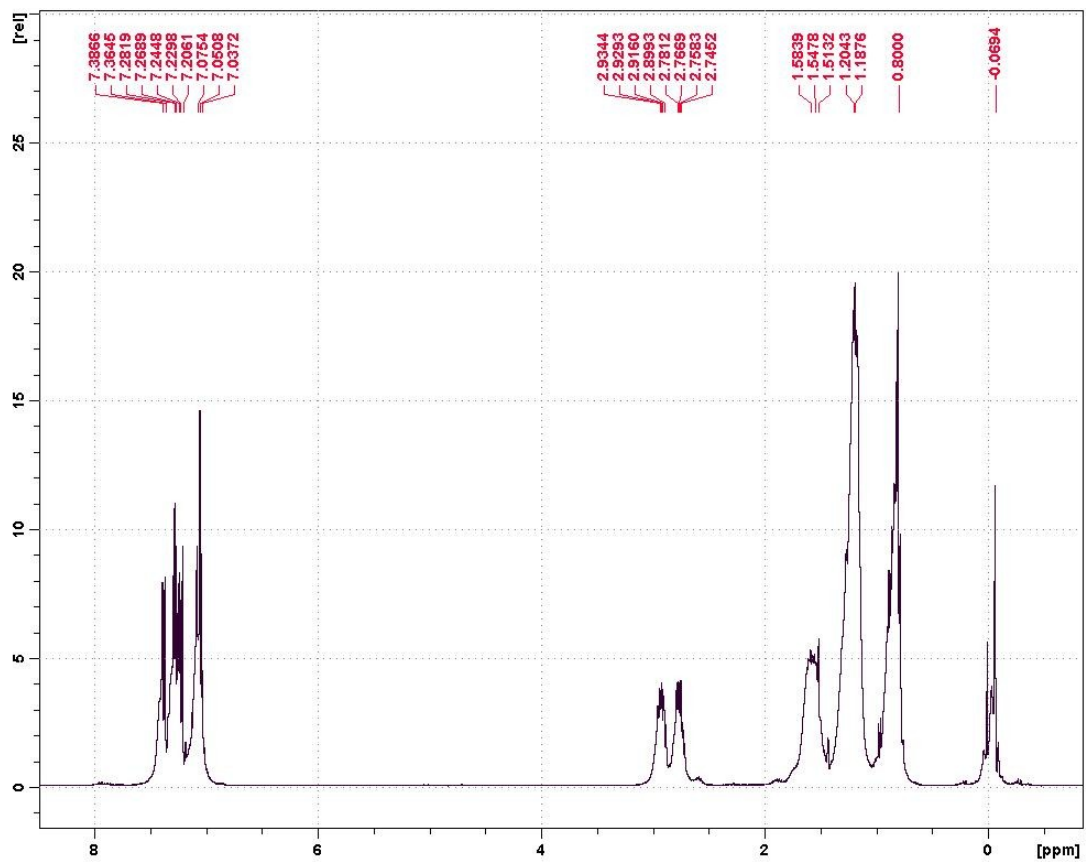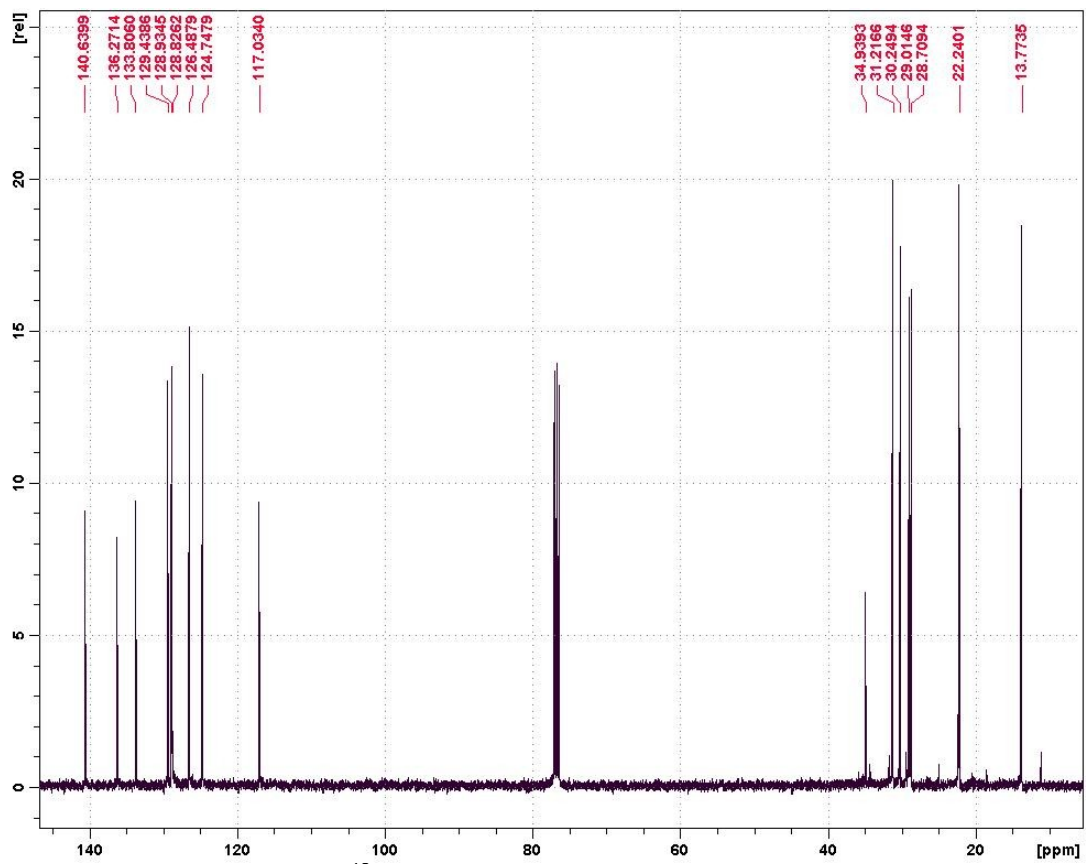
Figure A25. ^{13}C NMR of Tail In TMT (100 MHz, CDCl$_3$).
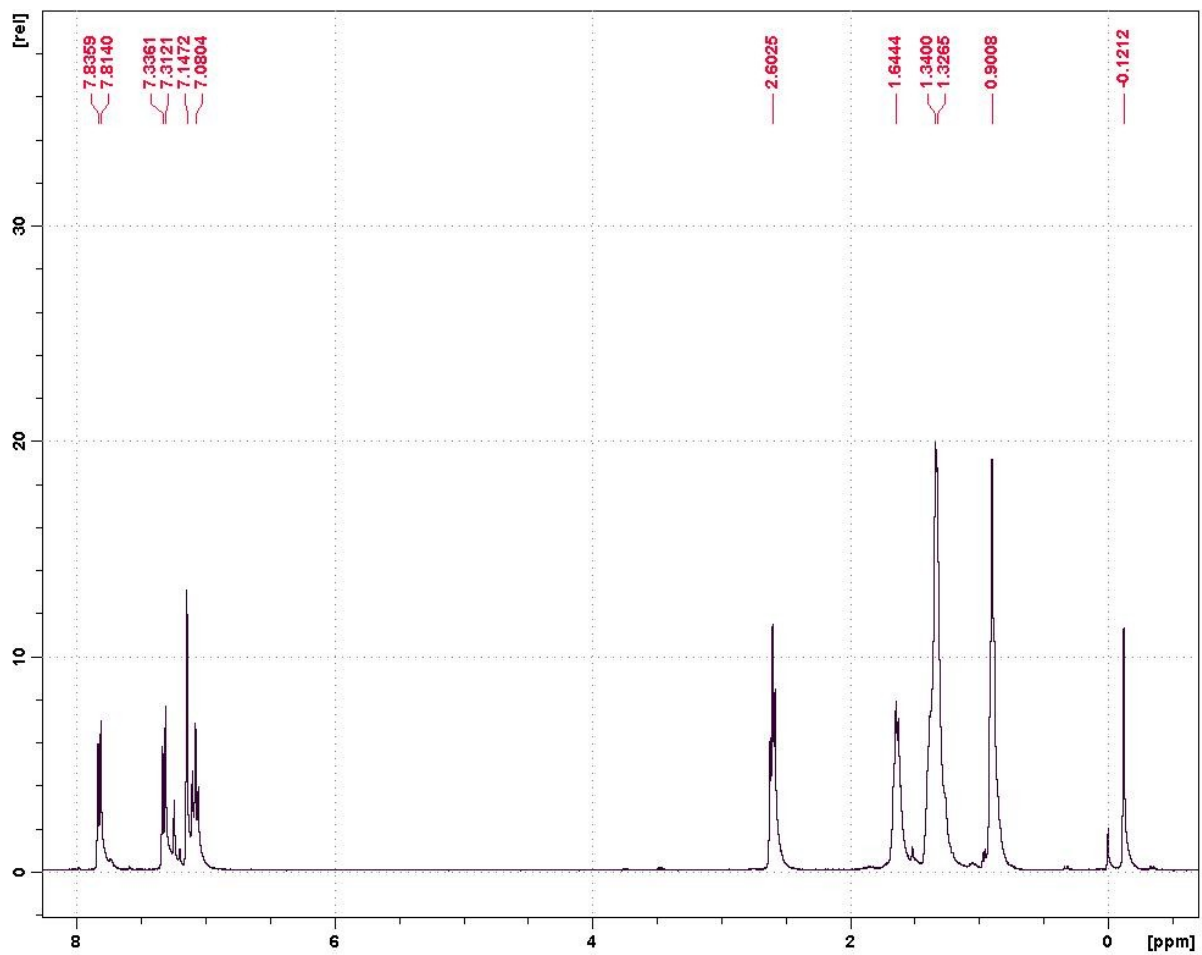
Figure A26. ^{1}H NMR of dibromo-Tail Out TMT (400 MHz, CDCl$_3$).
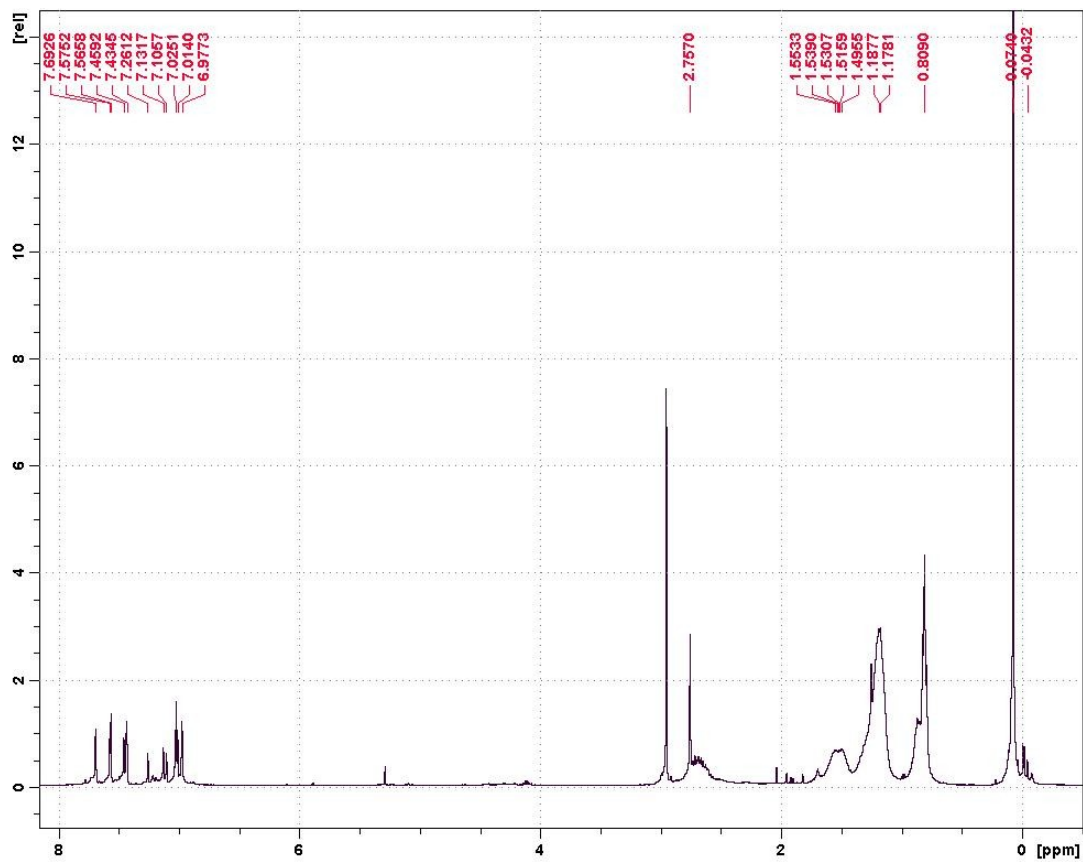
Figure A27. ^{1}H NMR of dibromo-Tail In TMT (400 MHz, CDCl$_3$).
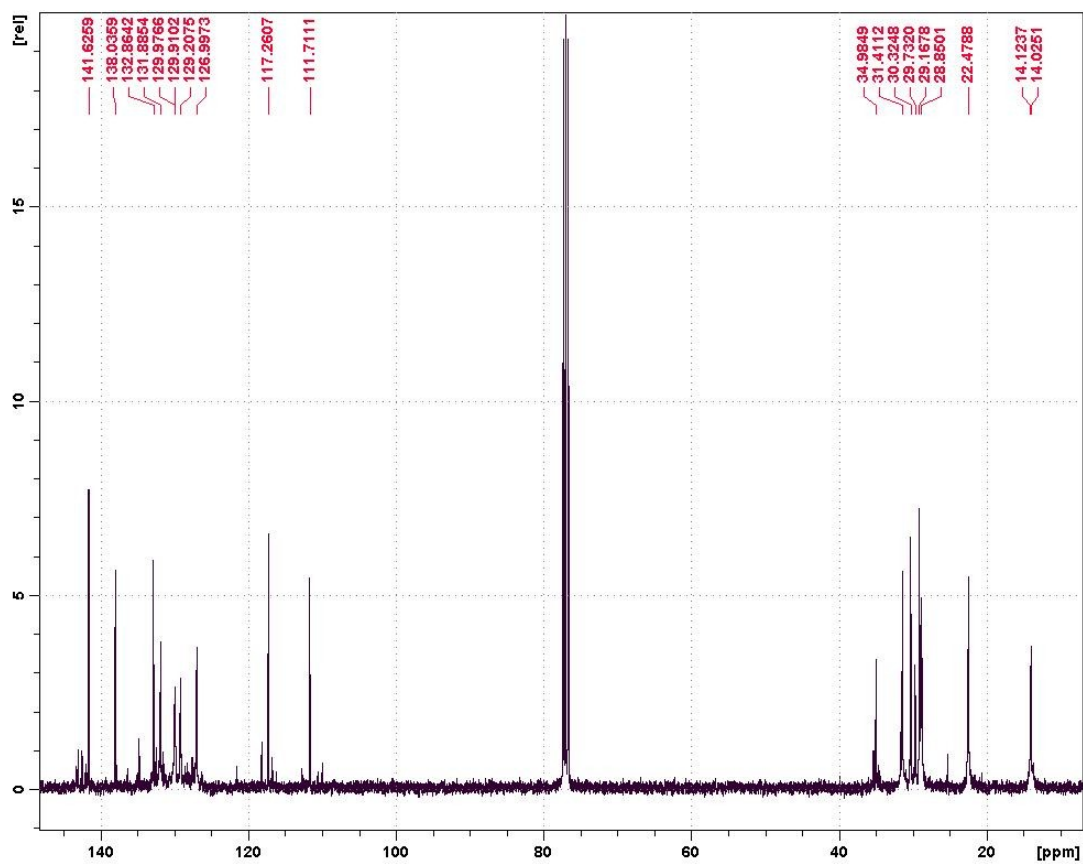
Figure A28. ^{13}C NMR of dibromo-Tail In TMT (100 MHz, CDCl$_3$).
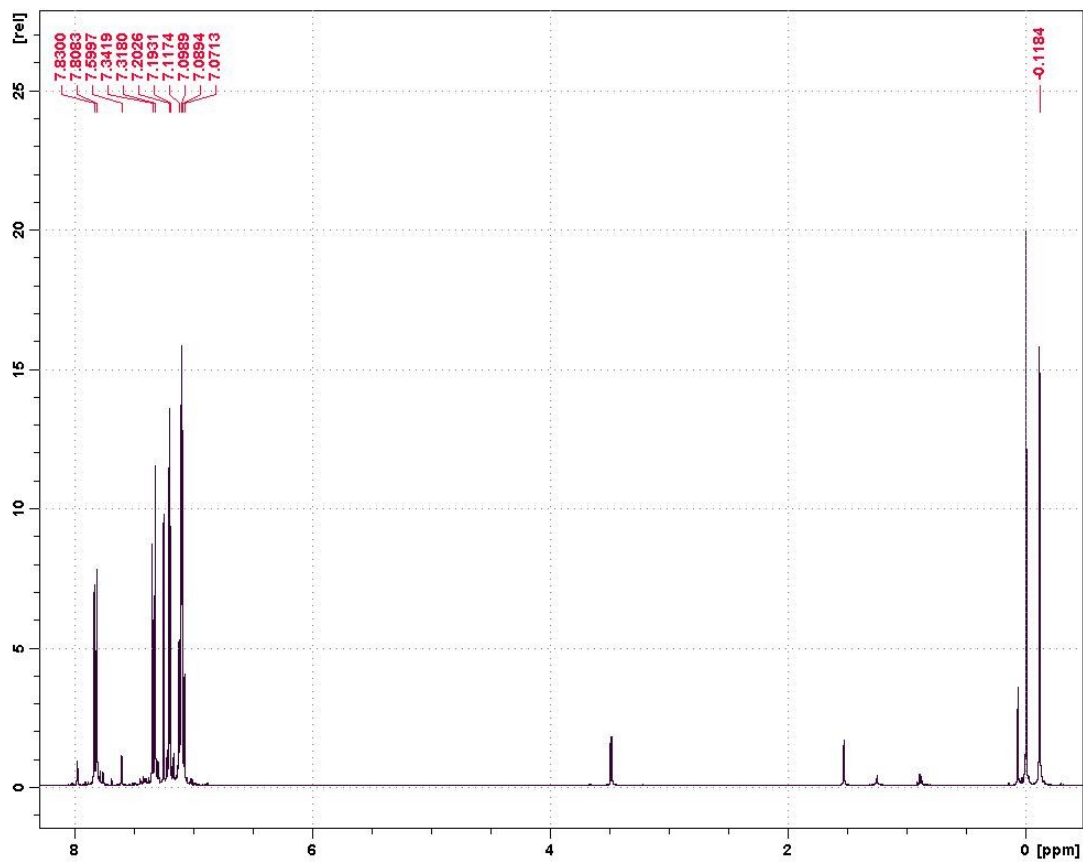
Figure A29. ^{1}H NMR of dibromo-No Tail TMT (400 MHz, CDCl$_3$).
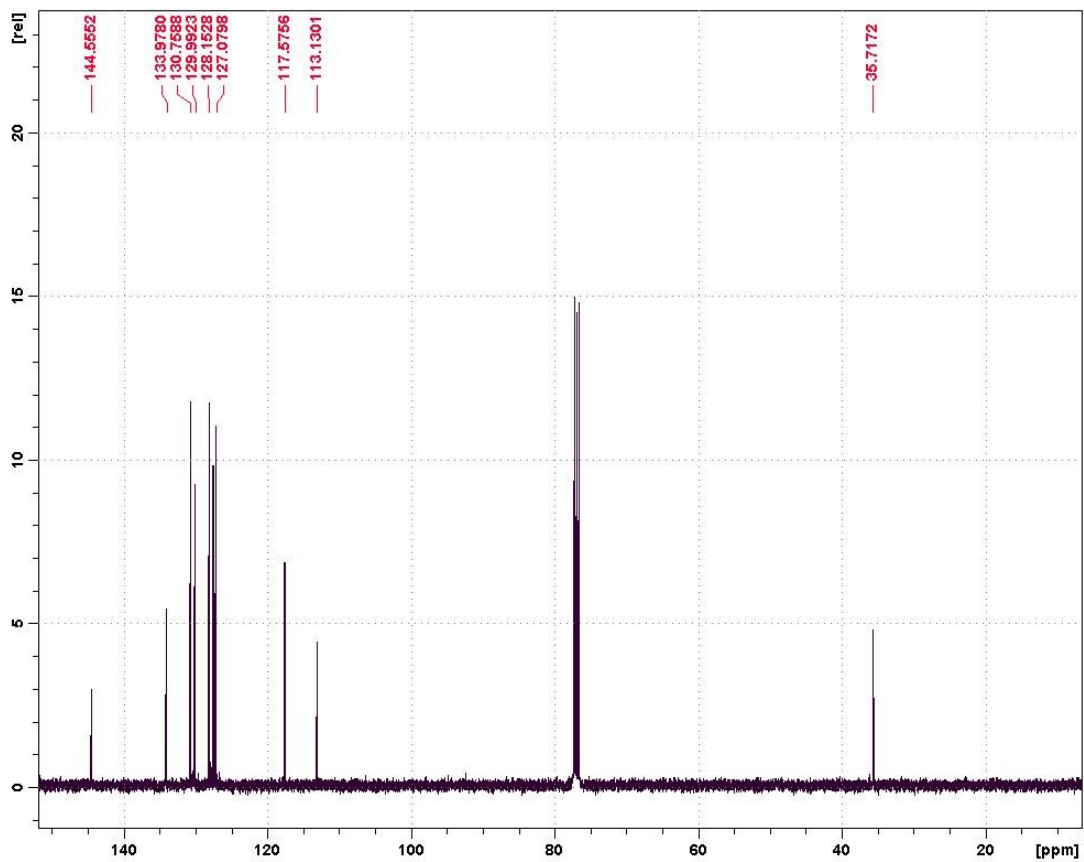
Figure A30. ^{13}C NMR of dibromo-No Tail TMT (100 MHz, CDCl$_3$).
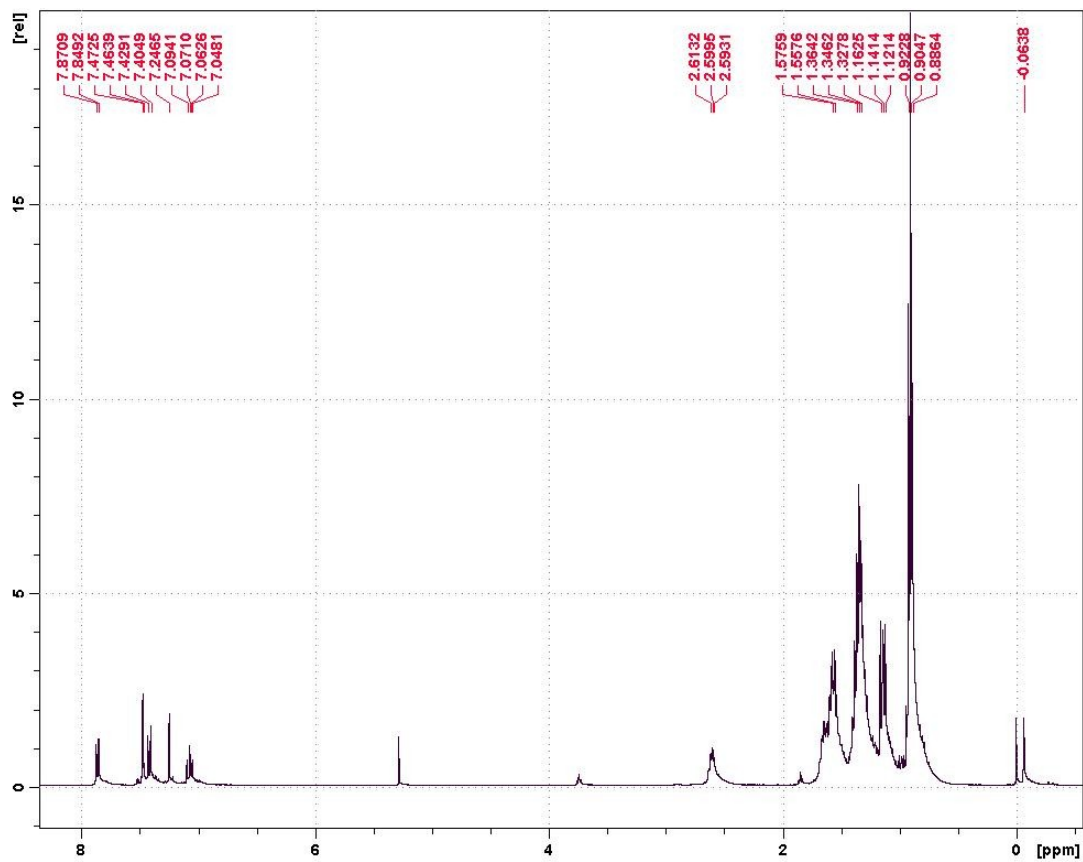
Figure A31. ^{1}H NMR of distannyl-Tail Out TMT (400 MHz, CDCl$_3$).
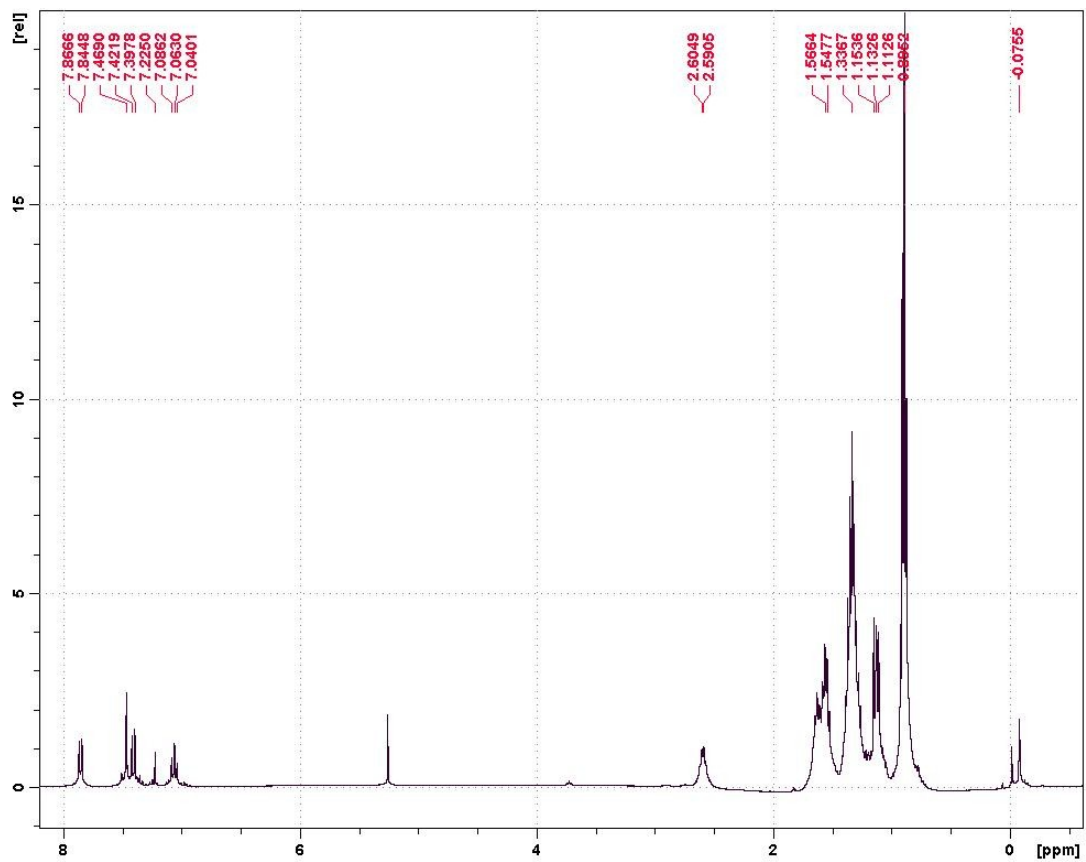
Figure A32. ^{1}H NMR of distannyl-Tail In TMT (400 MHz, CDCl$_3$).
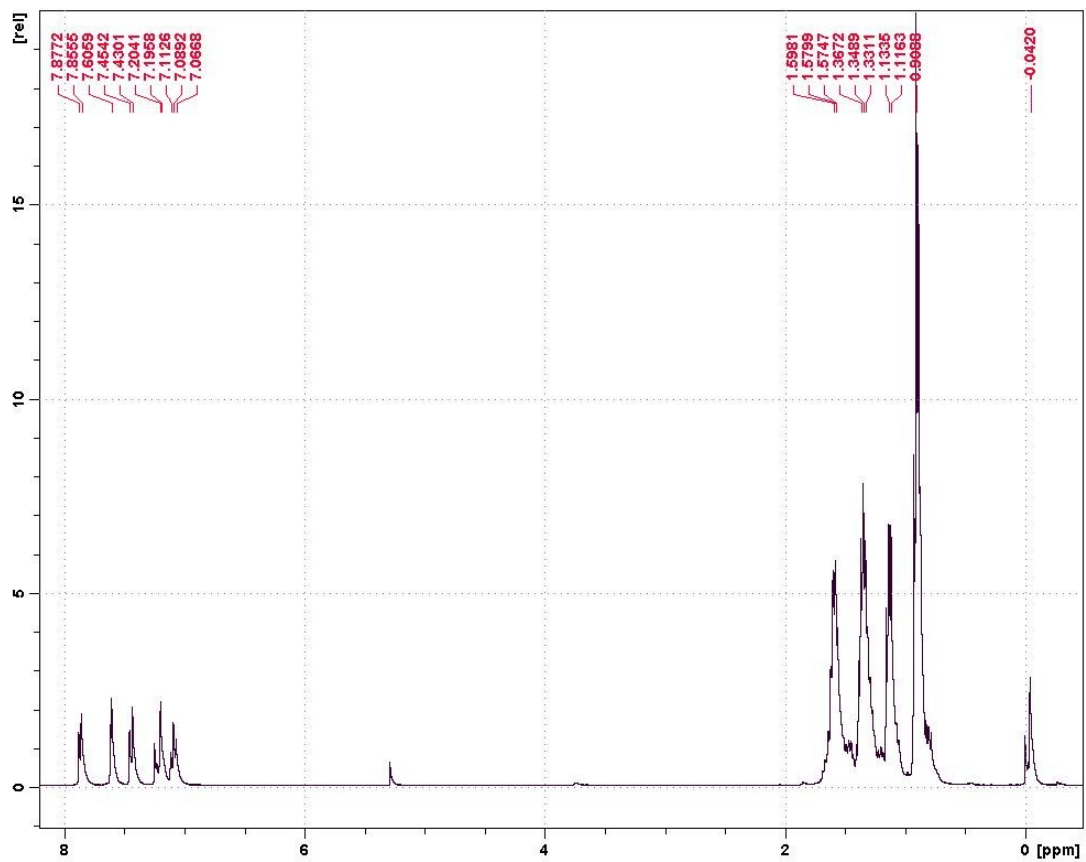
Figure A33. ^{1}H NMR of distannyl-No Tail TMT (400 MHz, CDCl$_3$).
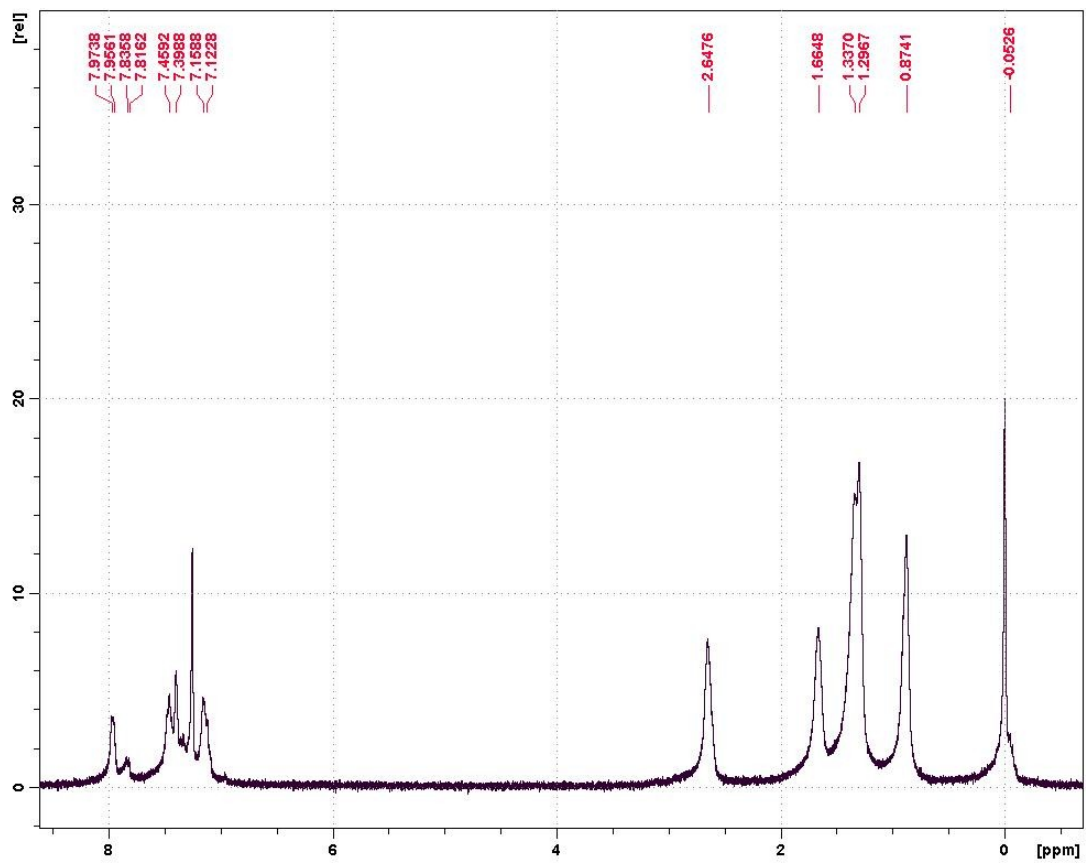
Figure A34. ^{1}H NMR of Tail Out PTMT (400 MHz, CDCl$_3$).
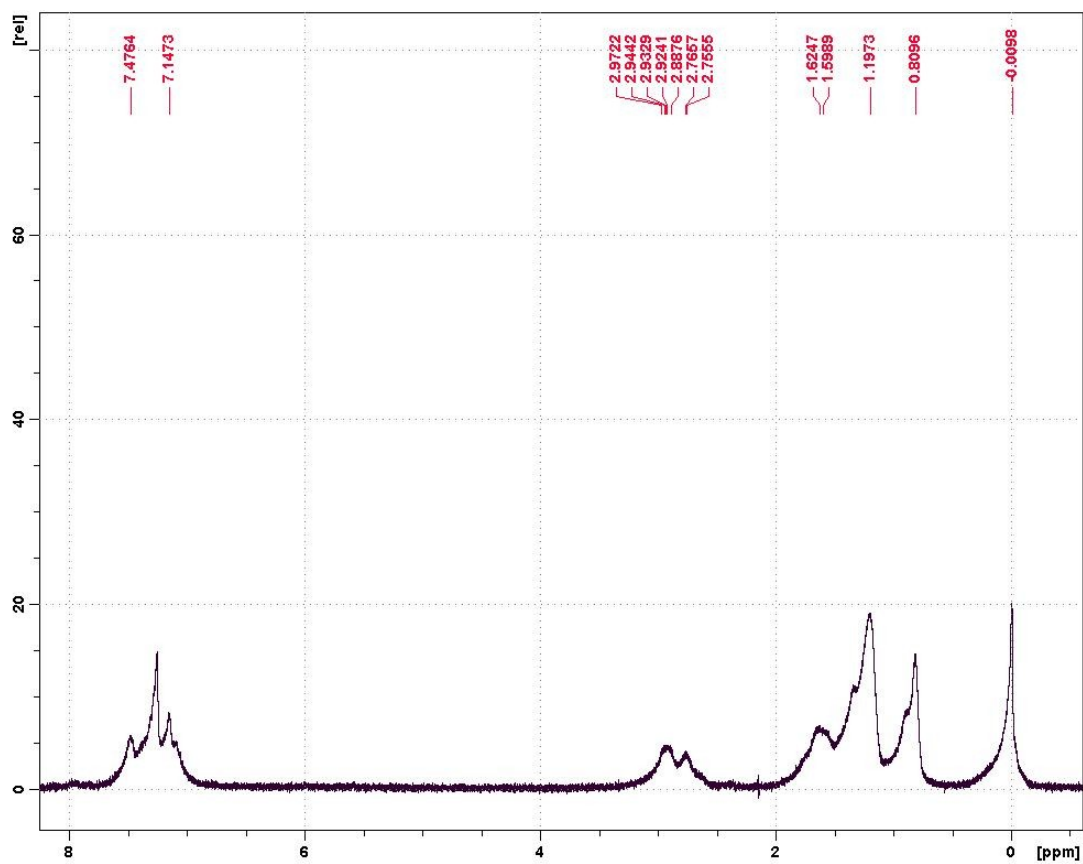
Figure A35. ^{1}H NMR of Tail In PTMT (400 MHz, CDCl$_3$).
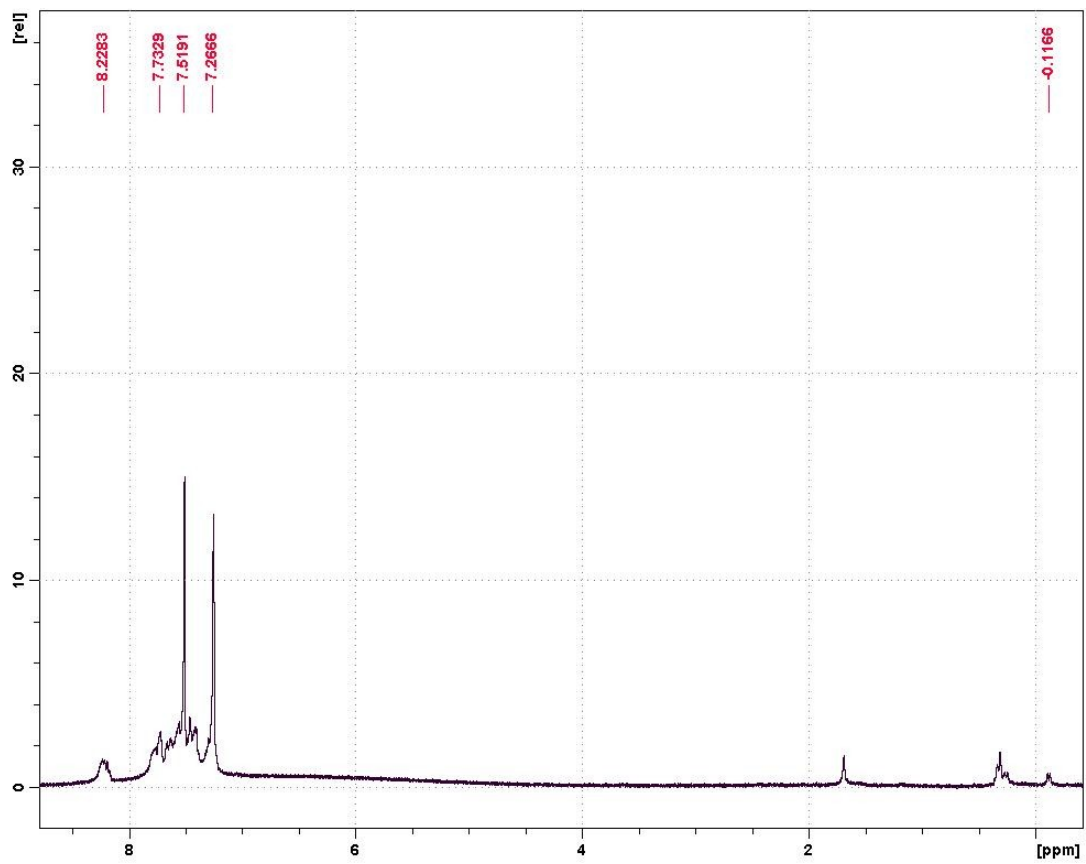
Figure A36. ^{1}H NMR of No Tail PTMT (400 MHz, CDCl$_3$).
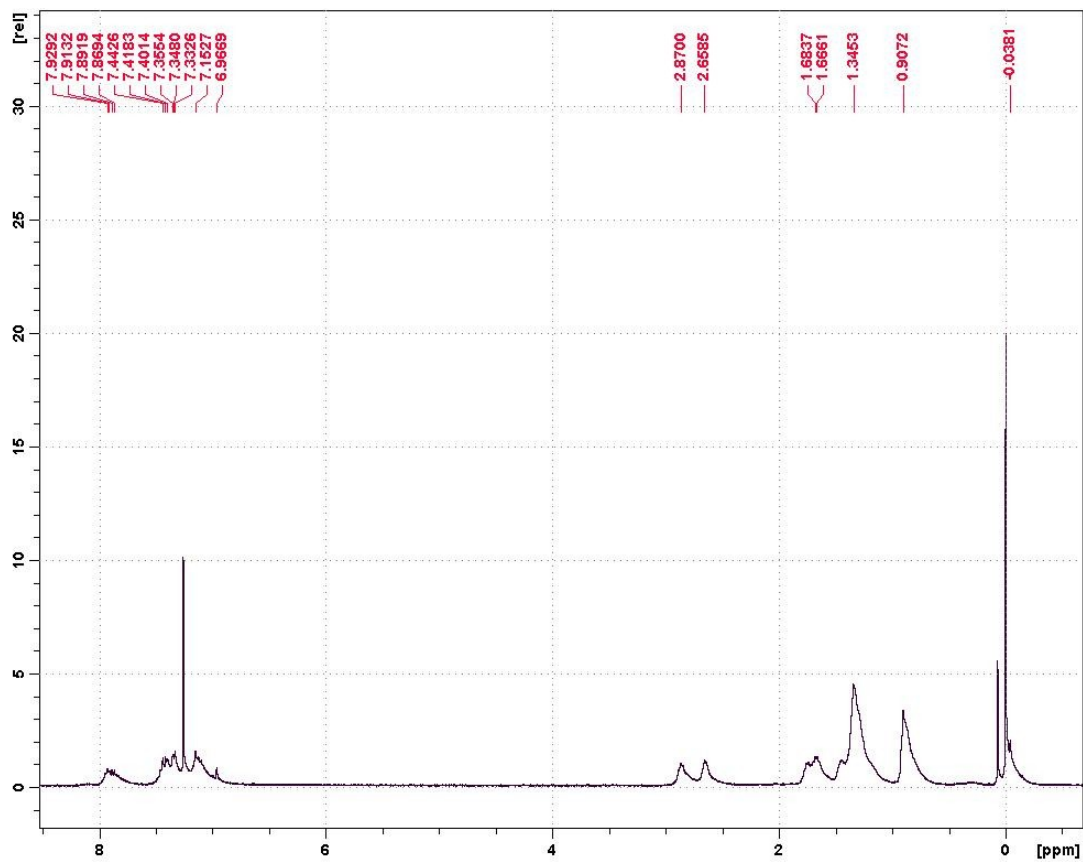
Figure A37. ^{1}H NMR of Tail Out PTMT-T (400 MHz, CDCl$_3$).
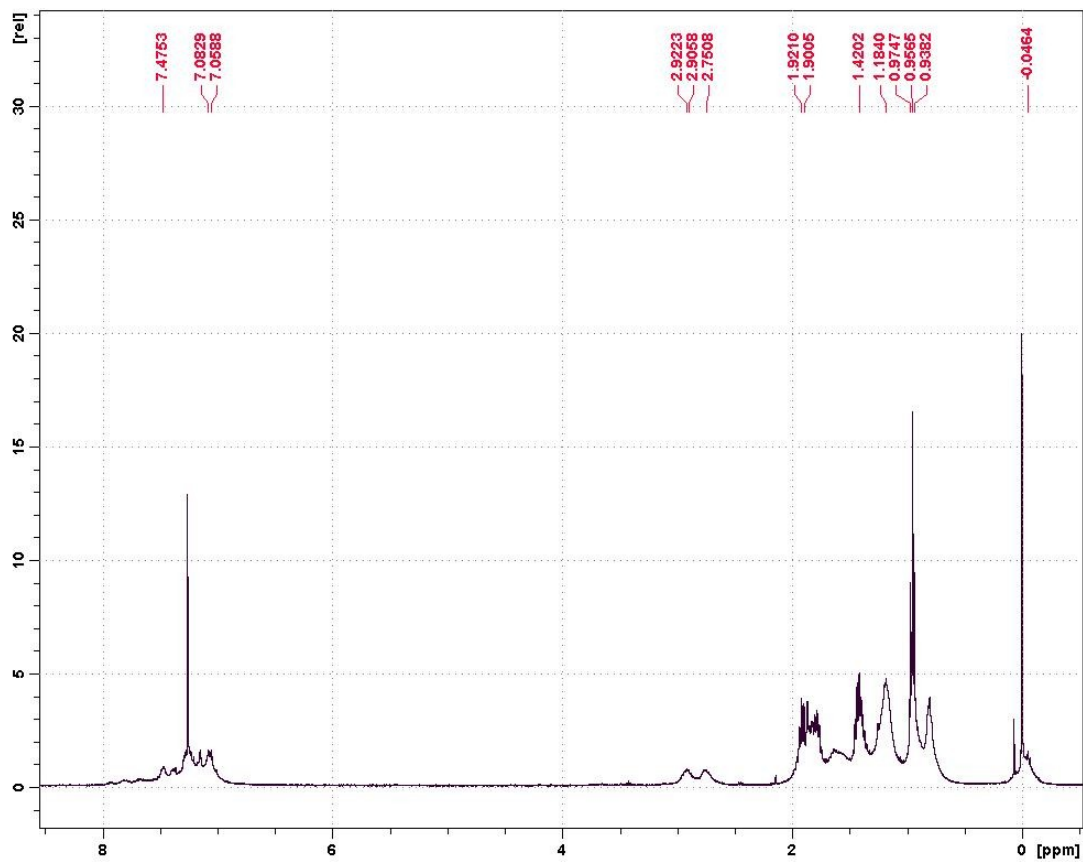
Figure A38. [^1]H NMR of Tail In PTMT-T (400 MHz, CDCl$_3$).
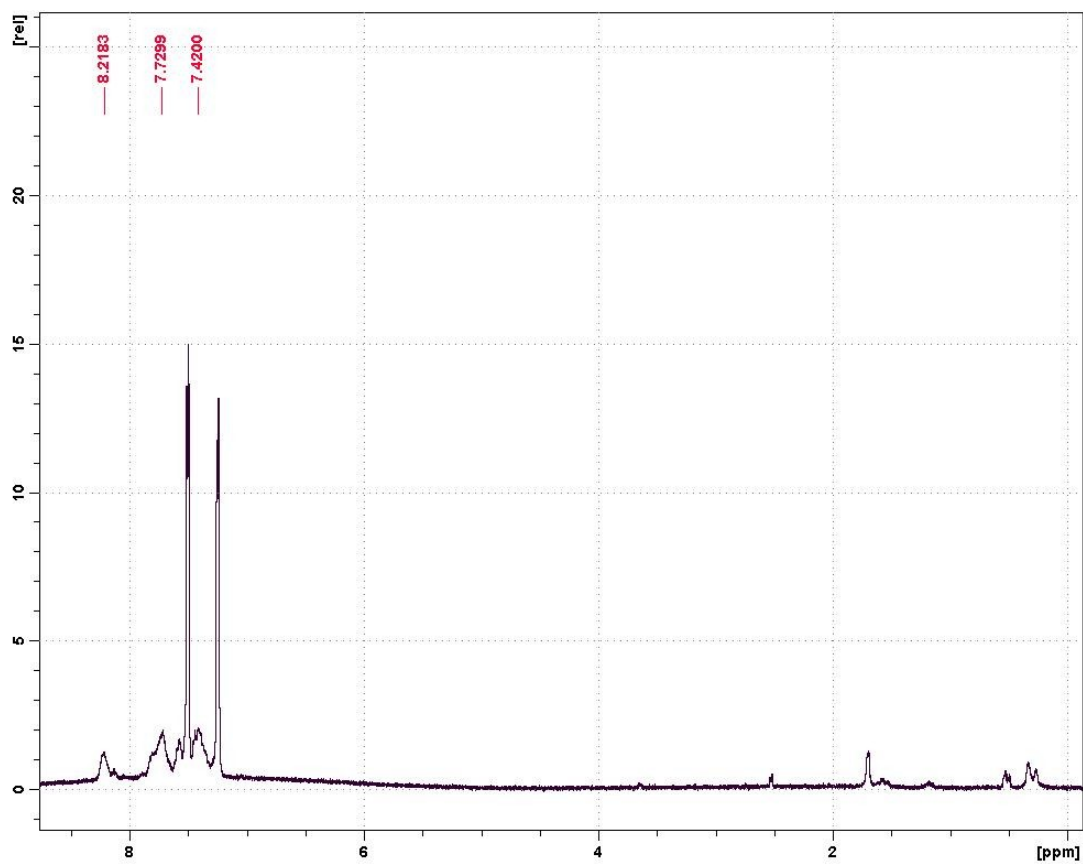
Figure A39. ^{1}H NMR of No Tail PTMT-T (400 MHz, CDCl$_3$).
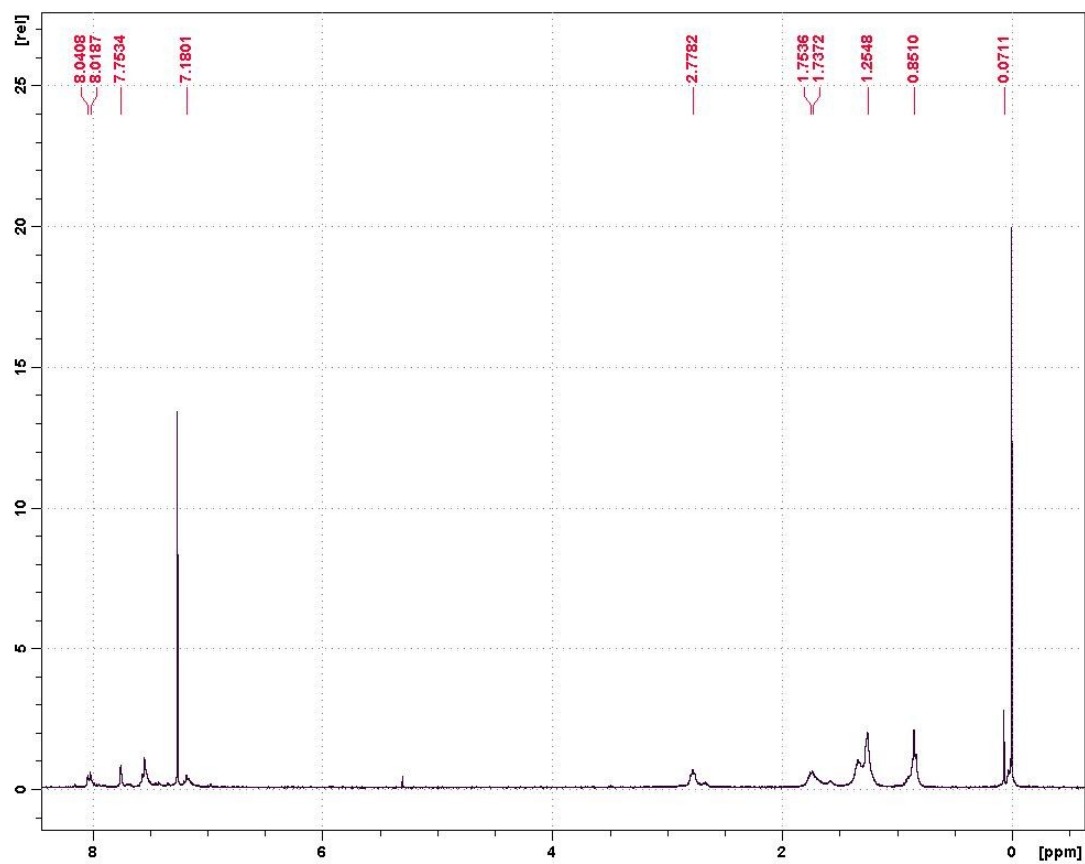
Figure A40. ^{1}H NMR of Tail Out PTMT-B (400 MHz, CDCl$_3$).
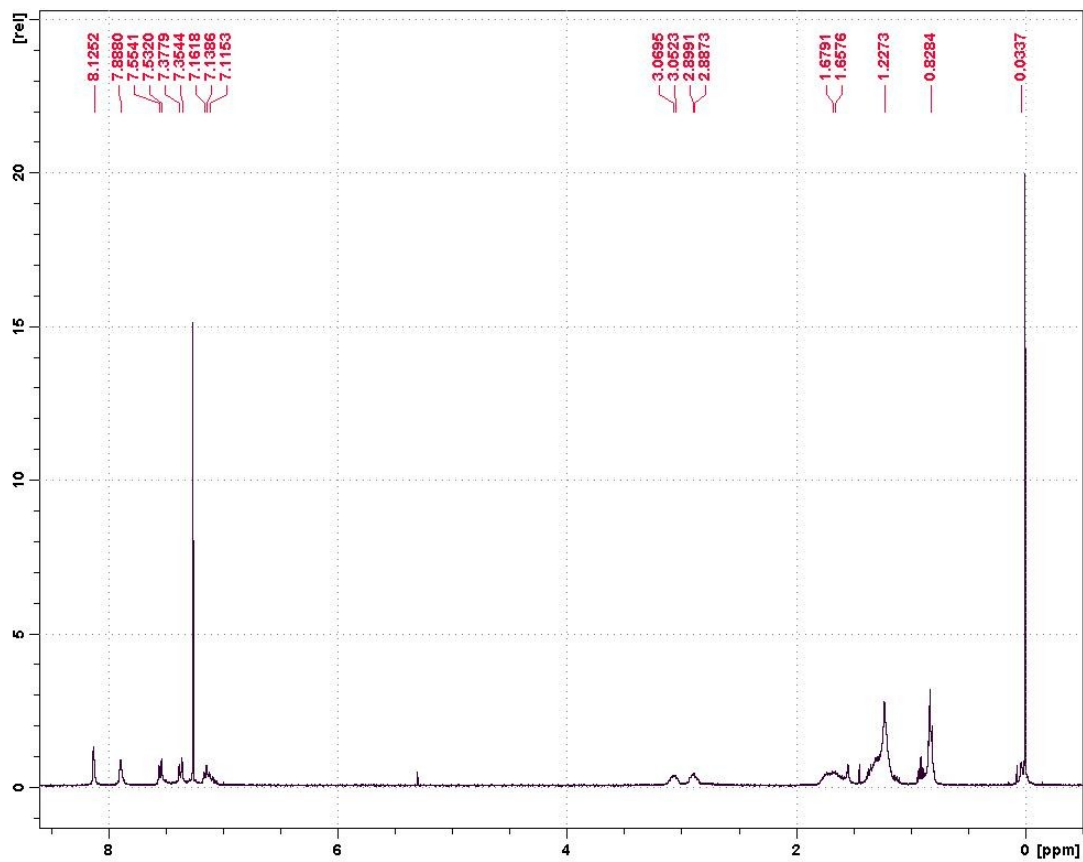
Figure A41. ^{1}H NMR of Tail In PTMT-B (400 MHz, CDCl$_3$).
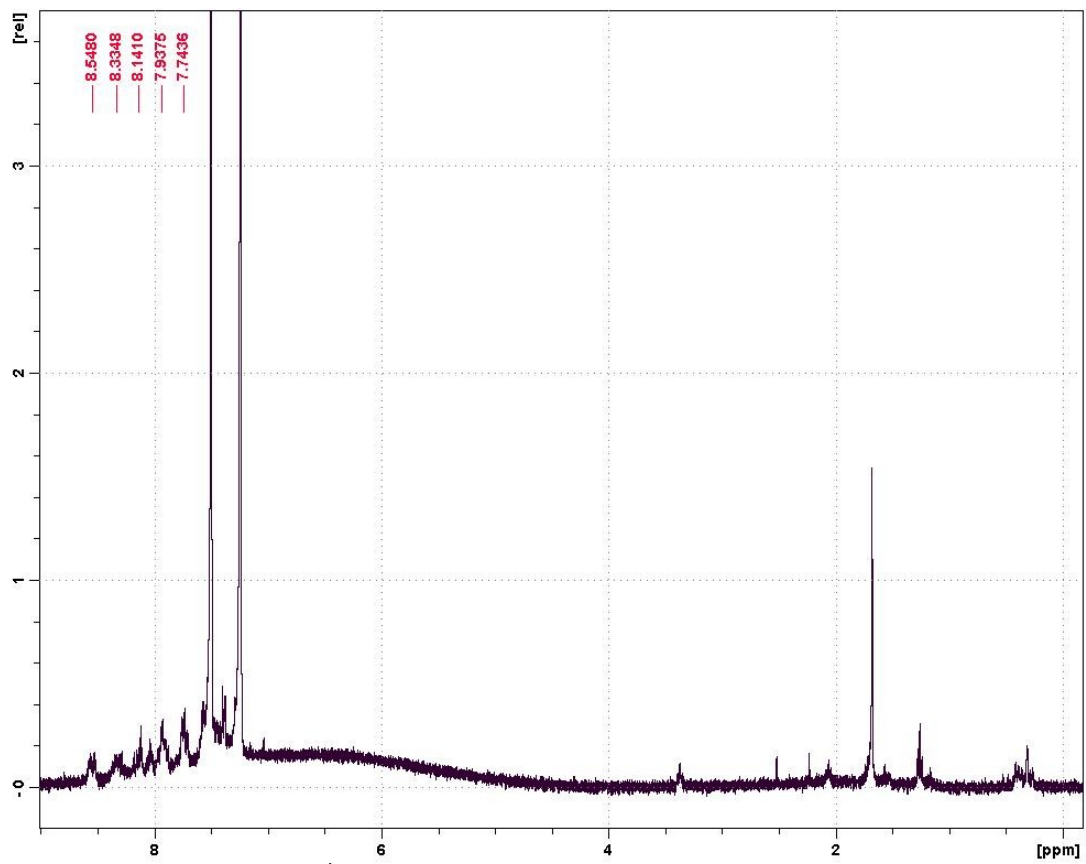
Figure A42. ^{1}H NMR of No Tail PTMT-B (400 MHz, CDCl$_3$).
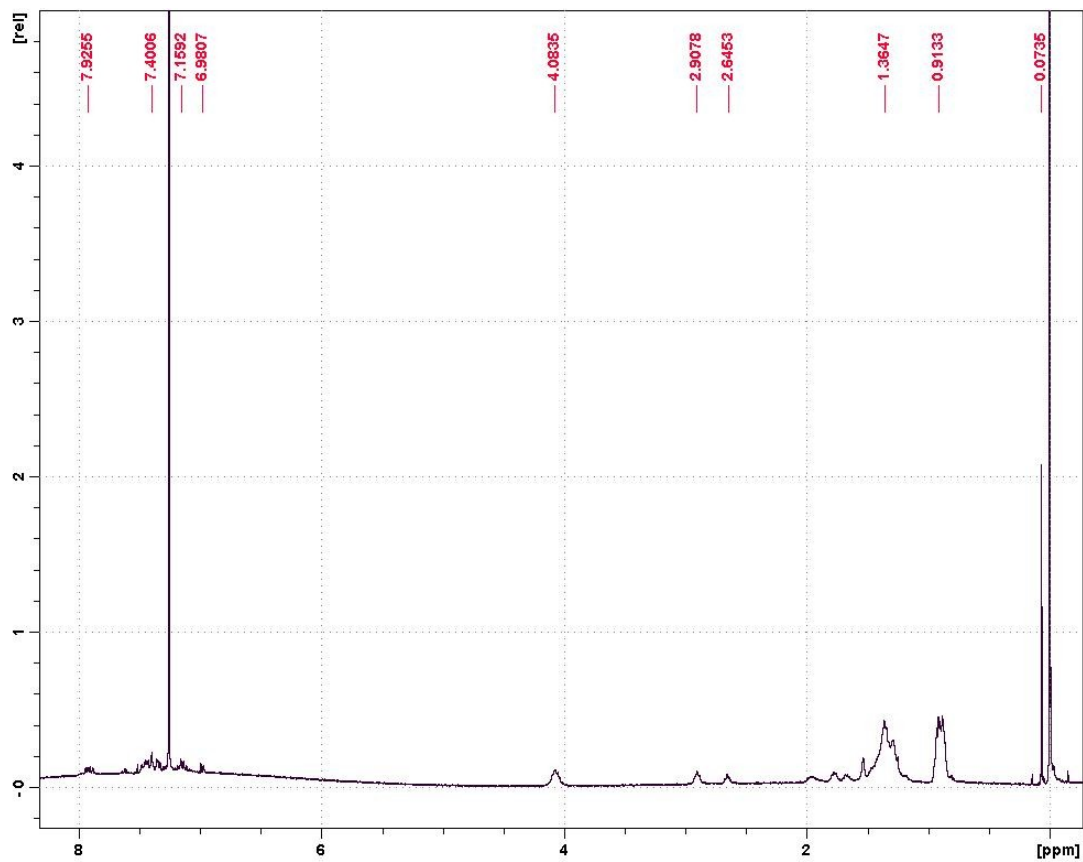
Figure A43. ^{1}H NMR of Tail Out PTMT-DPP (400 MHz, CDCl$_3$).
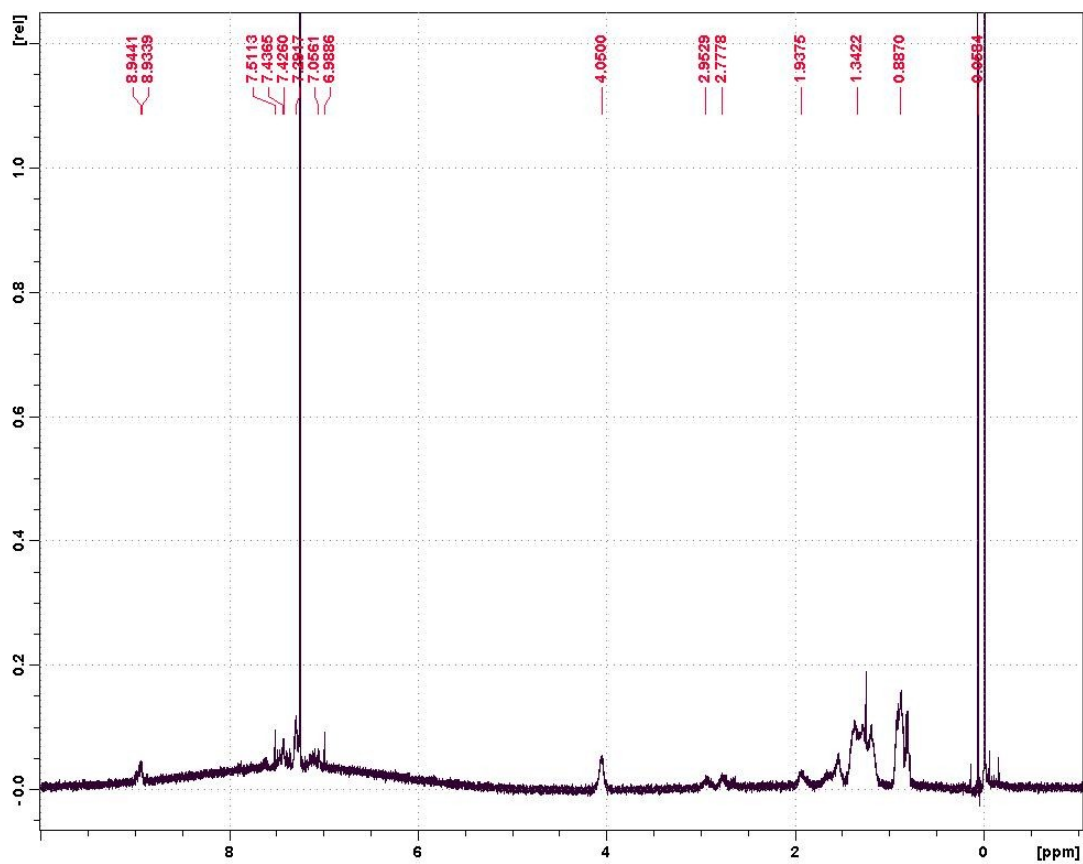
Figure A44. ^{1}H NMR of Tail In PTMT-DPP (400 MHz, CDCl$_3$).
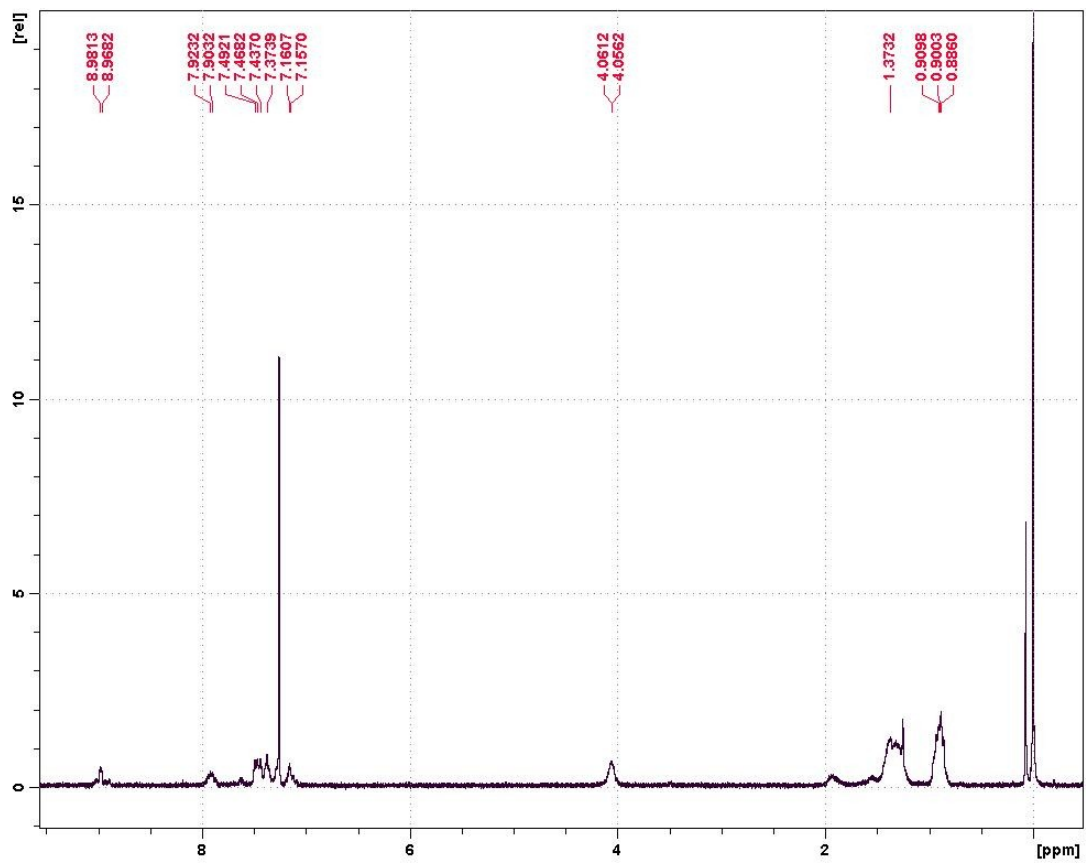
Figure A45. ^{1}H NMR of No Tail PTMT-DPP (400 MHz, CDCl$_3$).
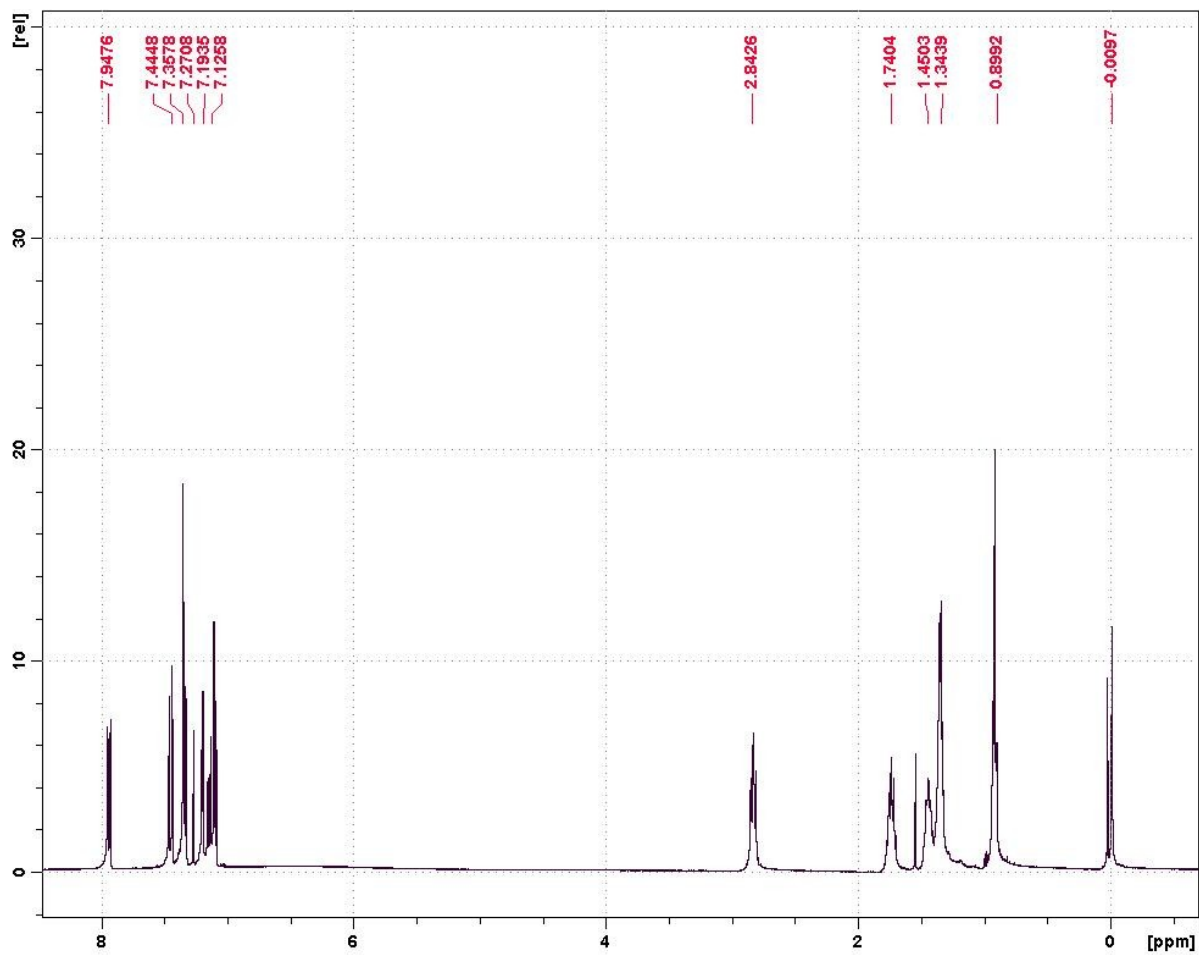
Figure A46. ^{1}H NMR of Tail Out TTMTT (400 MHz, CDCl$_3$).
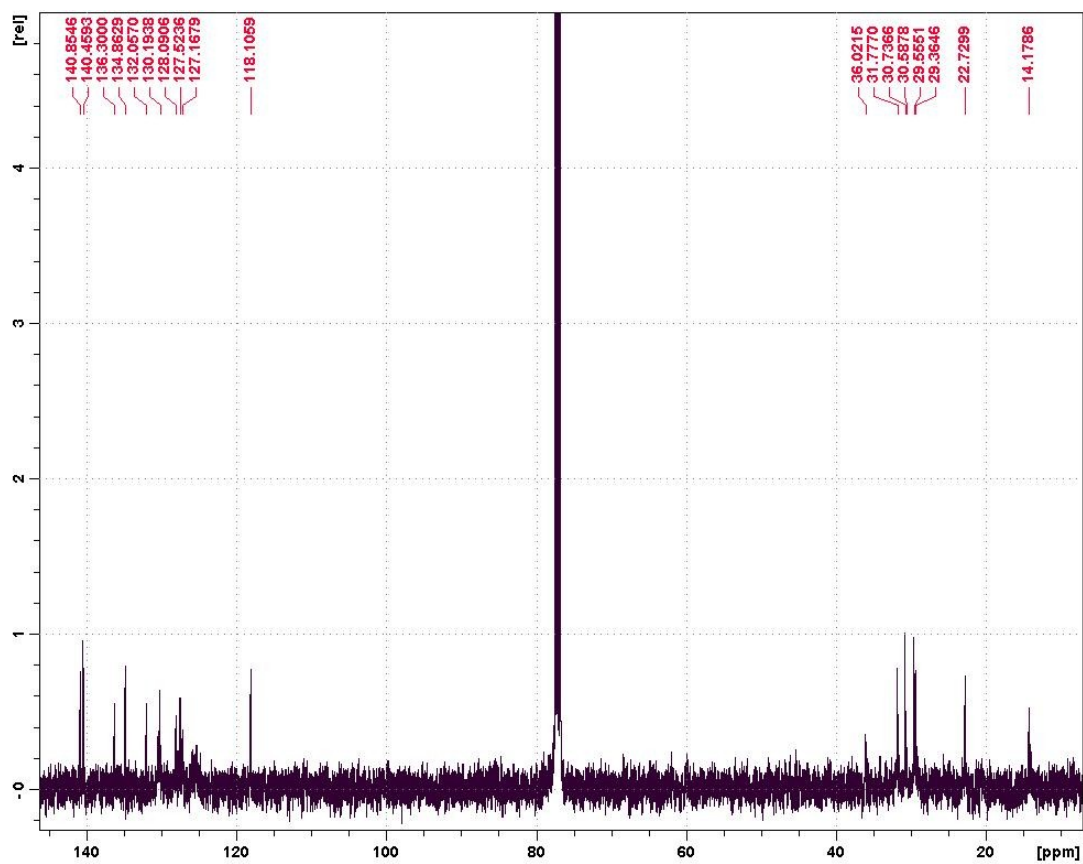
Figure A47. ^{13}C NMR of Tail Out TTMTT (100 MHz, CDCl$_3$).
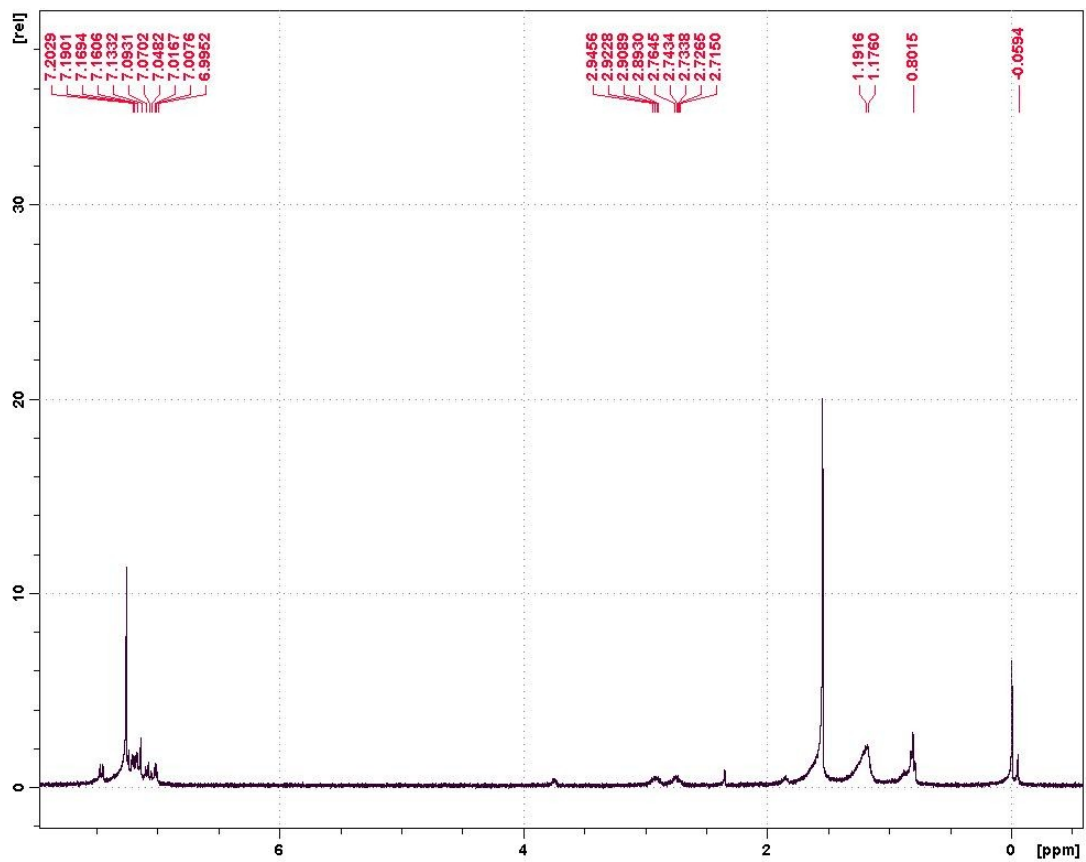
Figure A48. ^{1}H NMR of Tail In TTMTT (400 MHz, CDCl$_3$).
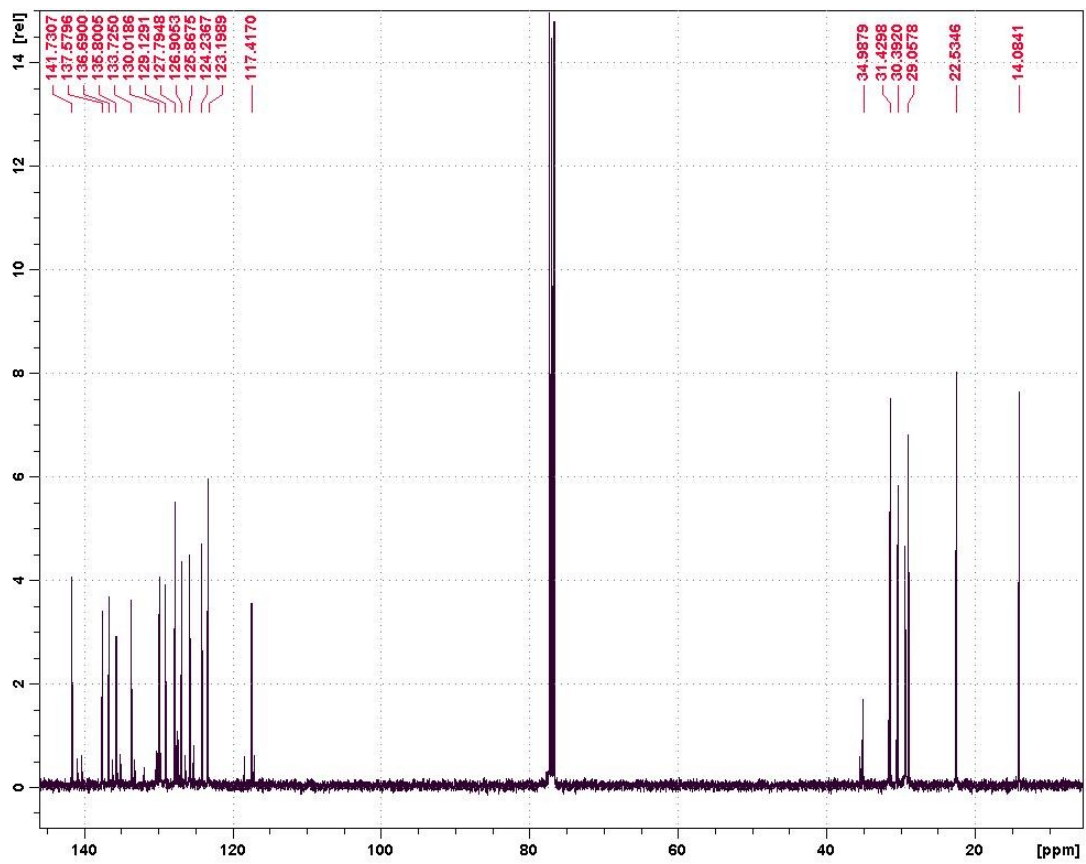
Figure A49. ^{13}C NMR of Tail In TTMTT (100 MHz, CDCl$_3$).
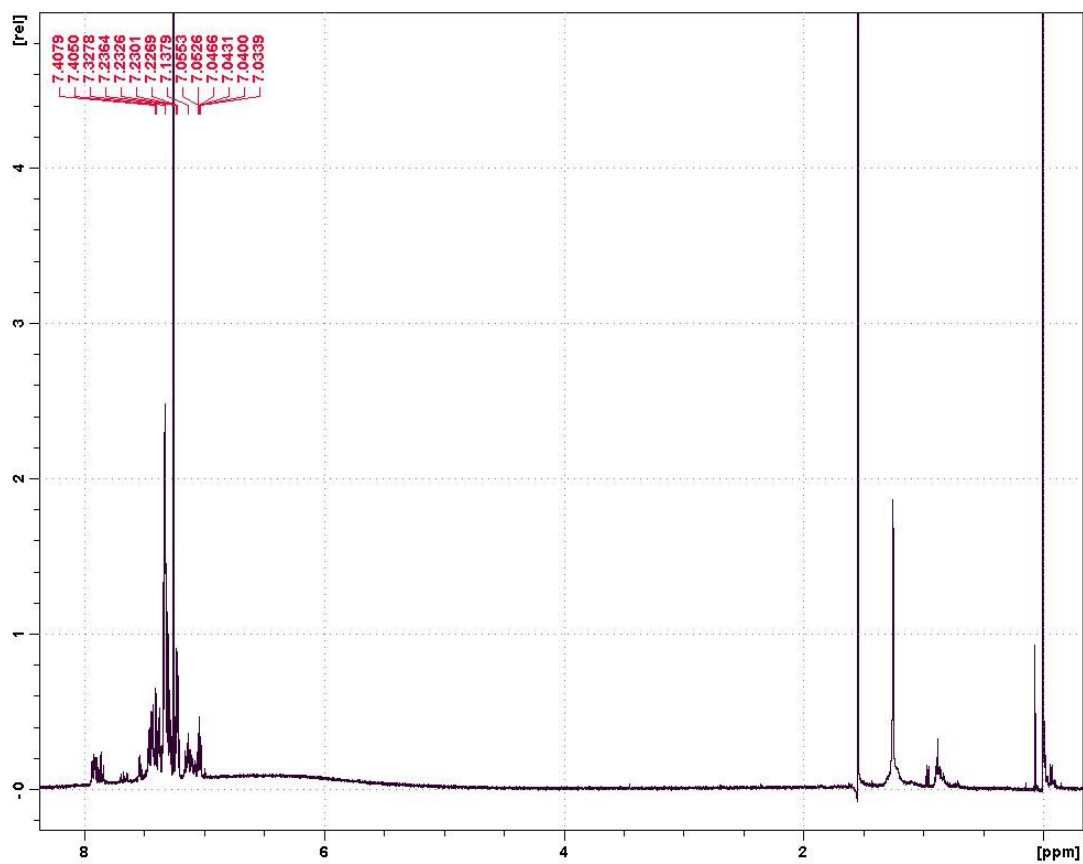
Figure A50. ^{1}H NMR of No Tail TTMTT (400 MHz, CDCl$_3$).
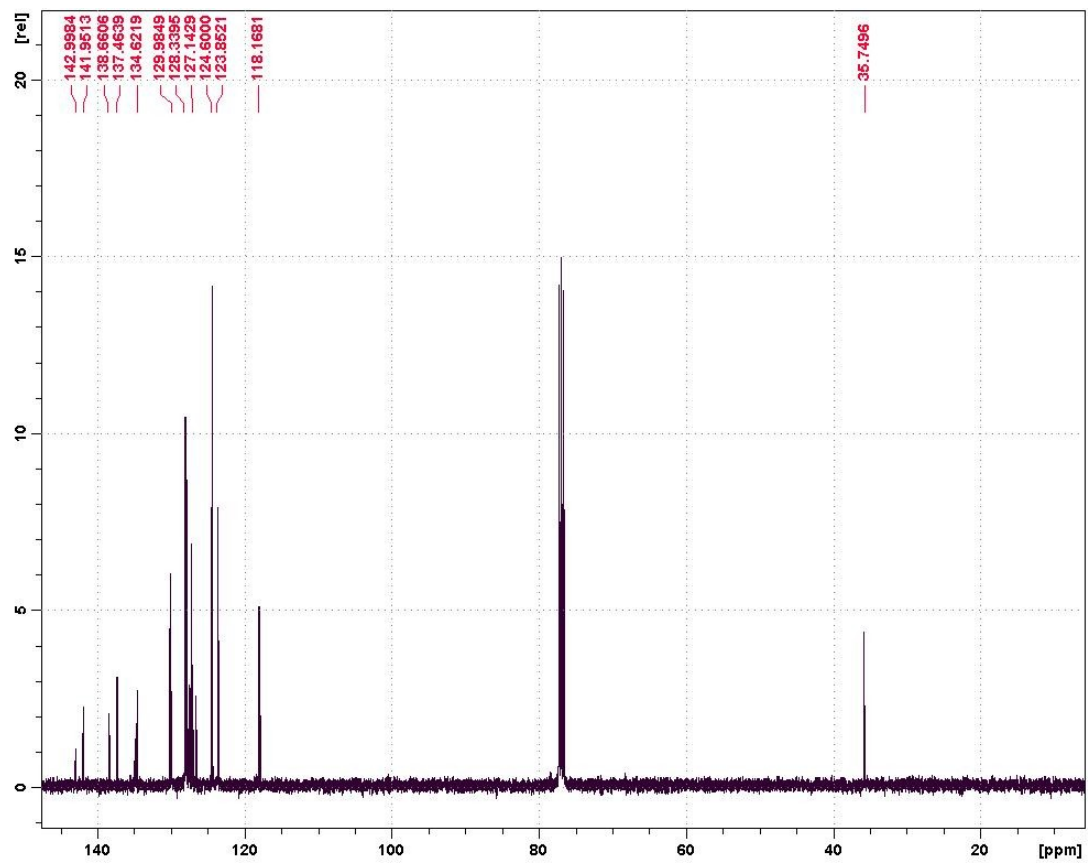
Figure A51. ^{13}C NMR of No Tail TTMTT (100 MHz, CDCl$_3$).
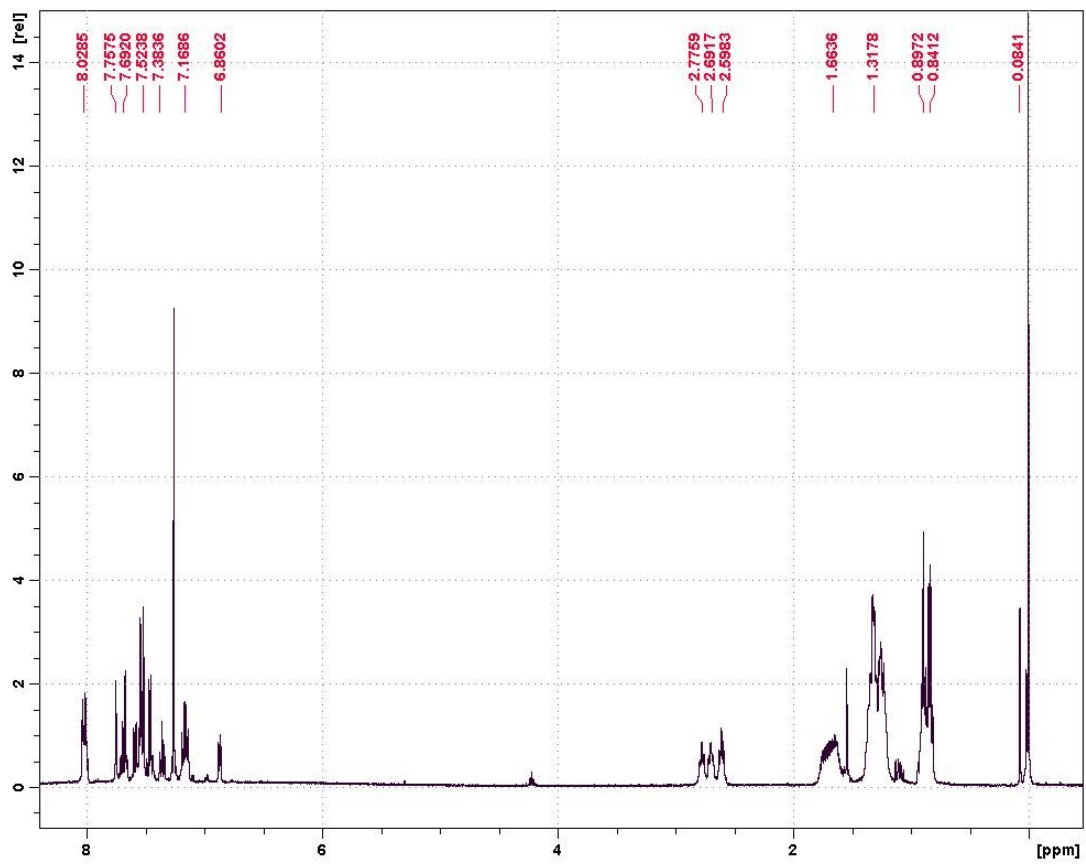
Figure A52. ^{1}H NMR of Tail Out BTMTB (400 MHz, CDCl$_3$).

Figure A53. ^{13}C NMR of Tail Out BTMTB (100 MHz, CDCl$_3$).
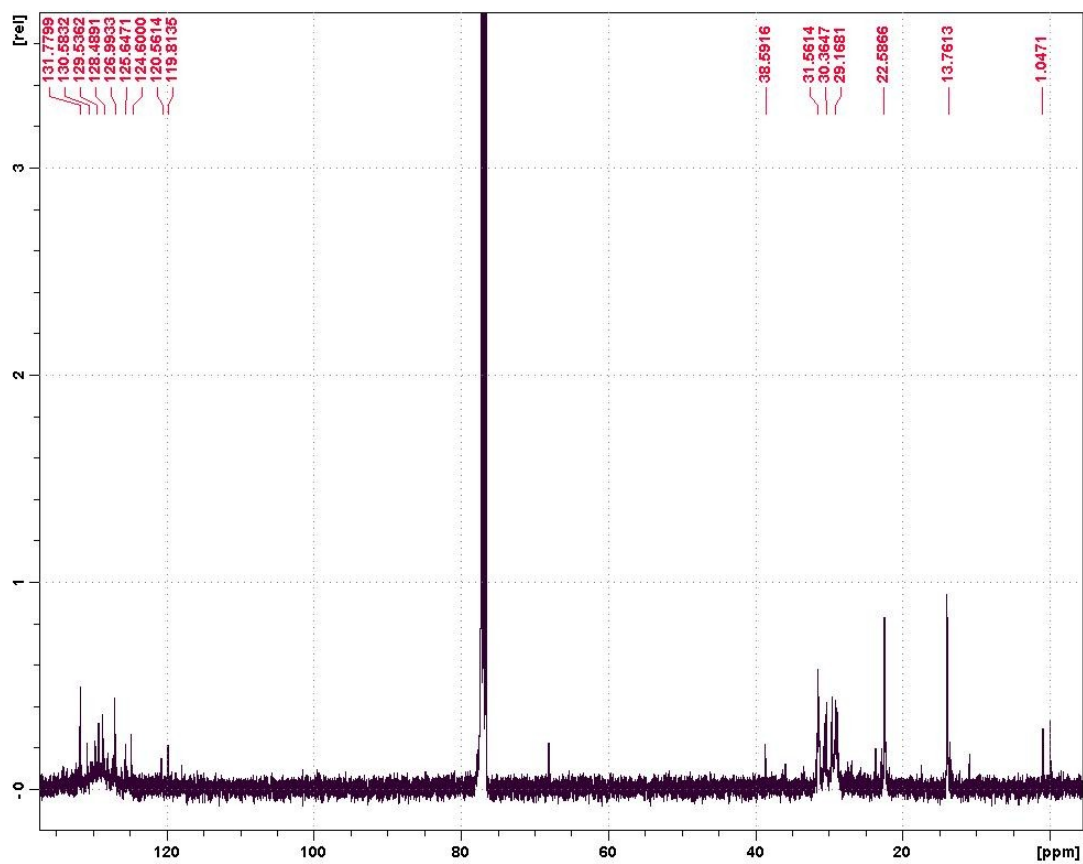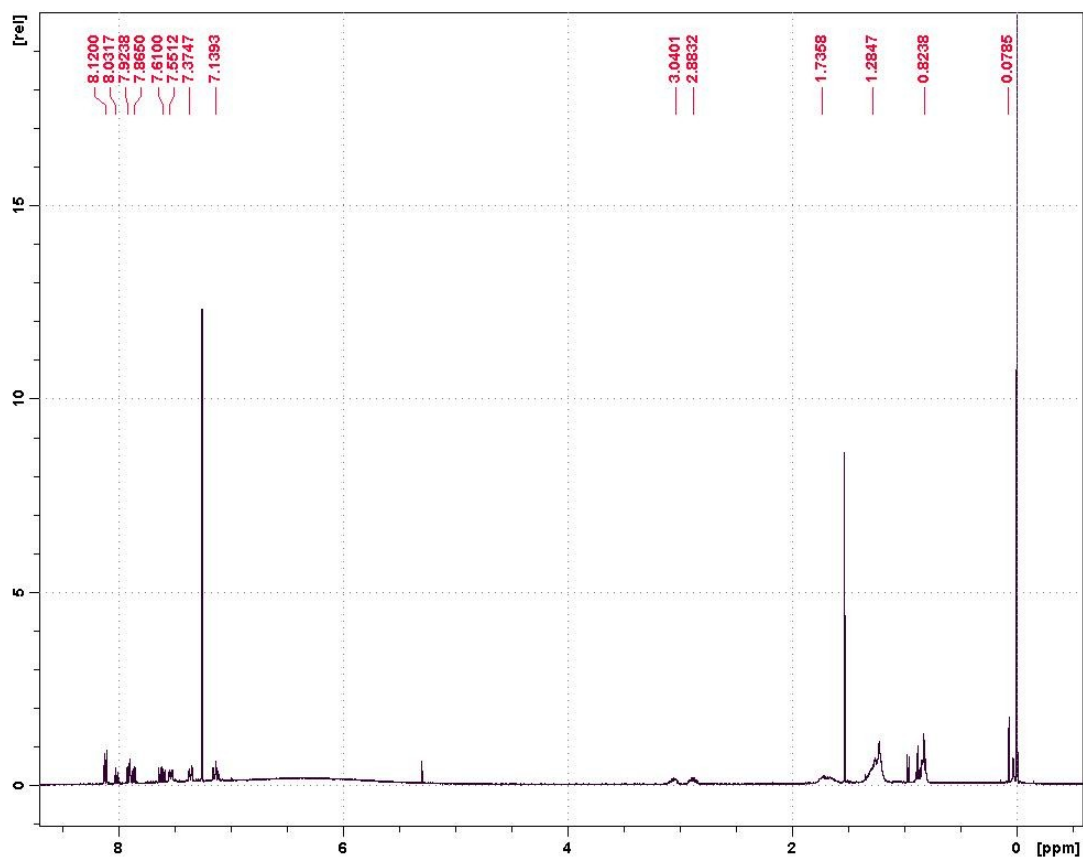
Figure A54. ^{1}H NMR of Tail In BTMTB (400 MHz, CDCl$_3$).
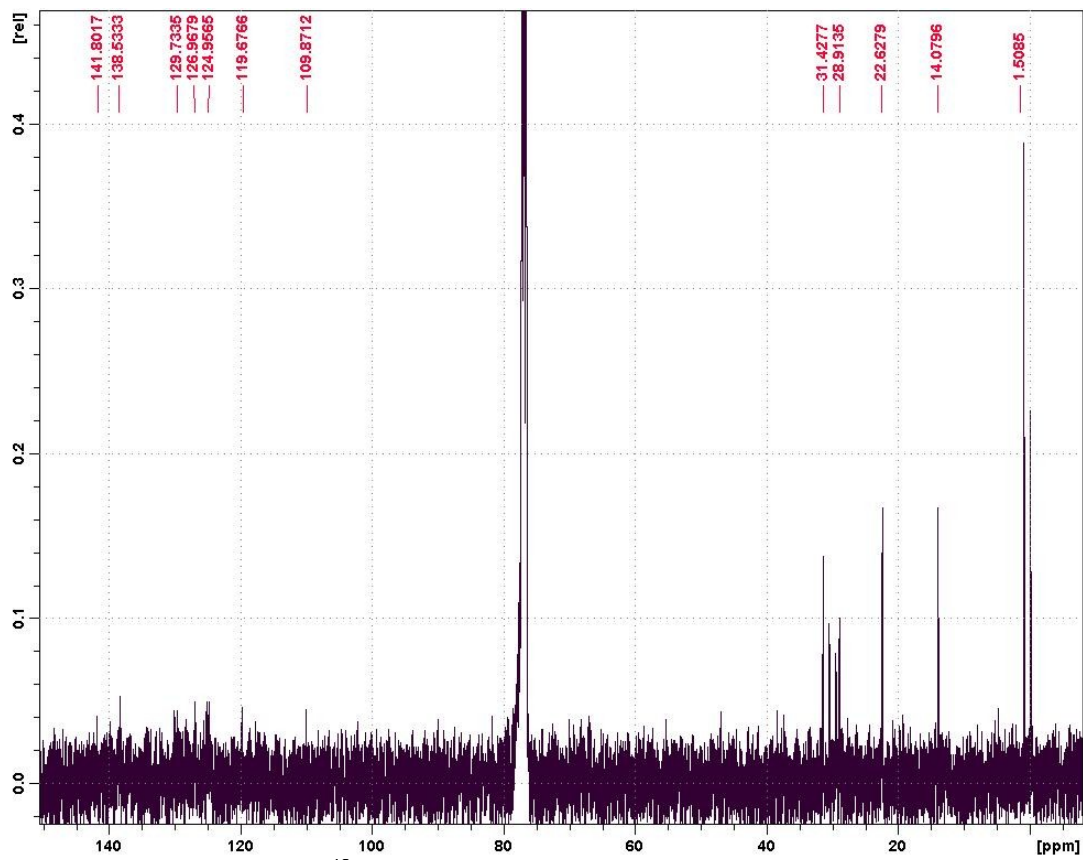
Figure A55. ^{13}C NMR of Tail In BTMTB (100 MHz, CDCl$_3$).
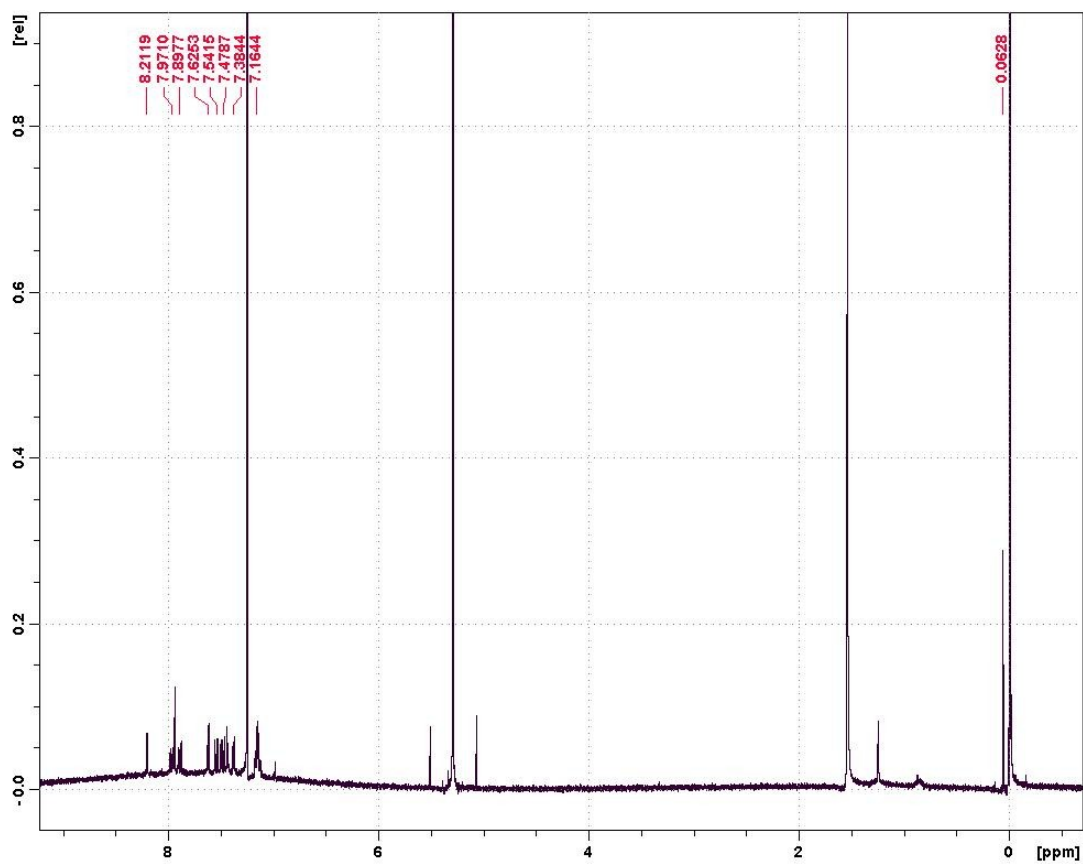
Figure A56. ^{1}H NMR of No Tail BTMTB (400 MHz, CDCl$_3$).
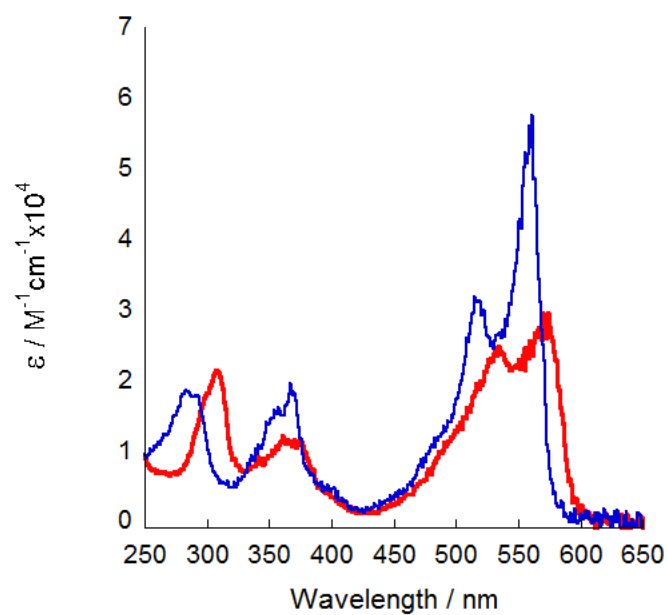
Figure A57. Solution UV-Vis absorption (CHCl$_3$) spectra for dibromo-dithienyl-DPP (red) and dibromo-difuryl-DPP (blue) monomers.
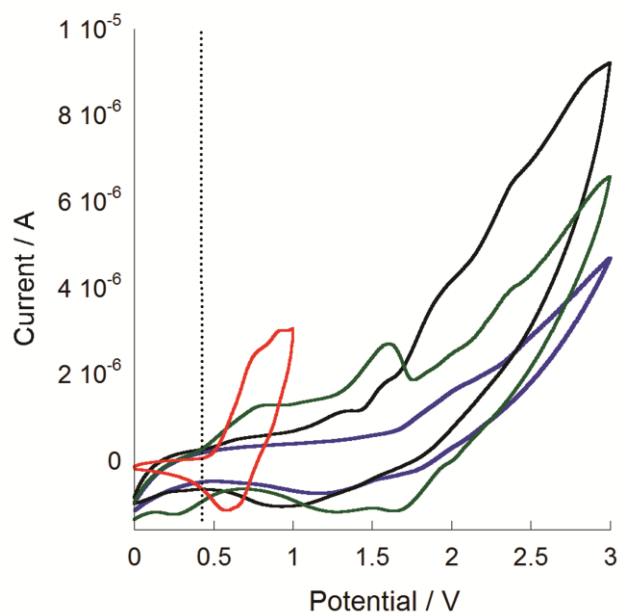
Figure A58. Cyclic voltammograms of PXY polymers (dotted line is approximate onset potential for each polymer). Red: PTT, Black: PTF, Blue: PFT, Green: PFF.
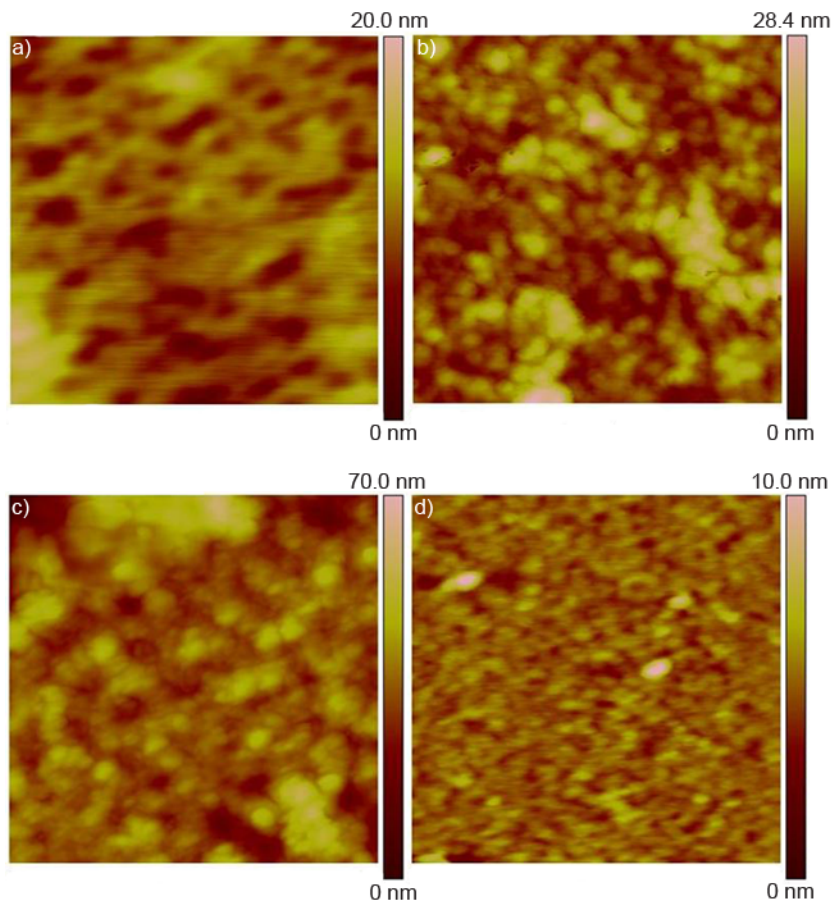
Figure A59. AFM height images of PXY polymers (2 μm x 2μm image area). a) PFF b) PFT c) PTF d) PTT.
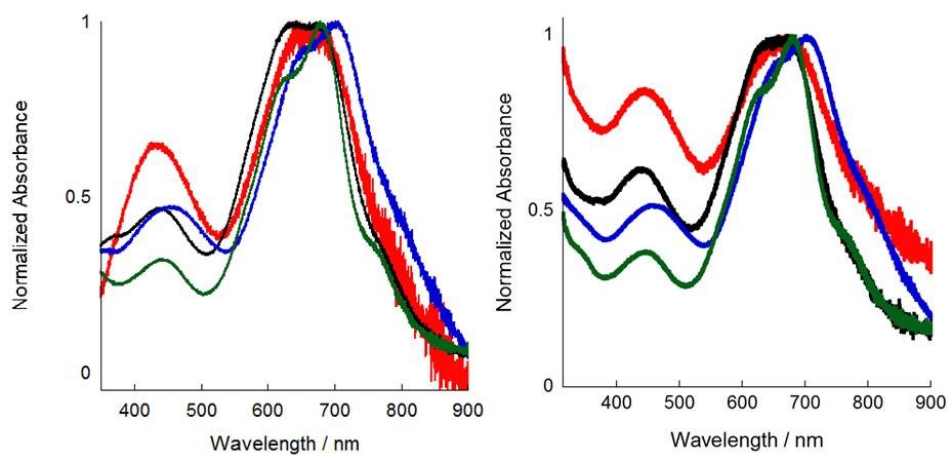
Figure A60. UV-Vis spectra of as-spun (left) and annealed (right, 1 h at 100°C) PXY polymer thin films.
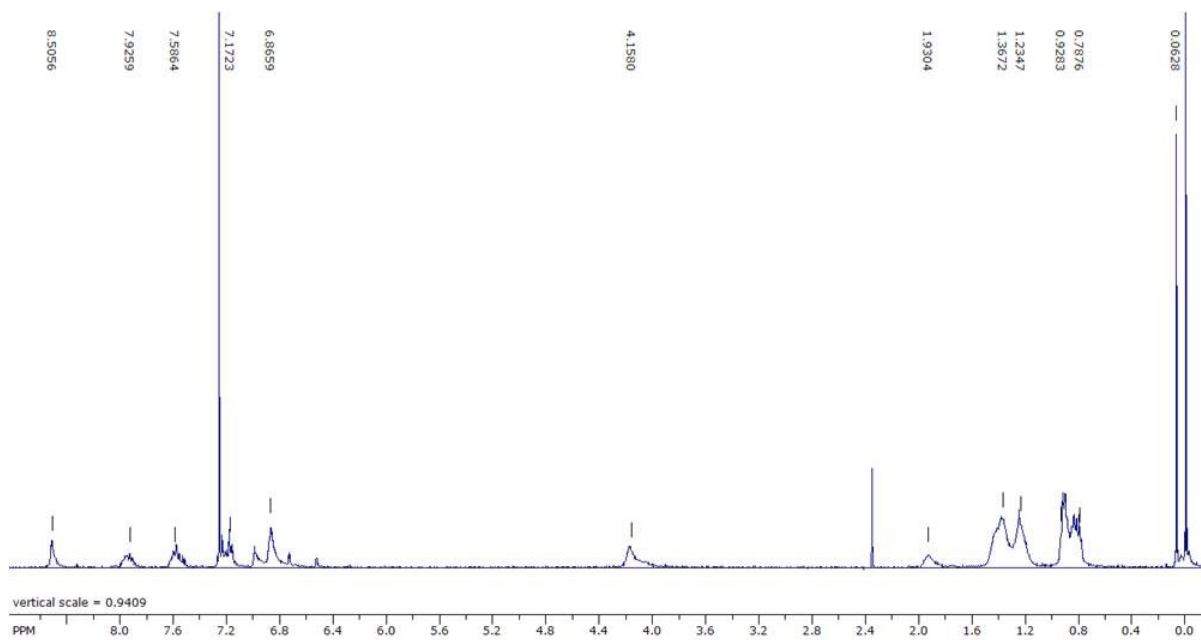
Figure A61. ^{1}H NMR of PFF (400 MHz, CDCl$_3$).
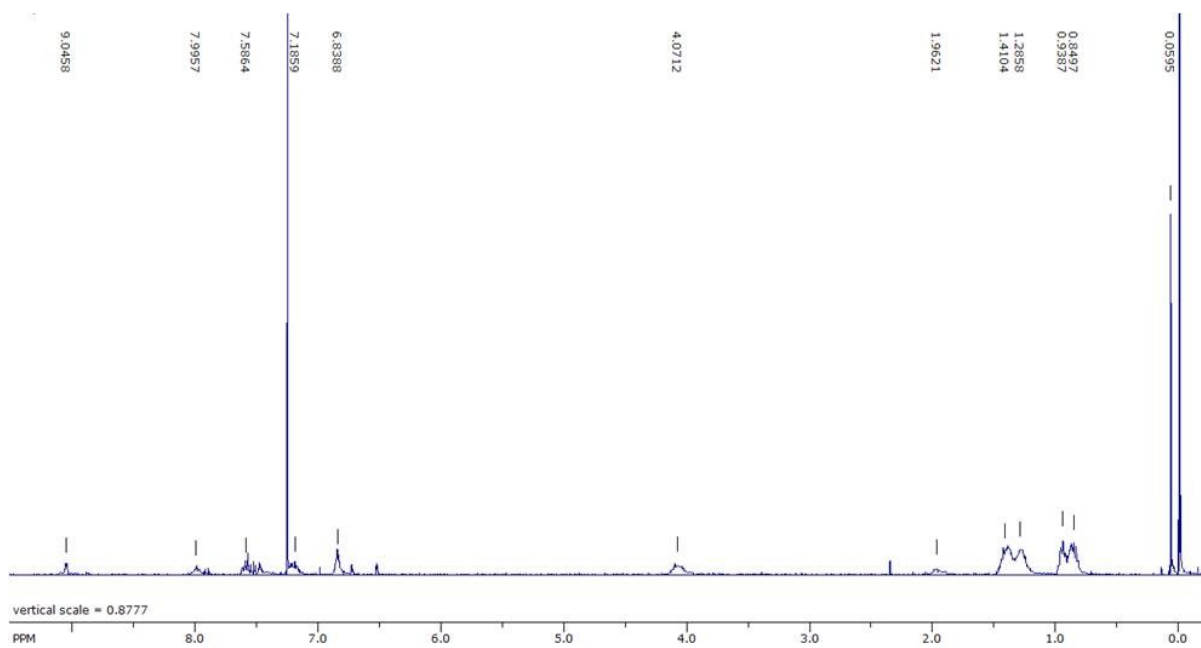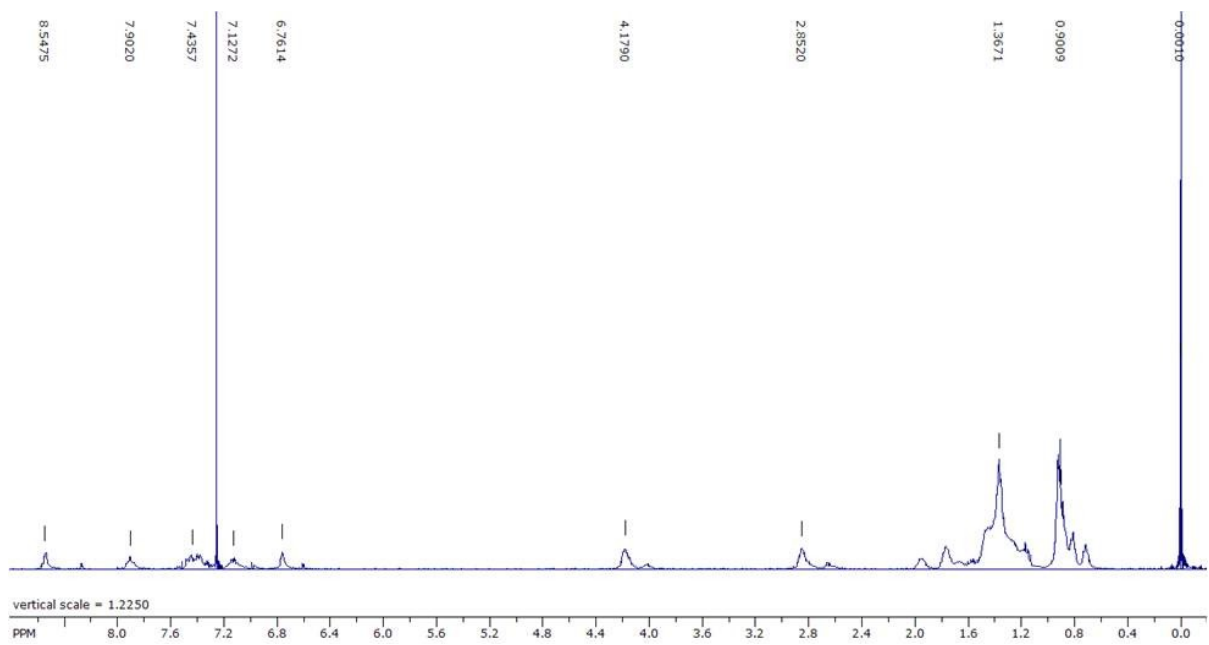

Figure A62. ^{1}H NMR of PFT (400 MHz, CDCl$_3$).

Figure A63. ^{1}H NMR of PTF (400 MHz, CDCl$_3$).
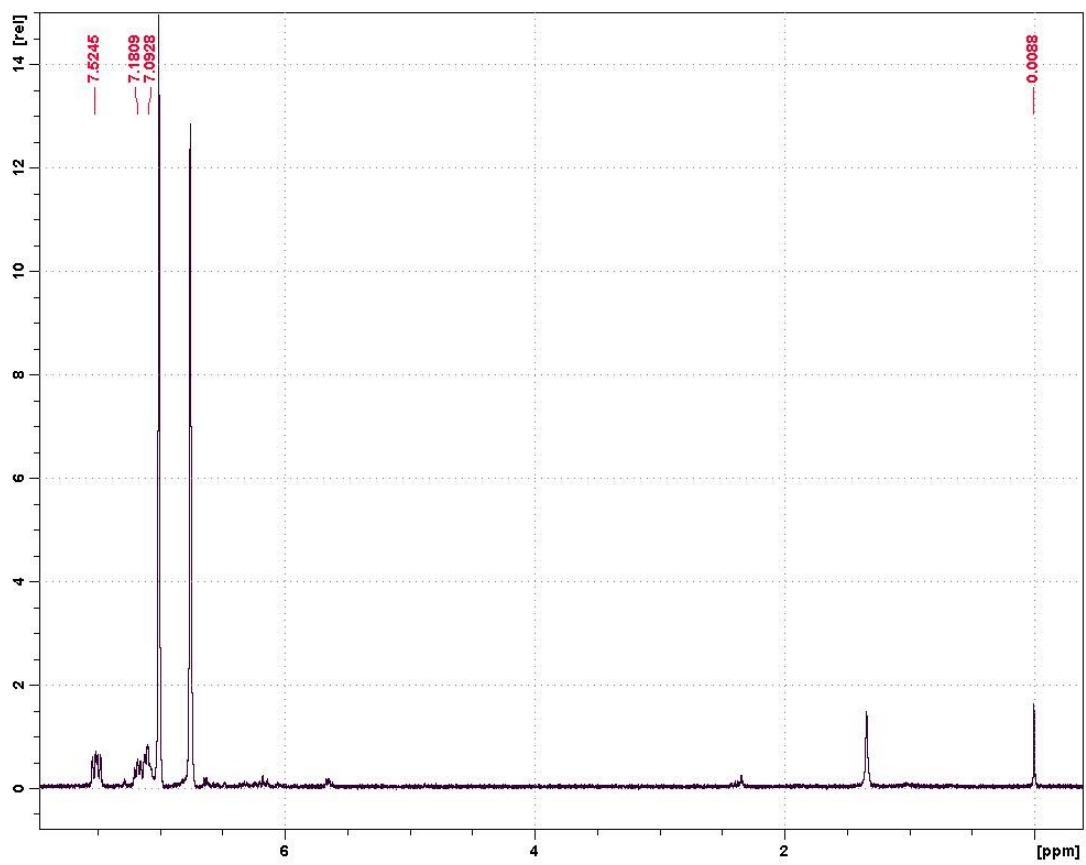

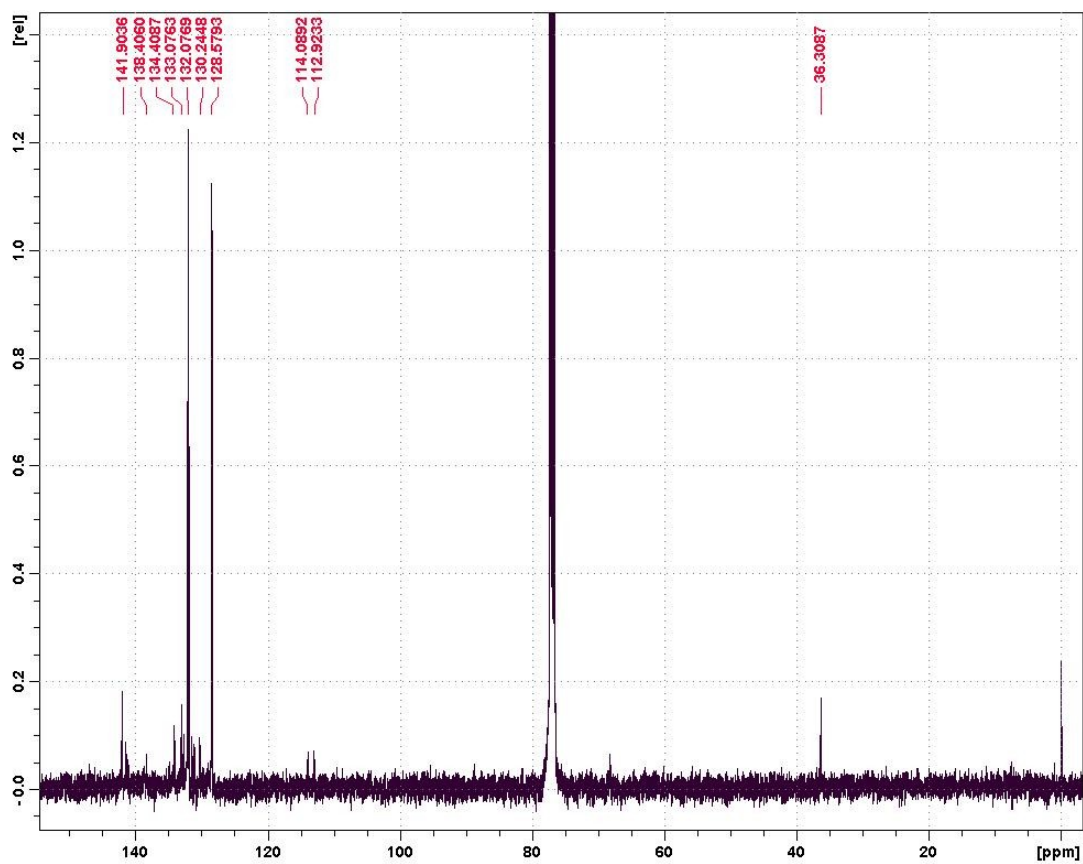**Figure A64.** ^{1}H NMR of TMTQ (400 MHz, CDCl$_3$).

Figure A65. ^{13}C NMR of TMTQ (400 MHz, CDCl$_3$).
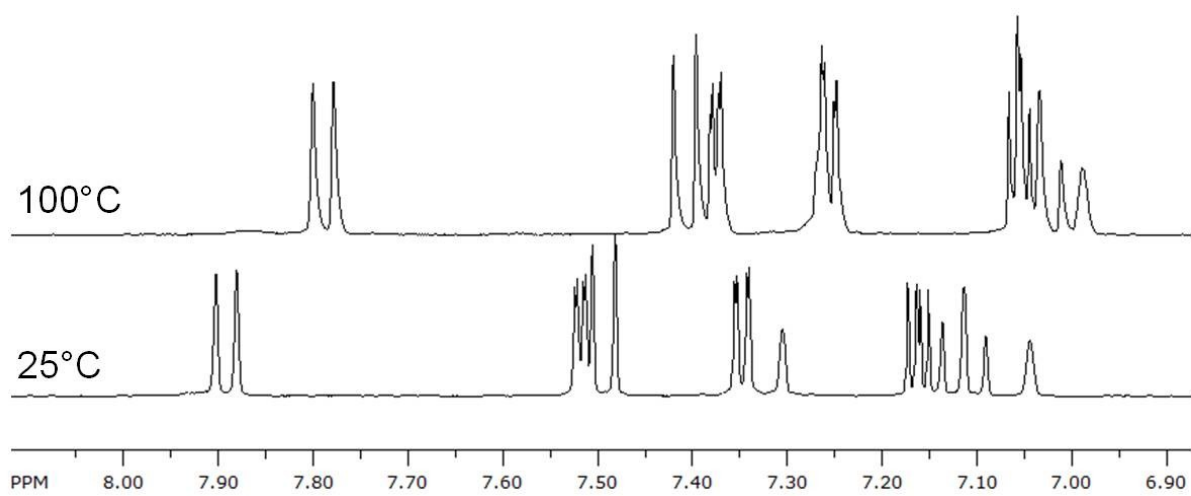

Figure A66. Variable temperature NMR of dibromo-TMT (400 MHz, d_4-o-dichlorobenzene).
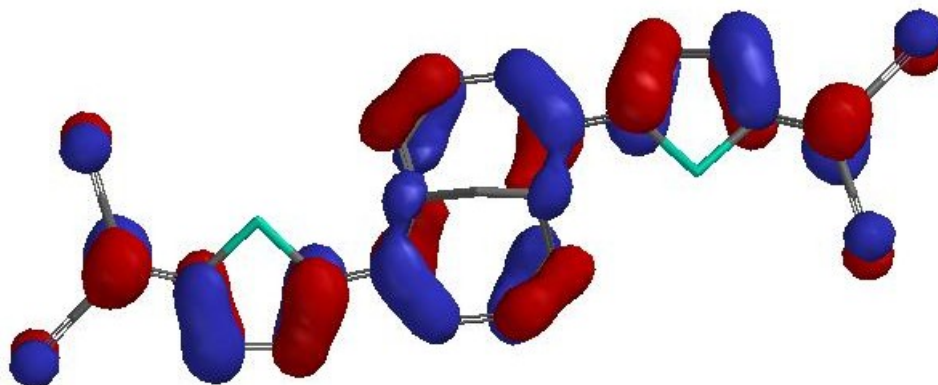
Figure A67. Singlet LUMO diagram of TMTQ (DFT, B3LYP/6-31G*).
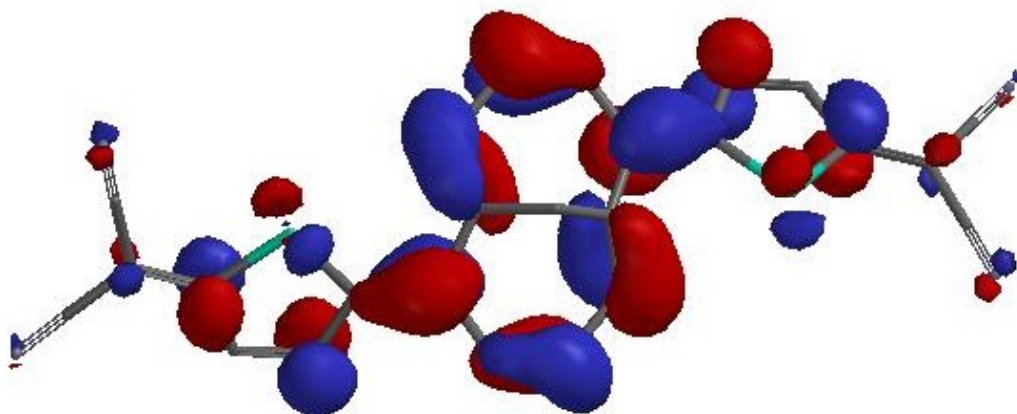

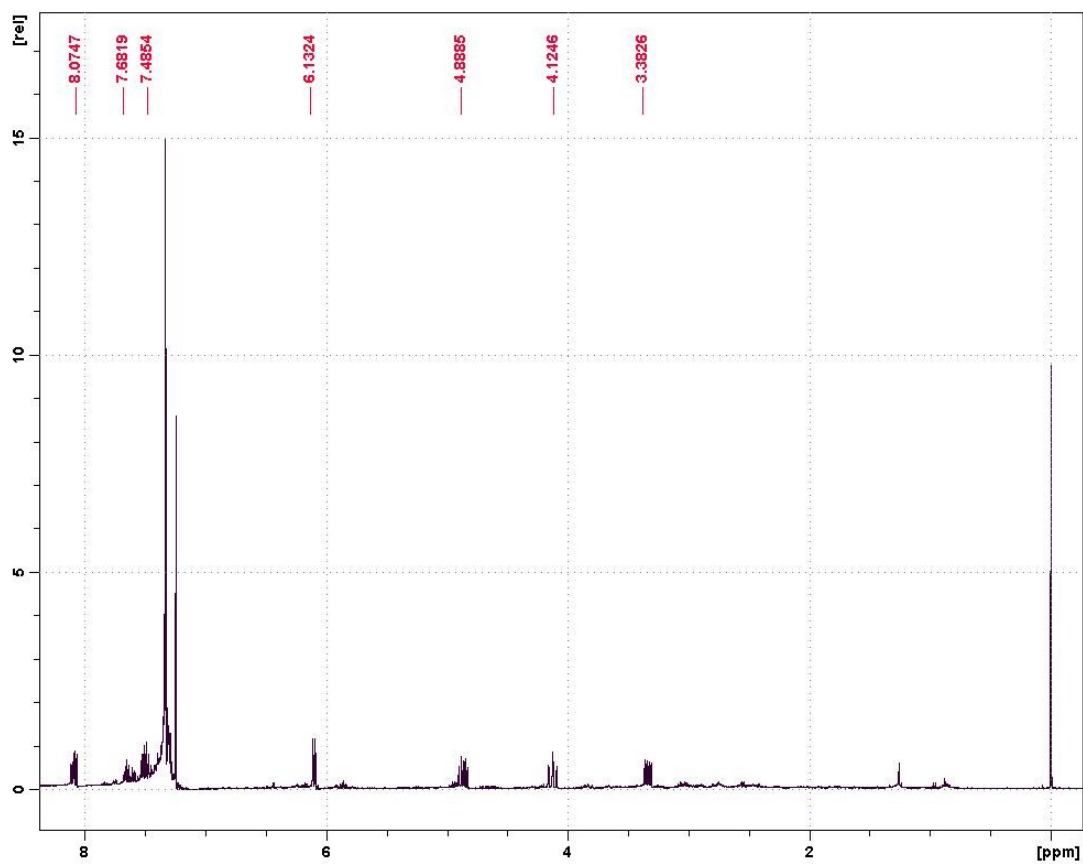**Figure A68.** Triplet LUMO diagram of TMTQ (DFT, B3LYP/6-31G*).

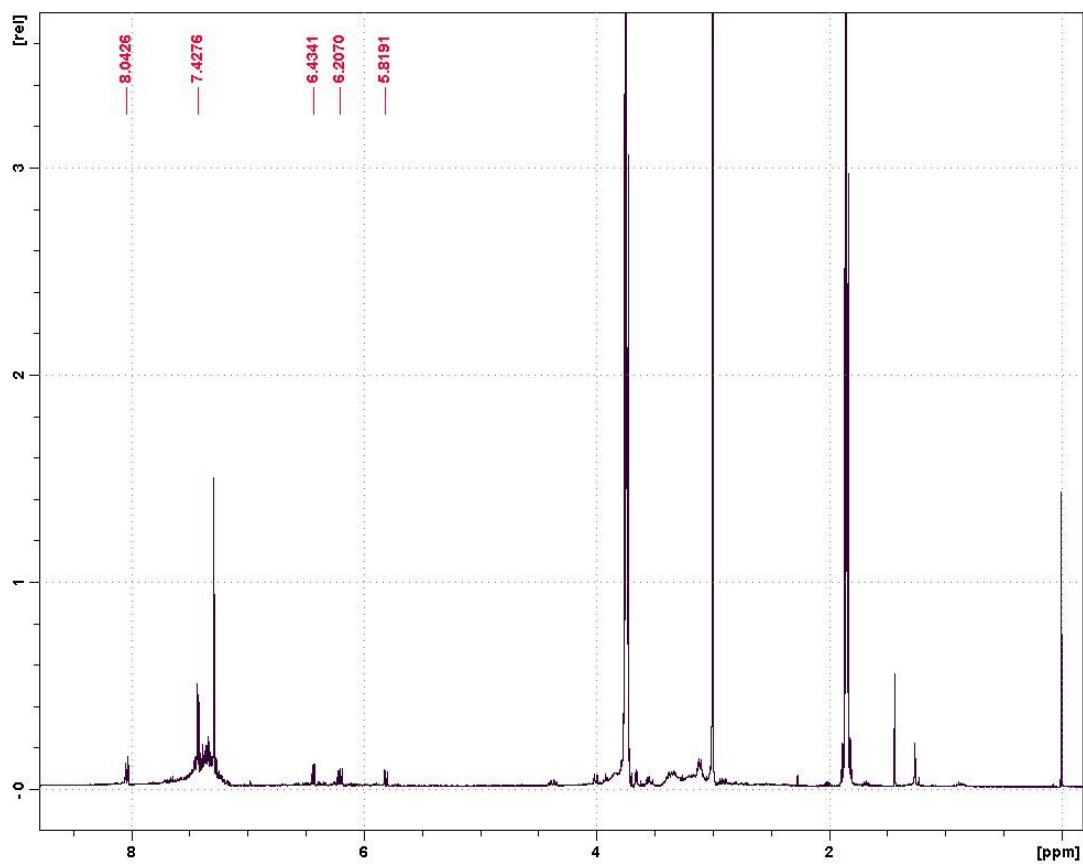**Figure A70.** ^{1}H NMR of 3,7-dibromo-1,5-diphenylcycloocta-1,5-diene (400 MHz, CDCl$_3$).

Figure A71. ^{1}H NMR of 1,5-diphenylcycloocta-1,3,5,7-tetraene (400 MHz, CDCl$_3$).
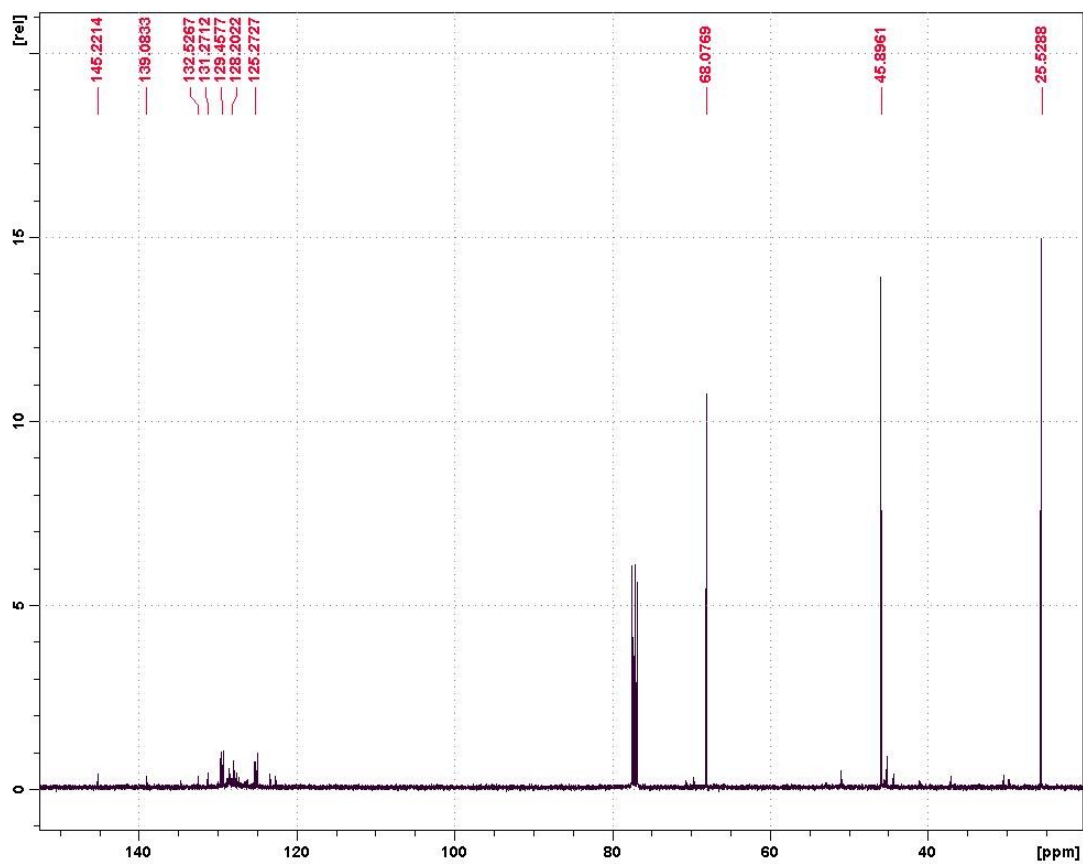
Figure A72. ^{13}C NMR of 1,5-diphenylcycloocta-1,3,5,7-tetraene (100 MHz, CDCl$_3$).

Chapter 7 - Curriculum Vitae

Benjamin C. Streifel was born in Auburn, Washington in the United States of America on November 19th, 1986. He attended Bellarmine Preparatory School in Tacoma, Washington. He matriculated into the University of San Diego in the fall of 2005 and studied chemistry under Dr. Peter Iovine and Dr. Steven Morrison. His undergraduate research revolved around the design, synthesis, and characterization of arylboroxine-core polyester dendrimers (Iovine) and the synthesis of a depsipeptide antibiotic serratamolide (Morrison). He graduated in 2009 and began his studies at Johns Hopkins University under the tutelage of Professor John D. Tovar. He began his work on synthesizing 1,6-methano[10]annulene-based π-conjugated polymers and continued to work with the unusual Hückel aromatic for the remainder of his graduate career. He began to investigate the spin-stabilizing properties of the annulene, as well as synthesizing furan-containing copolymers. While at Johns Hopkins University, he was a teaching assistant for organic chemistry courses.

Benjamin Christopher Streifel

Johns Hopkins University
Department of Chemistry (NCB 340)
3400 North Charles Street
Baltimore, MD 21218

Graduate Student
Tovar Research Group
Phone: (253)-370-8365
benjaminstreifel@gmail.com

Research Interests

Materials-oriented synthetic organic chemistry, polymer chemistry, π-conjugated small molecules and polymers, optoelectronic, spintronic, and thermoelectric materials.

Education

May 2014	Ph.D. Chemistry
	Johns Hopkins University
June 2011	M.A. Chemistry
	Johns Hopkins University
May 2009	B.A. Chemistry (ACS certified), Mathematics Minor
	University of San Diego

Research Experience

Doctoral Research: Chemistry Department, Department of Materials Science and Engineering, Johns Hopkins University, 2009-Present (Research Advisor: J.D. Tovar)

Rational design, synthesis, and characterization of π-conjugated polymers and small molecules for photovoltaic, transistor, thermoelectric, and spintronic device applications.

Fabrication and analysis of photovoltaic, transistor, and thermoelectric devices.

Synthesis and characterization of unusual Hückel and Möbius aromatic molecules to expand the state of the art in organic optoelectronic materials.

Undergraduate Research: Department of Chemistry and Biochemistry, University of San Diego, 2006-2009 (Research Advisor: P.M. Iovine)

Synthesized arylboroxine-core dendrimers as possible solubilizing reagents for chemical modification of lignin

Performed Lewis acid-base studies with arylboroxine-core dendrimers to characterize the reactivity of the boroxine functional group across different generations of dendrimer

Teaching Experience

Teaching assistant: Johns Hopkins University, Department of Chemistry
      Organic Chemistry Lecture: Fall 2009, Spring 2010, Spring 2011
      Spectroscopic Methods of Structure Determination: Fall 2010
Private Tutor: Johns Hopkins University
      Organic chemistry: Fall 2011-present
Tutor: University of San Diego, Academic Support Center
      Chemistry, Mathematics, and Physics 2006-2009

Awards, Grants, and Fellowships

National Research Council Postdoctoral Fellowship (2014)
Johns Hopkins University Owens Summer Fellowship (2013)
University of San Diego Department of Chemistry Excellence in Research Award (2009)
University of San Diego Associated Students Student Research Grant (2008)
University of San Diego Summer Undergraduate Research Experience Grant (2007)

Presentations

2013: Gordon Research Conferences (Polymers) - Poster Presentation
2012: IUPAC Macro 2012 World Polymer Congress - Poster presentation
2011: Gordon Research Conferences (Polymers) - Poster Presentation
2008: ACS National Meeting (Philadelphia) - Poster Presentation

Publications

B.C. Streifel; P.A. Peart; J.F. Martinez-Hardigree; H.E. Katz; J.D. Tovar, "Torsional influences within disordered organic electronic materials based upon non-benzenoid 1,6-methano[10]annulene rings" *Macromolecules*, **2012**, *45*, 7339-7349

B.C. Streifel; J.D. Tovar, "Pi-conjugated Furan-Based Polymers" Encyclopedia of Polymer Science and Technology, **2012**, Wiley and Sons.

M.C. Smith; J.A. Snyder; B.C. Streifel; A.E. Bragg, "Ultrafast excited-state dynamics of o-terphenyl and 1,2-diphenylcyclohexene: the role of 'ethylenic twisting' in the nonadiabatic photocyclization of stilbene analogs" *J. Phys. Chem. Lett.*, **2013**, *4*, 1895-1900